WATER MONOGRAPHS

#WaterMonographs

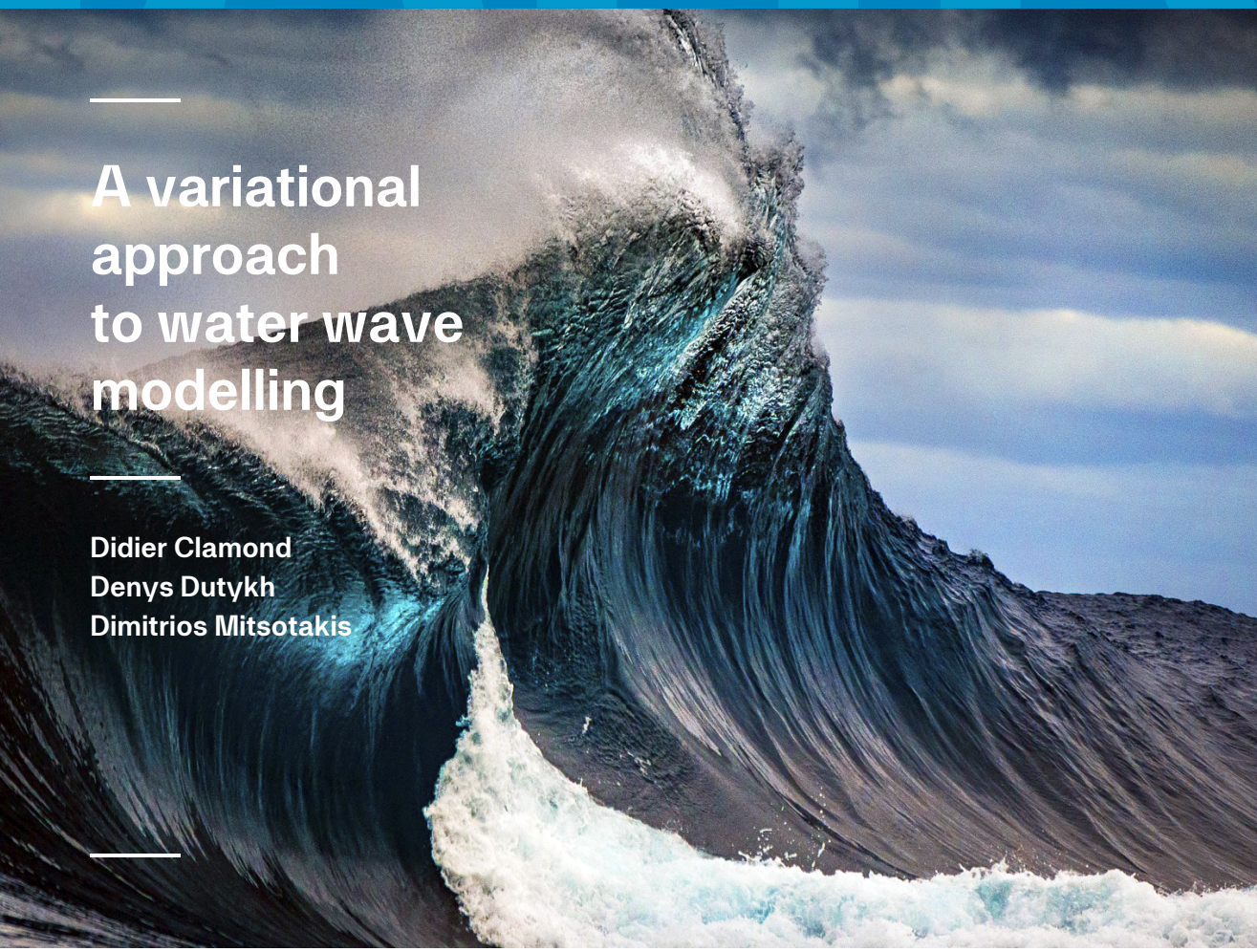

A variational approach to water wave modelling

Didier Clamond
Denys Dutykh
Dimitrios Mitsotakis

Supported by

جامعة خليفة
Khalifa University

OPEN ACCESS

IAHR AIRH
International Association for Hydro-Environment Engineering and Research
Hosted by
Spain Water and IWHR, China

IAHR.org

A variational approach to water wave modelling

Didier Clamond, Denys Dutykh and Dimitrios Mitsotakis

A variational approach to water wave modelling

Didier Clamond
Denys Dutykh
Dimitrios Mitsotakis

IAHR WATER MONOGRAPH SERIES

Series Editor

Damien Violeau
LNHE, EDF R&D, France.
Saint-Venant Hydraulics Laboratory, Ecole des Ponts ParisTech, France.
E-mail: damien.violeau@edf.fr

ISBN (electronic version): 978-90-833476-6-0

ISBN (printed version): 978-90-833476-7-7

ISSN 2959-7978

doi: 10.3850/978-90-833476-6-0_IAHR_Watermonograph_003

Published by:
IAHR — International Association for Hydro-Environment Engineering and Research

Madrid Office

Paseo Bajo Virgen del Puerto 3, 28005, Madrid, SPAIN
Tel: +34 913357908; Fax: +34 913357935

Beijing Office

A-1 Fuxing Road, Haidian District, 100038, Beijing, CHINA
Tel: +86 1068781128; Fax: +86 1068781890

The International Association for Hydro-Environment Engineering and Research (IAHR), founded in 1935, is a worldwide independent organisation of engineers and water specialists working in fields related to the hydro-environmental sciences and their practical application. Activities range from river and maritime hydraulics to water resources development and eco-hydraulics, through to ice engineering, hydro-informatics and continuing education and training. IAHR stimulates and promotes both research and it's application, and by so doing strives to contribute to sustainable development, the optimisation of the world's water resources management and industrial flow processes. IAHR accomplishes its goals by a wide variety of member activities including: working groups, research agenda, congresses, specialty conferences, workshops and short courses; Journals, Monographs and Proceedings; by involvement in international programmes such as UNESCO, WMO, IDNDR, GWP, ICSU, and by co-operation with other water-related (inter)national organisations.

The monitoring of publishing ethics is a major aspect of editorial and peer-review publications. IAHR is a well-established and long-standing organization whose primary mission is to foster knowledge exchange amongst its community and stakeholder base. Accordingly, IAHR takes its policies on ethics seriously.

The IAHR Water Monograph A *variational approach to water wave modelling* has been published under the IAHR Publications Ethics and Malpractice Statement. Additionally, IAHR publications follow the Ethical Guidelines and Codes of Conduct provided by the Committee of Publication Ethics (COPE).

Cover information:
Tall powerful cross ocean wave breaking during a dark, stormy evening. Philip Thurston / iStock by Getty Images.

Cover by Tres Estudio Creativo, Spain

Typeset by Research Publishing, Singapore

About the IAHR Water Monograph Series

The Water Monograph Series joins IAHR's portfolio of publications, which includes journals, magazines, conference proceedings, whitepapers, and books. Since its start in 1935, IAHR has been dedicated to supporting the development and dissemination of knowledge that aids hydro-environment engineering and research.

The Water Monographs are mid-sized publications (about 50–150 pages long) that bridge knowledge gaps, summarize existing knowledge, and publicize recent advances in technologies and methods. More narrowly focused than a book, the Water Monographs occupy the publication space between a journal paper and a book. They concisely present information on physical processes, measurement techniques, theoretical material, numerical modeling techniques, engineering applications, and historical and cultural matters, doing so in an appealingly readable and well-illustrated manner.

IAHR intends that the Water Monograph Series helps people understand specific longstanding, current, or emerging topics in hydro-environment engineering and research.

A specific IAHR Task Force on Water Monographs is responsible for making calls for proposals, receiving proposals and evaluating proposals. This Task Force is composed by:

Damien Violeau, EDF, France (**Chair**)
Claudia Adduce, Roma Tre University, Italy
Ioan Nistor, University of Ottawa, Canada
Robert Ettema, Colorado State University, USA
Vlad Nikora, University of Aberdeen, UK
Pengzhi Lin, Sichuan University, China
Massimo Guerrero, Università di Bologna-DICAM, Italy
Donatella Termini, University of Palermo, Italy

Once a proposal is approved by the majority of the members, an Editor is assigned to the draft monographe. The Editor is in charge of communications with the author(s) until the manuscript is ready. When the draft manuscript is ready for review, the Editor selects three reviewers - independent, with expertise in the field and external to IAHR staff. The reviewers conduct the review process When all

the reviews are received, they are sent to the author(s) and once they are addressed the Editor makes the final decision to accept the updated draft for publication. At that time, the names of the reviewers are shared with the author(s) and the reviewers are acknowledged in the Water Monograph.

IAHR Water Monographs are sponsored mainly by third institutions with the interest of spreading the knowledge in a specific field and by IAHR; sponsors receive visibility in exchange placing the logo in the cover.

Damien Violeau
Chair of IAHR Water Monograph Series

Table of Contents

Foreword

The realisation that variational principles might be useful in the theory of water waves appears to have been first noticed by Purser and Synge [191] in a 1962 letter to the Editor of Nature, with the detailed mathematics appearing in Synge [217]. Their observation was that "*ocean waves approaching a beach may be discussed by the method of geometrical optics*…", and it had already been noted by Hamilton over a century earlier that the rays in geometric optics theory could be characterized as a Hamiltonian system. Synge [217] adapted this theory to derive the Hamiltonian system for water wave rays.

Purser and Synge go further and write "*It may be useful to have a word, analogous to 'photon', 'phonon' and 'graviton', for a fictitious particle that travels with the ray (or group) velocity and carries energy: we suggest the name 'hydron'.*" However, neither the Hamiltonian theory of Synge nor the name hydron ever took off. Although ray theory is today a central part of coastal engineering and the theory of shoaling water waves, reference to Synge's Hamiltonian approach is almost nowhere to be found. Unfortunately, the word "hydron" was never taken up either. However, a few years later, using the same logic, Kruskal and Zabusky coined the term "solitron", eventually shortening it to "soliton", which did indeed take off.

It is the discoveries, just a few short years later, of Luke [155] (the Lagrangian theory) and Zakharov [243] (the Hamiltonian theory), of variational principles for the full, albeit irrotational, water wave problem, that firmly established the importance of variational principles in every aspect of the theory of water waves. Today, variational principles are a central part of the theory of water waves across the spectrum from pure to applied mathematics through to applications.

This monograph takes the subject of variational principles for water waves to a new level. Lagrangians such as Luke's are improved via *relaxation* where a sequence of constraints are added, enforced by Lagrange multipliers, that may be exact or approximate and, in the latter case, a range of new and surprising model equations for water waves emerge, without the need to introduce a small parameter. It is a highly effective strategy and produces Lagrangian, Hamiltonian and multisymplectic structures with equal ease.

The strategy recovers known equations and many new ones. It allows for the enforcement of boundary conditions, thereby including bottom topography without restriction on size, as well as time-dependent boundary conditions. The latter case, applied to time-varying topography, is shown to have great practical value in the modelling of tsunami waves, with the emergent models capturing the Synolakis mechanism of tsunami slowdown followed by acceleration nearshore. The heart of the monograph is chapter 4, which is a theme and variations on the Serre equations, re-deriving, re-interpreting the classical versions, and then taking Serre equations in new directions. A triumph here is the discovery via relaxation of a multisymplectic formation. Chapter 4 segues into chapter 5 with the dual problem of model equations in deep water. A range of new models PDEs are discovered, building on the authors' previous discovery of a generalised Klein–Gordon equation for deep water waves, with new and surprising Hamiltonian and multisymplectic structures emerging.

A strength of this monograph is that the new models are tested with high-quality numerical schemes. For simulations, finite-volume methods and pseudo-spectral methods are used. Variational principles feed into numerics in the improved preservation of local and global invariants like energy and momentum, as well as symplecticity. Variationally-designed numerical schemes also appear to preserve the properties of the dispersion relation.

Multisymplectic structures are a much more recent addition to the panoply of variational structures for water waves, first appearing in the 1990s [32, 33, 162]. In its simplest form, multisymplecticity is a collection of pre-symplectic forms (one for each space direction and time) and a scalar-valued function (serving the role of Hamiltonian function). The subject has a rich history with many variants. Historically, the concept emerged from a multidirectional Legendre transform, whereby each space direction as well as the time direction are transformed. However, this approach is limiting, and the modern approach is to define multisymplecticity axiomatically: a manifold or phase space $\mathcal{M}$ on which there is one (classical case) or many closed, but not necessarily non-degenerate, two forms. A pull-back of each two-forms by a vector field on $\mathcal{M}$ defines a scalar-valued function, the Hamiltonian. This axiomatic approach was initiated in [33]. A multisymplectic structure for Lagrangians on manifolds was developed in [162], with the restriction of first-order fields. In [35], a coordinate-free approach for multisymplectic structures on abstract manifolds was presented without recourse to a Lagrangian. The introduction to [35] also gives a history of multisymplecticity and its many variants (Dedonder–Weyl theory, Norris' soldering form, $k-$symplectic structures, Cartan form, polysymplecticity, the TEA bundle). Hamiltonian systems on a multisymplectic structure have been found to be important in a wide range of applications.

In this monograph, the authors take multisymplecticity in a new direction, showing how relaxed variational principles provide an efficient strategy for deriving new multisymplectic formulations, even in cases where it is by no means obvious. Two successes of this strategy are the discovery of a multisymplectic formulation of the Serre equation in shallow water and the construction of a multisymplectic structure for the generalized Klein–Gordon equations (gKG) equations in deep water.

This monograph is more of a starting point than a complete story. It paves the way for new research directions. For example, there is a wide open area of models for parametrically defined free surfaces, opening the door to the modelling of wave breaking, and there is a need for models that include vorticity and, most importantly, new models that capture the three-dimensionality of water waves.

Prof. Tom Bridges Surrey, UK
November 2021

Preface

Surface water waves represent an exceedingly complex field of physical study, characterized by a rich tapestry of underlying mechanisms and a long-standing history of scholarly investigation, see *e.g.* [65, 232]. Water waves serve as a distinct subclass within the broader category of fluid mechanical waves, uniquely characterized by their propagation along the interface that separates aqueous and atmospheric mediums. They play a central rôle in the interactions taking place between the ocean and atmosphere [138, 221]. In addition to their fundamental physical importance, understanding water waves is also important for many applications related to human safety and the economy, such as tsunamis, freak waves, harbour protections, and beach nourishment/erosion, just to mention a few examples. Water waves function as a paradigmatic example that encapsulates a wide array of nonlinear wave phenomena manifesting in diverse physical media. The famous physicist Richard P. Feynman wrote in his celebrated lectures [100]:

> *"Now, the next waves of interest, that are easily seen by everyone, and which are usually used as an example of waves in elementary courses, are water waves. As we shall soon see, they are the worst possible example, because they are in no respects like sound and light; they have all the complications that waves can have."*

It is precisely these intricate complexities that contribute to the richness and intellectual allure of the study of water waves. Indeed, despite numerous studies, new waves and new wave behaviour are still discovered (*e.g.*, [193, 194]), and wave dynamics are still far from being fully understood. The complete mathematical formulation describing the propagation of water waves is quite complex to deal with. The mathematical formulation cannot be solved analytically (unless in some asymptotic sense), and thus, efficient numerical algorithms have been developed since the 1970's [43].

The use of mathematical and numerical models is unavoidable for understanding water waves. Despite the apparent simplicity in formulating the foundational equations governing these waves, specifically the Navier–Stokes equations, the mathematical analysis required to solve them is exceptionally intricate. Furthermore, even the computational approaches aimed at their numerical resolution present significant challenges, demanding considerable computational resources and expertise.

Therefore, simplified models are crucial to gain insight and to derive operational numerical models. Moreover, the water wave theory has always been developed by constructing convenient and physically sound approximations [65]. Most of the time, simplified models are derived via some asymptotic expansions, exploiting a small parameter in the problem at hand. This approach is very effective leading to well-known equations, such as the Saint-Venant [68, 212, 232], Boussinesq [29], Serre–Green–Naghdi equations (SGN) [115, 203], Korteweg–deVries equation (KdV) [140] equations in shallow water and the Nonlinear Schrödinger equation (NSE) [165], Dysthe [98] equations in deep water. These governing equations are frequently derived through the application of various perturbation techniques. Such techniques generally yield models that are applicable primarily to waves characterized by small amplitude and/or a low ratio of wavelength to water depth. However, for a broad range of practical applications, it becomes imperative to employ models that are uniformly valid across all depths and that offer a high degree of accuracy even for waves with large amplitudes. It is worth noting that our understanding of the shallow water regime has significantly advanced in recent years. Within the context of shallow water, a well-structured hierarchy of hydrodynamic models has been firmly established:

- Nonlinear shallow water (Saint-Venant or Airy (especially in the UK) or fully nonlinear non-dispersive) equations [2, 68].
- Boussinesq-type (or weakly nonlinear weakly dispersive) equations [30, 196].
- Fully nonlinear weakly dispersive equations [134, 204].
- Fully nonlinear strongly dispersive equations [125, 233].
- Fully nonlinear fully dispersive Euler equations [159].

The deep water case is much less organised. The main difference between these two regimes comes from the dimensionless numbers which characterize the flow. When the depth d is finite, we have one parameter α_0/d which characterizes the wave non-linearity and another parameter d/λ to describe the flow 'shallowness'. Here α_0 refers to the typical wave amplitude, and λ is the typical wavelength. By applying asymptotic expansions in one or even two parameters, we can obtain various approximate models. Now, if we take the limit $d \to \infty$, both these parameters lose their sense in the deep water, making this case somehow special. Traditionally, deep water waves have been described as perturbations of a certain carrier wave. In this way, the wave field has been conveniently described using wave envelopes [21]. Then, the envelope function is shown to satisfy the nonlinear Schrödinger [243] or Dysthe-type [98] equations depending on the desired asymptotic order of accuracy. These equations can be also recast into the Hamiltonian framework [112]. In the present monograph, we

take an alternative route without appealing to wave envelope techniques. Moreover, some phenomena (see *e.g.* [193, 194]) do not involve any small parameter and do not bifurcate from rest. The problem is then to derive models without relying on a small parameter.

It is well-known in theoretical physics that variational formulations are tools of choice to derive approximations when small parameter expansions are inefficient. Fortunately, a variational principle is available for water waves that can be exploited to derive approximations. There are mainly two variational formulations for irrotational surface waves that are commonly used, namely the Lagrangian of Luke [155] and the Hamiltonian of Broer, Petrov and Zakharov [39, 190, 243]. Details on the variational formulations for surface waves can be found in review papers, *e.g.* [192, 197, 245]. The paper [34] gives variational formulations for water waves in curvilinear coordinates. A variational principle for fluid sloshing with vorticity was recently proposed in [7] in terms of the stream function. It also includes coupling to body motion.

In water wave theory, variational formulations are generally used together with a small parameter expansion. This is not necessary, however, because variational methods can also be fruitfully used without small parameters, as it is well-known in Quantum Mechanics, for example. This will be demonstrated in the present monograph. Here, only elementary knowledge in vector calculus is assumed, as well as some familiarity with the Euler–Lagrange equations and variational principles in Mechanics [110, 147].

Through the utilization of straightforward examples, we aim to elucidate the merits of employing relaxed variational principles, among other variational approaches. The benefits of adopting this particular methodology become even more pronounced in scenarios involving variable water depths. In such cases, this approach facilitates the derivation of simplified approximations that are not readily obtainable through the use of asymptotic expansions (see *e.g.* [83]). The relaxed variational principle provides a common platform for deriving several approximate equations from the same Ansatz in changing only the constraints. Besides the Ansätze and the subordinate conditions, no further approximations are needed to derive the equations. Using more general assumptions (*i.e.*, involving more free functions and parameters) and well-chosen constraints, one can hopefully derive more accurate approximations.

Although the possibility of using the variational methods without a small-parameter expansion has been overlooked in the context of water waves, it has long been recognized as a powerful tool in Theoretical Physics, in particular in Quantum Mechanics. This approach is even taught in some undergraduate lectures. For instance, from Berkeley's course on Quantum Mechanics [179]:

- *The perturbation theory is useful when there is a small dimensionless parameter in the problem, and the system is exactly solvable when the small parameter is sent to zero.*
- *[…] it is not required that the system has a small parameter, nor that the system is exactly solvable in a certain limit. Therefore, it has been useful in studying strongly correlated systems, such as the fractional quantum Hall effect.*

However, in order to be successful, the great power of the variational method needs to be harnessed with skill and care, as it is well-known in Theoretical Physics. Indeed, as quoted in the same lecture on Quantum Mechanics:

- *[…] there is no way to judge how close your result is to the true result. The only thing you can do is to try out many Ansätze and compare them.*
- *[…] the success of the variational method depends on the initial "guess" […] and an excellent physical intuition is required for a successful application.*

But it is also well-known that this approach can be very rewarding:

- *For example, R.B. Laughlin [148] proposed a trial wave function that beat other wave functions that had been proposed earlier, such as "Wigner crystal".*
- *Once your wave function gives a lower energy than your rival's, you won the race**.

Thus, despite its "dangers," the variational approach is a tool of choice for modelling water waves, especially for problems when there are no obvious small parameters or if approximations valid for a broad range are needed. We shall illustrate these claims in this monograph.

Prof. Didier Clamond — Nice, France
Assoc. Prof. Denys Dutykh — Abu Dhabi, UAE
Assoc. Prof. Dimitrios Mitsotakis — Wellington, New Zealand
October 2023

*R.B. Laughlin *et al.* earned the 1998 Physics Nobel prize.

CHAPTER 1

Introduction

The water wave problem in fluid mechanics has been known for more than two hundred years [65]. The classical mathematical formulation of surface gravity waves involves five equations: the irrotationality of the fluid motion, the incompressibility of the fluid, the bottom and the surface impermeabilities, and the surface isobarity [165]. This system of equations cannot generally be solved exactly, and historically, water wave theory has been developed by constructing various approximations. In shallow water, we have the equations of Korteweg and de Vries [140], Boussinesq [29], Benjamin *et al.* [19], Serre [203], Green and Naghdi [115], Camassa and Holm [40], Degasperis–Procesi [69], and many other model equations. In finite depth and deep water, there is the celebrated nonlinear Schrödinger equation [165] and the equations of Dysthe [98], Trulsen *et al.* [225], Kraenkel *et al.* [141], among others. These equations are most often derived via some perturbation techniques and are thus valid for waves of small amplitude. Moreover, these equations are generally valid for a very limited range of the ratio *wavelength/water-depth* and for narrow-banded wave spectra. However, for many applications, it is necessary to use models uniformly valid for all depths, which are accurate for large amplitudes. In the domain of theoretical physics, it is widely acknowledged that when the endeavour is to derive approximations, especially in scenarios where expansions predicated on small parameters prove to be inefficient, variational formulations are often the methodologies of choice. These formulations, characterised by their flexibility and robustness, provide a structured approach towards obtaining approximate solutions. By minimising or maximising a functional[1], they allow for the exploration of system dynamics under various conditions, thereby often yielding more accurate or insightful approximations compared to traditional small parameter expansion techniques. Furthermore, the variational approach often unveils underlying geometric or topological properties of the physical system under consideration, which can be instrumental in fostering a deeper understanding of the phenomena at hand.

There are mainly two variational formulations for irrotational surface waves that are commonly used, namely the Lagrangian of Luke [155] and the Hamiltonian of Petrov [190] and Zakharov [243]. Details on the variational formulations for surface waves can be found in review papers, *e.g.*, [192, 197, 245].

[1] In practice, we always look at stationary points of a given functional.

In tracing the lineage of such variational methodologies, it is intriguing to note the historical evolution of related formulations in theoretical physics. Specifically, the development of multi-symplectic formulations emerged as a significant stride towards a more comprehensive understanding of variational problems involving multiple variables. The history of multi-symplectic formulations can be traced back to V. Volterra (1890), who generalised Hamiltonian equations for variational problems involving several variables [229, 230]. Later, these ideas were developed in the 1930s [67, 150, 235]. Finally, in the 1970s, the multivariable Hamiltonian formulation was geometrised by several mathematical physicists [109, 135, 142, 143] similarly to the evolution of symplectic geometry originating from the ideas of J.-L. Lagrange [146, 211]. In our study, we have been inspired by modern works on multi-symplectic PDEs [33, 161]. Recently, the multisymplectic geometry has found many applications to the development of structure-preserving integrators [37, 47, 82, 174]. These variational principles have been exploited, in different variants, to build analytical and numerical approximations, *e.g.*, [11, 136] just to mention a few references. The water wave problem is also known to have a multi-symplectic structure [32].

Luke's Lagrangian is predicated on the assumption that the fluid flow under consideration is strictly irrotational; that is to say, the Lagrangian encapsulates a velocity potential while abstaining from direct incorporation of the velocity components. This formulation aligns with the theoretical underpinning that in an irrotational flow, the velocity field is derivable from a scalar potential function, thereby rendering the explicit articulation of velocity components unnecessary within the Lagrangian. Should the conditions of fluid incompressibility and bottom impermeability be satisfied identically, it consequently facilitates the derivation of the equations pertinent to the surface from Zakharov's Hamiltonian, as delineated in [243]. This formulation elucidates the inherent relationships and dynamics at play, particularly at the fluid-surface interface, thereby providing a robust analytical framework to explore the complex interactions therein. Zakharov's Hamiltonian, in this context, serves as a pivotal theoretical construct, linking the fundamental physical constraints of incompressibility and impermeability to the observable phenomena at the fluid surface, thus enriching the discourse on fluid dynamics and surface wave behaviour.

In both Luke's and Zakharov's variational formulations, there is an inherent assumption of exact irrotationality in the flow dynamics, a characteristic prominently featured in the water wave problem formulation. However, a discernible distinction arises in that Zakharov's Hamiltonian exhibits a more stringent constraint compared to Luke's Lagrangian. These variational formulations necessitate that either a portion or the entirety of the equations governing the fluid dynamics in the bulk of the fluid and at the bottom are satisfied identically. Concurrently, any residual relations are subject to

approximation in the course of constructing an approximate variational model, as expounded upon in [64]. The predilection towards satisfying irrotationality and incompressibility identically is attributed to their mathematical tractability, making them relatively straightforward to fulfil. Yet, beyond this allure of simplicity, there does not appear to be a compelling rationale to prioritize irrotationality and/or incompressibility over other conditions, such as the impermeability or the isobarity of the free surface. In the ensuing discourse of this monograph, we endeavour to underscore the advantages of relinquishing the rigid adherence to exact irrotationality and incompressibility. As we shall demonstrate, approximations of these relations suffice in a majority of practical scenarios, thereby offering a pragmatic and flexible approach to exploring the dynamical behaviour of fluid flows and surface waves.

Variational formulations involving as few dependent variables as possible are often regarded as simpler [241]. It is understandably tempting to solve exactly (*i.e.*, analytically) as many equations as possible in order to 'improve' the solution accuracy. However, this is not always a good idea. Indeed, there are many examples in numerical analysis and scientific computing where efficient and well-used algorithms do exactly the opposite. These so-called *relaxation methods — e.g.*, pseudo-compressibility for incompressible fluid flows [130] — have proven to be very efficient for stiff problems. When solving numerically a system of equations, the exact resolution of a few equations does not necessarily ensure that the overall error is reduced. What really matters is that the global error is minimized. A similar idea of relaxation may also be applied to analytical approximations. The interplay between continuous and discrete models has already been proven to be very fruitful. The paper [101] introduced the idea of a *numerical dispersion relation* and how it approximates the exact dispersion relation. One outcome of this study is that multi-symplectic schemes, such as the Preissmann scheme, preserve the monotonicity of the dispersion relation, thereby eliminating spurious group velocities in a numerical scheme.

In this study, we would like to elucidate the benefit of using relaxed variational methods for the water waves problem. In other words, we illustrate the advantage of using a variational principle involving as many dependent variables as possible. We emphasize that our primary purpose here is to provide a generalized framework for deriving model equations for water waves. This methodology is explained in various examples, some of them being new to our knowledge. However, the potential of the present approach is far from being fully exploited.

Our review would not be complete if we did not mention one less-known, but still remarkable variational model for shallow water waves. The Isobe-Kakinuma model was derived by M. Isobe and further expanded by T. Kakinuma as a mathematical approximation for long water waves (see [125] for

exact Japanese references). The Isobe-Kakinuma model is also derived from Luke's variational formulation of the full water wave problem. The Isobe-Kakinuma model, which is the Euler-Lagrange equation for an approximated Lagrangian, is established by approximating the velocity potential in Luke's Lagrangian. Various model systems can be obtained depending on the choice of function system used. The strength of the Isobe-Kakinuma model lies in its ability to provide a high-order approximation to the water wave equations without containing high-order derivative terms, which can be computationally burdensome. Specifically, the Isobe-Kakinuma model is considered a superior higher-order approximation to the water wave equations. However, this model did not gain much popularity in the water wave community. Due to this model's highly technical construction and approximations, it is not without limitations. It requires specific initial conditions and involves a number of complex calculations that may not be feasible for all practical applications. The variational structure of the Isobe-Kakinuma model originates from its foundation in the Lagrangian framework established by J.C. Luke for water wave problems.

The present manuscript is organized as follows. First, the water waves problem formulation is briefly reviewed in chapter 2. In chapter 3, several variational formulations are presented. In chapter 4, we present several examples in the shallow water regime, while chapter 5 focuses on the opposite, *i.e.* deep water regime. We also provide some guidance on how to address the intermediate depths in chapter 6. Some numerical methods and illustrations in shallow water regime are given in chapter 4.6. Finally, in chapter 7, we outline the main conclusions and perspectives of this study.

CHAPTER 2

Water wave problem formulation

Consider an ideal incompressible fluid of constant density ρ. The horizontal independent variables are denoted by $\boldsymbol{x} = (x_1, x_2)$ and the upward vertical one by y. The origin of the Cartesian coordinate system is chosen such that the surface $y = 0$ corresponds to the still water level. The fluid is bounded below by the bottom at $y = -d(\boldsymbol{x}, t)$ and above by the free surface at $y = \eta(\boldsymbol{x}, t)$. Usually, we assume that the total depth $h(\boldsymbol{x}, t) \overset{\text{def}}{=} d(\boldsymbol{x}, t) + \eta(\boldsymbol{x}, t)$ remains positive $h(\boldsymbol{x}, t) \geqslant h_0 > 0$ at all times t for some constant h_0. A sketch of the physical domain is shown in Figure 2.1.

Remark 2.1. In our analytical approach, we adhere to the classical assumption that the free surface is represented as a graph $y = \eta(\boldsymbol{x}, t)$, derived from a single-valued function. This assumption, while simplifying the analytical framework, inherently imposes a limitation on the scope of phenomena that can be effectively captured within this modelling approach. Specifically, by representing the free surface in such a manner, we are essentially restricting our analysis to scenarios where the surface profile can be described unambiguously at every spatial point for a given time. This simplification, albeit useful for analytical tractability, precludes the exploration of certain complex phenomena, notably wave breaking, which manifest beyond the confines of a single-valued function representation. Wave breaking, characterized by the overturning or steepening of wave crests to the point of discontinuity, challenges the single-valued function depiction and, thus, falls outside the ambit of the current modelling approach. This exclusion, while narrowing the scope of our investigation, allows for a more focused and manageable exploration within the defined analytical framework. Nevertheless, it is important to acknowledge this limitation, as it delineates the boundary between the simplified scenarios amenable to our analysis and the more intricate phenomena demanding a more nuanced or alternative modelling approach.

We denote $\boldsymbol{u} = (u_1, u_2)$ the horizontal velocity and v the vertical one. The fluid density is constant, and the mass conservation implies an isochoric motion, yielding the continuity equation valid everywhere in the fluid domain

$$\boldsymbol{\nabla} \cdot \boldsymbol{u} + \partial_y v = 0, \tag{2.1}$$

where $\boldsymbol{\nabla}$ denotes the horizontal gradient and $\cdot$ denotes the standard scalar (inner) product of two-dimensional Euclidean vectors. Here, ∂_y denotes the usual partial derivative with respect to the

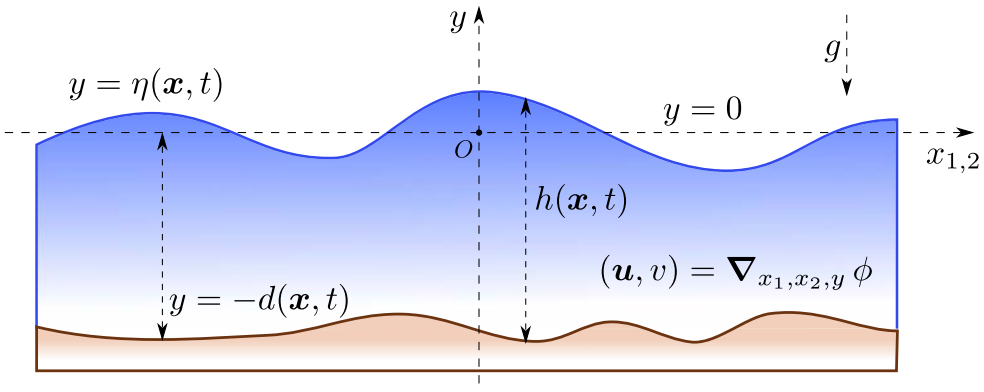

Figure 2.1 | Sketch of the fluid domain.

vertical variable y. Denoting with over 'tildes' and 'breves' are the quantities computed[2], respectively, at the free surface $y = \eta(\boldsymbol{x}, t)$ and at the bottom $y = -d(\boldsymbol{x}, t)$, the impermeabilities of these boundaries give the relations

$$\partial_t \eta + \tilde{\boldsymbol{u}} \cdot \boldsymbol{\nabla} \eta = \tilde{v}, \qquad \partial_t d + \breve{\boldsymbol{u}} \cdot \boldsymbol{\nabla} d = -\breve{v}. \tag{2.2}$$

Traditionally, in water wave modelling, the assumption of flow irrotationality is also adopted because it is relevant in many situations, and it brings considerable simplifications. The zero-curl velocity field condition can be written

$$\boldsymbol{\nabla} v = \partial_y \boldsymbol{u}, \qquad \boldsymbol{\nabla} \times \boldsymbol{u} = 0, \tag{2.3}$$

where $\times$ is a two-dimensional analogue of the cross[3] product. The irrotationality conditions (2.3) are satisfied identically, introducing a (scalar) velocity potential ϕ such that

$$\boldsymbol{u} = \boldsymbol{\nabla} \phi, \qquad v = \partial_y \phi. \tag{2.4}$$

For irrotational motions of incompressible fluids, the Euler momentum equations can be integrated into the scalar Lagrange–Cauchy equation

$$p + \partial_t \phi + g y + \tfrac{1}{2} |\boldsymbol{\nabla} \phi|^2 + \tfrac{1}{2} (\partial_y \phi)^2 = 0,$$

where p is the pressure divided by the density ρ and $g > 0$ is the acceleration due to gravity. At the free surface, the pressure can be set to zero without any loss of generality — *i.e.*, $\tilde{p} = 0$ — but surface

[2] For example $\tilde{\boldsymbol{u}} = \boldsymbol{u}(y = \eta)$, $\breve{v} = v(y = -d)$.
[3] For two two-dimensional vectors $\boldsymbol{a} = (a_1, a_2)$ and $\boldsymbol{b} = (b_1, b_2)$, $\boldsymbol{a} \times \boldsymbol{b} = a_1 b_2 - a_2 b_1$ is a scalar.

tension or other effects could be taken into account. Note that for steady flows, *i.e.* when the velocity field is independent of time, $\partial_t \phi = \text{constant} = -B$ and the Lagrange–Cauchy equation becomes the Bernoulli equation, B being a Bernoulli constant[4].

In summary, with the hypotheses stated above, the governing equations of the classical (non-overturning) surface water waves are [129, 212, 237]:

$$\boldsymbol{\nabla}^2 \phi + \partial_y^2 \phi = 0, \qquad -d(\boldsymbol{x}, t) < y < \eta(\boldsymbol{x}, t), \tag{2.5}$$

$$\partial_t \eta + (\boldsymbol{\nabla}\phi) \cdot (\boldsymbol{\nabla}\eta) - \partial_y \phi = 0, \qquad y = \eta(\boldsymbol{x}, t), \tag{2.6}$$

$$\partial_t \phi + \tfrac{1}{2}|\boldsymbol{\nabla}\phi|^2 + \tfrac{1}{2}(\partial_y \phi)^2 + g\eta = 0, \qquad y = \eta(\boldsymbol{x}, t), \tag{2.7}$$

$$\partial_t d + (\boldsymbol{\nabla} d) \cdot (\boldsymbol{\nabla}\phi) + \partial_y \phi = 0, \qquad y = -d(\boldsymbol{x}, t). \tag{2.8}$$

The assumptions of fluid incompressibility and flow irrotationality lead to the Laplace equation 2.5 for the velocity potential $\phi(\boldsymbol{x}, y, t)$. The main difficulty of the water wave problem is associated with the boundary conditions. Equations 2.6 and 2.8 express the free-surface kinematic condition and bottom impermeability, respectively, while the dynamic condition 2.7 expresses the free surface isobarity.

[4] We would like to mention that for unsteady flows, the 'constant' could actually be a function of time.

CHAPTER 3

Variational formulation

The water wave problem is known to encompass a multitude of variational structures as elucidated in seminal works [155, 236, 243]. These variational structures provide a robust framework for delving into the intricate dynamics of water waves, each offering a unique perspective and analytical tools for investigating the underlying physics. In the ensuing monograph, our discourse will be significantly channelled towards the exhaustive exploitation of the Lagrangian variational formalism. This particular formalism is revered for its profound ability to articulate the dynamics of water waves through a potent mathematical apparatus. Through a meticulous exploration of the Lagrangian formalism, we aim to contribute a nuanced understanding to the existing body of knowledge, thereby enriching the discourse on water wave dynamics and potentially unveiling novel facets or solutions pertinent to the problem at hand.

Equations 2.5–2.8 can be derived from the "stationary point" (the point where the variation is zero[5]) of the following functional

$$\mathcal{L} = \int_{t_1}^{t_2} \int_{\Omega} \mathscr{L}\, \rho \, \mathrm{d}^2\boldsymbol{x} \, \mathrm{d}t$$

(Ω the horizontal domain), where the Lagrangian density $\mathscr{L}$ is [155]:

$$\mathscr{L} = -\int_{-d}^{\eta} \left[g\, y + \partial_t \phi + \tfrac{1}{2} |\boldsymbol{\nabla}\phi|^2 + \tfrac{1}{2} (\partial_y \phi)^2 \right] \mathrm{d}y. \tag{3.1}$$

Upon examination, it becomes apparent that the Euler-Lagrange equations emanating from this particular functional lead directly to the water wave equations, thereby establishing a coherent mathematical bridge between the variational formalism and the governing equations of water wave dynamics. The derivation of these equations, though succinct in its nature, unveils a structured pathway connecting the variational principles to the fluid dynamics encapsulated in the water wave problem. A meticulous derivation of these equations is provided in the seminal work by Luke [155]. Furthermore, a more accessible exposition of this derivation is also available on Wikipedia[6],

[5] For a more precise definition of a stationary point we refer to classical books on variational methods in Mechanics such as [15, 147, 177, 202].

[6] http://en.wikipedia.org/wiki/Luke's_variational_principle.

providing a platform for a broader audience to grasp the underlying principles and the consequential Euler-Lagrange equations. The availability of these resources, ranging from scholarly articles to more publicly accessible platforms, facilitates a comprehensive understanding of the variational framework and its pivotal rôle in formulating the water wave equations.

If the fluid incompressibility and the bottom impermeability are satisfied identically, Luke's Lagrangian is reduced to a form leading directly to the Hamiltonian of Zakharov [243]. However, for many practical applications, it is advantageous *not* to fulfil a maximum of relations, as advocated in [52]. Note also that Luke's Lagrangian 3.1 can be extended to the case where the bottom function $d(\boldsymbol{x}, t)$ is unknown if a condition at $y = -d$ is added to the problem [220].

Integrating by parts and neglecting the terms at the horizontal and temporal boundaries because they do not contribute to the functional variations (this will be done repeatedly below without explicit mention), Luke's variational formulation 3.1 can be rewritten with the following Lagrangian density:

$$\mathscr{L} = \tilde{\phi}\,\eta_t + \breve{\phi}\,d_t - \frac{g\,\eta^2}{2} + \frac{g\,d^2}{2} - \int_{-d}^{\eta} \left[\frac{|\boldsymbol{\nabla}\phi|^2}{2} + \frac{\phi_y^2}{2} \right] \mathrm{d}y. \tag{3.2}$$

The alternative form 3.2 is somehow more convenient. Note that:

- the term $\tilde{\phi}\eta_t$, for example, can be replaced by $-\eta\tilde{\phi}_t$ after integration by parts;
- the term $g\,d^2/2$ can be omitted because d being prescribed, it does not contribute to the variational principle;
- the term $g\eta^2/2$ can be replaced by $g\,h^2/2$ via a change of definition of ϕ.

Luke's Lagrangian involves a velocity potential but not explicitly the velocity field. Thus, any approximation derived from 3.1 has an irrotational velocity field because the latter is calculated from the relations 2.4. The realm of water wave dynamics is characterized by a complex interplay of various equations, each encapsulating distinct physical phenomena pertinent to fluid motion and surface interactions. Within this intricate framework, there exists an array of conditions, namely irrotationality, incompressibility, and surface isobarity, each offering unique perspectives and constraints on the underlying fluid dynamics. The enforcement of irrotationality, in particular, is often seen as a conventional choice, however, there are, *a priori*, no foundational rationales dictating the exclusive enforcement of irrotationality over, say, incompressibility or surface isobarity or even a synthesis of these conditions. Each of these conditions delineates a unique facet of the fluid dynamics, and their enforcement or relaxation within the analytical framework can profoundly impact the nature and accuracy of

the resulting solutions to the water wave problem. For instance, the enforcement of incompressibility could shed light on the volume conservation aspects of fluid flow, while surface isobarity could provide insights into the pressure dynamics at the fluid-surface interface. As it is well known in numerical methods, enforcing an exact resolution of as many equations as possible is not always a good idea. Indeed, numerical analysis and scientific computing know many examples of when efficient and most-used algorithms do exactly the opposite. These so-called *relaxation methods* have proven to be very efficient for stiff problems. When solving numerically a system of equations, the exact resolution of a few equations does not necessarily ensure that the overall error is reduced. What really matters is that the global error is minimized. A similar idea of relaxation may also apply to analytical approximations, as advocated in [52].

In order to give us more freedom for building approximations, while keeping an exact formulation, the variational principle is modified (relaxed) by introducing explicitly the horizontal velocity $\boldsymbol{u} = \boldsymbol{\nabla}\phi$ and the vertical one $v = \phi_y$. The variational formulation can thus be reformulated with the Lagrangian density

$$\mathscr{L} = \tilde{\phi}\,\eta_t + \breve{\phi}\,d_t - \frac{g\,\eta^2}{2} - \int_{-d}^{\eta} \left[\frac{\boldsymbol{u}^2 + v^2}{2} + \boldsymbol{\mu}\cdot(\boldsymbol{\nabla}\phi - \boldsymbol{u}) + \nu(\phi_y - v) \right] \mathrm{d}y, \tag{3.3}$$

where the Lagrange multipliers $\boldsymbol{\mu}$ and ν have to be determined. By variations with respect of $\boldsymbol{u}$ and v, one finds at once the definition of the Lagrange multipliers:

$$\boldsymbol{\mu} = \boldsymbol{u}, \qquad \nu = v, \tag{3.4}$$

so $(\boldsymbol{\mu}, \nu)$ is another representation of the velocity field, in addition to $(\boldsymbol{u}, v)$ and $(\boldsymbol{\nabla}\phi, \phi_y)$. Using these definitions, 3.3 becomes

$$\mathscr{L} = \tilde{\phi}\,\eta_t + \breve{\phi}\,d_t - \tfrac{1}{2}\,g\,\eta^2 + \int_{-d}^{\eta} \left[\tfrac{1}{2}\,\boldsymbol{u}^2 + \tfrac{1}{2}\,v^2 - \boldsymbol{u}\cdot\boldsymbol{\nabla}\phi - v\,\phi_y \right] \mathrm{d}y. \tag{3.5}$$

The Lagrangian density 3.5 was used by Kim *et al.* [136] to derive the 'irrotational' Green–Naghdi equations for long waves in shallow water.

However, it is advantageous to keep the most general form of the Lagrangian. Indeed, it allows one to choose Ansätze for the Lagrange multipliers $\boldsymbol{\mu}$ and ν that can be different from the velocity field $\boldsymbol{u}$ and v. The Lagrangian density 3.3 involving six dependent variables $\{\eta, \phi, \boldsymbol{u}, v, \boldsymbol{\mu}, \nu\}$ — while the original Lagrangian 3.2 only two (η and ϕ) — it allows more and different subordinate relations to be fulfilled.

The connection of 3.3 with the variational formulation of the classical mechanics can be seen by applying Green's theorem to 3.3 that yields another equivalent variational formulation involving the Lagrangian density

$$\begin{aligned}\mathscr{L} = &\left(\partial_t \eta + \tilde{\boldsymbol{\mu}} \cdot \boldsymbol{\nabla}\eta - \tilde{\nu}\right)\tilde{\phi} + \left(\partial_t d + \breve{\boldsymbol{\mu}} \cdot \boldsymbol{\nabla} d + \breve{\nu}\right)\breve{\phi} - \tfrac{1}{2}\, g\, \eta^2 \\ &+ \int_{-d}^{\eta} \left[\, \boldsymbol{\mu} \cdot \boldsymbol{u} - \tfrac{1}{2}\boldsymbol{u}^2 \,+\, \nu v \,-\, \tfrac{1}{2} v^2 \,+\, \left(\boldsymbol{\nabla} \cdot \boldsymbol{\mu} + \partial_y \nu\right)\phi \,\right] \mathrm{d}y. \end{aligned} \tag{3.6}$$

We underline that the last Lagrangian is the most general (relaxed) form of Luke's variational principle, including two Lagrange multipliers $\boldsymbol{\mu}$ and ν. We remind also that $\tilde{\boldsymbol{\mu}}$, $\tilde{\nu}$, $\breve{\boldsymbol{\mu}}$ and $\breve{\nu}$ denote the traces of these Lagrange multipliers at the free surface and bottom, respectively. Perhaps other generalizations of Luke's variational principle are possible (see *e.g.* [61]). However, at the current stage, we are completely satisfied with 3.6.

If the relations 3.4 are used, the Lagrangian density 3.6 can be reduced to

$$\begin{aligned}\mathscr{L} = &\left(\partial_t \eta + \tilde{\boldsymbol{u}} \cdot \boldsymbol{\nabla}\eta - \tilde{v}\right)\tilde{\phi} + \left(\partial_t d + \breve{\boldsymbol{u}} \cdot \boldsymbol{\nabla} d + \breve{v}\right)\breve{\phi} - \tfrac{1}{2}\, g\, \eta^2 \\ &+ \int_{-d}^{\eta} \left[\, \tfrac{1}{2}\boldsymbol{u}^2 + \tfrac{1}{2} v^2 + \left(\boldsymbol{\nabla} \cdot \boldsymbol{u} + \partial_y v\right)\phi \,\right] \mathrm{d}y. \end{aligned} \tag{3.7}$$

Thus, the classical Hamilton principle is recovered, *i.e.*, the Lagrangian is the kinetic energy minus the potential energy plus constraints for the incompressibility and the boundary impermeabilities, as already pointed out by Miles [166]. In other words, the Lagrangian density 3.6 is the Hamilton principle in its most general form for irrotational surface gravity waves. Note finally that extensions of 3.3 and 3.6 including, *e.g.*, obstacles, surface tensions and stratifications in several homogeneous layers are straightforward generalizations. For instance, to include the surface tension, it is sufficient to add the term $-\sigma\left(\sqrt{1+(\boldsymbol{\nabla}\eta)^2}-1\right)$ into the definition of the Lagrangian density 3.6, the constant σ being the surface tension coefficient. The application of variational principles to capillary-gravity waves can be found in *e.g.* [55, 56, 103].

The Lagrangians 3.1, 3.2, 3.3, 3.6 and 3.7 yield the same exact relations. However, 3.3, 3.6 and 3.7 allow the constructions of approximations that are not exactly irrotational, that is not the case of Lagrangians 3.1 and 3.2. This advantage is illustrated below via some straightforward examples.

CHAPTER 4

Shallow water examples

If λ is a characteristic wavelength and h is an average water depth, the shallow water approximation consists of assuming that $h/\lambda \ll 1$ or, in other words, the water depth is much smaller compared to the typical wavelength. This regime is relevant in coastal engineering problems [156, 210, 238]. In the open ocean, only tsunami and tidal waves are in this regime [71, 133].

In this Section, we are going to derive various approximate water wave models in shallow waters. Some of these models are well-known[7] and some of them will be totally new.

4.1 | Serre equations: the first derivation

For surface waves propagating in shallow water, it is well known that the velocity fields vary little along the vertical. A reasonable Ansatz for the horizontal velocity is thus one such that u is independent of y, *i.e.*, and one can consider the approximation

$$u(x,y,t) \approx \bar{u}(x,t), \tag{4.1}$$

meaning that u is assumed to be close to its depth-averaged value.[8]

In order to introduce a suitable Ansatz for the vertical velocity, one can assume, for example, that the fluid incompressibility 2.1 and the bottom impermeability (2.2*b*) are fulfilled. These choices lead to the Ansatz

$$v(x,y,t) \approx -(y+d)\,\bar{u}_x. \tag{4.2}$$

Notice that, with this Ansatz, the velocity field is not exactly irrotational, *i.e.*

$$v_x - u_y \approx -(y+d)\,\bar{u}_{xx}.$$

[7] In this case, we just provide an alternative derivation procedure.
[8] $\bar{u} = \frac{1}{h}\int_{-d}^{\eta} u\,\mathrm{d}y$.

This does *not* mean that we are modelling a vortical motion but, instead, we are modelling a potential flow via a velocity field that is not exactly irrotational. This should not be more surprising than, *e.g.*, using an approximation such that the pressure at the free surface is not exactly zero.

With the Ansätze 4.1–4.2, the vertical acceleration (with $\mathrm{D}/\mathrm{D}t$ being the temporal derivative following the motion) is

$$\frac{\mathrm{D}\,v}{\mathrm{D}t} \;=\; \frac{\partial\, v}{\partial t} + u\,\frac{\partial\, v}{\partial x} + v\,\frac{\partial\, v}{\partial y} \;\approx\; -\,v\,\bar{u}_x - (y+d)\,\frac{\mathrm{D}\,\bar{u}_x}{\mathrm{D}t} = \gamma\,\frac{y+d}{h},$$

where γ is the vertical acceleration at the free surface:

$$\gamma \;\equiv\; \left.\frac{\mathrm{D}\,v}{\mathrm{D}t}\right|_{y=\eta} \;\approx\; h\,\left[\,\bar{u}_x^2 - \bar{u}_{xt} - \bar{u}\,\bar{u}_{xx}\,\right].$$

The kinetic energy per water column $\mathscr{K}$ is similarly easily derived[9]

$$\frac{\mathscr{K}}{\rho} = \int_{-d}^{\eta} \frac{u^2+v^2}{2}\,\mathrm{d}y \;\approx\; \frac{h\,\bar{u}^2}{2} + \frac{h^3\,\bar{u}_x^2}{6}.$$

The Hamilton principle 3.7 — *i.e.*, kinetic minus potential energies plus constraints for incompressibility and boundary impermeabilities — yields, for this Ansatz and after some elementary algebra, the Lagrangian density

$$\mathscr{L} = \tfrac{1}{2}\,h\,\bar{u}^2 + \tfrac{1}{6}\,h^3\,\bar{u}_x^2 - \tfrac{1}{2}\,g\,h^2 + \{\,h_t + [\,h\,\bar{u}\,]_x\,\}\,\tilde{\phi}\,.$$

The Euler–Lagrange equations for this functional are

$$\delta\tilde{\phi}: \quad 0 = h_t + [\,h\,\bar{u}\,]_x\,, \tag{4.3}$$

$$\delta\bar{u}: \quad 0 = \tilde{\phi}\,h_x - [\,h\,\tilde{\phi}\,]_x - \tfrac{1}{3}\,[\,h^3\,\bar{u}_x\,]_x + h\,\bar{u}, \tag{4.4}$$

$$\delta h: \quad 0 = \tfrac{1}{2}\,\bar{u}^2 - g\,h + \tfrac{1}{2}\,h^2\,\bar{u}_x^2 - \tilde{\phi}_t + \tilde{\phi}\,\bar{u}_x - [\,\bar{u}\,\tilde{\phi}\,]_x, \tag{4.5}$$

thence

$$\tilde{\phi}_x \;=\; \bar{u} - \tfrac{1}{3}\,h^{-1}\,[\,h^3\,\bar{u}_x\,]_x, \tag{4.6}$$

$$\tilde{\phi}_t \;=\; \tfrac{1}{2}\,h^2\,\bar{u}_x^2 - \tfrac{1}{2}\,\bar{u}^2 - g\,h + \tfrac{1}{3}\,\bar{u}\,h^{-1}\,[\,h^3\,\bar{u}_x\,]_x. \tag{4.7}$$

[9] This computation is straightforward and does not involve any approximations beyond the ones stated in the chosen Ansatz.

Differentiation of 4.7 with respect to x and differentiation of 4.6 with respect to t yield, after some algebra[10], the equation

$$\left[\, \bar{u} - \tfrac{1}{3}\, h^{-1}(h^3 \bar{u}_x)_x \,\right]_t + \left[\, \tfrac{1}{2}\, \bar{u}^2 + g\, h - \tfrac{1}{2}\, h^2\, \bar{u}_x^2 - \tfrac{1}{3}\, \bar{u}\, h^{-1}(h^3 \bar{u}_x)_x \,\right]_x = 0,$$

that can be rewritten in the non-conservative form

$$\bar{u}_t + \bar{u}\, \bar{u}_x + g\, h_x + \tfrac{1}{3}\, h^{-1}\, \partial_x \left[\, h^2 \gamma \,\right] = 0.$$

After multiplication by h and exploiting 4.3, we also derive the conservative equation

$$\left[\, h\, \bar{u} \,\right]_t + \left[\, h\, \bar{u}^2 + \tfrac{1}{2}\, g\, h^2 + \tfrac{1}{3}\, h^2 \gamma \,\right]_x = 0.$$

In summary, we have derived the system of equations

$$\begin{aligned} h_t + \partial_x \left[\, h\, \bar{u} \,\right] &= 0, \\ \partial_t \left[\, h\, \bar{u} \,\right] + \partial_x \left[\, h\, \bar{u}^2 + \tfrac{1}{2}\, g\, h^2 + \tfrac{1}{3}\, h^2 \gamma \,\right] &= 0, \\ h\, \bar{u}_x^2 - h\, \bar{u}_{xt} - h\, \bar{u}\, \bar{u}_{xx} &= \gamma, \end{aligned}$$

that are the Serre–Green–Naghdi equations (SGN). With the SGN equations, the irrotationality is not exactly satisfied, and thus, these equations cannot be derived from Luke's variational principle.

Assuming small derivatives (*i.e.*, long waves) but not small amplitudes, these equations were first derived by Serre [204] via a different route. They were independently rediscovered by Su and Gardner [215], and again by Green, Laws and Naghdi [114]. Another variational derivation based on the Lagrangian (fluid particle) formulation was given by Salmon [197]. These approximations are valid in shallow water without assuming small amplitude waves, and they are therefore sometimes called *weakly-dispersive fully-nonlinear approximation* [134, 239] and are a generalization of the

[10] The elimination of the variable $\tilde{\phi}$ aligns with expectations, given its designation as a Lagrange multiplier–a mathematical entity introduced to enforce certain constraints–rather than a variable fundamentally rooted in the physical essence of the problem at hand. This characteristic of $\tilde{\phi}$ is emblematic of the rôle of Lagrange multipliers, which serve as auxiliary constructs to ensure the satisfaction of specified conditions within the analytical framework yet do not carry intrinsic physical significance pertaining to the core dynamics of the problem. Their introduction facilitates a structured approach to navigating the constraints inherent in the system, allowing for a more disciplined exploration of the solution space. However, once these constraints are adequately addressed, the retention of such multipliers, including $\tilde{\phi}$, becomes superfluous, warranting their elimination from the ensuing analysis. This process of elimination, far from being arbitrary, underscores the transient utility of Lagrange multipliers in bridging the mathematical formulation with the physical constraints, while also delineating the boundary between auxiliary mathematical constructs and variables of core physical relevance.

Saint-Venant [212, 232] and of the Boussinesq equations. The variational derivation above is obvious and straightforward. Further details on the SGN equations concerning their properties and numerical resolutions can be easily found in the literature, *e.g.*, [87, 153, 216].

4.2 | Serre equations: the relaxed variational principle

For a long wave in shallow water, in potential motion on a horizontal impermeable sea bed at $y = -d$, it has long been noticed that the velocity field can be well approximated by truncating the following expansion[11] due to Lagrange [145]:

$$\boldsymbol{u} = \check{\boldsymbol{u}} - \tfrac{1}{2}(y+d)^2\,\boldsymbol{\nabla}^2\check{\boldsymbol{u}} + \tfrac{1}{24}(y+d)^4\,\boldsymbol{\nabla}^4\check{\boldsymbol{u}} + \cdots . \tag{4.8}$$

The methodological legacy of Lagrange, particularly his approach to expansion, found resonance among a myriad of subsequent scholars, including, but not limited to, notable figures such as Airy, Boussinesq, and Rayleigh. These scholars, inspired by Lagrange's pioneering work, embraced this genre of expansion as a potent tool in their analytical arsenal, employing it judiciously to derive their individual approximations tailored to address specific problems in the realm of fluid dynamics and wave theory. Each scholar, while drawing upon the foundational insights from Lagrange's expansion methodology, contributed their own nuanced understanding and refinements, thereby enriching the collective body of knowledge in the field. This tradition of methodological evolution, as chronicled in [65], not only pays homage to Lagrange's seminal contributions but also epitomizes the vibrant scholarly exchange and cumulative knowledge advancement emblematic of the scientific discourse in this domain.

We consider here a simple Ansatz of polynomial type, that is, a zeroth-order polynomial in y for ϕ and for $\boldsymbol{u}$, and a first-order one for v, *i.e.*, we approximate flows that are nearly uniform along the vertical direction. Our Ansatz thus reads

$$\phi \approx \bar{\phi}(\boldsymbol{x}, t), \qquad \boldsymbol{u} \approx \bar{\boldsymbol{u}}(\boldsymbol{x}, t), \qquad v \approx (y+d)\,(\eta+d)^{-1}\,\tilde{v}(\boldsymbol{x}, t). \tag{4.9}$$

Such Ansätze are the basis of most shallow water approximations. We have also to introduce suitable Ansätze for the Lagrange multiplier $\boldsymbol{\mu}$ and ν. Since $\boldsymbol{\mu} = \boldsymbol{u}$ and $\nu = v$ for the exact solution, a natural Ansatz for the multipliers is

$$\boldsymbol{\mu} \approx \bar{\boldsymbol{\mu}}(\boldsymbol{x}, t), \qquad \nu \approx (y+d)\,(\eta+d)^{-1}\,\tilde{\nu}(\boldsymbol{x}, t). \tag{4.10}$$

[11] We remind that in this expansion, the variable $\check{\boldsymbol{u}}$ denotes the trace of the horizontal velocity at the solid bottom.

With the Ansätze 4.9 and 4.10, the Lagrangian density 3.6 becomes

$$\mathscr{L} = (\eta_t + \bar{\boldsymbol{\mu}} \cdot \boldsymbol{\nabla}\eta)\,\bar{\phi} - \tfrac{1}{2}\,g\,\eta^2 \;+ (\eta + d)\left[\,\bar{\boldsymbol{\mu}} \cdot \bar{\boldsymbol{u}} - \tfrac{1}{2}\,\bar{\boldsymbol{u}}^2 + \tfrac{1}{3}\,\tilde{\nu}\,\tilde{v} - \tfrac{1}{6}\,\tilde{v}^2 \;+\; \bar{\phi}\,\boldsymbol{\nabla}\cdot\bar{\boldsymbol{\mu}}\,\right]. \tag{4.11}$$

Using the Green formula, the variational problem can also be written such that the Lagrangian density is in the following simpler form

$$\mathscr{L} = \bar{\phi}\,\eta_t - \tfrac{1}{2}\,g\eta^2 \;+\; (\eta + d)\left[\,\bar{\boldsymbol{\mu}} \cdot \bar{\boldsymbol{u}} \;-\; \tfrac{1}{2}\bar{\boldsymbol{u}}^2 \;+\; \tfrac{1}{3}\,\tilde{\nu}\tilde{v} \;-\; \tfrac{1}{6}\tilde{v}^2 - \bar{\boldsymbol{\mu}} \cdot \boldsymbol{\nabla}\bar{\phi}\,\right]. \tag{4.12}$$

The two Lagrangian densities 4.11 and 4.12 differing by a divergence term yield exactly the same equations. Thus, depending on the constraints, we use the Lagrangian density, leading to the simpler expression. We now investigate equations led by this shallow water model under various subordinate relations.

4.2.1 | Unconstrained approximation

Without further constraints, the Euler–Lagrange equations of 4.12 yield

$$\delta\,\bar{\boldsymbol{u}}: \qquad \mathbf{0} = \bar{\boldsymbol{\mu}} \;- \bar{\boldsymbol{u}}, \tag{4.13}$$

$$\delta\,\tilde{v}: \qquad 0 = \tilde{\nu} \;-\; \tilde{v}, \tag{4.14}$$

$$\delta\,\bar{\boldsymbol{\mu}}: \qquad \mathbf{0} = \bar{\boldsymbol{u}} \;- \boldsymbol{\nabla}\bar{\phi}, \tag{4.15}$$

$$\delta\,\tilde{\nu}: \qquad 0 = \tilde{v}, \tag{4.16}$$

$$\delta\,\bar{\phi}: \qquad 0 = \eta_t + \boldsymbol{\nabla}\cdot\left[\,(\eta + d)\,\bar{\boldsymbol{\mu}}\,\right], \tag{4.17}$$

$$\delta\,\eta: \qquad 0 = \bar{\boldsymbol{\mu}} \cdot \bar{\boldsymbol{u}} - \tfrac{1}{2}\,\bar{\boldsymbol{u}}^2 + \tfrac{1}{3}\,\tilde{\nu}\,\tilde{v} - \tfrac{1}{6}\,\tilde{v}^2 - \bar{\boldsymbol{\mu}} \cdot \boldsymbol{\nabla}\bar{\phi} - \bar{\phi}_t - g\,\eta. \tag{4.18}$$

The relations 4.13–4.16 imply that the motion is exactly irrotational, but the fluid incompressibility is not satisfied identically. With these four relations, the last two equations can be rewritten in the form:

$$h_t + \boldsymbol{\nabla}\cdot\left[\,h\,\bar{\boldsymbol{u}}\,\right] = 0, \tag{4.19}$$

$$\bar{\boldsymbol{u}}_t + \tfrac{1}{2}\,\boldsymbol{\nabla}\,|\bar{\boldsymbol{u}}|^2 + g\,\boldsymbol{\nabla}\,h = \mathbf{0}, \tag{4.20}$$

where $h = \eta + d$ is the total water depth. Equations 4.19–4.20 are the very well-known nonlinear shallow water equations, also known as Airy or Saint-Venant equations (Wehausen & Laitone [232, §28]). They are sometimes called *non-dispersive fully nonlinear approximation* because their classical

derivation assumes long waves without the extra hypothesis of small amplitudes. These equations have a canonical[12] Hamiltonian structure for the conjugate variables η and $\bar{\phi}$ with the Hamiltonian

$$\int_\Omega \left\{ \tfrac{1}{2}\, g\, \eta^2 + \tfrac{1}{2}\, (\eta + d) \left| \boldsymbol{\nabla} \bar{\phi} \right|^2 \right\} \mathrm{d}^2 \boldsymbol{x}.$$

The Saint-Venant equations do not admit smooth progressive wave solutions. They are nevertheless widely used because they can be solved locally analytically by the method of characteristics [212]. This analytical method translates into the celebrated Finite Volume method [13, 108] in the realm of numerical techniques.

4.2.2 | Constraining with free surface impermeability

We now constrain the Ansatz 4.9, 4.10, imposing that the impermeability of the free surface is satisfied identically. Since the surface impermeability is expressed through the velocity $(\boldsymbol{\mu}, \nu)$ in 3.6, we substitute

$$\tilde{\nu} = \eta_t + \bar{\boldsymbol{\mu}} \cdot \boldsymbol{\nabla} \eta, \tag{4.21}$$

into the Lagrangian density 4.11, and the subsequent Euler–Lagrange equations are

$$\delta\, \bar{\boldsymbol{u}} : \qquad \mathbf{0} = \bar{\boldsymbol{\mu}} \; - \bar{\boldsymbol{u}}, \tag{4.22}$$

$$\delta\, \tilde{v} : \qquad 0 = \eta_t + \bar{\boldsymbol{\mu}} \cdot \boldsymbol{\nabla} \eta \; - \; \tilde{v}, \tag{4.23}$$

$$\delta\, \bar{\boldsymbol{\mu}} : \qquad \mathbf{0} = \bar{\boldsymbol{u}} + \tfrac{1}{3}\, \tilde{v}\, \boldsymbol{\nabla} \eta - \boldsymbol{\nabla} \bar{\phi}, \tag{4.24}$$

$$\delta\, \bar{\phi} : \qquad 0 = \eta_t + \boldsymbol{\nabla} \cdot \left[(\eta + d)\, \bar{\boldsymbol{\mu}} \right], \tag{4.25}$$

$$\begin{aligned} \delta\, \eta : \qquad 0 = {} & \bar{\boldsymbol{\mu}} \cdot \bar{\boldsymbol{u}} - \tfrac{1}{2}\, \bar{\boldsymbol{u}}^2 - \tfrac{1}{6}\, \tilde{v}^2 - \bar{\boldsymbol{\mu}} \cdot \boldsymbol{\nabla} \bar{\phi} - \bar{\phi}_t - g\, \eta \\ & - \tfrac{1}{3}\, (\eta + d) \left[\tilde{v}_t + \bar{\boldsymbol{\mu}} \cdot \boldsymbol{\nabla} \tilde{v} + \tilde{v}\, \boldsymbol{\nabla} \cdot \bar{\boldsymbol{\mu}} \right]. \end{aligned} \tag{4.26}$$

The relations 4.22 and 4.24 link the velocity potential and the horizontal velocity as $\boldsymbol{\nabla} \bar{\phi} \neq \bar{\boldsymbol{u}} = \bar{\boldsymbol{\mu}}$ and, therefore, equations 4.22–4.26 cannot be derived from Luke's variational principle. Relations 4.22 and 4.25 provide the mass conservation, and hence, with 4.21, the approximation 4.22–4.26 implies that the fluid incompressibility is fulfilled identically.

[12] Along with a multitude of non-canonical Hamiltonian structures as well.

Eliminating $\bar{\phi}$, $\bar{\boldsymbol{\mu}}$ and $\tilde{v}$ from the horizontal gradient of 4.26, the system 4.22–4.26 becomes

$$h_t + \boldsymbol{\nabla}\cdot[\,h\,\bar{\boldsymbol{u}}\,] = 0, \tag{4.27}$$

$$\bar{\boldsymbol{u}}_t + \tfrac{1}{2}\,\boldsymbol{\nabla}|\bar{\boldsymbol{u}}|^2 + g\,\boldsymbol{\nabla}h + \tfrac{1}{3}\,h^{-1}\,\boldsymbol{\nabla}[\,h^2\,\tilde{\gamma}\,] = \tfrac{1}{3}\,(\bar{\boldsymbol{u}}\cdot\boldsymbol{\nabla}h)\,\boldsymbol{\nabla}(h\boldsymbol{\nabla}\cdot\bar{\boldsymbol{u}}) - \tfrac{1}{3}\,[\,\bar{\boldsymbol{u}}\cdot\boldsymbol{\nabla}(h\boldsymbol{\nabla}\cdot\bar{\boldsymbol{u}})\,]\,\boldsymbol{\nabla}h, \tag{4.28}$$

and where

$$\tilde{\gamma} = \tilde{v}_t + \bar{\boldsymbol{u}}\cdot\boldsymbol{\nabla}\tilde{v} = h\,\left\{(\boldsymbol{\nabla}\cdot\bar{\boldsymbol{u}})^2 - \boldsymbol{\nabla}\cdot\bar{\boldsymbol{u}}_t - \bar{\boldsymbol{u}}\cdot\boldsymbol{\nabla}\,[\,\boldsymbol{\nabla}\cdot\bar{\boldsymbol{u}}\,]\,\right\}, \tag{4.29}$$

is the fluid vertical acceleration at the free surface.

In the two-dimensional case (one horizontal dimension), the right-hand side of 4.28 vanishes, and the system 4.27, 4.28 reduces to the equations first derived by Serre [203], independently rediscovered by Su and Gardner [215] and again by Green, Laws and Naghdi [114]. It is sometimes called *weakly-dispersive fully-nonlinear approximation* [239]. These equations admit a travelling solitary wave solution propagating along the horizontal dimension

$$\eta = a\,\mathrm{sech}^2\,\tfrac{1}{2}\varkappa(x_1 - ct), \qquad c^2 = g\,(d+a), \qquad (\varkappa d)^2 = 3\,a\,(d+a)^{-1},$$

which is linearly stable [153]. Note that this solution does not impose any limitation on the wave amplitude, meaning that the Serre equations are physically inconsistent with the existence of the highest wave in the full Euler equations as it has been known since the brilliant argument by Stokes [214]. Note also that the Serre equations have a *non-canonical* Hamiltonian structure [153] along with the multi-symplectic structure [48].

In three dimensions, equations 4.27–4.28 were called by Kim *et al.* [136] 'irrotational' Green–Naghdi equations[13]. If the right-hand side of (4.28) is neglected, we recover the classical Green–Naghdi equations [115].

Remark 4.1. Craig and Grooves, as documented in [62], alongside a host of other scholars, have ventured into the derivation of various shallow water models, anchoring their efforts in a variational principle. Their approaches predominantly hinge on the introduction of small parameters to facilitate the derivation process. This is where our methodology diverges markedly. In our approach, we eschew

[13] See the original work [136] to see why this term was coined.

the incorporation of small parameters; instead, we channel our focus towards making well-founded assumptions regarding the vertical structure of the flow.

4.2.3 | Constraining with incompressibility and partial potential flow I

Here, we restrict the freedom by imposing that the velocity potential is related to the horizontal velocity as $\boldsymbol{u} = \boldsymbol{\nabla}\phi$, and that the fluid incompressibility $\boldsymbol{\nabla}\cdot\boldsymbol{u}+v_y = 0$ is fulfilled, together with the relations $\boldsymbol{\mu} = \boldsymbol{u}$ and $\nu = v$, *i.e.*, we take the subordinate conditions

$$\bar{\boldsymbol{\mu}} = \bar{\boldsymbol{u}}, \qquad \tilde{\nu} = \tilde{v}, \qquad \bar{\boldsymbol{u}} = \boldsymbol{\nabla}\bar{\phi}, \qquad \tilde{v} \;=\; -(\eta + d)\,\boldsymbol{\nabla}^2\bar{\phi}.$$

These constraints do not impose exact irrotationality because $v \neq \phi_y$. Undoubtedly, we aim to derive an approximation that resides intermediate to the Saint-Venant and Serre–Green–Naghdi equations (SGN) equations, potentially encapsulating aspects of both, thereby fostering a broader understanding of the fluid dynamics under investigation.

Thus, the Lagrangian density 4.12 becomes

$$\mathscr{L} = \bar{\phi}\,\eta_t - \tfrac{1}{2}\,g\,\eta^2 - \tfrac{1}{2}\,(\eta + d)\,\big(\boldsymbol{\nabla}\bar{\phi}\big)^2 + \tfrac{1}{6}\,(\eta + d)^3\,\big(\boldsymbol{\nabla}^2\bar{\phi}\big)^2, \tag{4.30}$$

and its Euler–Lagrange equations yield

$$\begin{aligned} \delta\,\bar{\phi}: \qquad & 0 = \eta_t + \boldsymbol{\nabla}\cdot\big[\,(\eta + d)\,\boldsymbol{\nabla}\bar{\phi}\,\big] + \tfrac{1}{3}\,\boldsymbol{\nabla}^2\big[\,(\eta + d)^3\,\big(\boldsymbol{\nabla}^2\bar{\phi}\big)\,\big], \\ \delta\,\eta: \qquad & 0 = \bar{\phi}_t + g\,\eta + \tfrac{1}{2}\,\big(\boldsymbol{\nabla}\bar{\phi}\big)^2 - \tfrac{1}{2}\,(\eta + d)^2\,\big(\boldsymbol{\nabla}^2\bar{\phi}\big)^2. \end{aligned}$$

It seems that these equations have never appeared before in the literature before our study [52]. They are a generalization of the so-called Kaup–Boussinesq (or canonical Boussinesq) equations [131, 144] and are thus referred to as the gKB equations. This can be seen by noticing that the gKB equations can be derived from the canonical Hamiltonian

$$\int_\Omega \Big\{\, \tfrac{1}{2}\,g\,\eta^2 + \tfrac{1}{2}\,(\eta + d)\,\big|\boldsymbol{\nabla}\bar{\phi}\,\big|^2 \;-\; \tfrac{1}{6}\,(\eta + d)^3\,\big(\boldsymbol{\nabla}^2\bar{\phi}\big)^2 \,\Big\}\,\mathrm{d}^2\boldsymbol{x}, \tag{4.31}$$

while the classical Kaup–Boussinesq equations (cKB) equations are obtained replacing $(\eta + d)^3$ by d^3 in 4.31 and restricting the resulting Hamiltonian to one horizontal dimension. Note that the Lagrangian 4.30 is cubic in η, meaning that it has (at most) one local minimum in η and not a global one.

The linearized gKB and cKB systems admit the special travelling wave solution

$$\eta = a\cos k(x_1 - ct), \qquad c^2 = g\,d\,(1 - \tfrac{1}{3}k^2d^2), \tag{4.32}$$

implying that these equations are linearly ill-conditioned ($c^2 < 0$ for $kd > \sqrt{3}$). Nevertheless, should the generalized Kaup–Boussinesq equations (gKB) equations exhibit integrability akin to that of the cKB equations, they may emerge as a somewhat intriguing model for investigating gravity waves in shallow water scenarios. The allure of integrability holds promise for facilitating a structured exploration of the complex wave dynamics inherent in shallow water environments. Despite this potential, it is important to note that a comprehensive study of these equations, to fully elucidate their applicability and the insights they might offer, remains an endeavor yet to be undertaken.

4.3 | Constraining with incompressibility and partial potential flow II

So far, all the approximations derived turned out to be such that $\boldsymbol{\mu} = \boldsymbol{u}$ and $\nu = v$. We propose here a novel approximation that does not satisfy one of these identities, and that is an interesting variant of the previous models.

We impose a partially potential flow such that $\boldsymbol{\mu} = \boldsymbol{\nabla}\phi$ and $\nu = \phi_y$, together with the incompressibility condition $\boldsymbol{\nabla}\cdot\boldsymbol{u} + v_y = 0$ and the condition $\boldsymbol{u} = \boldsymbol{\mu}$. Thus, substituting the constraints

$$\bar{\boldsymbol{\mu}} = \bar{\boldsymbol{u}} = \boldsymbol{\nabla}\bar{\phi}, \qquad \tilde{\nu} = 0, \qquad \tilde{v} = -(\eta + d)\,\boldsymbol{\nabla}^2\bar{\phi},$$

into the Lagrangian density 4.12 yields

$$\mathscr{L} = \bar{\phi}\,\eta_t - \tfrac{1}{2}\,g\,\eta^2 - \tfrac{1}{2}\,(\eta + d)\left(\boldsymbol{\nabla}\bar{\phi}\right)^2 - \tfrac{1}{6}\,(\eta + d)^3\left(\boldsymbol{\nabla}^2\bar{\phi}\right)^2 ,$$

and the corresponding Euler–Lagrange equations are

$$\delta\,\bar{\phi}: \qquad 0 = \eta_t + \boldsymbol{\nabla}\cdot\left[\,(\eta + d)\,\boldsymbol{\nabla}\bar{\phi}\,\right] - \tfrac{1}{3}\,\boldsymbol{\nabla}^2\left[\,(\eta + d)^3\left(\boldsymbol{\nabla}^2\bar{\phi}\right)\,\right], \tag{4.33}$$

$$\delta\,\eta: \qquad 0 = \bar{\phi}_t + g\,\eta + \tfrac{1}{2}\,\left(\boldsymbol{\nabla}\bar{\phi}\right)^2 + \tfrac{1}{2}\,(\eta + d)^2\left(\boldsymbol{\nabla}^2\bar{\phi}\right)^2 . \tag{4.34}$$

These equations can be derived from the canonical Hamiltonian

$$\int_\Omega \left\{ \tfrac{1}{2}\,g\,\eta^2 + \tfrac{1}{2}\,(\eta + d)\left|\boldsymbol{\nabla}\bar{\phi}\right|^2 + \tfrac{1}{6}\,(\eta + d)^3\left(\boldsymbol{\nabla}^2\bar{\phi}\right)^2 \right\} \mathrm{d}^2\boldsymbol{x}\,,$$

which is always positive (an interesting feature for modelling water waves). To the linear approximation, equations 4.33, 4.34 have the progressive wave solution

$$\eta = a\cos k\,(x_1 - ct), \qquad c^2 = g\,d\,(1 + \tfrac{1}{3}k^2d^2), \tag{4.35}$$

which is well-behaved (*i.e.*, c^2 is never negative). Comparisons with the gKB equations suggest to refer to equations 4.33–4.34 as regularized general Kaup–Boussinesq equations (rgKB).

However, the linear dispersion relation 4.35 approximates the dispersion relation of linear waves — *i.e.*, $c^2 = g \tanh(kd)/k$ — only to the order $\mathcal{O}(k^2)$, while the dispersion relation 4.32 to rgKB model is $\mathcal{O}(k^4)$. Therefore, the rgKB equations are not very interesting for modelling water waves, but these equations may be of interest in modelling other physical processes.

4.3.1 | Constraining with incompressibility and potential flow I

In the previous example, we have constructed an approximation such that $\boldsymbol{\mu} = \boldsymbol{u}$ but $\nu \neq v$. Now, we release the constraint $\boldsymbol{\mu} = \boldsymbol{u}$ and keep the other constraints. Thus, we impose

$$\bar{\boldsymbol{\mu}} = \boldsymbol{\nabla}\bar{\phi}, \qquad \tilde{\nu} = 0, \qquad \tilde{v} = -(\eta + d)\,\boldsymbol{\nabla}\cdot\bar{\boldsymbol{u}},$$

so that the pseudo velocity field $(\boldsymbol{\mu}, \nu)$ is irrotational while the velocity field $(\boldsymbol{u}, v)$ is incompressible. After some elementary algebra, the Lagrangian density becomes

$$\mathscr{L} = \bar{\phi}\, h_t - \tfrac{1}{2}\, g\, \eta^2 + h\, \bar{\boldsymbol{u}}\cdot\boldsymbol{\nabla}\bar{\phi} - \tfrac{1}{2}\, h\, \bar{\boldsymbol{u}}^2 - \tfrac{1}{6}\, h^3\, (\boldsymbol{\nabla}\cdot\bar{\boldsymbol{u}})^2 - h\, \big(\boldsymbol{\nabla}\bar{\phi}\big)^2\,,$$

The corresponding Euler–Lagrange equations read

$$\begin{aligned}
\delta\,\bar{\boldsymbol{u}}: \quad & \boldsymbol{0} = h\,\boldsymbol{\nabla}\bar{\phi} - h\,\bar{\boldsymbol{u}} + \tfrac{1}{3}\,\boldsymbol{\nabla}\left[\, h^3\,\boldsymbol{\nabla}\cdot\bar{\boldsymbol{u}}\,\right],\\
\delta\,\bar{\phi}: \quad & 0 = h_t - \boldsymbol{\nabla}\cdot\left[\, h\,\bar{\boldsymbol{u}}\,\right] + 2\,\boldsymbol{\nabla}\cdot\left[\, h\,\boldsymbol{\nabla}\bar{\phi}\,\right],\\
\delta\,\eta: \quad & 0 = \bar{\phi}_t + g\,\eta + \tfrac{1}{2}\,\bar{\boldsymbol{u}}^2 + \big(\boldsymbol{\nabla}\bar{\phi}\big)^2 - \bar{\boldsymbol{u}}\cdot\boldsymbol{\nabla}\bar{\phi} + \tfrac{1}{2}\,h^2\,(\boldsymbol{\nabla}\cdot\bar{\boldsymbol{u}})^2\,.
\end{aligned}$$

The linearization of this system of equations has a $(2\pi/k)$-periodic sinusoidal travelling wave solution with the dispersion relation

$$c^2 = gd\,(1 + \tfrac{2}{3}k^2d^2)\,(1 + \tfrac{1}{3}k^2d^2)^{-1} \;=\; gd\,(1 + \tfrac{1}{3}k^2d^2) + \mathcal{O}\,(k^4),$$

which, like the previous example, is not satisfactory for water waves. However, these equations may be of some Mathematical interest nevertheless.

4.3.2 | Constraining with incompressibility and potential flow II

We now assume that the pseudo velocity field $(\boldsymbol{\mu}, \nu)$ is divergence-free, while the velocity field $(\boldsymbol{u}, v)$ is irrotational, *i.e.*, we impose the constraints

$$\bar{\boldsymbol{u}} = \boldsymbol{\nabla}\bar{\phi}, \qquad \tilde{v} = 0, \qquad \tilde{\nu} = -(\eta + d)\,\boldsymbol{\nabla}\cdot\bar{\boldsymbol{\mu}}.$$

The Lagrangian density becomes

$$\mathscr{L} = \bar{\phi}\,\eta_t - \tfrac{1}{2}\,g\,\eta^2 \;-\; \tfrac{1}{2}\,(\eta + d)\,\big(\boldsymbol{\nabla}\bar{\phi}\big)^2\,,$$

which yields the Saint-Venant equations. Thus, these constraints do not bring anything new. It should be emphasized that this is the case for the special shallow water Ansatz we are considering here, but this is not necessarily the case for other Ansätze.

4.4 | Further possibilities

The constraints of sections 4.2.3 to 4.3.2 can be unified into a single formalism considering combinations. Indeed, the velocity field $(\boldsymbol{u}, v)$ being not more (nor less) physical than the pseudo-velocity field $(\boldsymbol{\mu}, \nu)$ and the potential velocity field $(\boldsymbol{\nabla}\phi, \phi_y)$, the constraints can be imposed by combinations of these three fields. For instance, we could impose irrotationality on the field

$$(c_1\boldsymbol{u} + c_2\boldsymbol{\mu} + (1-c_1-c_2)\boldsymbol{\nabla}\phi\,,\; c_1 v + c_2\nu + (1-c_1-c_2)\phi_y\,),$$

the fluid incompressibility for the field

$$(c_3\boldsymbol{u} + c_4\boldsymbol{\mu} + (1-c_3-c_4)\boldsymbol{\nabla}\phi\,,\; c_3 v + c_4\nu + (1-c_3-c_4)\phi_y\,),$$

and so on for any other constraint or field we may think of. The $\{\, c_n \,\} \subset \mathbb{R}$ are parameters at our disposal. We can choose them in a convenient way based on some mathematical and physical considerations. For example, imposing that the approximate equations derived must be linearly well-posed and/or have better dispersion relation properties.

In the examples above, only some kinematic constraints (irrotationality, incompressibility, impermeability) were used. We could have also considered dynamical constraints based on, *e.g.*, the Bernoulli equation, or other relevant dynamical equations.

The relaxed variational principle provided a common platform for deriving several shallow water equations from the same Ansatz in changing only the constraints. Besides the Ansatz, no further approximations were made, and the derivations required only some elementary algebra. Using more general Ansätze — *i.e.*, involving more free functions and parameters — one can introduce more constraints, if desired, and derives more accurate approximations.

4.5 | Modified Serre's equations

The Serre equations are named after François Serre, an engineer at École Nationale des Ponts et Chaussées, who derived this model for the first time in 1953 in his prominent paper entitled *"Contribution à l'étude des écoulements permanents et variables dans les canaux"* (see [203]). Later, these equations were independently rediscovered by Su and Gardner [215] and by Green, Laws and

Naghdi [114]. The extension of Serre equations for general uneven bathymetries was derived by Seabra-Santos *et al.* [201]. In the Soviet literature, these equations were known as the Zheleznyak–Pelinovsky model [249].

For the sake of simplicity, we consider here only one horizontal dimension, say x_1, and we set $x_1 = x$ and $u_1 = u$, for brevity. We also consider the special case $\mu = u$ and $\nu = v$ together with the constraint $\tilde{v} = \eta_t + \tilde{u}\eta_x$ (free surface's impermeability). The generalized shallow water Ansatz reads

$$\phi \approx \bar{\phi}(x,t), \qquad u \approx \bar{u}(x,t), \qquad v \approx \left[\frac{y+d}{\eta+d}\right]^{\lambda} \tilde{v}(x,t).$$

Thus, the Lagrangian density 3.6 yields

$$\mathscr{L} = (\eta_t + [(\eta+d)\bar{u}]_x)\,\tilde{\phi} - \tfrac{1}{2}g\eta^2 + \tfrac{1}{2}(\eta+d)\bar{u}^2 + \tfrac{1}{2}\beta^2(\eta+d)\,[\eta_t + \bar{u}\eta_x]^2\,, \tag{4.36}$$

where $\beta^2 = (2\lambda+1)^{-1}$.

After some algebra, the Euler–Lagrange equations are

$$h_t + [\,h\,\bar{u}\,]_x = 0, \tag{4.37}$$

$$\bar{u}_t + \bar{u}\,\bar{u}_x + g\,h_x + \beta^2\,h^{-1}\,[\,h^2\,\tilde{\gamma}\,]_x = 0, \tag{4.38}$$

where $\tilde{\gamma}$ is defined in 4.29. If $\beta = 1/\sqrt{3}$ the classical SGN equations are recovered.

Using equations 4.37 and 4.38 one can show that the following relations hold

$$[\,h\,\bar{u}\,]_t + \left[\,h\,\bar{u}^2 + \tfrac{1}{2}\,g\,h^2 + \beta\,h^2\,\tilde{\gamma}\,\right]_x = 0, \tag{4.39}$$

$$[\,\bar{u} - \beta\,h^{-1}(h^3\bar{u}_x)_x\,]_t + \left[\,\tfrac{1}{2}\,\bar{u}^2 + g\,h - \tfrac{1}{2}\,h^2\,\bar{u}_x^2 - \beta\,\bar{u}h^{-1}\,(h^3\bar{u}_x)_x\,\right]_x = 0, \tag{4.40}$$

$$[\,h\,\bar{u} - \beta\,(h^3\bar{u}_x)_x\,]_t + \left[\,h\,\bar{u}^2 + \tfrac{1}{2}\,g\,h^2 - 2\,\beta\,h^3\,\bar{u}_x^2 - \beta\,h^3\,\bar{u}\,\bar{u}_{xx} - h^2\,h_x\,\bar{u}\,\bar{u}_x\,\right]_x = 0, \tag{4.41}$$

$$\left[\,\tfrac{1}{2}\,h\,\bar{u}^2 + \tfrac{1}{2}\,\beta\,h^3\,\bar{u}_x^2 + \tfrac{1}{2}\,g\,h^2\,\right]_t + \left[\,\left(\tfrac{1}{2}\,\bar{u}^2 + \tfrac{1}{2}\,\beta\,h^2\,\bar{u}_x^2 + g\,h + \beta\,h\tilde{\gamma}\right)\,h\,\bar{u}\,\right]_x = 0. \tag{4.42}$$

Physically, these relations represent conservations of the momentum, quantity $\bar{q} = \bar{u} - \beta h^{-1}(h^3\bar{u}_x)_x$, its flux $\tilde{q} := h\bar{u} - \beta(h^3\bar{u}_x)_x$ and the total energy, respectively. Moreover, the Serre equations are invariant under the Galilean transformation. This property is naturally inherited from the full water wave problem since our Ansatz does not destroy this symmetry [20], and the derivation is made according to variational principles.

Remark 4.2. In some applications, such as coastal engineering, it is required to estimate the loading exerted by water waves onto vertical structures [59]. The pressure can be computed in the framework of the Serre equations as well. For the first time, these quantities were computed in the pioneering paper by Zheleznyak (1985) [248]. Here, for simplicity, we provide the expressions in two space dimensions, which were derived in [248]. The pressure distribution inside the fluid column is given by

$$\frac{\mathcal{P}(x,y,t)}{\rho g d} = \frac{\eta - y}{d} + \frac{1}{2}\left[\left(\frac{h}{d}\right)^2 - \left(1+\frac{y}{d}\right)^2\right]\frac{\tilde\gamma\, d}{g\, h},$$

one can compute the force $\mathcal{F}$ exerted on a vertical wall:

$$\frac{\mathcal{F}(x,t)}{\rho g d^2} = \int_{-d}^{\eta} \frac{\mathcal{P}}{\rho g d^2}\,\mathrm{d}y \;=\; \left(\frac{1}{2}+\frac{\tilde\gamma}{3\,g}\right)\left(\frac{h}{d}\right)^2.$$

Finally, the tilting moment $\mathcal{M}$ relative to the sea bed is given by the following formula:

$$\frac{\mathcal{M}(x,t)}{\rho g d^3} = \int_{-d}^{\eta} \frac{\mathcal{P}}{\rho g d^3}\,(y+d)\,\mathrm{d}y \;=\; \left(\frac{1}{6}+\frac{\tilde\gamma}{8\,g}\right)\left(\frac{h}{d}\right)^3.$$

Equations 4.37–4.38 admit a $(2\pi/k)$-periodic cnoidal travelling wave solution:

$$\bar u = \frac{c\,\eta}{d+\eta}, \qquad \eta = a\,\frac{\mathrm{dn}^2\left(\frac{1}{2}\varkappa\xi|m\right) - E/K}{1-E/K} = a \;-\; H\,\mathrm{sn}^2\left(\tfrac{1}{2}\varkappa\xi|m\right), \tag{4.43}$$

with $\xi := x - ct$, dn and sn being elliptic functions of Jacobi of parameter m ($0 \leqslant m \leqslant 1$), and where $K = \mathrm{K}(m)$ and $E = \mathrm{E}(m)$ are the complete elliptic integrals of the first and second kinds, respectively (see [1, Section §17.3]). The parameter $\varkappa$ plays the rôle of a wavenumber, a is the wave amplitude (mean level to crest elevation), H is the total wave height (trough to crest elevation), and c is the wave phase velocity observed in the frame of reference without mean flow. The wave parameters obey the relations

$$k = \frac{\pi\,\varkappa}{2\,K}, \qquad H = \frac{m\,a\,K}{K-E}, \qquad (\varkappa d)^2 = \frac{g\,H}{m\,\beta^2\,c^2}, \tag{4.44}$$

$$m = \frac{g\,H\,(d+a)\,(d+a-H)}{g\,(d+a)^2\,(d+a-H) - d^2\,c^2}. \tag{4.45}$$

In the limiting case $m \to 1$, we have $K \to \infty$, $E/K \to 0$, $k \to 0$, $H \to a$ and hence, a classical solitary wave solution is recovered

$$\eta = a\,\mathrm{sech}^2\tfrac{1}{2}\varkappa(x-ct), \qquad c^2 = g\,(d+a), \qquad \tfrac{a}{d} = \tfrac{(\beta\varkappa d)^2}{1-(\beta\varkappa d)^2}. \tag{4.46}$$

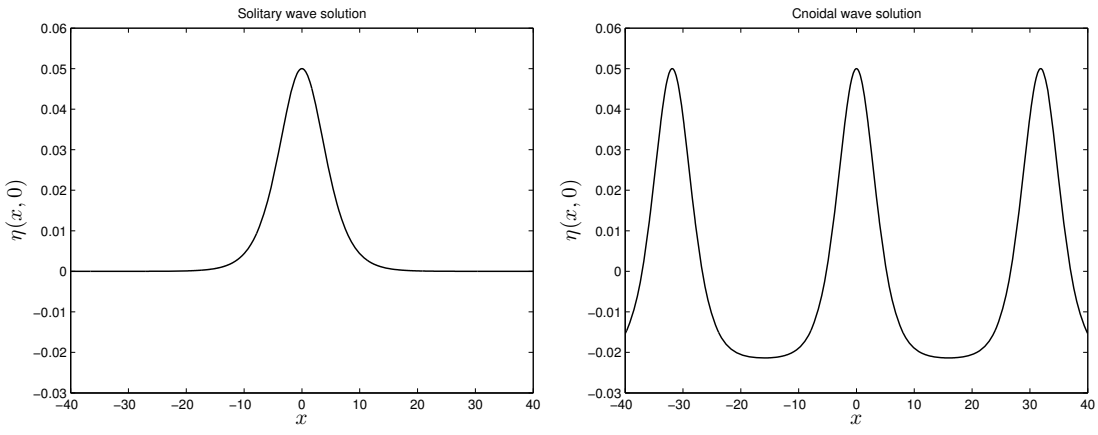

(a) Solitary wave (b) Cnoidal wave

Figure 4.1 | Two exact solutions to the Serre equations. The solitary wave amplitude is equal to $a/d = 0.05$. For the cnoidal wave parameters, m and a/d are equal to 0.99 and 0.05, respectively. Other cnoidal wave parameters can be deduced from relations 4.44, 4.45.

For illustrative purposes, a solitary wave along with a cnoidal wave of the same amplitude $a/d = 0.05$ are depicted in Figure 4.1.

Utilising the exact solitary wave solution delineated in equation 4.46, we are poised to assess the accuracy of the Serre equations (with $\beta = \frac{1}{3}$), through a comparative lens against the corresponding solutions to the original, potential full Euler equations[14]. The methodology that propels the construction of travelling wave solutions to the Euler equations is meticulously articulated in references [53, 84]. Further facilitating this exploration is a MATLAB script, dedicated to generating these profiles with a precision that approaches the machine limit. This script is readily accessible for download from the File Exchange server, as cited in [51], thereby providing an open avenue for rigorous computational examination.

As we unveil the outcomes of this comparative analysis for a spectrum of values attributed to the speed parameter c, encapsulated in Figure 4.2, a narrative of approximation accuracy begins to unfold. It is discernible that the solitary waves corresponding to the Serre equations exhibit a commendable approximation to the full Euler solutions, maintaining this fidelity up to an amplitude ratio

[14] Usually, we call this mathematical formulation to be the full water wave problem.

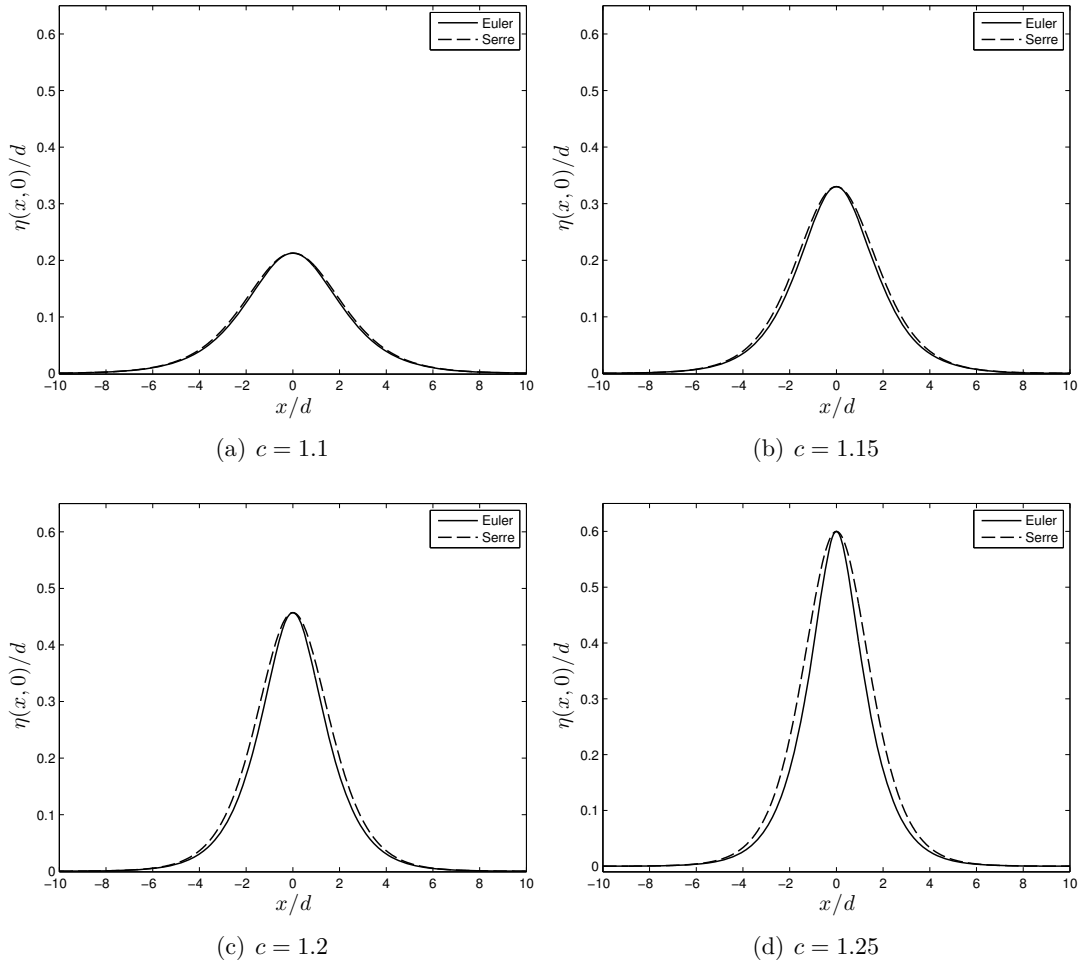

(a) $c = 1.1$ (b) $c = 1.15$

(c) $c = 1.2$ (d) $c = 1.25$

Figure 4.2 | Comparison of solitary wave solutions to the Serre and the full Euler equations.

of approximately $a/d \approx \frac{1}{2}$. This observed accuracy not only underscores the robustness of the Serre equations in encapsulating the dynamics of the Euler equations but also echoes a semblance of validation for the analytical frameworks employed.

It is noteworthy to mention that our findings resonate with the conclusions drawn in a prior investigative venture by Li *et al.* (2004) [154]. The harmony between these independent studies reinforces the narrative of approximation accuracy, thereby elevating the confidence in the utilisation of the Serre equations as a viable analytical tool for exploring the dynamics of solitary waves, especially in scenarios where the amplitude ratio hovers around or below the threshold of $a/d \lesssim \frac{1}{2}$. Through this

comparative analysis, we have not only benchmarked the accuracy of the Serre equations but also accentuated their potential as a reliable and efficacious conduit for delving into the complex realm of fluid dynamics governed by the Euler equations.

At this stage, β is still a free parameter. A suitable expression for this parameter may be obtained by substituting the solution 4.43 into the Lagrangian density 4.36, integrating $\mathscr{L}$ over one wavelength, then solving $\mathrm{d}\mathcal{L}/\mathrm{d}\beta = 0$ while keeping k and c constant (as well as g and d) and varying the other parameters according to relations 4.44–4.45. Thus, after some cumbersome algebra, we found $\beta = 0$ for this parameter, which is not very interesting for practical applications. A possible alternative here is to choose β such that the exact (for potential flow) relation $c^2 = g \tan(\varkappa d)/\varkappa$ is satisfied identically or up to some asymptotic order.

4.5.1 | Invariants of the Serre equations

Henceforth, until the end of this Section, we consider only the two-dimensional case. As pointed out by Li (2002) [153], the classical Serre equations possess a non-canonical Hamiltonian structure which can be easily generalized for the model 4.37, 4.38

$$\begin{pmatrix} h_t \\ \tilde{q}_t \end{pmatrix} = \mathbb{J} \cdot \begin{pmatrix} \delta\,\mathcal{H} / \delta\tilde{q} \\ \delta\,\mathcal{H} / \delta h \end{pmatrix},$$

where the Hamiltonian functional $\mathcal{H}$ and the symplectic operator $\mathbb{J}$ are defined as

$$\mathcal{H} = \tfrac{1}{2} \int_{\mathbb{R}} \left[h\,\bar{u}^2 + \beta\, h^3\, \bar{u}_x^2 + g\,\eta^2 \right] \mathrm{d}x, \qquad \mathbb{J} = -\begin{bmatrix} h_x & 0 \\ \tilde{q}_x + \tilde{q}\partial_x & h\partial_x \end{bmatrix}.$$

The variable $\bar{u}$ is related to $\tilde{q}$ as follows

$$\tilde{q} \;\equiv\; h\,\bar{u} - \beta\,[\,h^3\,\bar{u}_x\,]_x.$$

The conservation of the quantity $\tilde{q}$ was established in equation 4.41.

According to [153], one-parameter symmetry groups of Serre equations include the space translation $(x + \varepsilon, t, h, u)$, the time translation $(x, t + \varepsilon, h, u)$, the Galilean boost $(x + \varepsilon t, t, h, u + \varepsilon)$ and the scaling $\mathrm{e}^{\epsilon}(\mathrm{e}^{\epsilon} x, t, \mathrm{e}^{\epsilon} h, u)$. Using the first three symmetry groups and the symplectic operator $\mathbb{J}$, one may recover the following invariants:

$$\mathcal{Q} = \int_{\mathbb{R}} \frac{\eta\,\tilde{q}}{d + \eta}\,\mathrm{d}x, \qquad \mathcal{H}, \qquad \int_{\mathbb{R}} [\,t\,\tilde{q} - x\,\eta\,]\,\mathrm{d}x. \tag{4.47}$$

It is manifest that the equation 4.37 engenders an invariant that is intimately tethered to the mass conservation property[15], encapsulated by the integral expression $\int_{\mathbb{R}} \eta \, \mathrm{d}x$. The scaling symmetry, however, does not furnish any conserved quantity in relation to the symplectic operator $\mathbb{J}$. As we navigate further, our discourse will pivot on the utilisation of the total energy $\mathcal{H}$ and the generalized momentum $\mathcal{Q}$ conservation, employing these principles as pivotal instruments to rigorously evaluate the accuracy of the numerical schemes at our behest. These evaluations will not merely dwell in the abstract but will be juxtaposed against the exact analytical solution delineated in equation 4.46, thereby providing a grounded and comparative assessment of the fidelity and robustness of the numerical schemes in replicating the underlying dynamics of the SGN equations. Through this meticulous examination, we aim to forge a comprehensive understanding of the numerical schemes' performance, while concurrently illuminating the inherent conservation principles and their interplay with the accuracy and reliability of the numerical solutions generated.

4.5.2 | Multi-symplectic structure of the Serre equations

This section is devoted to a further study of the celebrated SGN model 4.37, 4.38 of fully nonlinear long water waves propagating in shallow water. For the sake of simplicity, we adopt the 'classical' value of the parameter $\beta = \frac{1}{\sqrt{3}}$. The Hamiltonian formulation for the SGN equations was revisited earlier. However, this structure is non-canonical and highly non-trivial, at least at first sight. Within this section, we elucidate a multi-symplectic structure pertaining to the same system of SGN equations, a structure whose initial unveiling in the scholarly domain was effectuated through the publication [48]. This exposition not only revisits the groundbreaking revelation from [48] but also ventures to delineate the nuanced intricacies and implications of this multi-symplectic structure in the context of the SGN equations. Through a meticulous examination, we aim to accentuate the profound analytical utility and the enriched understanding that this multi-symplectic framework bequeaths upon the SGN equations, thereby contributing to the broader comprehension and exploration of long wave dynamics in shallow waters.

The multi-symplectic structure generalizes the classical Hamiltonian formulations [15] to the case of PDEs such that the space and time variables are treated on the equal footing [33] (see also [149, Chapter 12]). The hint for deriving this multi-symplectic structure is given in Appendix C. The generalisation to a multi-symplectic structure from classical Hamiltonian formulations engenders a more holistic and nuanced analytical framework, especially conducive for the examination of PDEs.

[15] Indeed, this invariant should be rather termed as the mass perturbation conservation. However, we stick to the classical term even if it is not fully accurate.

By extending the Hamiltonian perspective to accommodate both space and time variables on an equal footing, this multi-symplectic vantage point fosters a more harmonised understanding and manipulation of the underlying dynamics encapsulated within the PDEs. This enriched framework consequently broadens the horizon for deriving conservation laws and invariant properties, thereby unveiling a more profound comprehension of the intricate interplay between spatial and temporal dimensions within the equations under scrutiny. Moreover, the multi-symplectic structure holds the promise of facilitating the derivation and analysis of numerical schemes that remain faithful to the conservation laws inherent in the continuous problem, thus significantly enhancing the accuracy and reliability of numerical solutions.

A system of PDEs in 1D is said to be multi-symplectic if it can written as a system of first-order equations of the form [33, 161]:

$$\mathbb{M} \cdot \boldsymbol{z}_t + \mathbb{K} \cdot \boldsymbol{z}_x = \boldsymbol{\nabla}_{\boldsymbol{z}} S(\boldsymbol{z}), \tag{4.48}$$

where a dot denotes the contracted (inner) product, $\boldsymbol{z} \in \mathbb{R}^n$ is a rank-one tensor (vector) of state variables, $\mathbb{M} \in \mathbb{R}^{n\times n}$ and $\mathbb{K} \in \mathbb{R}^{n\times n}$ are skew-symmetric constant rank-two tensors (matrices) and S is a smooth rank-zero tensor (scalar) function depending on $\boldsymbol{z}$. (We use tensor notations because they give more compact formulae than the matrix formalism [27].) The function S plays the rôle of the Hamiltonian functional in classical symplectic formulations [15]. Consequently, S is sometimes called the '*Hamiltonian*' function as well. It should be noted that the matrices $\mathbb{M}$ and $\mathbb{K}$ can be (and often are) degenerated [38].

It turns out that the SGN equations 4.37–4.38 have a multi-symplectic structure with $\boldsymbol{z} = h\,\boldsymbol{e}_1 + \phi\,\boldsymbol{e}_2 + u\,\boldsymbol{e}_3 + v\,\boldsymbol{e}_4 + p\,\boldsymbol{e}_5 + q\,\boldsymbol{e}_6 + r\,\boldsymbol{e}_7 + s\,\boldsymbol{e}_8$ ($\boldsymbol{e}_i$ unitary basis vectors) and

$$\mathbb{M} = \boldsymbol{e}_1 \otimes \boldsymbol{e}_2 - \boldsymbol{e}_2 \otimes \boldsymbol{e}_1 + \tfrac{1}{3}\,\boldsymbol{e}_1 \otimes \boldsymbol{e}_5 - \tfrac{1}{3}\,\boldsymbol{e}_5 \otimes \boldsymbol{e}_1, \tag{4.49}$$

$$\mathbb{K} = \tfrac{1}{3}\,\boldsymbol{e}_1 \otimes \boldsymbol{e}_7 - \tfrac{1}{3}\,\boldsymbol{e}_7 \otimes \boldsymbol{e}_1 - \boldsymbol{e}_2 \otimes \boldsymbol{e}_6 + \boldsymbol{e}_6 \otimes \boldsymbol{e}_2, \tag{4.50}$$

$$S = \left(\tfrac{1}{6}\,v^2 - \tfrac{1}{2}\,u^2 - \tfrac{1}{3}\,s\,u\,v\right) h - \tfrac{1}{2}\,g\,h^2 + \tfrac{1}{3}\,p\,(u\,s - v) + q\left(u + \tfrac{1}{3}\,s\,v\right) - \tfrac{1}{3}\,r\,s, \tag{4.51}$$

where $\otimes$ denotes the tensor product. Indeed, the substitution of these relations into 4.48 yields the equations[16]

$$\phi_t + \tfrac{1}{3}\,p_t + \tfrac{1}{3}\,r_x = \tfrac{1}{6}\,v^2 - \tfrac{1}{2}\,u^2 - \tfrac{1}{3}\,s\,u\,v - g\,h, \tag{4.52}$$

$$-h_t - q_x = 0, \tag{4.53}$$

[16] The variables p, q, r, and s are defined right after the system.

$$0 = q - h\,u + \tfrac{1}{3} s\,(\,p - h\,v\,)\,, \tag{4.54}$$

$$0 = \tfrac{1}{3}\,(\,h\,v - p\,) \;+\; \tfrac{1}{3}\,s\,(\,q - h\,u\,)\,, \tag{4.55}$$

$$-\tfrac{1}{3}\,h_t = \tfrac{1}{3}\,(\,s\,u - v\,)\,, \tag{4.56}$$

$$\phi_x = u + \tfrac{1}{3}\,s\,v, \tag{4.57}$$

$$-\tfrac{1}{3}\,h_x = -\tfrac{1}{3}\,s, \tag{4.58}$$

$$0 = \tfrac{1}{3}\,(\,p\,u + q\,v - r - h\,u\,v\,)\,. \tag{4.59}$$

These equations have the following physical meaning. Equation 4.58 gives $s = h_x$, so s is the surface slope. Equations 4.54 and 4.55 yield $p = hv$ and $q = hu$, which are the vertical and horizontal momenta, respectively. It follows that 4.53 is the mass conservation $h_t + [hu]_x = 0$ and 4.56 is the impermeability of the free surface $h_t + uh_x = v$ (v is then the vertical velocity at the free surface). Equation 4.57 shows that the velocity field is not exactly irrotational for the SGN equations (a well-known result). The definition above of p and q substituted into 4.59 gives $r = huv$. Finally, substituting all the preceding results into 4.52, after some algebra, one obtains

$$\phi_t + \tfrac{1}{2}\,u^2 + \tfrac{1}{6}\,h^2\,u_x^2 + g\,h - \tfrac{1}{3}\,h^2\,u_{xt} - \tfrac{1}{3}\,h\,u\,\partial_x\,[\,h\,u_x\,] \;=\; 0.$$

Differentiating this equation with respect to x, eliminating ϕ using 4.57 and exploiting the mass conservation, one gets equation 4.40.

It should be noted that after eliminating p, q and r, the '*Hamiltonian*' S becomes

$$S = \tfrac{1}{2}\,h\,u^2 - \tfrac{1}{6}\,h\,v^2 - \tfrac{1}{2}\,g\,h^2 = \tfrac{1}{2}\,h\,u^2 - \tfrac{1}{6}\,h^3\,u_x^2 \;-\; \tfrac{1}{2}\,g\,h^2,$$

so S is neither a density of total energy nor a Lagrangian density.

Conservation laws

A multi-symplectic system of partial differential equations has local conservation laws for the energy and momentum [37, 38]

$$\partial_t E(\boldsymbol{z}) + \partial_x F(\boldsymbol{z}) = 0, \qquad \partial_t I(\boldsymbol{z}) + \partial_x G(\boldsymbol{z}) = 0,$$

where

$$E(\boldsymbol{z}) = S(\boldsymbol{z}) + \tfrac{1}{2}\,\boldsymbol{z}_x \cdot \mathbb{K} \cdot \boldsymbol{z}, \qquad F(\boldsymbol{z}) = -\tfrac{1}{2}\,\boldsymbol{z}_t \cdot \mathbb{K} \cdot \boldsymbol{z},$$
$$G(\boldsymbol{z}) = S(\boldsymbol{z}) + \tfrac{1}{2}\,\boldsymbol{z}_t \cdot \mathbb{M} \cdot \boldsymbol{z}, \qquad I(\boldsymbol{z}) = -\tfrac{1}{2}\,\boldsymbol{z}_x \cdot \mathbb{M} \cdot \boldsymbol{z}.$$

For the SGN equations, from the results given above (*cf.* 4.50–4.51), we thus find

$$
\begin{aligned}
E &= \tfrac{1}{6}\, r\, h_x - \tfrac{1}{6}\, h\, r_x + \tfrac{1}{2}\, \phi\, q_x - \tfrac{1}{2}\, q\, \phi_x - \tfrac{1}{2}\, g\, h^2 + \tfrac{1}{2}\, h\, u^2 - \tfrac{1}{6}\, h\, v^2, \\
F &= \tfrac{1}{6}\, h\, r_t - \tfrac{1}{6}\, r\, h_t + \tfrac{1}{2}\, q\, \phi_t - \tfrac{1}{2}\, \phi\, q_t, \\
G &= \tfrac{1}{6}\, p\, h_t - \tfrac{1}{6}\, h\, p_t + \tfrac{1}{2}\, \phi\, h_t - \tfrac{1}{2}\, h\, \phi_t - \tfrac{1}{2}\, g\, h^2 + \tfrac{1}{2}\, h\, u^2 - \tfrac{1}{6}\, h\, v^2, \\
I &= \tfrac{1}{6}\, h\, p_x - \tfrac{1}{6}\, p\, h_x + \tfrac{1}{2}\, h\, \phi_x - \tfrac{1}{2}\, \phi\, h_x.
\end{aligned}
$$

Furthemore, after using the relations 4.52–4.59 and some algebra, one gets the expression of quantities E, F, G and I in terms of initial physical variables

$$
\begin{aligned}
-E &= \tfrac{1}{2}\, h\, u^2 + \tfrac{1}{2}\, g\, h^2 + \tfrac{1}{6}\, h^2\, u_x^2 - \partial_x \left[\tfrac{1}{2}\, \phi\, h\, u + \tfrac{1}{6}\, h^3\, u\, u_x \right], \\
-F &= \left(\tfrac{1}{2}\, u^2 + \tfrac{1}{6}\, h^2\, u_x^2 + g\, h + \tfrac{1}{3}\, h \gamma \right) h\, u + \partial_t \left[\tfrac{1}{2}\, \phi\, h\, u + \tfrac{1}{6}\, h^3\, u\, u_x \right], \\
G &= h\, u^2 + \tfrac{1}{2}\, g\, h^2 + \tfrac{1}{3}\, h^2\, \gamma + \partial_t \left[\tfrac{1}{2}\, \phi\, h + \tfrac{1}{6}\, h^3\, u_x \right], \\
I &= h\, u - \partial_x \left[\tfrac{1}{2}\, \phi\, h + \tfrac{1}{6}\, h^3\, u_x \right].
\end{aligned}
$$

So the momentum and energy conservation equations 4.39 and 4.42 are recovered, though $-E$, $-F$, G and I are not exactly the densities of energy, energy flux, momentum flux and impulse, respectively.

Intermediate conclusions

In the discourse of this section, we have delved into the multi-symplectic structure pertinent to the SGN equations, which have garnered substantial acclaim in recent times as a robust model for long waves navigating shallow water terrains. Our understanding underscores the publication [48] as a seminal piece, heralding the initial unveiling of such a structure within the academic literature, thereby contributing a novel lens through which to interpret the SGN equations. While a non-canonical Hamiltonian structure of the SGN equations has been previously delineated, for instance in [128], our exploration has led us to discern that the corresponding multi-symplectic structure emanates as a more intuitive and streamlined framework for these equations. A salient feature of this multi-symplectic structure is its egalitarian treatment of both spatial and temporal variables, as elucidated in [161], thereby furnishing a balanced analytical perspective. The merits of such a formulation are well-documented and recognized, with references such as [33] shedding light on its advantageous disposition. This multi-symplectic formulation, hence, not only augments the analytical rigour but also enhances the intuitive understanding of the dynamics encapsulated within the SGN equations, thereby fostering a more comprehensive and nuanced exploration of long waves in shallow waters.

The elucidation of the multi-symplectic structure in the exact water wave equations, as showcased in [33], naturally engenders the conjecture that such a structure might extend to approximate equations as well, a notion echoed in [79]. However, the terrain becomes nuanced with the SGN equations, which do not embody exact irrotationality, thereby casting a veil of uncertainty on an *a priori* basis, over the existence of such a multi-symplectic structure within them. The quest to unearth this structure directly from the SGN equations, as enumerated in equations 4.37–4.38, transcends a mere trivial endeavour, presenting a complex analytical challenge.

In light of this, our investigative journey commenced with the relaxed variational principle, an exemplification of the generalized Hamilton principle, as expounded in [52]. This choice of starting point proved propitious, rendering the derivation of the multi-symplectic formulation of the SGN equations considerably lucid, as substantiated in appendix C. This route not only illuminated the coveted multi-symplectic structure but also underscored the nuanced interplay between irrotationality and the symplectic characteristics of the SGN equations. The transparent derivation ensuing from the relaxed variational principle accentuates the profound utility and the insightful lens it provides in navigating the complex mathematical landscape of the SGN equations, thereby contributing significantly to the understanding and analytical treatment of long waves in shallow waters.

The SGN equations can be extended to 3D in several ways. One extension of special interest concerns the so-called *irrotational Green–Naghdi equations* [52, 136] for which a multi-symplectic structure can be obtained following the same route as for the SGN equations, *i.e.*, starting from the relaxed variational principle.

This form of structure revelation unveils fresh avenues for the fabrication of structure-preserving integrators pertaining to the SGN equations. To our current understanding, this realm of inquiry remains largely unexplored in contemporary times. There have been endeavours to resolve SGN equations employing a variety of methodological approaches, including conventional finite volume techniques [45], pseudo-spectral methods [87], and finite element methods [171], each with its unique set of merits and considerations.

However, it is noteworthy that these attempts do not invariably ensure the preservation of the variational structures, be they symplectic or multi-symplectic, at the discrete level as well. The quintessence of preserving these structures transcends a mere mathematical formality, venturing into the realm of ensuring a faithful representation of the underlying physics even in a discretised computational framework. The discourse presented in this manuscript sheds light on pivotal findings that could significantly ease the application of finite difference [9, 37, 174, 231] and pseudo-spectral

[47, 111] variational schemes. These schemes are lauded for their capability to preserve, with exactitude, the multi-symplectic conservation law even at the discrete echelon. This preservation is instrumental in engendering numerical solutions that are not only accurate but also imbued with the essential physical attributes inherent in continuous equations.

A meticulous numerical comparison has been orchestrated, juxtaposing symplectic, multi-symplectic, and pseudo-spectral schemes, as articulated in [80, 82]. This comparison, pivoted on the renowned KdV equation, unveils the nuanced performance and the fidelity of these schemes in capturing the essence of the continuous problem in a discrete setting. The insights gleaned from this comparison, in tandem with the findings elucidated in this manuscript, offer a promising pathway towards not only constructing but also discerning the efficacy of variational schemes that hold the promise of preserving the essential symplectic and multi-symplectic structures. This, in turn, augments the robustness and reliability of numerical solutions, thereby fostering a more informed and accurate exploration of the complex dynamics inherent in the SGN equations.

4.6 | Numerical applications

In this Section, we shall consider the classical SGN equations corresponding to the choice of $\beta = \frac{1}{\sqrt{3}}$. A variety of numerical methods have been applied to discretize dispersive wave models and, more specifically, the Serre equations [87]. A pseudo-spectral method was applied in [73], an implicit finite difference scheme in [14, 169] and a compact higher-order scheme in [49, 50]. Some Galerkin and Finite Element type methods have been successfully applied to Boussinesq-type equations [6, 10, 75, 91, 170–172]. A finite difference discretization based on an integral formulation was proposed by Bona and Chen [25]. Recently, efficient high-order explicit or implicit-explicit finite difference [46] and finite volume schemes for dispersive wave equations have been developed [45, 93, 93]. The robustness of the proposed numerical schemes also allowed simulation of the run-up of long waves on a beach with high accuracy [93].

4.6.1 | Finite volume scheme and numerical results

In the present study, we propose a finite-volume discretization procedure [12, 13] for the Serre equations 4.37, 4.38, which we rewrite here as

$$h_t + [\, h\, u\,]_x = 0, \tag{4.60}$$

$$u_t + \left[\, \tfrac{1}{2}\, u^2 \,+\, g\, h\,\right]_x = \beta\, h^{-1}\, \left[\, h^3\, (u_{xt} \,+\, u\, u_{xx} \,-\, u_x^2)\,\right]_x, \tag{4.61}$$

where the over-bars have been omitted for brevity. (In this section, over-bars denote quantities averaged over a cell, as explained below.)

We begin our presentation with a discretization of the hyperbolic part of the equations (which are simply the classical (Airy–)Saint-Venant equations) and subsequently discuss the treatment of dispersive terms. The Serre equations can be formally put into the quasi-linear form

$$\boldsymbol{V}_t + [\,\boldsymbol{F}(\boldsymbol{V})\,]_x = \boldsymbol{S}(\boldsymbol{V}), \tag{4.62}$$

where $\boldsymbol{V}$, $\boldsymbol{F}(\boldsymbol{V})$ are the conservative variables and the advective flux function, respectively

$$\boldsymbol{V} \equiv \begin{pmatrix} h \\ u \end{pmatrix}, \quad \boldsymbol{F}(\boldsymbol{V}) \equiv \begin{pmatrix} h\,u \\ \frac{1}{2}\,u^2 + g\,h \end{pmatrix}.$$

The source term $\boldsymbol{S}(\boldsymbol{V})$ denotes the right-hand side of 4.60, 4.61 and thus, depends also on space and time derivatives of $\boldsymbol{V}$. The Jacobian of the advective flux $\boldsymbol{F}(\boldsymbol{V})$ can be straightforwardly computed

$$\mathbb{A}(\boldsymbol{V}) = \frac{\partial \boldsymbol{F}(\boldsymbol{V})}{\partial \boldsymbol{V}} = \begin{bmatrix} u & h \\ g & u \end{bmatrix}.$$

The Jacobian $\mathbb{A}(\boldsymbol{V})$ has two distinctive eigenvalues

$$\lambda^{\pm} = u \pm c_s, \qquad c_s \equiv \sqrt{g\,h}.$$

The corresponding right and left eigenvectors are provided here

$$\mathbb{R} = \begin{bmatrix} h & -h \\ c_s & c_s \end{bmatrix}, \qquad \mathbb{L} = \mathbb{R}^{-1} = \frac{1}{2}\begin{bmatrix} h^{-1} & c_s^{-1} \\ -h^{-1} & c_s^{-1} \end{bmatrix}.$$

We consider a partition of the real line $\mathbb{R}$ into cells (or finite volumes) $\mathcal{C}_i = [x_{i-\frac{1}{2}}, {}_{i+\frac{1}{2}}]$ with cell centers $x_i = \frac{1}{2}(x_{i-\frac{1}{2}} + x_{i+\frac{1}{2}})$ $(i \in \mathbb{Z})$. Let Δx_i denote the length of the cell $\mathcal{C}_i$. In the sequel, we will consider only uniform partitions with $\Delta x_i = \Delta x, \forall i \in \mathbb{Z}$. We would like to approximate the solution $\boldsymbol{V}(x,t)$ by discrete values. In order to do so, we introduce the cell average of $\boldsymbol{V}$ on the cell $\mathcal{C}_i$ (denoted with an over-bar), *i.e.*,

$$\bar{\boldsymbol{V}}_i(t) \equiv \big(\,\bar{h}_i(t)\,,\,\bar{u}_i(t)\,\big) = \frac{1}{\Delta x}\int_{\mathcal{C}_i} \boldsymbol{V}(x,t)\,\mathrm{d}x.$$

A simple integration of 4.62 over the cell $\mathcal{C}_i$ leads the following exact relation:

$$\frac{\mathrm{d}\bar{\boldsymbol{V}}}{\mathrm{d}t} + \frac{1}{\Delta x}\Big[\,\boldsymbol{F}(\boldsymbol{V}(x_{i+\frac{1}{2}},t)) - \boldsymbol{F}(\boldsymbol{V}(x_{i-\frac{1}{2}},t))\Big] = \frac{1}{\Delta x}\int_{\mathcal{C}_i} \boldsymbol{S}(\boldsymbol{V})\,\mathrm{d}x \equiv \bar{\boldsymbol{S}}_i.$$

Since the discrete solution is discontinuous at cell interfaces $x_{i+\frac{1}{2}}$ ($i \in \mathbb{Z}$), we replace the flux at the cell faces with the so-called numerical flux function

$$\boldsymbol{F}(\boldsymbol{V}(x_{i\pm\frac{1}{2}}, t)) \approx \mathcal{F}_{i\pm\frac{1}{2}}(\bar{\boldsymbol{V}}^{L}_{i\pm\frac{1}{2}}, \bar{\boldsymbol{V}}^{R}_{i\pm\frac{1}{2}}),$$

where $\bar{\boldsymbol{V}}^{L,R}_{i\pm\frac{1}{2}}$ denotes the reconstructions of the conservative variables $\bar{\boldsymbol{V}}$ from the left and right sides of each cell interface (the reconstruction procedure employed in the present study will be described below). Consequently, the semi-discrete scheme takes the form

$$\frac{\mathrm{d}\bar{\boldsymbol{V}}_i}{\mathrm{d}t} + \frac{1}{\Delta x}\left[\mathcal{F}_{i+\frac{1}{2}} - \mathcal{F}_{i-\frac{1}{2}}\right] = \bar{\boldsymbol{S}}_i. \tag{4.63}$$

In order to discretize the advective flux $\boldsymbol{F}(\boldsymbol{V})$, we use the FVCF scheme[17] [105, 106]:

$$\mathcal{F}(\boldsymbol{V}, \boldsymbol{W}) = \frac{\boldsymbol{F}(\boldsymbol{V}) + \boldsymbol{F}(\boldsymbol{W})}{2} - \mathbb{U}(\boldsymbol{V}, \boldsymbol{W}) \cdot \frac{\boldsymbol{F}(\boldsymbol{W}) - \boldsymbol{F}(\boldsymbol{V})}{2}.$$

The first part of the numerical flux is centred, and the second part is the upwinding introduced through the Jacobian sign-matrix $\mathbb{U}(\boldsymbol{V}, \boldsymbol{W})$ defined as

$$\mathbb{U}(\boldsymbol{V}, \boldsymbol{W}) = \mathrm{sign}\left[\mathbb{A}\left(\tfrac{1}{2}(\boldsymbol{V} + \boldsymbol{W})\right)\right], \qquad \mathrm{sign}(\mathbb{A}) = \mathbb{R} \cdot \mathrm{diag}(s^{+}s^{-}) \cdot \mathbb{L},$$

where $s^{\pm} \equiv \mathrm{sign}(\lambda^{\pm})$. After some simple algebraic computations, one can find

$$\mathbb{U} = \frac{1}{2}\begin{bmatrix} s^{+} + s^{-} & (h/c_s)\,(s^{+} - s^{-}) \\ (g/c_s)\,(s^{+} - s^{-}) & s^{+} + s^{-} \end{bmatrix},$$

the sign-matrix $\mathbb{U}$ being evaluated at the average state of left and right values.

4.6.2 | High order reconstruction

In order to obtain a higher-order scheme in space, we need to replace the piecewise constant data by a piecewise polynomial representation. This goal is achieved by various so-called reconstruction procedures such as MUSCL TVD [137, 226, 227], UNO [120], ENO [119], WENO [240] and many others. In our previous study on Boussinesq-type equations [92], the UNO2 scheme showed a good performance with small dissipation in realistic propagation and run-up simulations. Consequently, we retain this scheme for the discretization of the advective flux in Serre equations.

[17] This scheme is slightly dissipative and non-variational. However, we choose finite volumes due to their excellent shock-capturing properties, whose importance can hardly be underestimated for shallow water flows.

Remark 4.3. In TVD schemes, the numerical operator is required (by definition) not to increase the total variation of the numerical solution at each time step. It follows that the value of an isolated maximum may only decrease in time, which is not a good property for the simulation of coherent structures such as solitary waves. The non-oscillatory UNO2 scheme, employed in our study, is only required to diminish the *number* of local extrema in the numerical solution. Unlike TVD schemes, UNO schemes are not constrained to dampen the values of each local extremum at every time step.

The main idea of the UNO2 scheme is to construct a non-oscillatory piecewise-parabolic interpolant $\boldsymbol{Q}(x)$ to a piecewise smooth function $\boldsymbol{V}(x)$ (see [120] for more details). On each segment containing the face $x_{i+\frac{1}{2}} \in [x_i, x_{i+1}]$, the function $\boldsymbol{Q}(x) = \boldsymbol{q}_{i+\frac{1}{2}}(x)$ is locally a quadratic polynomial and wherever $v(x)$ is smooth we have

$$\boldsymbol{Q}(x) - \boldsymbol{V}(x) = \boldsymbol{0} + \mathcal{O}(\Delta x^3), \qquad \frac{\mathrm{d}\boldsymbol{Q}}{\mathrm{d}x}(x \pm 0) - \frac{\mathrm{d}\boldsymbol{V}}{\mathrm{d}x} = \boldsymbol{0} + \mathcal{O}(\Delta x^2).$$

Also, $\boldsymbol{Q}(x)$ should be non-oscillatory in the sense that the number of its local extrema does not exceed that of $\boldsymbol{V}(x)$. Since $\boldsymbol{q}_{i+\frac{1}{2}}(x_i) = \bar{\boldsymbol{V}}_i$ and $\boldsymbol{q}_{i+\frac{1}{2}}(x_{i+1}) = \bar{\boldsymbol{V}}_{i+1}$, it can be written in the form

$$\boldsymbol{q}_{i+\frac{1}{2}}(x) = \bar{\boldsymbol{V}}_i + \mathfrak{d}_{i+\frac{1}{2}}\{\boldsymbol{V}\} \times \frac{x - x_i}{\Delta x} + \tfrac{1}{2}\,\mathfrak{D}_{i+\frac{1}{2}}\{\boldsymbol{V}\} \times \frac{(x - x_i)(x - x_{i+1})}{\Delta x^2},$$

where $\mathfrak{d}_{i+\frac{1}{2}}\{\boldsymbol{V}\} \equiv \bar{\boldsymbol{V}}_{i+1} - \bar{\boldsymbol{V}}_i$ and $\mathfrak{D}_{i+\frac{1}{2}}\boldsymbol{V}$ is closely related to the second derivative of the interpolant since $\mathfrak{D}_{i+\frac{1}{2}}\{\boldsymbol{V}\} = \Delta x^2\, \boldsymbol{q}''_{i+\frac{1}{2}}(x)$. The polynomial $\boldsymbol{q}_{i+\frac{1}{2}}(x)$ is chosen to be the least oscillatory between two candidates interpolating $\boldsymbol{V}(x)$ at (x_{i-1}, x_i, x_{i+1}) and (x_i, x_{i+1}, x_{i+2}). This requirement leads to the following choice of $\mathfrak{D}_{i+\frac{1}{2}}\{\boldsymbol{V}\} \equiv \mathrm{minmod}\,(\mathfrak{D}_i\{\boldsymbol{V}\}, \mathfrak{D}_{i+1}\{\boldsymbol{V}\})$ with

$$\mathfrak{D}_i\{\boldsymbol{V}\} = \bar{\boldsymbol{V}}_{i+1} - 2\,\bar{\boldsymbol{V}}_i + \bar{\boldsymbol{V}}_{i-1}, \qquad \mathfrak{D}_{i+1}\{\boldsymbol{V}\} = \bar{\boldsymbol{V}}_{i+2} - 2\,\bar{\boldsymbol{V}}_{i+1} + \bar{\boldsymbol{V}}_i,$$

and where $\mathrm{minmod}(x, y)$ is the usual minmod function defined as

$$\mathrm{minmod}(x, y) \;\equiv\; \tfrac{1}{2}\,[\,\mathrm{sign}(x) + \mathrm{sign}(y)\,] \times \min(|x|, |y|).$$

To achieve the second order $\mathcal{O}(\Delta x^2)$ accuracy, it is sufficient to consider piecewise linear reconstructions in each cell. Let $L(x)$ denote this approximately reconstructed function, which can be written in this form

$$L(x) = \bar{\boldsymbol{V}}_i + \boldsymbol{S}_i \times \frac{x - x_i}{\Delta x}, \qquad x \in [x_{i-\frac{1}{2}}, x_{i+\frac{1}{2}}].$$

In order for $L(x)$ to be a non-oscillatory approximation, we use the parabolic interpolation $\boldsymbol{Q}(x)$ constructed below to estimate the slopes $\boldsymbol{S}_i$ within each cell

$$\boldsymbol{S}_i = \Delta x \times \text{minmod}\left(\frac{\mathrm{d}\boldsymbol{Q}}{\mathrm{d}x}(x_i - 0), \frac{\mathrm{d}\boldsymbol{Q}}{\mathrm{d}x}(x_i + 0)\right).$$

In other words, the solution is reconstructed on the cells, while the solution gradient is estimated on the dual mesh as it is often performed in more modern schemes [12, 13]. A brief summary of the UNO2 reconstruction can also be found in [92, 93].

4.6.3 | Treatment of the dispersive terms

In this section, we explain how we treat the dispersive terms of Serre equations 4.60, 4.61. We begin the exposition by discussing the space discretization, and then, we propose a way to remove the intrinsic stiffness of the dispersion by partial implicitation.

For the sake of simplicity, we split the dispersive terms into three parts:

$$\mathbb{M}(\boldsymbol{V}) \equiv \beta\, h^{-1}\left[h^3\, u_{xt}\right]_x, \quad \mathbb{D}_1(\boldsymbol{V}) \equiv \beta\, h^{-1}\left[h^3\, u\, u_{xx}\right]_x, \quad \mathbb{D}_2(\boldsymbol{V}) \equiv \beta\, h^{-1}\left[h^3\, u_x^2\right]_x.$$

We propose the following approximations in space (which are all of the second order $\mathcal{O}(\Delta x^2)$ to be consistent with UNO2 advective flux discretization presented above)

$$\begin{aligned}
\mathbb{M}_i(\bar{\boldsymbol{V}}) &= \beta\, \bar{h}_i^{-1}\, \frac{\bar{h}_{i+1}^3\,(\bar{u}_{xt})_{i+1} - \bar{h}_{i-1}^3\,(\bar{u}_{xt})_{i-1}}{2\,\Delta x} \\
&= \frac{\beta\, \bar{h}_i^{-1}}{2\,\Delta x}\left[\bar{h}_{i+1}^3\,\frac{(\bar{u}_t)_{i+2} - (\bar{u}_t)_i}{2\,\Delta x} - \bar{h}_{i-1}^3\,\frac{(\bar{u}_t)_i - (\bar{u}_t)_{i-2}}{2\,\Delta x}\right] \\
&= \frac{\beta\, \bar{h}_i^{-1}}{4\,\Delta x^2}\left[\bar{h}_{i+1}^3\,(\bar{u}_t)_{i+2} - (\bar{h}_{i+1}^3 + \bar{h}_{i-1}^3)\,(\bar{u}_t)_i + \bar{h}_{i-1}^3\,(\bar{u}_t)_{i-2}\right].
\end{aligned}$$

The last relation can be rewritten in a short-hand form if we introduce the matrix $\mathbb{M}(\bar{\boldsymbol{V}})$ such that the i-th component of the product $\mathbb{M}(\bar{\boldsymbol{V}}) \cdot \bar{\boldsymbol{V}}_t$ gives exactly the expression $\mathbb{M}_i(\bar{\boldsymbol{V}})$.

In a similar way, we discretize the other dispersive terms without giving the intermediate steps

$$\begin{aligned}
\mathbb{D}_{1i}(\bar{\boldsymbol{V}}) &= \frac{\beta\, \bar{h}_i^{-1}}{2\,\Delta x^3}\left[\bar{h}_{i+1}^3\,\bar{u}_{i+1}\,(\bar{u}_{i+2} - 2\bar{u}_{i+1} + \bar{u}_i) - \bar{h}_{i-1}^3\,\bar{u}_{i-1}\,(\bar{u}_i - 2\bar{u}_{i-1} + \bar{u}_{i-2})\right], \\
\mathbb{D}_{2i}(\bar{\boldsymbol{V}}) &= \frac{\beta\, \bar{h}_i^{-1}}{8\Delta x^3}\left[\bar{h}_{i+1}^3\,(\bar{u}_{i+2} - \bar{u}_i)^2 - \bar{h}_{i-1}^3\,(\bar{u}_i - \bar{u}_{i-2})^2\right].
\end{aligned}$$

In a more general non-periodic case, asymmetric finite differences should be used near the boundaries. If we denote by $\mathbb{I}$ the identity matrix, we can rewrite the semi-discrete scheme 4.63 by expanding the right-hand side $\boldsymbol{S}_i$

$$\frac{\mathrm{d}\bar{h}}{\mathrm{d}t} + \frac{1}{\Delta x}\left[\mathcal{F}_+^{(1)}(\bar{\boldsymbol{V}}) - \mathcal{F}_-^{(1)}(\bar{\boldsymbol{V}})\right] = 0, \tag{4.64}$$

$$(\mathbb{I} - \mathbb{M}) \cdot \frac{\mathrm{d}\bar{u}}{\mathrm{d}t} + \frac{1}{\Delta x}\left[\mathcal{F}_+^{(2)}(\bar{\boldsymbol{V}}) - \mathcal{F}_-^{(2)}(\bar{\boldsymbol{V}})\right] = \mathbb{D}(\bar{\boldsymbol{V}}) \cdot \bar{u}, \tag{4.65}$$

where $\mathcal{F}_\pm^{(1,2)}(\bar{\boldsymbol{V}})$ are the two components of the advective numerical flux vector $\mathcal{F}$ at the right $(+)$ and left $(-)$ faces correspondingly and $\mathbb{D}(\bar{\boldsymbol{V}}) \equiv \mathbb{D}_1(\bar{\boldsymbol{V}}) - \mathbb{D}_2(\bar{\boldsymbol{V}})$.

Finally, in order to obtain the semi-discrete scheme, one has to solve a linear system to find explicitly the time derivative $\mathrm{d}\bar{u}/\mathrm{d}t$. A mathematical study of the resulting matrix $\mathbb{I} - \mathbb{M}$ is not straightforward to perform. However, in our numerical tests, we have never experienced any difficulties in inverting it.

4.6.4 | Temporal scheme

We rewrite the inverted semi-discrete scheme 4.64–4.65 as a system of ODEs:

$$\partial_t\, w = \mathcal{L}(w, t), \qquad w(0) = w_0,$$

where $w := (\,\bar{h},\, \bar{u}\,)^\top$.

In order to solve numerically the last system of equations, we apply the Bogacki–Shampine method [24]. It is a third-order Runge–Kutta scheme with four stages. It has an embedded second-order method, which is used to estimate the local error and, thus, to adapt the time step size. Moreover, the Bogacki–Shampine method enjoys the First Same As Last (FSAL) property, so it needs three function evaluations per step. This method is also implemented in the `ode23` function in MATLAB [205]. A step of the Bogacki–Shampine method is given by

$$\begin{aligned}
k_1 &= \mathcal{L}(w^{(n)}, t_n),\\
k_2 &= \mathcal{L}(w^{(n)} + \tfrac{1}{2}\Delta t_n k_1, t_n + \tfrac{1}{2}\Delta t),\\
k_3 &= \mathcal{L}(w^{(n)}) + \tfrac{3}{4}\Delta t_n k_2, t_n + \tfrac{3}{4}\Delta t),\\
w^{(n+1)} &= w^{(n)} + \Delta t_n \times \left(\tfrac{2}{9}k_1 + \tfrac{1}{3}k_2 + \tfrac{4}{9}k_3\right),\\
k_4 &= \mathcal{L}(w^{(n+1)}, t_n + \Delta t_n),\\
w_2^{(n+1)} &= w^{(n)} + \Delta t_n \times \left(\tfrac{4}{24}k_1 + \tfrac{1}{4}k_2 + \tfrac{1}{3}k_3 + \tfrac{1}{8}k_4\right).
\end{aligned}$$

Here $w^{(n)} \approx w(t_n)$, Δt is the time step and $w_2^{(n+1)}$ is a second-order approximation to the solution $w(t_{n+1})$, so the difference between $w^{(n+1)}$ and $w_2^{(n+1)}$ gives an estimation of the local error. The FSAL property consists of the fact that k_4 is equal to k_1 in the next time step, thus saving one function evaluation.

If the new time step Δt_{n+1} is given by $\Delta t_{n+1} = \rho_n \Delta t_n$, then according to the H211b digital filter approach [208, 209], the proportionality factor ρ_n is given by:

$$\rho_n = \left(\frac{\delta}{\varepsilon_n}\right)^{\beta_1} \left(\frac{\delta}{\varepsilon_{n-1}}\right)^{\beta_2} \rho_{n-1}^{-\alpha}, \tag{4.66}$$

where ε_n is a local error estimation at time step t_n, δ is the desired tolerance, and the constants β_1, β_2 and α are defined as

$$\alpha = \frac{1}{4}, \qquad \beta_1 = \beta_2 = \frac{1}{4\,p}.$$

The parameter p is the order of the scheme ($p = 3$ in our case).

Remark 4.4. The adaptive strategy 4.66 can be further improved if we smooth the factor ρ_n before computing the next time step Δt_{n+1}

$$\Delta t_{n+1} = \hat{\rho}_n \, \Delta t_n, \qquad \hat{\rho}_n = \omega(\rho_n).$$

The function $\omega(\rho)$ is called *the time step limiter* and should be smooth, monotonically increasing and should satisfy the following conditions

$$\omega(0) < 1, \qquad \omega(+\infty) > 1, \qquad \omega(1) = 1, \qquad \omega'(1) = 1.$$

One possible choice is suggested in [209]:

$$\omega(\rho) = 1 + \kappa \arctan\left(\frac{\rho - 1}{\kappa}\right).$$

In our computations, the parameter κ is set to 1.

4.6.5 | Pseudo-spectral Fourier-type method for the Serre equations

In this section, we describe a pseudo-spectral solver to integrate numerically the Serre equations in periodic domains. With spectral methods, it is more convenient to take as variables the free surface

elevation $\eta(x,\,t)$ and the conserved quantity $q(x,\,t)$. Hence, we consider the system of equations:

$$\eta_t + \left[\,(d+\eta)\,\bar{u}\,\right]_x = 0, \tag{4.67}$$

$$q_t + \left[\,q\,u \;-\; \tfrac{1}{2}\,\bar{u}^2 \;+\; g\,\eta \;-\; \tfrac{1}{2}\,(d+\eta)^2\,\bar{u}_x^2\,\right]_x = 0, \tag{4.68}$$

$$q - \bar{u} + \tfrac{1}{3}(d+\eta)^2\bar{u}_{xx} + (d+\eta)\eta_x\bar{u}_x = 0. \tag{4.69}$$

The first two equations 4.67 and 4.68 are of evolution type, while the third one 4.69 relates the conserved variable q to the primitive variables: the free surface elevation η and the velocity $\bar{u}$. In order to solve the relation 4.69 with respect to the velocity $\bar{u}$, we extract the linear part as

$$\bar{u} - \tfrac{1}{3}\,d^2\,\bar{u}_{xx} - q = \underbrace{\tfrac{1}{3}\,(2d\eta+\eta^2)\,\bar{u}_{xx} + (d+\eta)\,\eta_x\,\bar{u}_x}_{N(\eta,\bar{u})}\,.$$

Then, we apply to the last relation the following fixed point type iteration in Fourier space

$$\hat{\bar{u}}_{j+1} = \frac{\hat{q}}{1+\frac{1}{3}(kd)^2} + \frac{\mathcal{F}\{N(\eta,\bar{u}_j)\}}{1+\frac{1}{3}(kd)^2}, \qquad j=0,1,2,\cdots, \tag{4.70}$$

where $\hat{\psi}\equiv\mathcal{F}\{\psi\}$ denotes the Fourier transform of a quantity ψ. The last iteration is repeated until the desired convergence. For example, for moderate amplitude solitary waves (≈ 0.2), the accuracy 10^{-16} is attained in approximately 20 iterations if the velocity $\bar{u}_0$ is initialized from the previous time step. We note that the usual $3/2$-rule is applied to the nonlinear terms for anti-aliasing [58, 102, 224].

Remark 4.5. One can improve the fixed point iteration 4.70 employing the so-called relaxation approach [126]. The relaxed scheme takes the following form

$$\hat{\bar{u}}_{j+1} = \left(\frac{\hat{q}}{1+\frac{1}{3}(kd)^2} + \frac{\mathcal{F}\{N(\eta,\bar{u}_j)\}}{1+\frac{1}{3}(kd)^2}\right)\theta + (1-\theta)\hat{\bar{u}}_j\,, \qquad j=0,1,2,\cdots,$$

where $\theta\in[0,\,1]$ is a free parameter. We obtained the best convergence rate for $\theta=\frac{1}{2}$.

In order to improve the numerical stability of the time-stepping method, we integrate exactly the linear terms in evolution equations

$$\eta_t + d\,\bar{u}_x = -[\,\eta\,\bar{u}\,]_x,$$

$$q_t + g\,\eta_x = \left[\,\tfrac{1}{2}\,\bar{u}^2 \;+\; \tfrac{1}{2}\,(d+\eta)^2\,\bar{u}_x^2 \;-\; q\,u\,\right]_x.$$

Taking the Fourier transform and using the relation 4.69 between $\bar{u}$ and q, we obtain the following system of ODEs:

$$\hat{\eta}_t + \frac{\mathrm{i}kd}{1+\frac{1}{3}(kd)^2}\,\hat{q} = -\mathrm{i}k\,\mathcal{F}\{\eta\bar{u}\} - \frac{\mathrm{i}kd\,\mathcal{F}\{N(\eta,\bar{u}_j)\}}{1+\frac{1}{3}(kd)^2},$$

$$\hat{q}_t + \mathrm{i}kg\,\hat{\eta} = \mathrm{i}k\,\mathcal{F}\left\{\tfrac{1}{2}\bar{u}^2 + \tfrac{1}{2}(d+\eta)^2\bar{u}_x^2 - qu\right\}.$$

The next step consists in introducing the vector of dimensionless variables in Fourier space $\hat{\boldsymbol{V}} \equiv (\mathrm{i}k\hat{\eta}, \mathrm{i}\omega\hat{q}/g)$, where $\omega^2 = gk^2d/[1+\frac{1}{3}(kd)^2]$ is the dispersion relation of the linearized Serre equations. With unscaled variables in vectorial form, the last system becomes

$$\hat{\boldsymbol{V}}_t + \mathcal{L}\cdot\hat{\boldsymbol{V}} = \mathcal{N}(\hat{\boldsymbol{V}}), \qquad \mathcal{L} \equiv \begin{bmatrix} 0 & \mathrm{i}\omega \\ \mathrm{i}\omega & 0 \end{bmatrix}.$$

On the right-hand side, we put all the nonlinear terms

$$\mathcal{N}(\hat{\boldsymbol{V}}) = \begin{pmatrix} k^2\,\mathcal{F}\{\eta\bar{u}\} + dk^2\,\mathcal{F}\{N(\eta,\bar{u}_j)\}/(1+\frac{1}{3}(kd)^2) \\ -(k\omega/g)\,\mathcal{F}\left\{\frac{1}{2}\bar{u}^2 + \frac{1}{2}(d+\eta)^2\bar{u}_x^2 - qu\right\} \end{pmatrix}.$$

In order to integrate the linear terms, we make a last change of variables [102, 168]:

$$\hat{\boldsymbol{W}}_t = \mathrm{e}^{(t-t_0)\mathcal{L}}\cdot\mathcal{N}\left\{\mathrm{e}^{-(t-t_0)\mathcal{L}}\cdot\hat{\boldsymbol{W}}\right\}, \qquad \hat{\boldsymbol{W}}(t) \equiv \mathrm{e}^{(t-t_0)\mathcal{L}}\cdot\hat{\boldsymbol{V}}(t), \qquad \hat{\boldsymbol{W}}(t_0) = \hat{\boldsymbol{V}}(t_0).$$

Finally, the last system of ODEs is discretized in time by Verner's embedded[18] adaptive 9(8) Runge–Kutta scheme [228]. The time step is chosen adaptively using the so-called H211b digital filter [208, 209]

[18] Embedded Runge–Kutta schemes are a quintessence of numerical ingenuity in the realm of differential equations' resolution, embodying a dual-tier architecture that furnishes not only the sought-after solution but also an estimate of the local truncation error. This dual-faceted construct is eloquently manifest in the Verner embedded adaptive 9(8) Runge–Kutta scheme, a paradigm that unveils a confluence of accuracy and adaptability. At the heart of this scheme lies a pair of intertwined Runge-Kutta methods, one of the ninth order and its counterpart of the eighth order. The orchestration of these methods is such that they share common function evaluations, thereby entwining efficiency with precision.

The crux of adaptivity in this scheme emanates from the discrepancy between the solutions procured by the ninth and eighth-order methods, a discrepancy that serves as a harbinger of the local error. This local error estimation, devoid of additional function evaluations, furnishes the fodder for an adaptive strategy, wherein the step size is meticulously modulated to ensure that the error dovetails with a preordained tolerance. The Verner scheme, thus, transcends a mere solver to embody a self-adjusting algorithm, acclimatising to the terrain of the differential equation at hand.

Furthermore, the Verner scheme's elegance is not confined to its adaptive prowess alone but extends to its error control strategy. The scheme's architecture is meticulously crafted to ensure that the error estimation is robust, a feature indispensable for the scheme's adaptive strategy. This symbiosis of a high-order method with a reliable error estimator, encapsulated within a singular scheme, underscores the essence of embedded Runge-Kutta schemes. The Verner embedded adaptive 9(8) Runge–Kutta scheme epitomises a harmonious blend of precision, efficiency, and adaptability, rendering it a potent tool in the arsenal of a computational scientist venturing into the intricate domain of differential equations resolution.

Table 4.1 | Values of various parameters used in convergence tests.

Undisturbed water depth: d	1
Gravity acceleration: g	1
Solitary wave amplitude: a	0.05
Final simulation time: T	2
Free parameter: β	1/3

to meet some prescribed error tolerance (generally of the same order of the fixed point iteration 4.70 precision). Since the numerical scheme is implicit in the velocity variable $\bar{u}$, the resulting time step Δt is generally of the order of the spatial discretization $\mathcal{O}(\Delta x)$.

4.6.6 | Numerical results

In this section, we present some numerical results using the finite volume scheme described above. First, we validate the discretization and check the convergence of the scheme using an analytical solution. Then, we demonstrate the ability of the scheme to simulate the practically important solitary wave interaction problem. Throughout this Section, we consider the initial value problem with periodic boundary conditions unless a special remark is made.

Convergence test and invariants preservation

Consider the Serre equations 4.60 and 4.61 posed in the periodic domain $[\,-40,\,40\,]$. We solve numerically the initial-periodic boundary value problem with an exact solitary wave solution 4.46 posed as an initial condition. Then, this specific initial disturbance will be translated into space with known celerity under the system dynamics. This particular class of solutions plays an important rôle in water wave theory [76, 77], and it will allow us to assess the accuracy of the proposed scheme. The values of the various physical parameters used in the simulation are given in Table 4.1.

The error is measured using the discrete L_∞ norm for various successively refined discretizations. The result is shown in Figure 4.3. As anticipated, the finite volume scheme (black solid line with circles) shows a fairly good second-order convergence (with estimated slope ≈ 1.99). During all the numerical tests, the mass conservation was satisfied with the accuracy of the order $\approx 10^{-14}$. This remarkable result is due to the excellent local conservative properties of the finite volume method. We also investigate the numerical behaviour of the scheme with respect to the invariants $\mathcal{H}$ and Q defined in 4.47. These invariants can be computed analytically[19] for solitary wave solutions. However, we do not

[19] In the sense of closed-form solutions.

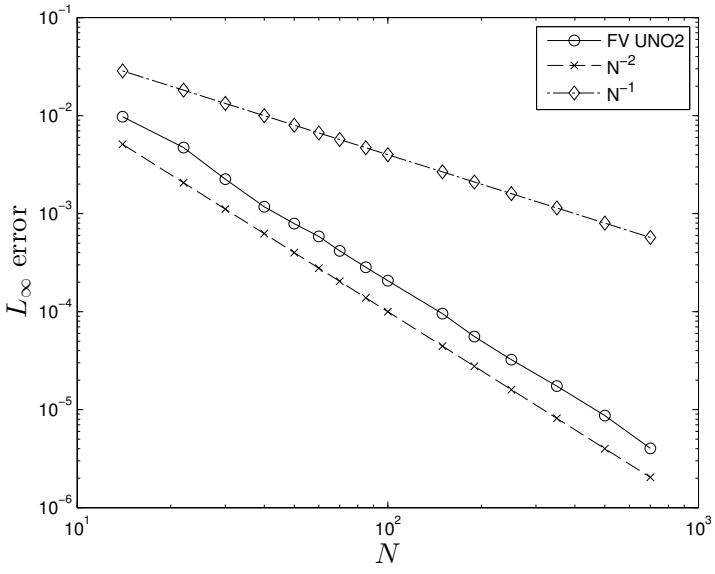

Figure 4.3 | Convergence of the numerical solution in the L_∞ norm computed using the finite volume method. Circles represent the error measured in our numerical solution. Two other curves demonstrate typical first and second-order convergence for the sake of comparison.

provide them to avoid cumbersome expressions. For the solitary wave with parameters given in Table 4.1, the generalized energy and momentum are given by the following expressions:

$$\mathcal{H}_0 = \frac{21\sqrt{7}}{100} + \frac{7\sqrt{3}}{10}\log\frac{\sqrt{21}-1}{\sqrt{21}+1} \approx 0.0178098463,$$

$$Q_0 = \frac{62\sqrt{15}}{225} + \frac{2\sqrt{35}}{5}\log\frac{\sqrt{21}-1}{\sqrt{21}+1} \approx 0.017548002.$$

These values are used to measure the error on these quantities at the end of the simulation. The convergence of this error under the mesh refinement is shown in Figure 4.4. One can observe a slight super-convergence phenomenon of the finite volume scheme. This effect is due to the special nature of the solution we use to measure the convergence. This solution is only translated under the system dynamics. For more general initial conditions, we expect a fair theoretical 2nd order convergence for the finite volume scheme. As anticipated, the pseudo-spectral scheme shows the exponential error decay with respect to the number of spectral modes.

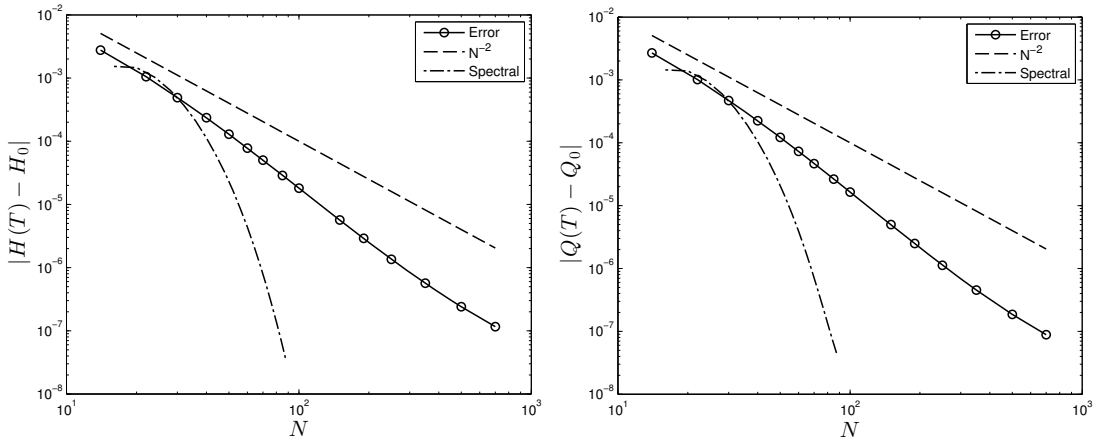

(a) Hamiltonian $\mathcal{H}$ (b) Momentum Q

Figure 4.4 | Hamiltonian and generalized momentum conservation convergence computed using the finite volume and spectral methods under the mesh refinement. The conserved quantities are measured at the final simulation time.

Solitary wave interaction

Solitary wave interactions are an important phenomenon in nonlinear dispersive waves, which have been studied by numerical and analytical methods, and results have been compared to experimental data. They also often serve as robust nonlinear benchmark test cases for numerical methods. We mention only a few works in the existing literature. For example, in [63, 163, 195] solitary wave interactions were studied experimentally. The head-on collision of solitary waves was studied in the framework of full Euler equations in [42, 63]. Studies of solitary waves in various approximate models can be found in [5, 74, 92, 93, 154]. To our knowledge, solitary wave collisions for the Serre equations were studied numerically for the first time in the PhD thesis of Seabra-Santos [200]. Finally, there are also a few studies devoted to simulations with full Euler equations [63, 102, 154].

Head-on collision

Consider the Serre equations posed in the domain $[-40,\ 40]$ with periodic boundary conditions. In the present section, we study the head-on collision (weak interaction) of two solitary waves of equal amplitude moving in opposite directions. Initially, two solitary waves of amplitude $a = 0.15$ are located at $x_0 = \pm 20$ (other parameters can be found in Table 4.1). The computational domain is divided into $N = 1000$ intervals (finite volumes in 1D) of the uniform length $\Delta x = 0.08$. The time step is chosen to be $\Delta t \approx 10^{-3}$. The process is simulated up to time $T = 36$. The numerical results

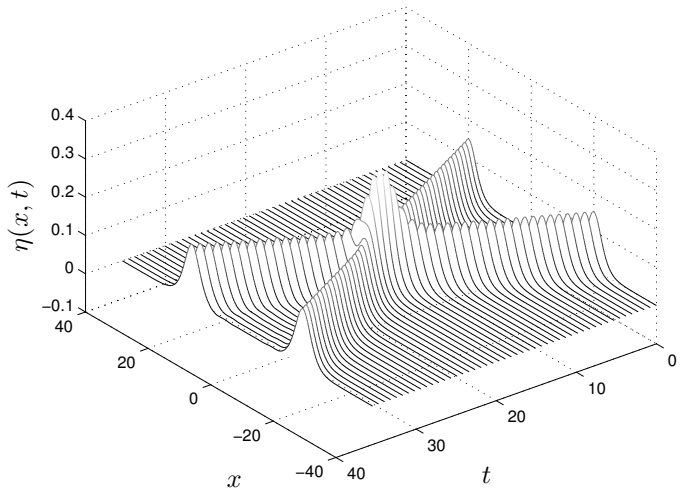

Figure 4.5 | Head-on collision of two equal solitary waves simulated with the finite volume scheme.

are presented in Figure 4.5. As expected, the solitary waves collide quasi-elastically and continue to propagate in opposite directions after the interaction. The value of importance is the maximum amplitude during the interaction process, sometimes referred to as the run-up. Usually, it is larger than the sum of the amplitudes of the two initial solitary waves. In this case, we obtain a run-up of $0.3130 > 2a = 0.3$.

In order to validate the finite volume simulation, we performed the same computation with the pseudo-spectral method presented briefly in section 4.6.5. We used a fine grid of 1024 nodes and adaptive time stepping. The overall interaction process is visually identical to the finite volume result shown in Figure 4.5. The run-up value according to the spectral method is 0.3127439, showing again the accuracy of our simulation. A small inelasticity is evident from the small dispersive wave train emerging after the interaction (for example, in a slightly different setting described below, see Figure 4.15, as first found numerically and experimentally by Seabra-Santos [200].

Overtaking collision

A second type of solitary wave interaction is the *overtaking collision* (or *strong interaction*) of two solitary waves of different amplitudes moving in the same direction. Sometimes, this situation is also referred to as the following collision or strong interaction. For this case, we consider a physical domain

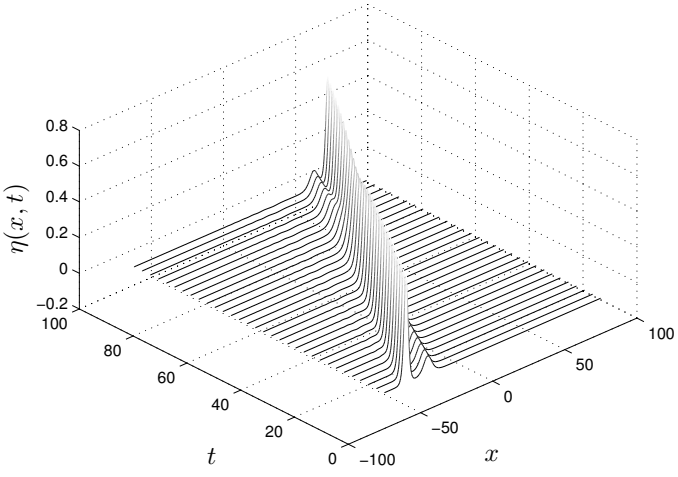

Figure 4.6 | Overtaking (or following) collision of two solitary waves simulated with the finite volume scheme.

Table 4.2 | Values of various parameters used to simulate the overtaking collision.

Undisturbed water depth: d	1
Gravity acceleration: g	1
Large solitary wave amplitude: a_1	0.6
Initial position: x_1	-60
Small solitary wave amplitude: a_2	0.1
Initial position: x_2	-45
Final simulation time: T	96
Free parameter: β	1/3

$[-75, 75]$ divided into $N = 1000$ equal control volumes. The initial data consists of two separated solitary waves of different amplitudes moving in the same direction. The solitary wave with larger amplitude moves faster and will overtake the smaller wave. This situation was simulated with the finite volume scheme, and the numerical results are presented in Figure 4.6. The parameters used in this simulation are given in Table 4.2. The strong interaction is also inelastic, with a small dispersive tail emerging after the over-taking (see Figure 4.14 for a magnification).

Experimental validation

In this Section, we present a comparison between the classical Serre model solved with our finite volume scheme and one head-on collision experiment from [63]. This specific experiment was already considered in the context of Boussinesq-type systems [92].

Table 4.3 | Values of various parameters used to simulate the head-on collision.

Undisturbed water depth: d [cm]	5
Gravity acceleration: g [m s^{-2}]	9.81
Right-going SW amplitude: a_1 [cm]	1.077
Initial position of the SW-1: x_1 [m]	0.247
Left-going SW amplitude: a_1 [cm]	1.195
Initial position of the SW-2: x_2 [m]	1.348
Final simulation time: T [s]	20.5

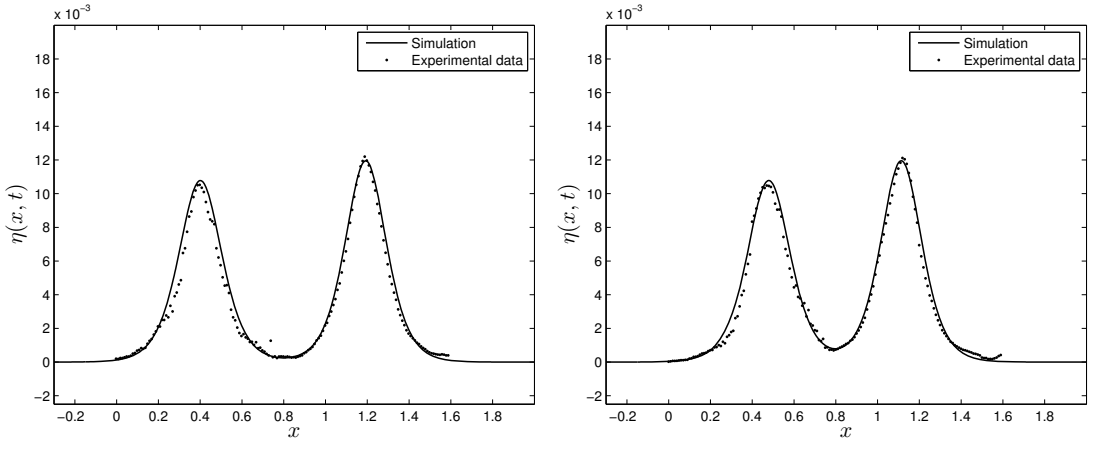

(a) $t = 18.5$ s (b) $t = 18.6$ s

Figure 4.7 | Head-on collision of two solitary waves of different amplitudes. Comparison with experimental data [63].

We simulate a portion of the wave tank $[-0.9,\ 2.7]$ (divided into $N = 1000$ equal control volumes) where the interaction process takes place. The initial data consists of two solitary waves (of different amplitudes in this case) moving in opposite directions. The exact parameters are given in Table 4.3. Simulation snapshots are presented in Figures 4.7–4.15. The general agreement is very good, validating the Serre equations in water wave theory, along with our numerical developments. Figure 4.15 shows visible dispersive oscillations after the interaction process, numerical evidence of the inelastic character of solitary wave interactions in the framework of the Serre equations. This simulation thereby not only validates the theoretical constructs of the Serre equations but also augments our numerical understanding of solitary wave interactions, paving the way for further analytical and numerical explorations in elucidating the complex dynamics of water wave interactions.

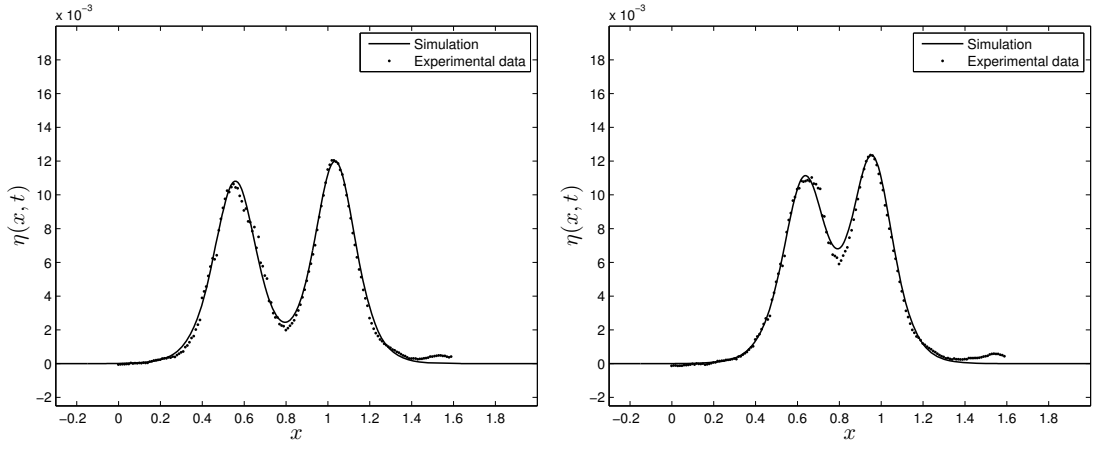

(a) $t = 18.7$ s (b) $t = 18.8$ s

Figure 4.8 | Head-on collision of two solitary waves of different amplitudes. Comparison with experimental data [63].

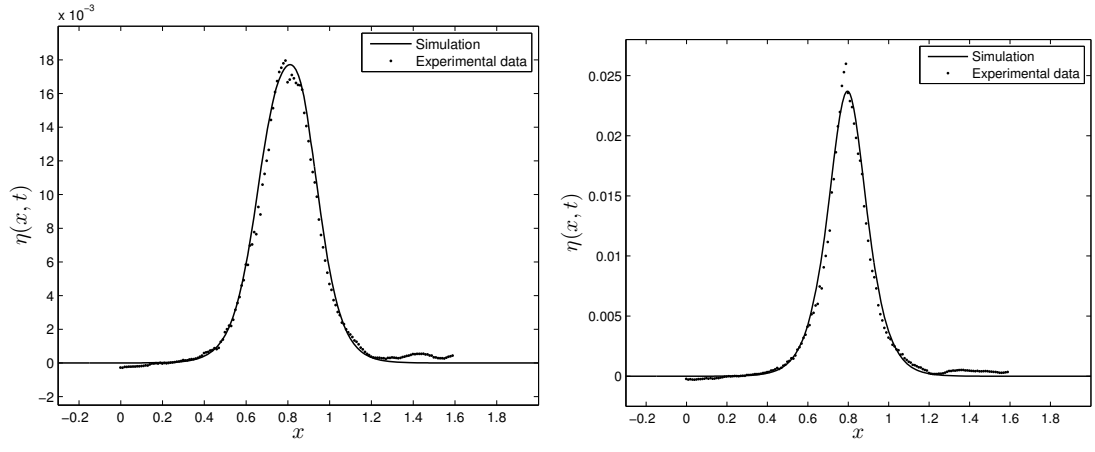

(a) $t = 18.92$ s (b) $t = 19.0$ s

Figure 4.9 | Head-on collision of two solitary waves of different amplitudes. Comparison with experimental data [63]. Note the difference in vertical scales on the left and right images.

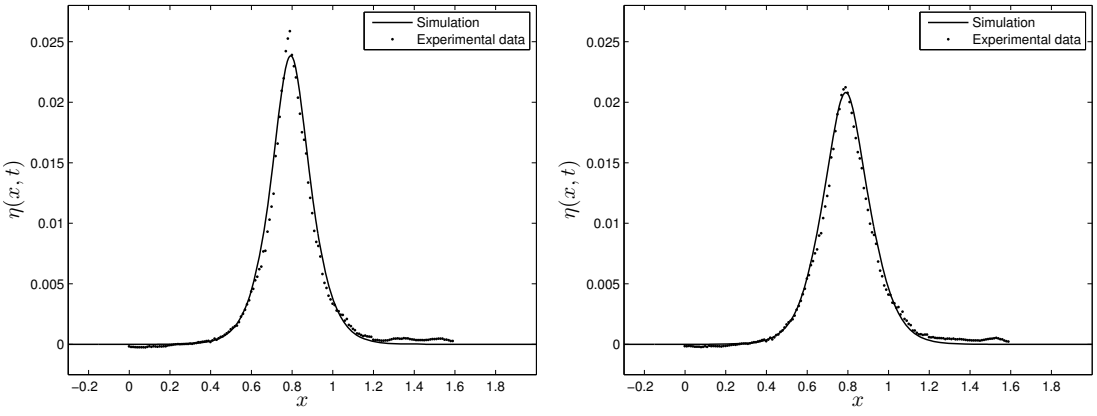

(a) $t = 19.05$ s (b) $t = 19.1$ s

Figure 4.10 | Head-on collision of two solitary waves of different amplitudes. Comparison with experimental data [63].

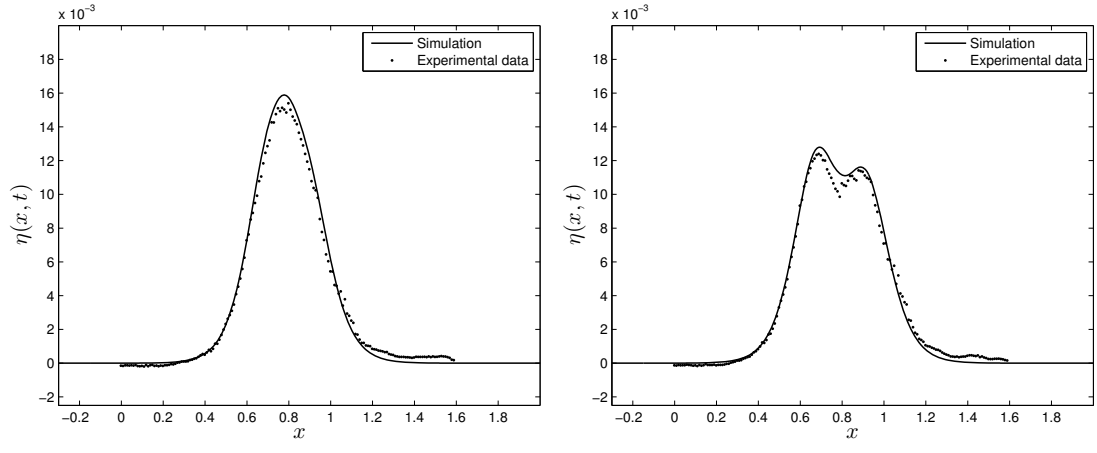

(a) $t = 19.15$ s (b) $t = 19.19$ s

Figure 4.11 | Head-on collision of two solitary waves of different amplitudes. Comparison with experimental data [63].

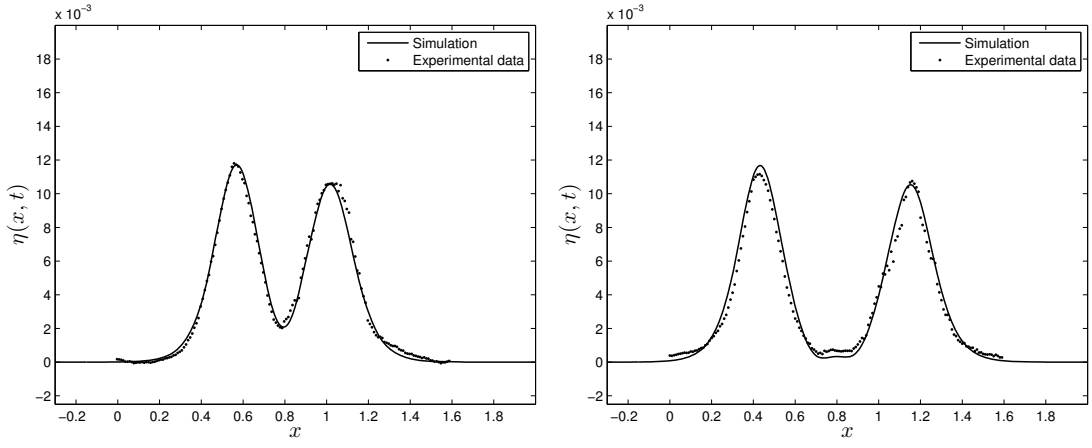

(a) $t = 19.33$ s (b) $t = 19.5$ s

Figure 4.12 | Head-on collision of two solitary waves of different amplitudes. Comparison with experimental data [63].

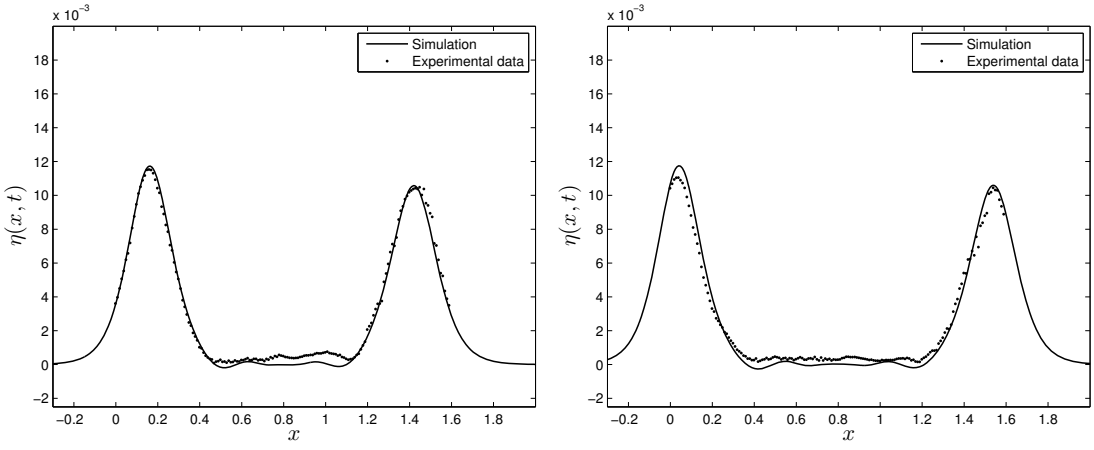

(a) $t = 19.85$ s (b) $t = 20.0$ s

Figure 4.13 | Head-on collision of two solitary waves of different amplitudes. Comparison with experimental data [63].

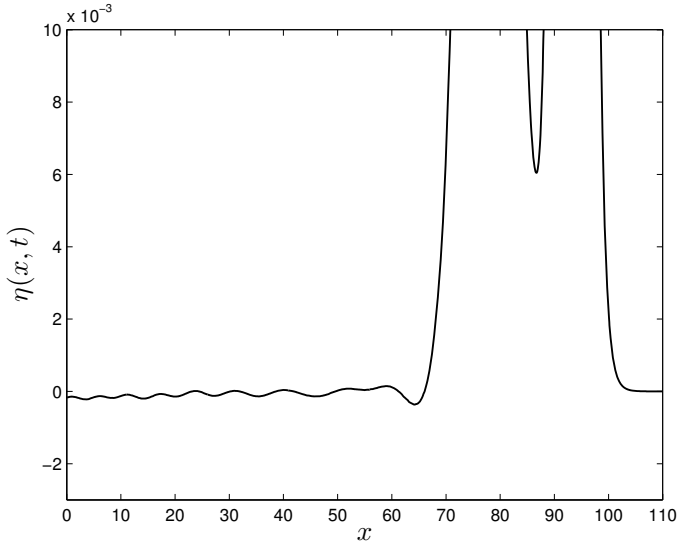

Figure 4.14 | Dispersive tail after overtaking collision of two solitary waves (strong interaction) at $T = 120.0$.

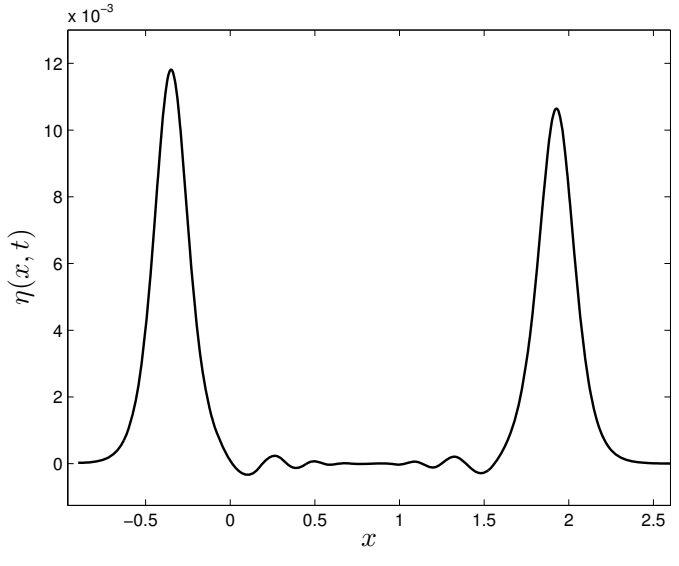

Figure 4.15 | Dispersive tail after head-on collision of two solitary waves (weak interaction). Small wavelets between two solitary waves clearly indicate that the collision is inelastic.

4.7 | Modified shallow water equations for significantly varying bottoms

The celebrated classical nonlinear shallow water equations (NSWE) were derived in 1871 by A. J. C. de Saint-Venant [68]. Currently, these equations are widely used in practice, and one can find thousands of publications devoted to the applications, validations and numerical solutions of these equations [95, 96, 164].

The interaction of surface waves with mild or tough bottoms has always attracted the particular attention of researchers [8, 44, 94, 180]. There are, however few studies which attempt to include the bottom curvature effect into the classical Saint-Venant [68, 212] or Savage–Hutter[20] [113, 198] equations. One of the first studies in this direction is perhaps due to Dressler [78]. Much later, this research was pursued almost at the same time by Berger, Keller, Bouchut and their collaborators [22, 28, 132]. We note that all these authors used some variants of the asymptotic expansion method. Recently, the model proposed by Dressler was validated in laboratory experiments [70]. The present study is a further attempt to improve the classical Saint-Venant equations by including a better representation of the bottom shape. Dressler's model includes the bottom curvature effects, which require the computation of the bottom's profile second-order derivatives. For irregular shapes, it can be problematic. Consequently, we try below to propose a model which requires only the first spatial derivatives of the bathymetry to be continuous.

The Saint-Venant equations are derived under the assumption of a hydrostatic pressure field, resulting in a non-dispersive system of equations. Many non-hydrostatic improved models have long been proposed; see [18, 158, 181, 239] for reviews. These Boussinesq-like and/or mild-slope [18, 181] equations are dispersive (*i.e.*, the wave speed depends on the wavelength) and involve (at least) third-order derivatives. Although these models capture more physical effects than the classical Saint-Venant shallow water equations, they have several drawbacks. First, the dispersive effects are often negligible for very long waves such as tsunamis and tidal waves. Second, the higher-order derivatives introduce stiffness into the equations, and thus, their numerical resolution is significantly more involved and costly than for the Saint-Venant equations. Third, the Boussinesq-like equations are not hyperbolic and, unlike the Saint-Venant equations, the method of characteristics cannot be employed (unless the operators are split, *e.g.* [26]). Therefore, it is not surprising that various dispersive shallow water models are not systematically[21] used in coastal modelling.

[20] The Savage–Hutter equations are usually posed on inclined planes, and they are used to model various gravity-driven currents, such as snow avalanches [4].

[21] There is a notable exception of the SGN equations, which gained a certain popularity even in more applied circles.

In the presence of varying bathymetry, the shallow water equations are derived under the assumption that the bottom variations are very weak. However, even for very long surface waves, significant variations of the bathymetry can play an important rôle in wave propagation. These bottom slope effects can be even more important when the wave travels over many oscillations of the seabed, due to the accumulation of bottom slope influences. Therefore, even for a shallow water long waves model, it is important to take properly into account the significant bottom variations [44]. In this article, we present a modification of the Saint-Venant equations in the presence of a seabed of significant variations. This model is derived from a variational principle, which is a powerful method to derive approximations that cannot be obtained from more classical asymptotic expansions.

Within the domain of water wave theory, variational principles are typically employed in concert with small parameter expansions, a methodology that often proves instrumental in deriving approximations. When undertaken, this approach may yield approximations that mirror those acquired from asymptotic expansions applied directly to the governing equations. A salient advantage of such congruence is the preservation of the variational structure, a fundamental attribute that lends a coherent framework for the ensuing analysis. However, should this congruence falter, the approximation procedure risks fracturing the invaluable variational structure, thereby potentially obfuscating the analytical clarity and coherence. The allure of variational methods extends beyond mere elegance and streamlined derivations, although these are notable merits. Principally, these methods exude a capacity for preserving the intrinsic variational structure even as they navigate the complexities of the problem at hand.

Variational methods transcend this conventional framework, showcasing their prowess in deriving approximations even in the absence of reliance on asymptotic expansions. This feature burgeons into a significant asset, particularly in scenarios where the identification of a discernible small parameter proves elusive. The robustness of variational methods in such scenarios underscores their versatility and the breadth of their analytical potential. They not only offer a pathway to deriving approximations but do so in a manner that retains the core variational structure, thereby ensuring a structured and disciplined analytical discourse. This capacity for adapting to the nuanced demands of the problem, sans a tether to asymptotic expansions, amplifies the appeal and the utility of variational methods in tackling the intricate and diverse challenges endemic to water wave theory.

Here, we adopt the same philosophy, applying it to the long water waves propagating over a seabed with significant variations. Namely, the shallow water Ansatz from [52] is additionally constrained to respect the bathymetry variations in space and time. Then, applying the variational principle, we arrive naturally at some modified Saint-Venant (mSV) equations. These mSV equations, like the

classical Saint-Venant equations, are hyperbolic and can be solved with similar techniques, which is an interesting feature in the prospect of integration/modification of existing operational codes. The derivation of mSV equations presented below were communicated by the same authors in a short note announcing the main results [83]. In the present study, we investigate the properties of the proposed mSV system along with its solutions through analytical and numerical methods. We especially focus on predictions of interest for ocean modelling, in particular the fact that the waves are slowed down by the seabed slope.

4.7.1 | Model derivation

In order to simplify the full water wave problem, we choose some approximate but physically relevant representations of all dependent variables in the relaxed variational principle. In this study, we choose a simple shallow water Ansatz, which is a velocity field, and velocity potential independent of the vertical coordinate y such that

$$\phi \approx \bar{\phi}(\boldsymbol{x}, t), \qquad \boldsymbol{u} = \boldsymbol{\mu} \approx \bar{\boldsymbol{u}}(\boldsymbol{x}, t), \qquad v = \nu \approx \check{v}(\boldsymbol{x}, t), \tag{4.71}$$

where $\bar{\boldsymbol{u}}(\boldsymbol{x}, t)$ is the depth-averaged horizontal velocity and $\check{v}(\boldsymbol{x}, t)$ is the vertical velocity at the bottom. In this Ansatz, we take for simplicity the pseudo-velocities to be equal to the velocity field $\boldsymbol{u} = \boldsymbol{\mu}$, $v = \nu$. However, in other situations, they can differ (see [52] for more examples).

Physically, the Ansatz 4.71 means that we are considering a so-called *columnar flow* [167], which is a sensible model for long waves in shallow water, as long as their amplitudes are not too large. Mathematically, the Ansatz 4.71 implies that the vertical variation of the velocity field does not contribute (*i.e.*, is negligible) to the Lagrangian 3.6. Thus, with the Ansatz 4.71, the Lagrangian density 3.6 becomes

$$\mathscr{L} = (\partial_t h + \bar{\boldsymbol{u}} \cdot \boldsymbol{\nabla} h + h \boldsymbol{\nabla} \cdot \bar{\boldsymbol{u}})\, \bar{\phi} - \tfrac{1}{2}\, g\, \eta^2 + \tfrac{1}{2}\, h\, (\bar{\boldsymbol{u}}^2 + \check{v}^2), \tag{4.72}$$

where we introduced the total water depth $h = \eta + d$.

Since we are considering a columnar flow model, each vertical water column can be considered as a moving rigid body. In the presence of bathymetry variations, the columnar flow paradigm then yields the fluid vertical velocity must be equal to the one at the bottom because the bottom is impermeable. Thus, we require that the fluid particles follow the bottom profile, *i.e.*,

$$\check{v} = -\partial_t\, d - \bar{\boldsymbol{u}} \cdot \boldsymbol{\nabla} d\,, \tag{4.73}$$

this identity being the bottom impermeability condition expressed with the Ansatz 4.71.

Remark 4.6. Note that for Ansatz 4.71 the horizontal vorticity $\boldsymbol{\omega}$ and the vertical one ζ are given by:

$$\boldsymbol{\omega} = \Big(\partial_{x_2} \check{v} \,,\, -\partial_{x_1} \check{v} \Big), \qquad \zeta = \partial_{x_1} \bar{u}_2 - \partial_{x_2} \bar{u}_1 .$$

Consequently, the flow is not exactly irrotational in general. It will be confirmed below one more time when we establish the connection between $\bar{\boldsymbol{u}}$ and $\boldsymbol{\nabla} \bar{\phi}$. We would like to mention also that it was demonstrated in [36] that perturbations of horizontal vorticity in shallow water models are not stable when embedded in the Euler equations.

After substitution of the relation 4.73 into the Lagrangian density 4.72, the Euler–Lagrange equations yield:

$$\delta \bar{\boldsymbol{u}} \;:\quad \mathbf{0} = \bar{\boldsymbol{u}} - \boldsymbol{\nabla} \bar{\phi} - \check{v}\, \boldsymbol{\nabla} d, \tag{4.74}$$

$$\delta \bar{\phi} \;:\quad 0 = \partial_t\, h + \boldsymbol{\nabla} \cdot [\, h\, \bar{\boldsymbol{u}}\,], \tag{4.75}$$

$$\delta \eta \;:\quad 0 = \partial_t\, \bar{\phi} + g\, \eta + \bar{\boldsymbol{u}} \cdot \boldsymbol{\nabla} \bar{\phi} - \tfrac{1}{2} (|\, \bar{\boldsymbol{u}}\,|^2 + \check{v}^2). \tag{4.76}$$

Taking the gradient of 4.76 and eliminating of $\bar{\phi}$ from 4.74 gives the system of governing equations:

$$\partial_t\, h + \boldsymbol{\nabla} \cdot [\, h\, \bar{\boldsymbol{u}}\,] = 0, \tag{4.77}$$

$$\partial_t [\, \bar{\boldsymbol{u}} \,-\, \check{v}\, \boldsymbol{\nabla} d\,] + \boldsymbol{\nabla} \left[\, g\, \eta + \tfrac{1}{2}\, |\, \bar{\boldsymbol{u}}\,|^2 + \tfrac{1}{2}\, \check{v}^2 + \check{v}\, \partial_t d\,\right] \,=\, 0, \tag{4.78}$$

together with the auxiliary relations

$$\bar{\boldsymbol{u}} = \boldsymbol{\nabla} \bar{\phi} + \check{v}\, \boldsymbol{\nabla} d = \boldsymbol{\nabla} \bar{\phi} - \frac{\partial_t d + (\boldsymbol{\nabla} \bar{\phi}) \cdot (\boldsymbol{\nabla} d)}{1 \,+\, |\boldsymbol{\nabla} d|^2}\, \boldsymbol{\nabla} d, \tag{4.79}$$

$$\check{v} \;= -\partial_t\, d - \bar{\boldsymbol{u}} \cdot \boldsymbol{\nabla} d = -\,\frac{\partial_t d \,+\, (\boldsymbol{\nabla} \bar{\phi}) \cdot (\boldsymbol{\nabla} d)}{1 \,+\, |\boldsymbol{\nabla} d|^2}. \tag{4.80}$$

Hereafter, every time the variables $\bar{\boldsymbol{u}}$ and $\check{v}$ appear in equations, it is *always* assumed that they are defined by the relations 4.79–4.80.

Remark 4.7. The classical irrotational NSWE or Saint-Venant equations [68, 212] can be recovered by substituting $\check{v} = 0$ into the last system:

$$\partial_t\, h + \boldsymbol{\nabla} \cdot [\, h\, \bar{\boldsymbol{u}}\,] = 0,$$

$$\partial_t\, \bar{\boldsymbol{u}} + \boldsymbol{\nabla} \left[\, g\, \eta + \tfrac{1}{2}\, |\, \bar{\boldsymbol{u}}\,|^2 \,\right] = 0,$$

where $\bar{\boldsymbol{u}} = \boldsymbol{\nabla} \bar{\phi}$.

4.7.2 | Properties of the mSV model

From the governing equations 4.77, 4.78 one can derive an equation for the horizontal velocity $\bar{\boldsymbol{u}}$:

$$\partial_t \bar{\boldsymbol{u}} + \tfrac{1}{2}\boldsymbol{\nabla}|\bar{\boldsymbol{u}}|^2 + g\,\boldsymbol{\nabla}\eta = \gamma\,\boldsymbol{\nabla}d + \bar{\boldsymbol{u}} \wedge (\boldsymbol{\nabla}\check{v} \wedge \boldsymbol{\nabla}d), \tag{4.81}$$

where γ is the vertical acceleration at the bottom defined as:

$$\gamma \;\equiv\; \frac{\mathrm{d}\,\check{v}}{\mathrm{d}t} = \partial_t \check{v} + (\bar{\boldsymbol{u}} \cdot \boldsymbol{\nabla})\,\check{v}. \tag{4.82}$$

Remark 4.8. Note that in 4.81, the last term on the right-hand side cancels out for two-dimensional waves (*i.e.*, one horizontal dimension). It can be seen from the following analytical representation, which degenerates to zero in one horizontal dimension:

$$\bar{\boldsymbol{u}} \wedge (\boldsymbol{\nabla}\check{v} \wedge \boldsymbol{\nabla}d) = (\boldsymbol{\nabla}\check{v})\,(\bar{\boldsymbol{u}} \cdot \boldsymbol{\nabla}d) - (\boldsymbol{\nabla}d)\,(\bar{\boldsymbol{u}} \cdot \boldsymbol{\nabla}\check{v}).$$

This property has an interesting geometrical interpretation since $\bar{\boldsymbol{u}} \wedge (\boldsymbol{\nabla}\check{v} \wedge \boldsymbol{\nabla}d)$ is a horizontal vector orthogonal to $\bar{\boldsymbol{u}}$ and thus vanishes for two-dimensional waves.

Defining the depth-averaged total (kinetic plus potential) energy density $\mathscr{E}$ together with the Ansatz 4.71, *i.e.*,

$$\mathscr{E} = \int_{-d}^{\eta} \left[\frac{|\boldsymbol{u}|^2 + v^2}{2} + g\,y \right] \mathrm{d}y \;\approx\; h\,\frac{\bar{\boldsymbol{u}}^2 + \check{v}^2}{2} + g\,\frac{\eta^2 - d^2}{2}, \tag{4.83}$$

and using 4.79–4.80, after some algebra, one derives the energy equation

$$\partial_t \mathscr{E} + \boldsymbol{\nabla} \cdot \left[\mathscr{E}\,\bar{\boldsymbol{u}} + \tfrac{1}{2}\,g\,h^2\,\bar{\boldsymbol{u}} \right] \;=\; -(g + \gamma)\,h\,\partial_t d. \tag{4.84}$$

Obviously, the source term on the right-hand side vanishes if the bottom is fixed $d = d(x)$ or, equivalently, if $\partial_t d = 0$.

The mSV equations 4.74–4.76 possess a Hamiltonian structure with canonical variables h and $\bar{\phi}$, *i.e.*,

$$\frac{\partial\, h}{\partial t} = \frac{\delta\,\mathcal{H}}{\delta\bar{\phi}}, \qquad \frac{\partial\,\bar{\phi}}{\partial t} = -\frac{\delta\,\mathcal{H}}{\delta h},$$

where the Hamiltonian $\mathcal{H}$ is defined as

$$2\,\mathcal{H} = \int \left\{ g(h-d)^2 - g\,d^2 \;+\; h|\boldsymbol{\nabla}\bar{\phi}|^2 \;-\; \frac{h\,[\,\partial_t d + (\boldsymbol{\nabla}\bar{\phi}) \cdot (\boldsymbol{\nabla}d)\,]^2}{1 + |\boldsymbol{\nabla}d|^2} \right\} \mathrm{d}^2\boldsymbol{x}. \tag{4.85}$$

One can easily check, after computing the variations, that the Hamiltonian 4.85 yields

$$\partial_t h = -\boldsymbol{\nabla}\cdot\left[h\boldsymbol{\nabla}\bar{\phi} - \frac{\partial_t d + (\boldsymbol{\nabla}\bar{\phi})\cdot(\boldsymbol{\nabla} d)}{1+|\boldsymbol{\nabla} d|^2}\, h\,\boldsymbol{\nabla} d\right],$$

$$\partial_t \bar{\phi} = -g\,(h-d) - \frac{|\boldsymbol{\nabla}\bar{\phi}|^2}{2} + \frac{[\,\partial_t d + (\boldsymbol{\nabla}\bar{\phi})\cdot(\boldsymbol{\nabla} d)\,]^2}{2+2\,|\boldsymbol{\nabla} d|^2},$$

which are equivalent to the system 4.75–4.76 after introduction of the auxiliary variables $\bar{\boldsymbol{u}}$ and $\check{v}$ defined in 4.79 and 4.80.

Remark 4.9. If we rewrite the Hamiltonian 4.85 in the following equivalent form:

$$2\,\mathcal{H} = \int \left\{\, g\,\eta^2 - g\,d^2 + h\,|\,\bar{\boldsymbol{u}}\,|^2 + h\,\check{v}^2 + 2\,h\,\check{v}\,\partial_t d\,\right\} \mathrm{d}^2\boldsymbol{x}, \tag{4.86}$$

one can see that the Hamiltonian density is actually the physical energy density $\mathscr{E}$ if the bottom is static (*i.e.*, if $\partial_t d = 0$), but these two quantities are different if the bottom moves. In other words, the Hamiltonian is the energy only if there is no external input of energy into the system. Note also that the Hamiltonian structure of the classical Saint-Venant equations can be recovered substituting $\check{v} = 0$ into the last Hamiltonian 4.86:

$$2\,\mathcal{H}_0 = \int \left\{\, g\,\eta^2 - g\,d^2 + h\,|\,\bar{\boldsymbol{u}}\,|^2\,\right\} \mathrm{d}^2\boldsymbol{x},$$

where $\bar{\boldsymbol{u}} = \boldsymbol{\nabla}\bar{\phi}$.

4.7.3 | Steady solutions

We consider here the two-dimensional case (*i.e.*, one horizontal dimension) in order to derive a closed-form solution for a steady state flow over a general bathymetry. We assume the following upstream conditions at $x \to -\infty$:

$$\eta \to 0, \qquad d \to d_0, \qquad \bar{u} \to u_0 \geqslant 0.$$

Physically, these conditions mean that far upstream, we consider a uniform current over a horizontal bottom. The mass conservation in steady condition yields

$$h\,\bar{u} = d_0\,u_0,$$

while the momentum conservation equation becomes

$$g\,h + \tfrac{1}{2}\,\bar{u}^2\left[\,1 + (\partial_x d)^2\,\right] = g\,d_0 + \tfrac{1}{2}\,u_0^2.$$

The last two relations yield the following cubic equations for the total water depth (with the dimensionless height $Z = h/d_0 > 0$ and the Froude number $\mathcal{F} = u_0/\sqrt{g\,d_0} \geqslant 0$)

$$G(Z) \equiv Z^3 - (1 + \tfrac{1}{2}\mathcal{F}^2)\,Z^2 + \tfrac{1}{2}\mathcal{F}^2\,[1 + (\partial_x d)^2] = 0. \tag{4.87}$$

Note that $G(0) > 0$ for all $\mathcal{F} > 0$, G has a maximum at $Z = 0$ and a minimum at $Z = Z_1 = (2+\mathcal{F}^2)/3$. Therefore, 4.87 has two positive solutions if $G(Z_1) < 0$, one positive solution if $G(Z_1) = 0$, and no positive solutions if $G(Z_1) > 0$. Equation 4.87 always has a real negative root, which is of no interest for obvious physical reasons.

If $G(Z_1) < 0$, the two positive solutions may be presented as

$$Z^+ = \left[2\sqrt{A/3}\cos\left(\tfrac{1}{3}\arccos\left(-3^{-1/2}BA^{-3/2}\right) - \tfrac{2}{3}\pi\right)\right]^{-1}$$

and

$$Z^- = \left[2\sqrt{A/3}\cos\left(\tfrac{1}{3}\arccos\left(-3^{-1/2}BA^{-3/2}\right)\right)\right]^{-1},$$

where

$$A \equiv \frac{1 + 2\,\mathcal{F}^{-2}}{1 + (\partial_x d)^2} \geqslant 0, \qquad B \equiv \frac{9\,\mathcal{F}^{-2}}{1 + (\partial_x d)^2} \geqslant 0.$$

We note that $Z^- < Z^+$. The root $Z = Z^+$ corresponds to the sub-critical regime, while $Z = Z^-$ corresponds to a supercritical regime. For the special case $\mathcal{F} = 1$, we have $Z^+ > 1$ and $Z^- < 1$.

If $G(Z_1) = 0$, for a given Froude number $\mathcal{F}$, there is only one absolute value of the slope for which this identity is satisfied, that is

$$(\partial_x d)^2 = (\mathcal{F}^2 - 1)^2\,(\mathcal{F}^2 + 8)\,/\,27\,\mathcal{F}^2.$$

For instance, if $\partial_x d = 0$ then $G(Z_1) = 0$ if and only if $\mathcal{F} = 1$.

Remark 4.10. It is straightforward to derive a similar equation for steady solutions to the classical Saint-Venant equations

$$Z^3 - (1 + \tfrac{1}{2}\mathcal{F}^2)\,Z^2 + \tfrac{1}{2}\mathcal{F}^2 = 0.$$

The last relation can also be obtained from equation 4.87 taking $\partial_x d = 0$. Consequently, we can say that steady solutions to the classical Saint-Venant equations do not take into account the bottom slope local variations.

Table 4.4 | Values of various parameters used for the steady state computation.

Parameter	*Value*
Gravity acceleration g:	$1\,\mathrm{m\,s^{-2}}$
Undisturbed water depth d_0:	1 m
Deformation amplitude a:	0.5 m
Half-length of the uplift area b:	2.5 m
Upstream flow speed, u_0:	$2.0\,\mathrm{m\,s^{-1}}$

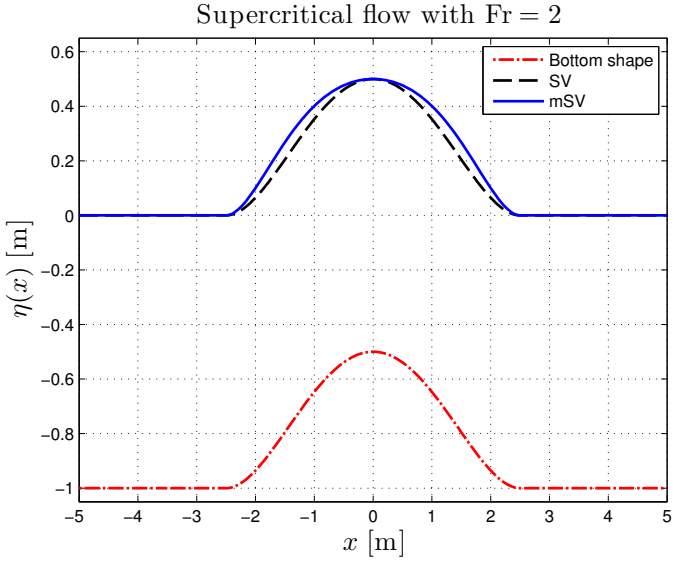

Figure 4.16 | Supercritical steady state solutions over a bump for the Froude number $\mathcal{F} = 2$. Comparison between the classical and modified Saint-Venant equations.

In order to illustrate the developments made above, we compute a steady flow over a bump. The bottom takes the form

$$d(x) = d_0 - a\,b^{-4}\left(x^2 - b^2\right)^2 \mathrm{H}(b^2 - x^2),$$

where $\mathrm{H}(x)$ is the Heaviside step function [1], a and b being the bump amplitude and its half-length, respectively. The values of various parameters are given in Table 4.4. We consider here, for illustrative purposes, the supercritical case for the classical and new models. The result is shown in Figure 4.16 where some small differences can be noted with respect to the classical Saint-Venant equations.

4.7.4 | Hyperbolic structure

From now on, we consider equations 4.77, 4.78 written in one horizontal space dimension (two-dimensional waves) for simplicity:

$$\partial_t\, h + \partial_x \left[\, h\, \bar{u}\,\right] = 0, \tag{4.88}$$

$$\partial_t \left[\, \bar{u} - \check{v}\, \partial_x\, d\,\right] + \partial_x \left[\, g\, \eta + \tfrac{1}{2}\, \bar{u}^2 + \tfrac{1}{2}\, \check{v}^2 + \check{v}\, \partial_t\, d\,\right] = 0. \tag{4.89}$$

In order to present the equations in a more suitable conservative form, we will introduce the potential velocity variable $U = \partial_x \bar{\phi}$. From equation 4.74, it is straightforward to see that U satisfies the relation

$$U = \bar{u} - \check{v}\, \partial_x\, d,$$

Depth averaged, and vertical bottom velocities can also be easily expressed in terms of the potential velocity U

$$\bar{u} = \frac{U \;-\; (\partial_t d)\,(\partial_x d)}{1 + (\partial_x d)^2}, \qquad \check{v} = -\frac{\partial_t d + U\, \partial_x d}{1 + (\partial_x d)^2}.$$

Consequently, using this new variable, equations 4.88 and 4.89 can be rewritten as a system of conservation laws

$$\partial_t\, h + \partial_x \left[\, h\, \frac{U - (\partial_t d)\,(\partial_x d)}{1 + (\partial_x d)^2}\,\right] = 0,$$

$$\partial_t\, U + \partial_x \left[\, g\,(h - d) + \frac{1}{2}\frac{U^2 - 2\,U\,(\partial_t d)\,(\partial_x d) - (\partial_t d)^2}{1 + (\partial_x d)^2}\,\right] = 0.$$

For the sake of simplicity, we rewrite the above system in the following quasi-linear vectorial form:

$$\partial_t\, w + \partial_x\, f(w) = 0,$$

where we introduced the vector of conservative variables w and the advective flux $f(w)$:

$$w = \begin{pmatrix} h \\ U \end{pmatrix}, \qquad f(w) = \begin{pmatrix} h\dfrac{U - (\partial_t d)(\partial_x d)}{1 + (\partial_x d)^2} \\[2ex] g(h - d) + \dfrac{U^2 - 2U(\partial_x d)(\partial_t d) - (\partial_t d)^2}{2\,[1 + (\partial_x d)^2]} \end{pmatrix}.$$

The Jacobian matrix of the advective flux $f(w)$ can be easily computed:

$$\mathbb{A}(w) \;=\; \frac{\partial\, f(w)}{\partial w} \;=\; \frac{1}{1 + (\partial_x d)^2} \begin{bmatrix} U - (\partial_t d)(\partial_x d) & h \\ g\,(1 + (\partial_x d)^2) & U - (\partial_t d)(\partial_x d) \end{bmatrix} \;=\; \begin{bmatrix} \bar{u} & \dfrac{h}{1 + (\partial_x d)^2} \\ g & \bar{u} \end{bmatrix}.$$

The matrix $\mathbb{A}(w)$ has two distinct eigenvalues:

$$\lambda^{\pm} = \frac{U - (\partial_t d)\,(\partial_x d)}{1 + (\partial_x d)^2} \pm c = \bar{u} \pm c, \qquad c^2 \equiv \frac{g\,h}{1 + (\partial_x d)^2}.$$

Remark 4.11. Physically, the quantity c represents the phase celerity of long gravity waves. In the framework of the Saint-Venant equations, it is well known that $c = \sqrt{gh}$. Both expressions differ by the factor $1/\sqrt{1 + (\partial_x d)^2}$. In our model, the long waves are slowed down by strong bathymetric variations since fluid particles are constrained to follow the seabed[22]. We also note that a similar factor was previously introduced in [107] to account for steepness in the bathymetry. In our case, it appears naturally when one studies the hyperbolicity property of the model.

Right and left eigenvectors coincide with those of the Saint-Venant equations, and they are given by the following matrices

$$R = \begin{bmatrix} -h & h \\ \sqrt{gh} & \sqrt{gh} \end{bmatrix}, \qquad L = \frac{1}{2}\begin{bmatrix} -h^{-1} & (gh)^{-1/2} \\ h^{-1} & (gh)^{-1/2} \end{bmatrix}.$$

Columns of the matrix R constitute eigenvectors corresponding to eigenvalues λ^- and λ^+, respectively. Corresponding left eigenvectors are conventionally written in lines of the matrix L.

4.7.5 | Group velocity

We would like to compute also the group velocity in the framework of the modified Saint-Venant (mSV) equations. This quantity is traditionally associated with the wave energy propagation speed [89, 212]. Recall that in the classical linearized shallow water theory, the phase c and group c_g velocities are equal [212]:

$$c = \frac{\omega}{k} = \sqrt{gh}, \qquad c_g = \frac{\mathrm{d}\,\omega}{\mathrm{d}\,k} = \sqrt{gh},$$

where $\omega = k\sqrt{gh}$ is the dispersion relation for linear long waves, k being the wavenumber and ω being the angular frequency.

In order to assess the wave energy propagation speed, we will consider a quasi-linear system of equations composed of mass and energy conservation laws:

$$\partial_t h + \partial_x \left[h\,\frac{U - (\partial_x d)(\partial_t d)}{1 + (\partial_x d)^2} \right] = 0,$$

$$\partial_t E + \partial_x \left[(E + \tfrac{1}{2} g h^2)\,\tfrac{U - (\partial_x d)(\partial_t d)}{1 + (\partial_x d)^2} \right] = -(g + \gamma)\,h\,\partial_t d,$$

[22] This property is rooted in the Ansatz that yields the mSV equations.

where γ is defined in 4.82 and E is the total energy considered already above 4.84:

$$E = h\frac{\bar{u}^2+\check{v}^2}{2} + \frac{g\,(\eta^2-d^2)}{2} = \frac{h}{2}\frac{U^2+(\partial_t d)^2}{1+(\partial_x d)^2} + \frac{g\,(h^2-2hd)}{2}.$$

The last formula can be inverted to express the potential velocity in terms of the wave energy:

$$U^2 = [\,1+(\partial_x d)^2\,]\left(\frac{2E}{h} - gh + 2gd\right) - (\partial_t d)^2.$$

In the spirit of computations performed in the previous section, we compute the Jacobian matrix $\mathbb{J}$ of the mass-energy advection operator:

$$\mathbb{J} = \frac{1}{1+(\partial_x d)^2}\begin{bmatrix} U - (\partial_x d)(\partial_t d) + h\dfrac{\partial U}{\partial h} & h\dfrac{\partial U}{\partial E} \\ gh[U-(\partial_x d)(\partial_t d)] + (E+\frac{1}{2}gh^2)\dfrac{\partial U}{\partial h} & U-(\partial_x d)(\partial_t d) + (E+\frac{1}{2}gh^2)\dfrac{\partial U}{\partial E}\end{bmatrix},$$

where partial derivatives are given here:

$$\frac{\partial U}{\partial h} = -\,[\,1+(\partial_x d)^2\,]\,\frac{gh^2+2E}{2h^2U}, \qquad \frac{\partial U}{\partial E} = \frac{1+(\partial_x d)^2}{hU}.$$

Computation of the Jacobian $\mathbb{J}$ eigenvalues leads the following expression for the *group velocity* of the mSV equations:

$$c_g^2 = \frac{g\,h}{1+(\partial_x d)^2}\frac{U-(\partial_x d)(\partial_t d)}{U}.$$

The last formula is very interesting. It means that in the moving bottom case, the group velocity c_g is modified and does not coincide anymore with the phase velocity $c^2 = gh[1+(\partial_x d)^2]^{-1}$. This fact represents another new and non-classical feature of the modified Saint-Venant equations. The relative difference between phase and group velocities squared is

$$\frac{c^2-c_g^2}{c^2} = \frac{(\partial_x d)\,(\partial_t d)}{U},$$

which is not necessarily always positive. When it is negative, the energy is injected into the system at a higher rate than can be spread, thus leading to energy accumulation and possibly favouring the breaking events.

4.7.6 | Numerical results

In this section, we also employ the finite volume method [85] very similar to the one presented above to solve SGN equations. This scheme has already been validated in several studies, even in the case

of dispersive waves [92, 93]. Consequently, we do not present here the standard convergence tests, which can be found in the references cited above. In the present Section, we show numerical results which illustrate some properties of the mSV equations with respect to their classical counterpart. In the sequel, we consider only a one-dimensional case for simplicity. The physical domain will also be limited by wall-boundary conditions. Other types of boundary conditions obviously could also be considered.

Wave propagation over the oscillatory bottom.

We begin the exposition of numerical results by presenting a simple test case of a wave propagating over a static but highly oscillatory bottom. Let us consider a one-dimensional physical domain $[-10,\ 10]$ which is discretized into $N = 350$ equal control volumes. The tolerance parameter δ in the time stepping algorithm is chosen to be 10^{-4}. The initial condition is simply a bump localized near the centre $x = 0$ and posed on the free surface with an initial zero velocity field

$$\eta_0(x) = b\,\mathrm{sech}^2(\kappa x), \qquad u_0(x) = 0.$$

The bottom is given analytically by the function

$$d(x) = d_0 + a\sin(kx).$$

In other words, the bathymetry function $d(x)$ consists of uniform level d_0, which is perturbed by uniform oscillations of amplitude a. Since the bathymetry is static, the governing equations 4.88 and 4.89 are simplified at some point.

Hereafter, we fix two wavenumbers k_1 and k_2 ($k_1 < k_2$) and perform a comparison between numerical solutions to the classical and mSV equations. The main idea behind this comparison is to show the similarity between two solutions for gentle bottoms and, correspondingly, to highlight the differences for stronger gradients. The values of various physical parameters used in numerical simulations are given in Table 4.5.

Several snapshots of the free surface elevation during the wave propagation test case are presented in Figures 4.17–4.23. The left image refers to the gentle bottom gradient case ($k_1 = 2$) while the right image corresponds to the oscillating bottom ($k_2 = 6$). Everywhere, the solid blue line represents a solution to the mSV equations, while the dotted black line refers to the classical solution. Numerical results on left images indicate that both models give very similar results when bathymetry gradients are gentle. The two solutions are almost indistinguishable from graphical resolutions, especially at the beginning. However, some divergences are accumulated with time. At the end of the simulation,

Table 4.5 | Values of various parameters used for the wave propagation over an oscillatory bottom test case.

Parameter	*Value*
Initial wavenumber κ:	$1\,\mathrm{m}^{-1}$
Gravity acceleration g:	$1\,\mathrm{m\,s}^{-2}$
Final simulation time T:	24 s
Initial wave amplitude b:	0.2 m
Undisturbed water depth d_0:	1 m
Bathymetry oscillation amplitude a:	0.1 m
Low bathymetry oscillation wavelength k_1:	$2\,\mathrm{m}^{-1}$
High bathymetry oscillation wavelength k_2:	$6\,\mathrm{m}^{-1}$

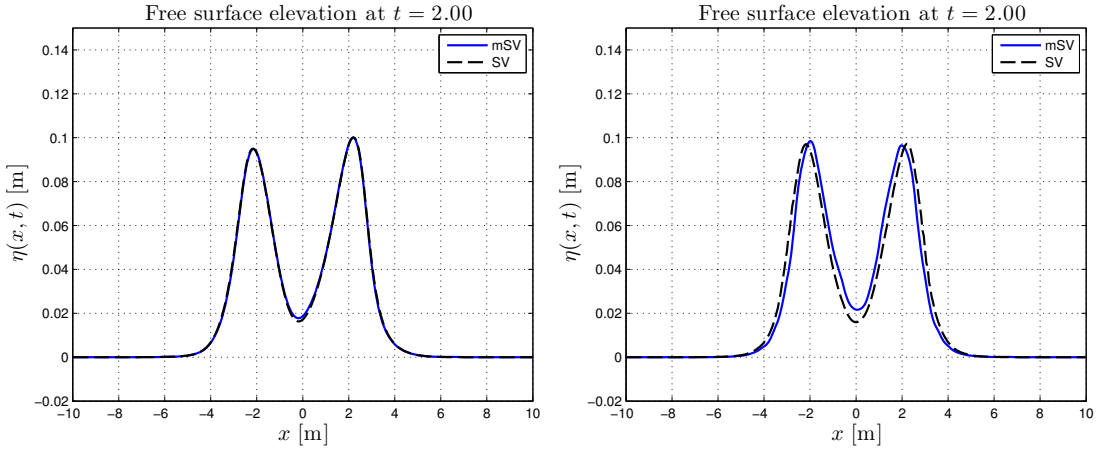

(a) *Low oscillations,* k_1 (b) *High oscillations,* k_2

Figure 4.17 | Wave propagation over an oscillatory bottom, $t = 2$ s.

some differences become visible in the graphic resolution. On the other hand, numerical solutions on the right images are substantially different from the first instants of the wave propagation. In accordance with theoretical predictions (see Remark 4.11), the wave in mSV equations propagates with speed effectively reduced by bottom oscillations. This fact explains a certain lag between two numerical solutions in the highly oscillating case. We note that the wave shape is also different in classical and improved equations. Finally, in Figure 4.24, we show the evolution of the local time step during the simulation. It can be easily seen that the time adaptation algorithm very quickly finds the optimal value of the time step, which is then maintained during the whole simulation. This observation is even more flagrant on the right image corresponding to the highly oscillating case.

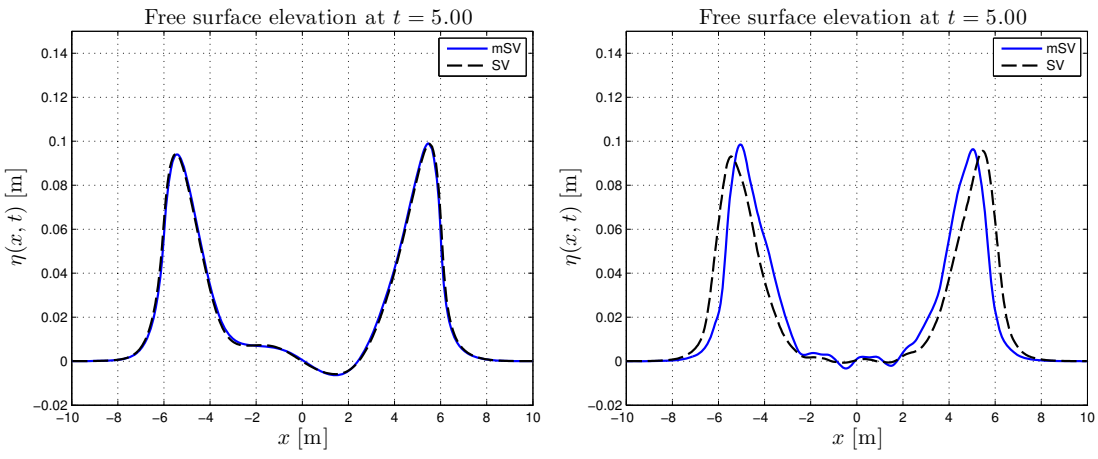

(a) *Low oscillations,* k_1 (b) *High oscillations,* k_2

Figure 4.18 | Wave propagation over an oscillatory bottom, $t = 5$ s.

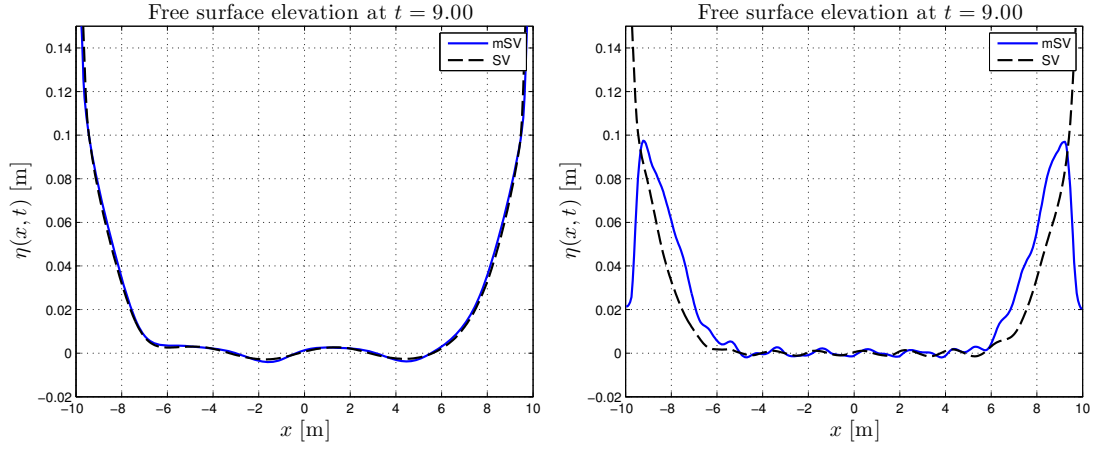

(a) *Low oscillations,* k_1 (b) *High oscillations,* k_2

Figure 4.19 | Wave propagation over an oscillatory bottom, $t = 9$ s.

Wave generation by sudden bottom uplift

We continue to investigate various properties of the modified Saint-Venant equations. In this Section, we present a simple test case which involves the bottom motion. More precisely, we will investigate two cases of slow and fast uplifts of a portion of the bottom. This simple situation has some important implications for tsunami genesis problems [90, 118, 223].

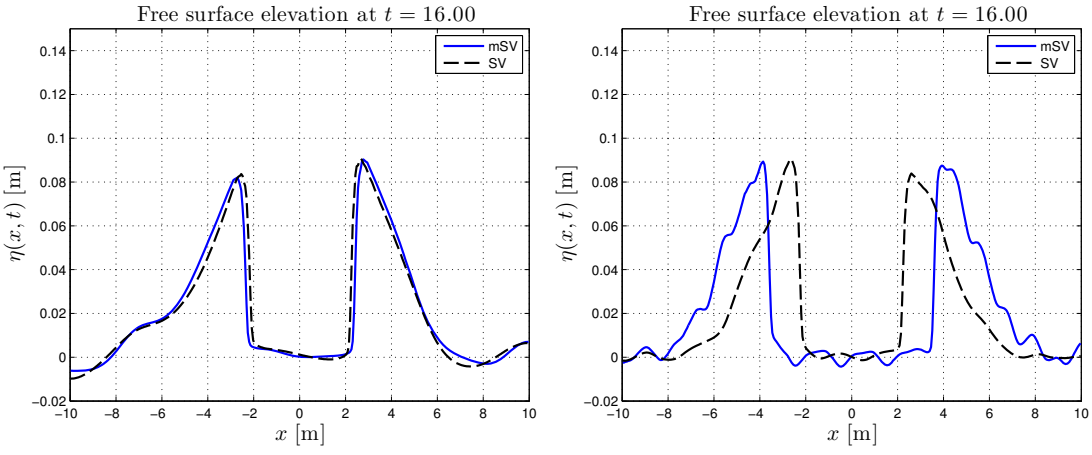

(a) *Low oscillations,* k_1 (b) *High oscillations,* k_2

Figure 4.20 | Wave propagation over an oscillatory bottom, $t = 16$ s.

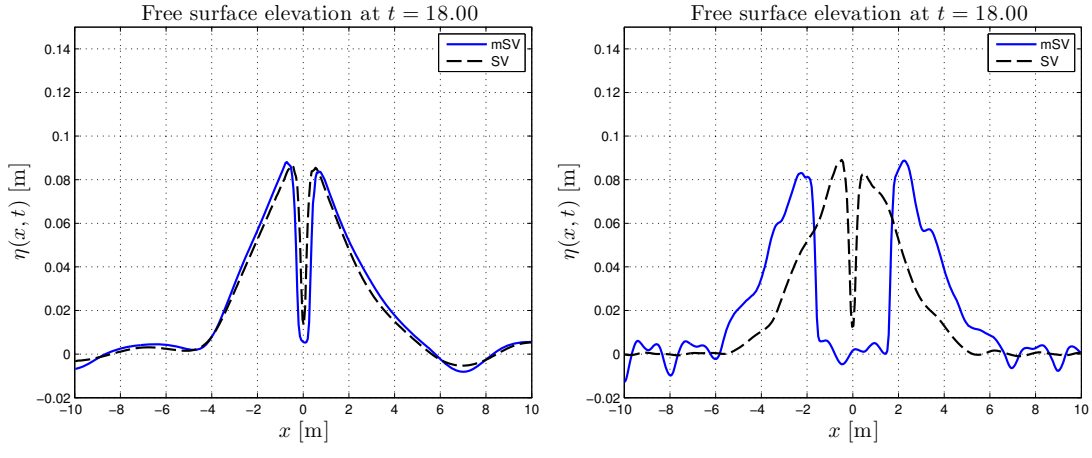

(a) *Low oscillations,* k_1 (b) *High oscillations,* k_2

Figure 4.21 | Wave propagation over an oscillatory bottom, $t = 18$ s.

The physical domain and discretization parameters are inherited from the last section. The bottom is given by the following function:

$$d(x,t) = d_0 - a\,T(t)\,\mathrm{H}(b^2 - x^2)\left[\left(\frac{x}{b}\right)^2 - 1\right]^2, \qquad T(t) = 1 - \mathrm{e}^{-\alpha t},$$

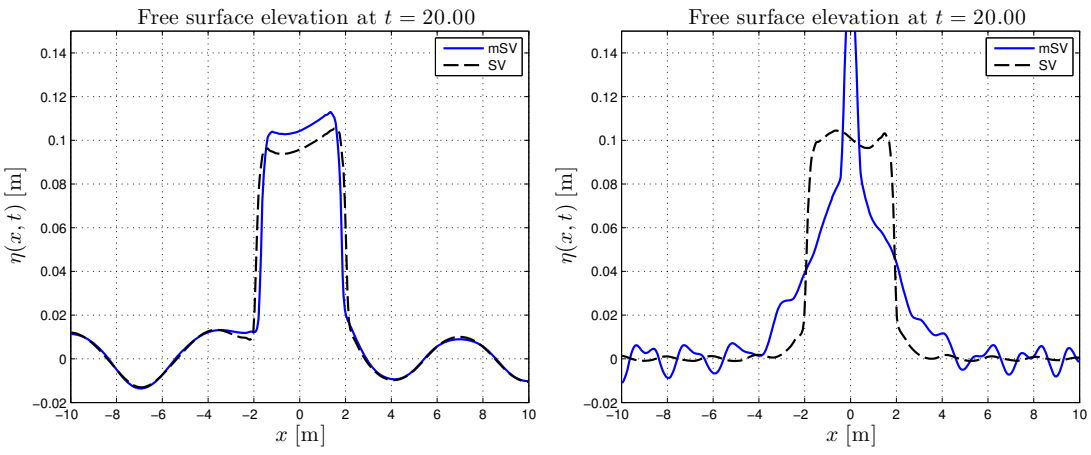

(a) *Low oscillations,* k_1 (b) *High oscillations,* k_2

Figure 4.22 | Wave propagation over an oscillatory bottom, $t = 20$ s.

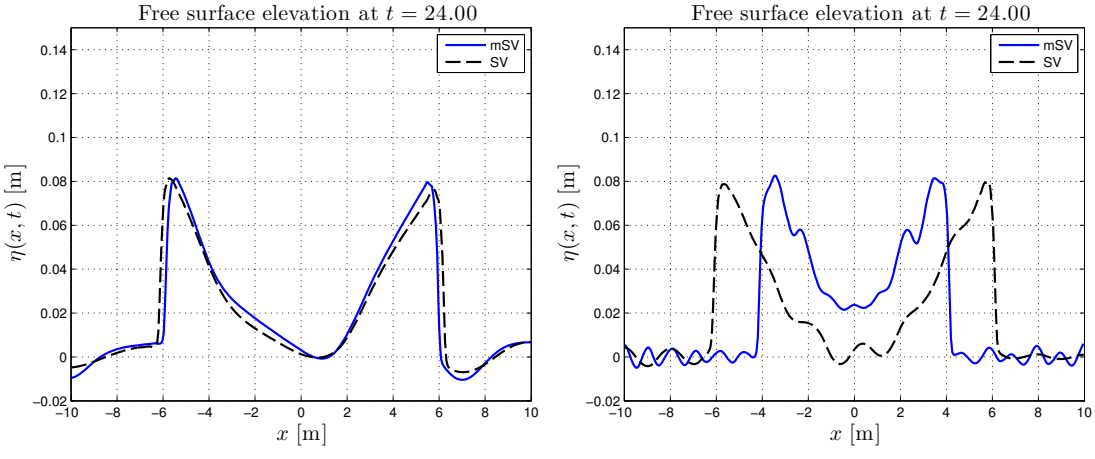

(a) *Low oscillations* (k_1) (b) *High oscillations* (k_2)

Figure 4.23 | Wave propagation over an oscillatory bottom, $t = 24$ s.

where $\mathrm{H}(x)$ is the Heaviside step function [1], a is the deformation amplitude and b is the half-length of the uplifting sea floor area. The function $T(t)$ provides us with complete information on the dynamics of the bottom motion. In tsunami wave literature, it is called a *dynamic scenario* [88, 118, 133]. Obviously, other choices of time dependence are possible. Initially, the free surface is undisturbed, and the velocity field is taken to be identically zero. The values of various parameters are given in Table 4.6.

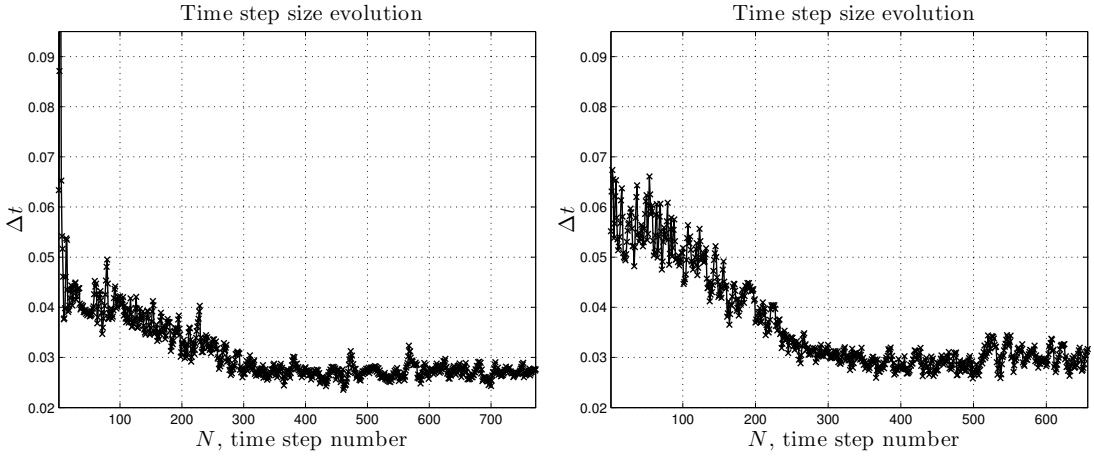

(a) *Low oscillations* (k_1) (b) *High oscillations* (k_2)

Figure 4.24 | Local time step size during the simulation of a wave propagating over an oscillatory bottom test case.

Table 4.6 | Values of various parameters used for the wave generation by a moving bottom.

Parameter	*Value*
Slow uplift parameter α_1:	$2.0\,\mathrm{s}^{-1}$
Fast uplift parameter α_2:	$12.0\,\mathrm{s}^{-1}$
Gravity acceleration g:	$1\,\mathrm{m\,s}^{-2}$
Final simulation time T:	5 s
Undisturbed water depth d_0:	1 m
Deformation amplitude a:	0.25 m
Half-length of the uplift area b:	2.5 m

Numerical results of the moving bottom test case are shown in Figures 4.25–4.30. In all these images, the blue solid line corresponds to the mSV equations, while the black dashed line refers to its classical counterpart. The dash-dotted line shows the bottom profile, which evolves in time as well.

First, we present numerical results (see Figures 4.25–4.26) corresponding to a relatively slow uplift of a portion of the bottom ($\alpha_1 = 2.0$). There is a very good agreement between the two computations. We note that the amplitude of bottom deformation $a/d = 0.25$ is strong, which explains some small discrepancies in Figure 4.26(a) between the two models. This effect is rather due to the bottom shape than to its dynamic motion.

Then we test the same situation, but the bottom uplift is fast with the inverse characteristic time $\alpha_2 = 12.0$. In this case, the differences between the two models are very flagrant. As it can be seen

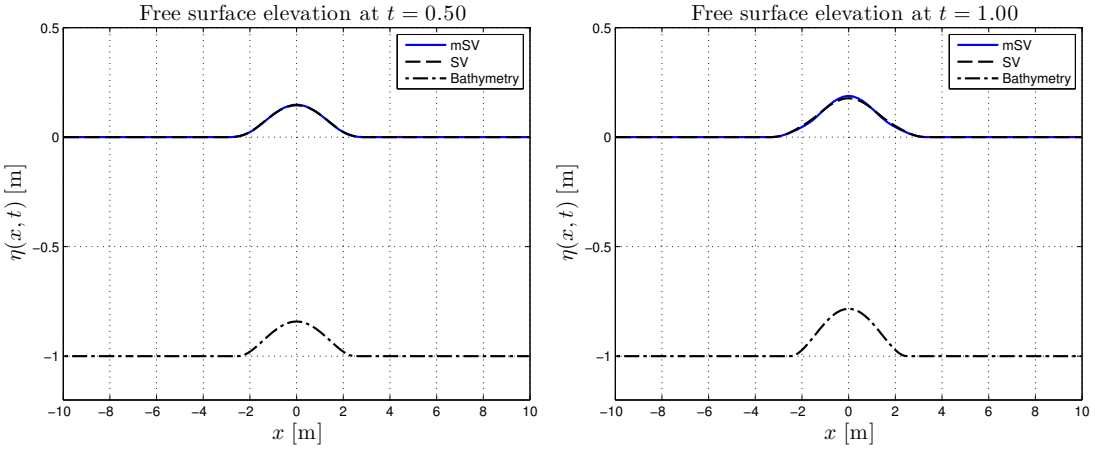

(a) $t = 0.5\,\mathrm{s}$ (b) $t = 1.0\,\mathrm{s}$

Figure 4.25 | Slow bottom uplift test-case ($\alpha_1 = 2$).

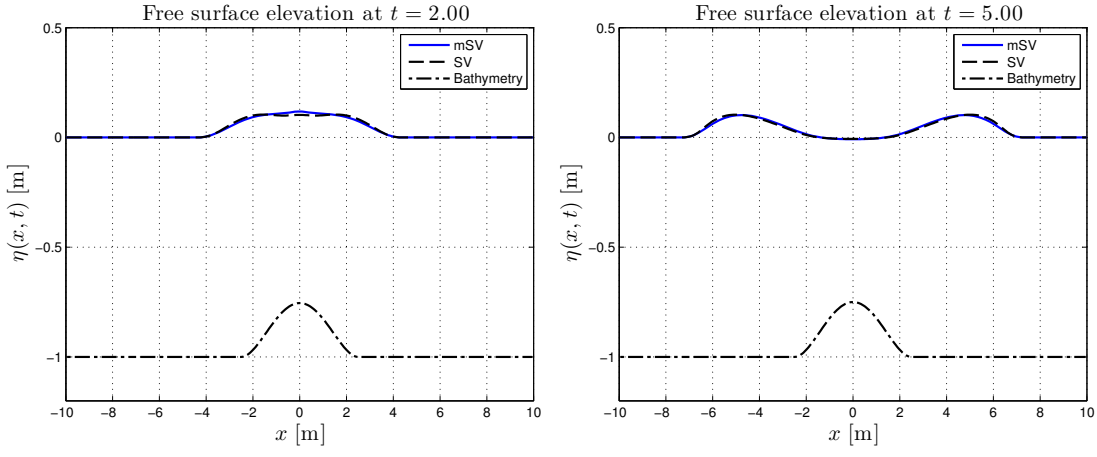

(a) $t = 2.0\,\mathrm{s}$ (b) $t = 5.0\,\mathrm{s}$

Figure 4.26 | Slow bottom uplift test-case ($\alpha_1 = 2$).

in Figure 4.28, for example, the mSV equations give a wave with almost two times higher amplitude. Some differences in the wave shape persist even during the propagation (see Figure 4.30). This test case clearly shows another advantage of the modified Saint-Venant equations in better representation of the vertical velocity field.

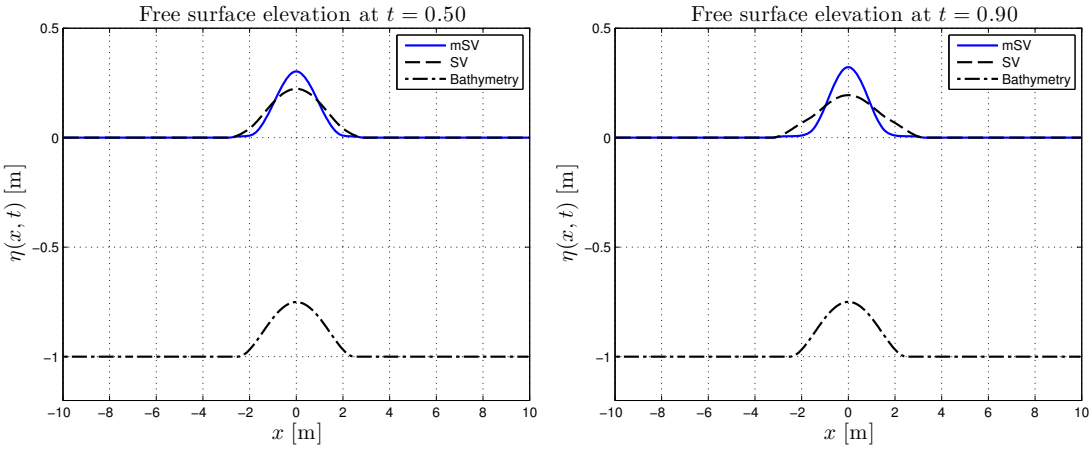

(a) $t = 0.5\,\mathrm{s}$ (b) $t = 0.9\,\mathrm{s}$

Figure 4.27 | Fast bottom uplift test-case ($\alpha_2 = 12$).

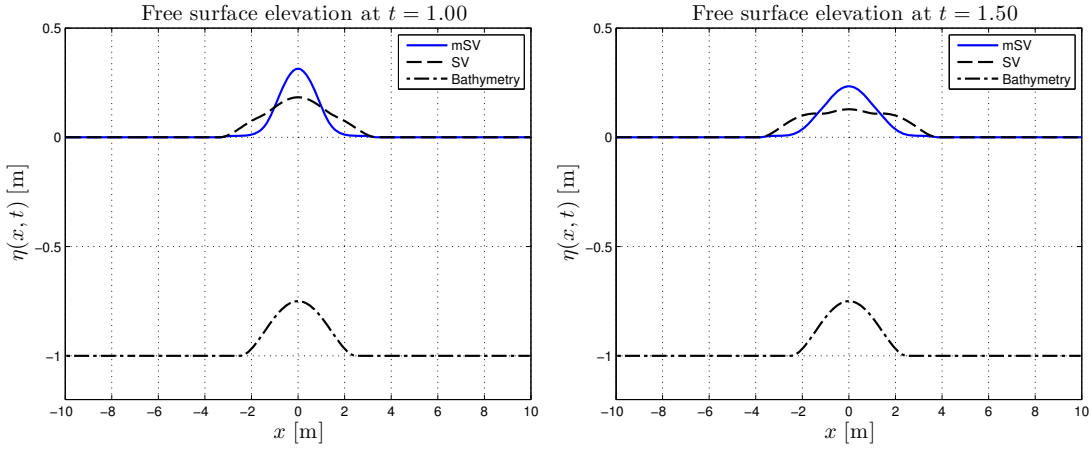

(a) $t = 1.0\,\mathrm{s}$ (b) $t = 1.5\,\mathrm{s}$

Figure 4.28 | Fast bottom uplift test-case ($\alpha_2 = 12$).

In Figure 4.31, we show the evolution of the local time step adapted while solving the mSV equations with moving bottom (up to $T = 5$ s). We can observe a behaviour very similar to the result presented above (see Figure 4.24) for the wave propagation test case.

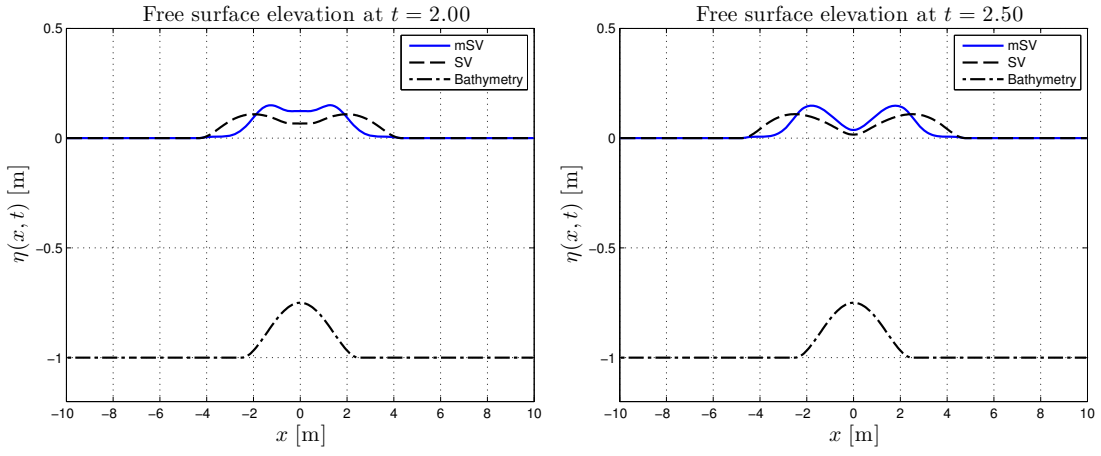

(a) $t = 2.0\,\mathrm{s}$ (b) $t = 2.5\,\mathrm{s}$

Figure 4.29 | Fast bottom uplift test-case ($\alpha_2 = 12$).

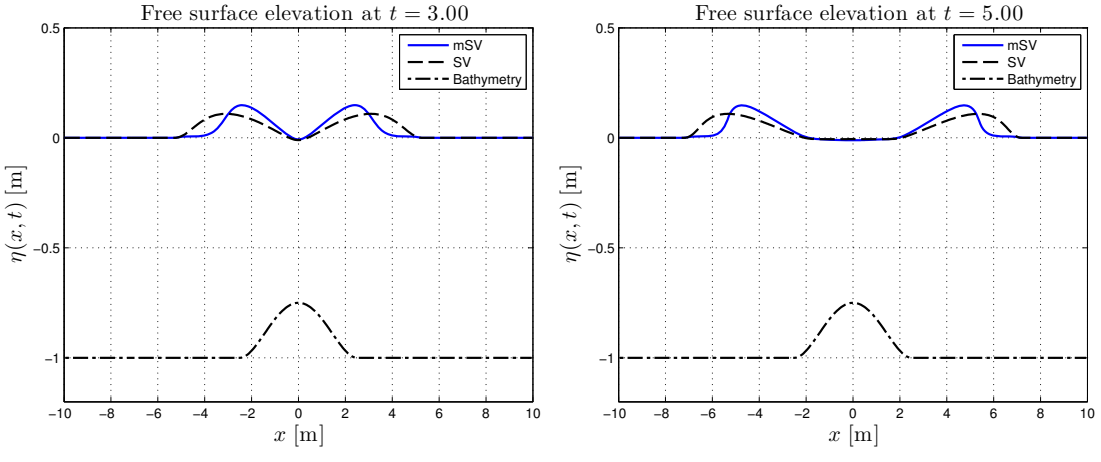

(a) $t = 3.0$ s (b) $t = 5.0$ s

Figure 4.30 | Fast bottom uplift test-case ($\alpha_2 = 12$).

Application to tsunami waves

Tsunami waves continue to pose various difficult problems to scientists, engineers and local authorities. There is one question initially stemming from the PhD thesis of Synolakis [218]. On page 85 of his manuscript, one can find a comparison between a theoretical (NSWE) and experimental wavefront paths during a solitary wave runup onto a plane beach. In particular, his results show some

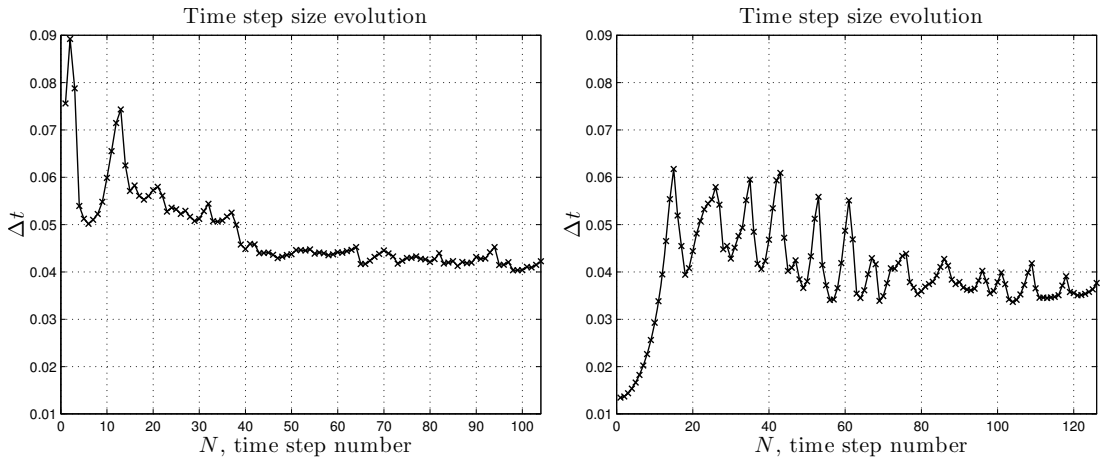

(a) *Slow uplift* (α_1) (b) *Fast uplift* (α_2)

Figure 4.31 | Local time step size evolution during the numerical experiment on wave generation by moving bottom.

discrepancies whose importance was not completely recognized until the wide availability of videos of the Tsunami Boxing Day 2004 [3, 182, 222]. In the same line of thinking, we quote here a recent review by Synolakis and Bernard [219], which contains a very interesting paragraph:

> *"In a video taken near the Grand Mosque in Aceh, one can infer that the wavefront first moved at speeds less than 8 km h^{-1}, then accelerated to 35 km h^{-1}. The same phenomenon is probably responsible for the mesmerization of victims during tsunami attacks, first noted in a series of photographs of the 1946 Aleutian tsunami approaching Hilo, Hawaii, and noted again in countless photographs and videos from the 2004 mega-tsunami. The wavefront appears slow as it approaches the shoreline, leading to a sense of false security, it appears as if one can outrun it, but then the wavefront accelerates rapidly as the main disturbance arrives."*

Since our new mSV model is able to take into account the local bottom slope into the wave speed computation, we propose a simple numerical setup which intends to shed some light on possible mechanisms of the reported above wavefront propagation anomalies. Consider a one-dimensional domain $[-20,\ 20]$ with wall boundary conditions. This domain is discretized into $N = 4000$ control volumes in order to resolve local bathymetry oscillations. The bottom has a uniform slope, which is perturbed on the left side ($x < 0$) by fast oscillations which model the bottom "steepness"

$$d(x) = d_0 - x\tan(\delta) + a\,[\,1\, - \mathrm{H}(x)\,]\sin(kx), \tag{4.90}$$

Table 4.7 | Values of various physical parameters used for the wave propagation over a sloping bottom.

Parameter	*Value*
Undisturbed water depth d_0:	1 m
Gravity acceleration g:	1 m s^{-2}
Bottom slope $\tan(\delta)$:	0.02
Oscillation amplitude a:	0.1 m
Oscillation wavenumber k:	20 m^{-1}
Final simulation time T:	19 s
Solitary wave amplitude A:	0.3 m
Solitary wave initial position x_0:	-12.0 m

where $\mathrm{H}(x)$ is the Heaviside function. The initial condition is a solitary wave moving rightwards as it was chosen in [218]:

$$\frac{\eta_0(x)}{d(x_0)} = A\,\mathrm{sech}^2\left(\tfrac{1}{2}\kappa(x-x_0)\right), \qquad u_0(x) = \frac{c_0\,\eta_0(x)}{d(x_0)+\eta_0(x)},$$
$$\kappa d(x_0) = \sqrt{\frac{3\,A}{1+A}}, \qquad \frac{c_0^2}{g\,d(x_0)} = 1+A.$$

This configuration aims to model a wave transition from steep to gentle bottoms. The values of various physical parameters are given in Table 4.7.

Then, the wave propagation and transformation over the sloping bottom 4.90 was computed using the classical and modified Saint-Venant (mSV) equations. The wavefront position was measured along this simulation, and the computation result is presented in Figure 4.32. The slope of these curves physically represents the wavefront propagation speed. Recall also that the point $x = 0$ corresponds to the transition between steep and gentle regions of the sloping beach.

As one can expect, the classical model does not really 'see' a region with bathymetry variations except from tiny oscillations. An observer situated on the beach, looking at the upcoming wave modelled by the classical Saint-Venant equations, will not see any change in the wave celerity. More precisely, the slope of the black dashed curve in Figure 4.32 is rather constant up to the graphical resolution. On the other hand, one can see a drastic change in the wavefront propagation speed predicted by the mSV equations when the bottom variation disappears.

The scenario we present in this section is only a first attempt to shed some light on the reported anomalies in tsunami wave arrival time on the beaches. For instance, a comprehensive study of Wessel [234] shows that the reported tsunami travel time often exceeds slightly the values predicted by the classical shallow water theory (see, for example, Figures 5 and 6 in [234]). This fact indirectly supports our theory. Certainly, this mechanism does not apply to laboratory experiments, but it can be

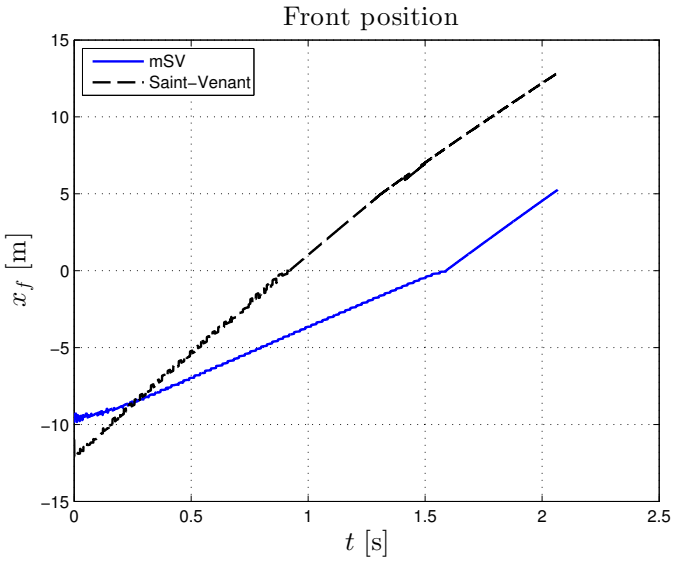

Figure 4.32 | Wave front position computed with modified and classical Saint-Venant equations.

a good candidate to explain the wavefront anomalies in natural environments. The mechanism we propose is only an element of explanation. Further investigations are needed to bring more validation to this approach.

We underline that the computational results rely on sound physical modelling without any *ad hoc* phenomenological terms in the governing equations. Only an accurate bathymetry description is required to take full advantage of the mSV equations.

4.7.7 | Intermediate conclusions

We derived a novel non-hydrostatic, non-dispersive model of shallow water type, which takes into account large bathymetric variations. Previously, some attempt was already made in the literature to derive shallow water systems for arbitrary slopes and curvature [22, 28, 78, 132]. However, our model contains a certain number of new elements with respect to the existing state of the art. Namely, our derivation procedure relies on a generalized Lagrangian principle of the water wave problem [52], which allows easily the derivations of approximations that cannot be obtained with more conventional asymptotic expansions. Indeed, we do not introduce explicitly any small parameter and our approximation is made through the choice of a suitable Ansatz. The resulting governing equations have a simple form and physically sound structure. Another new element is the introduction of

arbitrary bottom-time variations. Finally, the non-hydrostatic character of obtained equations is fundamentally different from the well-known Boussinesq-type and mild-slope models. The reason for the non-hydrostaticity of mSV equations lies in the pressure term and not in the frequency dispersion.

The proposed model was discretised with a finite volume scheme with adaptive time stepping to capture the underlying complex dynamics. The performance of this scheme is then illustrated in several test cases. Some implications for tsunami wave modelling are also suggested at the end of this study. For ocean modelling, the most interesting feature of the model is perhaps the prediction that a wave slows down due to the bottom slope. Among various perspectives, we would like to underline the importance of a robust runup algorithm development using the current model. This research should shift forward the accuracy and our comprehension of a water wave runup onto complex shores [92, 94].

CHAPTER 5

Deep water examples

The deep water approximation is the opposite of the shallow water case when $h/\lambda \gg 1$, *i.e.* the water depth is much larger than the typical wavelength. In practice, some deep water effects (defocussing type of the Nonlinear Schrödinger equation (NSE) equation) can already manifest when $kh = 2\pi h/\lambda \gtrsim 1.36$. This regime is relevant for most wave evolution problems in open oceans [23]. The sketch of the fluid domain is shown in Figure 5.1. Some classical variational structures of water wave equations in the deep water regime are described in appendix D.

For waves in deep water, measurements show that the velocity field varies nearly exponentially along the vertical [117, 127], even for very large, unsteady waves (including breaking waves). Thus, this property is exploited here to derive a simple approximation for gravity waves in deep water (*cf.* Figure 5.1).

5.1 | State of the art

The golden standard in deep water wave modelling is incontestably the cubic Zakharov model used, recently *e.g.* in [97, 139] to study wave (weak) turbulence [246]. These equations are obtained by expanding the Hamiltonian in the wave steepness parameter

$$\mathcal{H} = \mathcal{H}_0 + \mathcal{H}_1 + \mathcal{H}_2 + \cdots .$$

The cubic Zakharov equations (*cf.* Appendix B) are obtained by truncating this expansion after quartic terms (thus, the governing equations are effectively cubic after taking the variations). This model is weakly nonlinear, but it is valid for the whole spectrum of gravity waves. Cubic Zakharov equations are well understood nowadays. Consequently, in the present study, we focus on models which do the opposite: on the one hand, there are *a priori* no assumptions on the nonlinearity parameter. On the other hand, we describe waves around a certain wavenumber κ. Let us review the state of the art by following the main steps of [141]. However, below, we generalize their computations to the three-dimensional case.

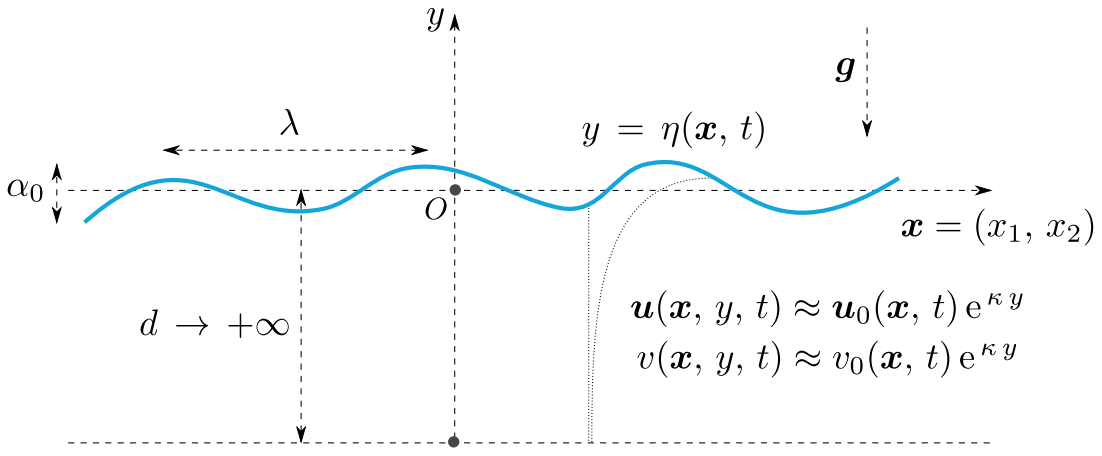

Figure 5.1 | Sketch of the physical fluid domain in the deep water case.

Consider the incompressible Euler equations:

$$\boldsymbol{\nabla} \cdot \boldsymbol{u} + v_y = 0, \tag{5.1}$$

$$\dot{\boldsymbol{u}} + \boldsymbol{\nabla} p = \boldsymbol{0}, \tag{5.2}$$

$$\dot{v} + p_y + g = 0, \tag{5.3}$$

where p is the fluid pressure, and the over dot denotes the total material derivative, *i.e.*

$$\dot{(\cdot)} \stackrel{\text{def}}{=} (\cdot)_t + \boldsymbol{u} \cdot \boldsymbol{\nabla}(\cdot) + v\,(\cdot)_y.$$

The governing equations are completed with the following boundary conditions:

$$\eta_t + \boldsymbol{u} \cdot \boldsymbol{\nabla}\eta = v, \qquad y = \eta(\boldsymbol{x}, t), \tag{5.4}$$

$$p = p_a, \qquad y = \eta(\boldsymbol{x}, t), \tag{5.5}$$

$$|\boldsymbol{u}|,\ |v| \to 0, \qquad y \to -\infty, \tag{5.6}$$

where p_a is the constant atmospheric pressure.

In order to derive an approximate model, Kraenkel *et al.* [141] propose to take the following solution Ansatz for the Euler equations 5.1–5.3:

$$\boldsymbol{u}(\boldsymbol{x}, y, t) = \boldsymbol{u}_0(\boldsymbol{x}, t)\, \mathrm{e}^{\kappa y}, \quad v(\boldsymbol{x}, y, t) = -\frac{1}{\kappa}\, (\boldsymbol{\nabla} \cdot \boldsymbol{u}_0)\, \mathrm{e}^{\kappa y}. \tag{5.7}$$

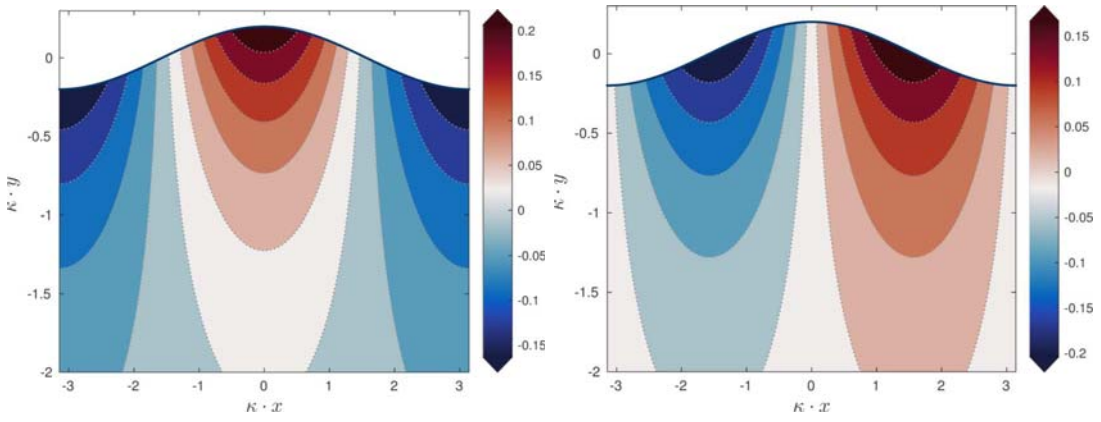

(a) $u_1(x_1, y, t)$ (b) $v(x_1, y, t)$

Figure 5.2 | Vertical structure of the chosen Ansatz 5.7 under a simple linear travelling periodic wave: (a) the horizontal and (b) vertical components of the velocity field. The periodic wave amplitude is $\alpha = 0.2$.

From the above Ansatz, it is straightforward to understand the physical sense of the variable $\boldsymbol{u}_0$ — it is simply the value of the 3D horizontal velocity $\boldsymbol{u}$ on the surface[23] $y = 0$. Other Ansätze will be considered below. Here, $\kappa = \text{const}$ is the wavenumber around which we model water waves in the spectral domain. The vertical velocity Ansatz is chosen to satisfy identically the free surface incompressibility 5.1. The velocity fields under a linear periodic wave predicted by this Ansatz are represented in Figure 5.2.

Substituting Ansatz 5.7 into the kinematic boundary condition 5.4, we readily obtain the mass conservation equation:

$$\kappa \eta_t + \boldsymbol{\nabla} \cdot \left[\boldsymbol{u}_0 \, \mathrm{e}^{\kappa \eta} \right] = 0. \tag{5.8}$$

In order to derive momentum balance equations, we first compute the material derivatives using Ansatz 5.7:

$$\dot{\boldsymbol{u}} = \boldsymbol{u}_{0t} \, \mathrm{e}^{\kappa y} + \mathscr{C} \, \mathrm{e}^{2\kappa y},$$
$$-\kappa \, \dot{v} = \mathscr{A} \, \mathrm{e}^{\kappa y} + \mathscr{B} \, \mathrm{e}^{2\kappa y},$$

[23] It is a direct consequence of the Asatz 5.7.

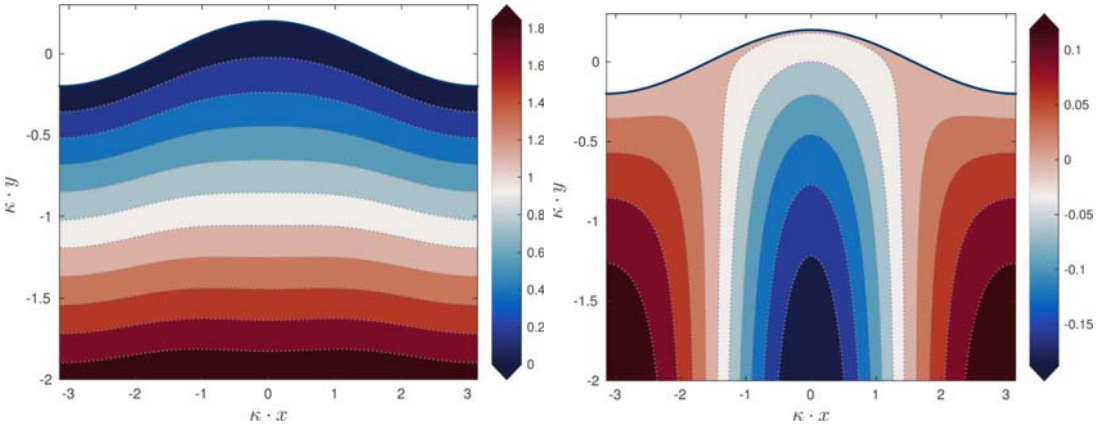

(a) $(p - p_a)(x_1, y, t)$ (b) $p_d(x_1, y, t)$

Figure 5.3 | Fluid pressure distribution under a linear travelling wave as predicted by equation 5.9 (a). The right panel (b) shows the dynamic pressure $p_d \overset{\text{def}}{=} p - p_a - g(\eta - y)$ distribution (*i.e.* without hydrostatic effects). The periodic wave amplitude is $\alpha = 0.2$.

where $\mathscr{A}$, $\mathscr{B}$ and $\mathscr{C} = \left(\mathscr{C}_1, \mathscr{C}_2\right)$ are defined as

$$\mathscr{A} = \boldsymbol{\nabla} \cdot \boldsymbol{u}_{0\,t}, \qquad \mathscr{B} = \boldsymbol{\nabla}(\boldsymbol{\nabla} \cdot \boldsymbol{u}_0) \cdot \boldsymbol{u}_0 - (\boldsymbol{\nabla} \cdot \boldsymbol{u}_0)^2,$$
$$\mathscr{C}_1 = u_2 \frac{\partial u_1}{\partial x_2} - u_1 \frac{\partial u_2}{\partial x_2}, \qquad \mathscr{C}_2 = u_1 \frac{\partial u_2}{\partial x_1} - u_2 \frac{\partial u_1}{\partial x_1}.$$

By substituting $\dot{v}$ into 5.3 and taking into account the boundary condition 5.5, we obtain the pressure distribution in the fluid bulk:

$$p - p_a = g(\eta - y) + \frac{1}{\kappa^2}\left[\left(\mathrm{e}^{\kappa y} - \mathrm{e}^{\kappa \eta}\right)\mathscr{A} + \frac{1}{2}\left(\mathrm{e}^{2\kappa y} - \mathrm{e}^{2\kappa \eta}\right)\mathscr{B}\right]. \tag{5.9}$$

Notice that the pressure field p diverges when $y \to -\infty$ due to the hydrostatic effects (in agreement with the Archimedes law). The pressure distribution under a linear periodic wave is shown in Figure 5.3.

The problem now is to satisfy in some sense equation 5.2 with available expressions for $\dot{\boldsymbol{u}}$ and p. Kraenkel *et al.* proposed the following weak formulation:

$$\int_{-\infty}^{\eta} \left[\dot{\boldsymbol{u}} + \boldsymbol{\nabla} p\right] \mathrm{e}^{\mathfrak{m} y}\, \mathrm{d}y = \boldsymbol{0},$$

where $\mathfrak{m} > 0$ is a modelling parameter to be chosen later. So, the Newton law is satisfied in a weak sense. The exponential weight function allows us to overcome the problem of Archimedian pres-

sure divergence. In order to derive the momentum equation in a conservative form, we shall use the equivalent form:

$$\int_{-\infty}^{\eta} \dot{\boldsymbol{u}}\, \mathrm{e}^{\mathrm{m}y}\, \mathrm{d}y + \boldsymbol{\nabla}\left[\int_{-\infty}^{\eta} p\, \mathrm{e}^{\mathrm{m}y}\, \mathrm{d}y\right] - p_a\, \mathrm{e}^{\mathrm{m}\eta}\cdot\boldsymbol{\nabla}\eta = \mathbf{0}.$$

After performing all computations, we obtain the desired horizontal momentum equation:

$$\frac{\mathrm{e}^{(\mathrm{m}+\kappa)\eta}}{\mathrm{m}+\kappa}\left[\boldsymbol{u}_{0t} + \frac{\mathrm{m}+\kappa}{\mathrm{m}+2\,\kappa}\,\mathrm{e}^{\kappa\eta}\,\mathscr{C}\right] + \boldsymbol{\nabla}\left[g\,\frac{\mathrm{e}^{\mathrm{m}\eta}}{\mathrm{m}^2} - \mathscr{A}\,\frac{\mathrm{e}^{(\mathrm{m}+\kappa)\eta}}{\kappa\,\mathrm{m}\,(\mathrm{m}+\kappa)} - \frac{1}{2}\,\mathscr{B}\,\frac{\mathrm{e}^{(\mathrm{m}+2\kappa)\eta}}{\kappa\,\mathrm{m}\,(\mathrm{m}+2\kappa)}\right] = \mathbf{0}. \tag{5.10}$$

These equations 5.8 and 5.10 constitute a closed system which describes the evolution of water waves in deep water.

Remark 5.1. In order to make a check of the derivation made above, we shall restrict our attention to the two-dimensional case. Here we can set $u_{01} \rightsquigarrow u$, $u_{02} \rightsquigarrow 0$ and dependent coefficients become:

$$\mathscr{A} \rightsquigarrow u_{xt}, \qquad \mathscr{B} \rightsquigarrow u\,u_{xx} - u_x^2, \qquad \mathscr{C} \rightsquigarrow \mathbf{0}.$$

Thus, Equations 5.8 and 5.10 in 2D become:

$$\kappa\,\eta_t + \left[u\,\mathrm{e}^{\kappa\eta}\right]_x = 0, \tag{5.11}$$

$$\frac{\mathrm{e}^{(\mathrm{m}+\kappa)\eta}}{\mathrm{m}+\kappa}\,u_t + \left[g\,\frac{\mathrm{e}^{\mathrm{m}\eta}}{\mathrm{m}^2} - u_{xt}\,\frac{\mathrm{e}^{(\mathrm{m}+\kappa)\eta}}{\kappa\,\mathrm{m}\,(\mathrm{m}+\kappa)} - \left(u\,u_{xx} - u_x^2\right)\frac{\mathrm{e}^{(\mathrm{m}+2\kappa)\eta}}{\kappa\,\mathrm{m}\,(\mathrm{m}+2\kappa)}\right]_x = 0. \tag{5.12}$$

By switching to dimensionless variables ($g \rightsquigarrow 1$, $\kappa \rightsquigarrow 1$) we recover equations (2.18) and (2.20) from [141].

As we saw above, the water wave problem possesses Hamiltonian and Lagrangian variational structures. The question we can ask is whether just derived equations 5.8, 5.10 (which are supposed to approximate the full Euler equations) possess at least one of these structures. By looking at equations 5.8, 5.10 the answer is not clear. Even in the 'Conclusion and comments' section in [141], the Authors admit that they did not succeed in finding a Hamiltonian formulation even for the short wave limit of these equations. We shall propose some fixes to this problem below.

5.1.1 | Choice of the modelling parameter

In order to derive a physically sound value for the modelling parameter m, we consider the governing equations in 2D, and we linearize Equations 5.11, 5.12:

$$\kappa\,\eta_t + u_x = 0,$$

$$\frac{1}{\mathrm{m}+\kappa}\,u_t + \left[\frac{g}{\mathrm{m}}\,\eta - \frac{1}{\kappa\,\mathrm{m}\,(\mathrm{m}+\kappa)}\,u_{xt}\right]_x = 0.$$

It is easy to eliminate the variable η from the above equations to obtain the linear version of the so-called *improved* Boussinesq *equation*:

$$\mathfrak{m}\,\kappa\,u_{tt} - g\,(\mathfrak{m}+\kappa)\,u_{xx} - u_{ttxx} = 0.$$

Then, we look for plane wave solutions of the form:

$$u(x,t) = \alpha_0\,\mathrm{e}^{\mathrm{i}(kx-\omega t)}.$$

Such solutions exist only if wave frequency ω and wavenumber k are related by the following relation, which is called the *dispersion relation*:

$$c_p(k) = \frac{\omega(k)}{k} = \sqrt{g\,\frac{\mathfrak{m}+\kappa}{\mathfrak{m}\,\kappa + k^2}}.$$

The ratio $c_p(k)$ is called the *phase velocity*. Notice that in the limit $k \to \kappa$ we obtain

$$\lim_{k\to\kappa}\frac{\omega(k)}{k} = \sqrt{\frac{g}{\kappa}},$$

which coincides with the exact phase velocity of the full Euler equations in deep water. Finally, in order to determine the modelling parameter $\mathfrak{m}$, we consider the *group velocity*:

$$c_g(k) \stackrel{\text{def}}{=} \frac{\partial\omega(k)}{\partial k}.$$

In the limit $k \to \kappa$, we obtain

$$\lim_{k\to\kappa} c_g(k) = \frac{\mathfrak{m}}{\mathfrak{m}+\kappa}\cdot\sqrt{\frac{g}{\kappa}}.$$

Now, it is straightforward to notice that we recover the exact expression $c_g(\kappa) = \frac{1}{2}\cdot\sqrt{\frac{g}{\kappa}}$ for deep water Euler equations only if $\mathfrak{m} \equiv \kappa$. This is the desired value of the modelling parameter $\mathfrak{m}$.

5.2 | Variational derivations

In the ensuing section, we are poised to present alternative derivations of the model equations akin to equations 5.8, 5.10, albeit rooted in the relaxed variational principle embodied in equation D.4. It is pivotal to note that the models emergent from this variational derivation might exhibit distinctions, and as will be elucidated, they indeed deviate from equations 5.8, 5.10. The crux of this alternative approach lies in the preservation of the Lagrangian structure, a feature inherent to the construction of the variational principle employed. This preservation is not merely a mathematical nicety, but a profound attribute that facilitates a coherent and structured exploration of the dynamical

behavior underpinning the model equations. By anchoring our derivations in the relaxed variational principle D.4, we are effectively harnessing a robust framework that not only engenders alternative model equations but also upholds the Lagrangian structural integrity.

5.2.1 | Weakly compressible Ansatz

Consider an Ansatz similar to 5.7:

$$\phi(\boldsymbol{x}, y, t) = \phi_0(\boldsymbol{x}, t)\, \mathrm{e}^{\kappa y},\ \boldsymbol{u}(\boldsymbol{x}, y, t) = \boldsymbol{u}_0(\boldsymbol{x}, t)\, \mathrm{e}^{\kappa y},\ v(\boldsymbol{x}, y, t) = v_0(\boldsymbol{x}, t)\, \mathrm{e}^{\kappa y}. \tag{5.13}$$

The main difference with 5.7 is that here, the vertical velocity approximation v_0 is kept independent from $\boldsymbol{u}_0$, and it will be chosen by the variational principle. Substituting 5.13 into Lagrangian D.4 and performing exactly all the integrations over the depth, we obtain the following Lagrangian density:

$$\begin{aligned}\mathcal{L} = &-\Big[\eta_t + \big(\boldsymbol{u}_0 \cdot \boldsymbol{\nabla}\eta - v_0\big)\, \mathrm{e}^{\kappa\eta}\Big]\, \phi_0\, \mathrm{e}^{\kappa\eta} + \frac{1}{2}\, g\, \eta^2 \\ &- \frac{1}{2\,\kappa}\, \Big[\tfrac{1}{2}\big(|\boldsymbol{u}_0|^2 + v_0^2\big) - \big(\boldsymbol{\nabla}\cdot\boldsymbol{u}_0 + \kappa\, v_0\big)\, \phi_0\Big]\, \mathrm{e}^{2\kappa\eta}.\end{aligned} \tag{5.14}$$

The governing equations are then obtained by computing variations of this functional:

$$\begin{aligned}\delta\phi_0:&\quad \eta_t + \big(\boldsymbol{u}_0 \cdot \boldsymbol{\nabla}\eta - v_0\big)\, \mathrm{e}^{\kappa\eta} = \frac{1}{2\,\kappa}\, \big(\boldsymbol{\nabla}\cdot\boldsymbol{u}_0 + \kappa\, v_0\big)\, \mathrm{e}^{\kappa\eta}, \\ \delta\boldsymbol{u}_0:&\quad \boldsymbol{u}_0 + \boldsymbol{\nabla}\phi_0 + 4\,\kappa\,\phi_0\,\boldsymbol{\nabla}\eta = \boldsymbol{0}, \\ \delta v_0:&\quad \phi_0 - \frac{1}{2\,\kappa}\, \big(v_0 - \kappa\,\phi_0\big) = 0, \\ \delta\eta:&\quad \big(\phi_0\, \mathrm{e}^{\kappa\eta}\big)_t + \boldsymbol{\nabla}\cdot\big[\phi_0\, \boldsymbol{u}_0\, \mathrm{e}^{2\kappa\eta}\big] + g\,\eta \\ &\quad - \Big[\tfrac{1}{2}\big(|\boldsymbol{u}_0|^2 + v_0^2\big) - \big(\boldsymbol{\nabla}\cdot\boldsymbol{u}_0 + \kappa\, v_0\big)\, \phi_0\Big]\, \mathrm{e}^{2\kappa\eta} \\ &\quad - \kappa\, \Big[\eta_t + 2\,\big(\boldsymbol{u}_0 \cdot \boldsymbol{\nabla}\eta - v_0\big)\, \mathrm{e}^{\kappa\eta}\Big]\, \phi_0\, \mathrm{e}^{\kappa\eta} = 0.\end{aligned}$$

The Euler–Lagrange equations turn out to be rather complicated. However, we can learn some lessons nevertheless. The variation $\delta\boldsymbol{u}_0$ gives us the connection between the horizontal velocity $\boldsymbol{u}_0$ and the velocity potential ϕ_0 (thus, $\boldsymbol{u}_0$ can be, in principle, eliminated from the equations). In particular, one can see that the flow is *not* irrotational. The variation δv_0 gives us the expression of the vertical velocity $v_0 = 3\kappa\phi_0$ in terms of the velocity potential. The variation with respect to η gives the analogue of the Cauchy–Lagrange integral (*i.e.* an *unsteady* Bernoulli equation). Finally, the variation with respect to

ϕ_0 gives us the mass conservation equation, and in order to have a conservative form, it is better to reinforce the flow incompressibility, *i.e.*

$$\boldsymbol{\nabla} \cdot \boldsymbol{u}_0 + \kappa\, v_0 \;\equiv\; 0.$$

It will be done in the following section.

5.2.2 | Exactly incompressible Ansatz

Now, we take the same Ansatz 5.13, but the vertical velocity approximation v_0 is chosen in order to satisfy identically the incompressibility condition. It is not difficult to see that this goal can be achieved by taking $v_0 \;\equiv\; -\frac{1}{\kappa}\;\boldsymbol{\nabla} \cdot \boldsymbol{u}_0$. In this way, we recover Ansatz 5.7 proposed by Kraenkel *et al.* [141]. Substituting this expression for v_0 into the Lagrangian density 5.14, we obtain the following slightly more compact density functional:

$$\mathcal{L} = -\Big[\, \eta_t + \big(\boldsymbol{u}_0 \cdot \boldsymbol{\nabla}\eta + \frac{1}{\kappa}\;\boldsymbol{\nabla} \cdot \boldsymbol{u}_0\big)\; \mathrm{e}^{\kappa\eta} \,\Big]\; \phi_0\, \mathrm{e}^{\kappa\eta} + \frac{1}{2}\, g\, \eta^2 - \frac{1}{4\,\kappa}\, \Big[\, |\boldsymbol{u}_0|^2 + \frac{1}{\kappa^2}\, (\boldsymbol{\nabla} \cdot \boldsymbol{u}_0)^2 \,\Big]\; \mathrm{e}^{2\kappa\eta}.$$

The Euler–Lagrange equations yield the following system:

$$\begin{aligned}
\delta\phi_0 :\quad & \kappa\, \eta_t + \boldsymbol{\nabla} \cdot \big(\boldsymbol{u}_0\, \mathrm{e}^{\kappa\eta}\big) \;=\; 0, \\
\delta\boldsymbol{u}_0 :\quad & \boldsymbol{\nabla}\Big(\big(\boldsymbol{\nabla} \cdot \boldsymbol{u}_0\big)\, \mathrm{e}^{2\kappa\eta}\Big) - \kappa^2\, \boldsymbol{u}_0\, \mathrm{e}^{2\kappa\eta} = 2\,\kappa^3\, \phi_0\, \boldsymbol{\nabla}\eta\, \mathrm{e}^{2\kappa\eta} - 2\,\kappa^2\, \boldsymbol{\nabla}\Big(\phi_0\, \mathrm{e}^{2\kappa\eta}\Big), \\
\delta\eta :\quad & \big(\phi_0\, \mathrm{e}^{\kappa\eta}\big)_t + \boldsymbol{\nabla} \cdot \big[\, \phi_0\, \boldsymbol{u}_0\, \mathrm{e}^{2\kappa\eta} \,\big] + g\, \eta \\
& - \kappa\, \boldsymbol{\nabla} \cdot \Big(\boldsymbol{u}_0\, \mathrm{e}^{\kappa\eta}\Big)\, \phi_0\, \mathrm{e}^{2\kappa\eta} - \frac{1}{2}\, \Big[\, |\boldsymbol{u}_0|^2 + \frac{1}{\kappa^2}\, (\boldsymbol{\nabla} \cdot \boldsymbol{u}_0)^2 \,\Big] = 0.
\end{aligned}$$

Even if these equations are more compact (than the system we obtained in section 5.2.1) and the mass conservation coincides exactly with 5.8, still, this system seems to be quite complicated. This time, it follows from the variation $\delta\boldsymbol{u}_0$ that in order to reconstruct the horizontal velocity $\boldsymbol{u}_0$ from the velocity potential ϕ_0, one has to solve an elliptic (vectorial) equation.

Intermediate conclusions. We saw above that the variational method can easily lead to complicated and unamenable equations, even if the latter naturally inherits the variational structure. Consequently, the choice of good Ansatz is absolutely crucial for the derivation of an approximate model. In this respect, a better Ansatz will be proposed below.

5.3 | Alternative deep water Ansatz

Let $\kappa > 0$ be a characteristic wavenumber corresponding, *e.g.*, to the carrier wave of a modulated wave group or to the peak frequency of a JONSWAP spectrum. Following the discussion above, it is

natural to seek approximations in the form

$$\{\,\phi\,;\,u\,;\,v\,\} \approx \{\,\tilde{\phi}\,;\,\tilde{u}\,;\,\tilde{v}\,\}\,\mathrm{e}^{\kappa(y-\eta)}, \tag{5.15}$$

where $\tilde{\phi}$, $\tilde{u}$ and $\tilde{v}$ are functions of x and t that can be determined using the variational principle (with or without additional constraints). The Ansatz 5.15 is certainly the simplest possible that is consistent with experimental pieces of evidence.

The Ansatz 5.15 substituted into the Lagrangian density 3.7 yields

$$2\,\kappa\,\mathscr{L} = 2\kappa\,\tilde{\phi}\,\eta_t - g\,\kappa\,\eta^2 + \tfrac{1}{2}\,\tilde{u}^2 + \tfrac{1}{2}\,\tilde{v}^2 - (\tilde{\phi}_x - \kappa\,\tilde{\phi}\,\eta)\,\tilde{u} - \kappa\,\tilde{v}\,\tilde{\phi}. \tag{5.16}$$

With (or without) subordinate relations, this Lagrangian gives various equations.

5.4 | Unconstrained approximation

We present here the case without further constraints; thus, the Euler–Lagrange equations to Lagrangian density 5.16 yield [81]:

$$\begin{aligned}
\delta\,\tilde{u}: &\quad 0 = \tilde{u} - \tilde{\phi}_x + \kappa\,\tilde{\phi}\,\eta_x,\\
\delta\,\tilde{v}: &\quad 0 = \tilde{v} - \kappa\,\tilde{\phi},\\
\delta\,\tilde{\phi}: &\quad 0 = 2\kappa\,\eta_t + \tilde{u}_x - \kappa\,\tilde{v} + \kappa\,\tilde{u}\,\eta_x,\\
\delta\,\eta: &\quad 0 = 2\,g\,\kappa\,\eta + 2\,\kappa\,\tilde{\phi}_t + \kappa\,[\,\tilde{\phi}\,\tilde{u}\,]_x.
\end{aligned}$$

The two first relations imply that this approximation is exactly rotational, and their use in the last two equations gives

$$\eta_t + \tfrac{1}{2}\,\kappa^{-1}\,\tilde{\phi}_{xx} - \tfrac{1}{2}\,\kappa\,\tilde{\phi} = \tfrac{1}{2}\,\tilde{\phi}\,\left[\,\eta_{xx} + \kappa\,\eta_x^2\,\right], \tag{5.17}$$

$$\tilde{\phi}_t + g\,\eta = -\tfrac{1}{2}\,\left[\,\tilde{\phi}\,\tilde{\phi}_x - \kappa\,\tilde{\phi}^2\,\eta_x\,\right]_x. \tag{5.18}$$

Since Equations 5.17, 5.18 derive from an irrotational motion, they can also be obtained from Luke's Lagrangian 3.1 under the Ansatz 5.15. That would not be the case if, for example, we had enforced the incompressibility in the Ansatz because, here, that leads to a rotational Ansatz (see [52, Section §4.3]). Equations 5.17 and 5.18 are a deep water counterpart of Saint-Venant equations for shallow water waves.

It is straightforward to verify that the gKG equations possess a canonical Hamiltonian structure

$$\begin{pmatrix}\partial_t\eta\\ \partial_t\tilde{\phi}\end{pmatrix} = \mathbb{J}\cdot\begin{pmatrix}\delta\,\mathcal{H}\,/\,\delta\tilde{\phi}\\ \delta\,\mathcal{H}\,/\,\delta\eta\end{pmatrix}, \qquad \mathbb{J} = \begin{pmatrix}0 & -1\\ 1 & 0\end{pmatrix},$$

where the Hamiltonian functional $\mathcal{H}$ is defined as

$$\mathcal{H} = \int_\Omega \left\{ \tfrac{1}{2}\, g\, \eta^2 + \tfrac{1}{4}\, \kappa^{-1} \left[\boldsymbol{\nabla} \tilde{\phi} - \kappa\, \tilde{\phi}\, \boldsymbol{\nabla} \eta \right]^2 + \tfrac{1}{4}\, \kappa\, \tilde{\phi}^2 \right\} \mathrm{d}^2 \boldsymbol{x}. \tag{5.19}$$

This Hamiltonian is quartic in nonlinearities and involves only first-order derivatives. It has to be compared with Zakharov's quartic Hamiltonian B.2, which involves second-order derivatives and pseudo-differential operators. However, Zakharov's quartic Hamiltonian is valid for broad spectra. Note that the Hamiltonian 5.19 cannot be derived from the exact one B.1, since the latter assumes that irrotationality and incompressibility are both satisfied identically in bulk, while the incompressibility is not fulfilled by equations 5.17, 5.18.

To the linear approximation, after elimination of $\tilde{\phi}$, equations 5.17, 5.18 yield

$$\eta_{tt} - (g/2\kappa)\, \eta_{xx} + (g\kappa/2)\, \eta = 0, \tag{5.20}$$

that is a Klein–Gordon equation. For this reason, equations 5.17 and 5.18 are named here generalized Klein–Gordon equations (gKG). The Klein–Gordon equation is prominent in mathematical physics and appears, *e.g.*, as a relativistic generalization of the Schrödinger equation. The Klein–Gordon equation 5.20 admits a special $(2\pi/k)$-periodic travelling wave solution

$$\eta = a \cos k(x - ct), \qquad c^2 = g \left(k^2 + \kappa^2 \right) / \left(2\, \kappa\, k^2 \right).$$

Therefore, if $k = \kappa$ the exact dispersion relation of linear waves (*i.e.*, $c^2 = g/k$) is recovered, as it should be. This means, in particular, that the gKG model is valid for spectra narrow-banded around the wavenumber κ. Further details and properties of the gKG are given in [52, Section §4.2] and in [81].

5.4.1 | Stokes wave

We focus now on $(2\pi/\kappa)$-periodic progressive waves solution of the gKG equations 5.17, 5.18, *i.e.*, we seek for solutions depending only on the variable $\theta = \kappa(x_1 - ct)$. We were not able to find an exact analytic solution, but a Stokes-like expansion gives some interesting insights. To the seventh order, we have

$$\begin{aligned} \kappa\, \eta = {} & \alpha \cos\theta + \tfrac{1}{2}\alpha^2 \left(1 + \tfrac{25}{12}\alpha^2 + \tfrac{1675}{192}\alpha^4 \right) \cos 2\theta \\ & + \tfrac{3}{8}\alpha^3 \left(1 + \tfrac{99}{16}\alpha^2 + \tfrac{11807}{320}\alpha^4 \right) \cos 3\theta + \tfrac{1}{3}\alpha^4 \left(1 + \tfrac{64}{5}\alpha^2 \right) \cos 4\theta \\ & + \tfrac{125}{384}\alpha^5 \left(1 + \tfrac{6797}{300}\alpha^2 \right) \cos 5\theta + \tfrac{27}{80}\alpha^6 \cos 6\theta + \tfrac{16807}{46080}\alpha^7 \cos 7\theta + \mathcal{O}(\alpha^8), \end{aligned}$$

$$
\begin{aligned}
g^{-\frac{1}{2}}\kappa^{\frac{3}{2}}\,\tilde{\phi} &= \alpha\left(1-\tfrac{1}{4}\alpha^2-\tfrac{\mathbf{59}}{96}\alpha^4-\tfrac{\mathbf{4741}}{1536}\alpha^6\right)\sin\theta+\tfrac{1}{2}\alpha^2\left(1+\tfrac{\mathbf{11}}{12}\alpha^2+\tfrac{\mathbf{547}}{\mathbf{192}}\alpha^4\right)\sin 2\theta\\
&\quad+\tfrac{3}{8}\alpha^3\left(1+\tfrac{\mathbf{163}}{\mathbf{48}}\alpha^2+\tfrac{\mathbf{221}}{\mathbf{15}}\alpha^4\right)\sin 3\theta+\tfrac{1}{3}\alpha^4\left(1+\tfrac{\mathbf{149}}{\mathbf{20}}\alpha^2\right)\sin 4\theta\\
&\quad+\tfrac{125}{384}\alpha^5\left(1+\tfrac{\mathbf{5057}}{\mathbf{375}}\alpha^2\right)\sin 5\theta+\tfrac{27}{80}\alpha^6\sin 6\theta+\tfrac{16807}{46080}\alpha^7\sin 7\theta+\mathcal{O}(\alpha^8),\\
g^{-\frac{1}{2}}\kappa^{\frac{1}{2}}\,c &= 1+\tfrac{1}{2}\alpha^2+\tfrac{1}{2}\alpha^4+\tfrac{\mathbf{899}}{384}\alpha^6+\mathcal{O}(\alpha^8).
\end{aligned}
$$

The expansions of η and $\tilde{\phi}$ match the exact Stokes wave (*cf.* Appendix A) up to the third order (non-matching coefficients are displayed in bold). This is not surprising since the gKG equations are cubic in nonlinearities. A bit more surprising is that the phase velocity c is correct up to the fifth order. But the most interesting is that, to the leading order, the n^{th} Fourier coefficient is (for all n up to infinity)

$$
\frac{n^{n-2}\,\alpha^n}{2^{n-1}\,(n-1)!}\,, \tag{5.21}
$$

which is also the case for the exact Stokes wave (Appendix A).

In a comparative vein, when examining the cubic Zakharov equations as delineated in equations B.3–B.4, it is observed that the phase velocity retains accuracy only up to the third order, and the Fourier coefficients do not adhere to the asymptotic behaviour described in equation 5.21 (refer to Appendix B for a detailed discussion). Upon truncating Zakharov's Hamiltonian at the order of $N+1$ in nonlinearities, the ensuing Stokes double series manifests correctness up to the order N with respect to the expansion parameter. However, it is noteworthy that none of these elevated approximations attain the exact asymptotic behaviour outlined in equation 5.21 regarding their Fourier coefficients. This discrepancy emanates from the fact that they encapsulate expansions centred around $\eta = 0$, a feature not shared by the generalized Klein–Gordon equations (gKG) equations. The Zakharov equations, on the other hand, hold validity across a broad spectrum of conditions, showcasing a level of versatility. Yet, they diverge from the gKG equations, which do not exhibit the same breadth in applicability. This comparative analysis underscores the nuanced differences in the performance and applicability of these mathematical formulations, illuminating the inherent trade-offs and the contextual efficacy of the Zakharov and gKG equations in capturing the complex dynamics of water wave phenomena.

5.4.2 | Multi-symplectic structure

The gKG equations have multiple variational structures. First of all, they appear as Euler–Lagrange equations of an approximate Lagrangian that also possesses a canonical Hamiltonian formulation

[52]. In this study, we show that the gKG system can be recast into the multi-symplectic form [37, 161] as well. The main idea behind this formulation is to treat the time and space variables on equal footing [38] while, for instance, in Hamiltonian systems, the time variable is privileged with respect to the space. Based on this special structure, numerous multi-symplectic schemes have been proposed for multi-symplectic PDEs, including the celebrated KdV, NSE equations [37, 173, 199, 247] and the Boussinesq family of equations [79]. These schemes are specifically designed to preserve exactly the discrete multi-symplectic form [80]. However, these schemes turn out to be fully implicit and, thence, advantageous only for long-time simulations using larger time steps. Since in the present study, we focus on the mid-range dynamics; we opt for a pseudo-spectral method which can ensure a high accuracy with an explicit time discretization [58, 102, 168, 224]. Since the periodic and localised solutions play an important rôle in the nonlinear wave dynamics [187], we use the numerical method to study the behaviour of these solutions.

In addition to the Lagrangian and Hamiltonian formulations, the gKG equations 5.17 and 5.18 can be recast into a first-order PDE system:

$$2\,\kappa\,\partial_t\eta + \boldsymbol{\nabla}\cdot\tilde{\boldsymbol{u}} = \kappa^2\,\tilde{\phi} - \kappa\,\tilde{\boldsymbol{u}}\cdot\boldsymbol{\alpha}, \tag{5.22}$$

$$-2\,\kappa\,\partial_t\tilde{\phi} - \boldsymbol{\nabla}\cdot\boldsymbol{\gamma} = 2\,\kappa\,g\,\eta, \tag{5.23}$$

$$-\boldsymbol{\nabla}\tilde{\phi} = -\tilde{\boldsymbol{u}} - \kappa\,\tilde{\phi}\,\boldsymbol{\alpha}, \tag{5.24}$$

$$\boldsymbol{\nabla}\eta = \boldsymbol{\alpha}, \tag{5.25}$$

$$\boldsymbol{0} = \boldsymbol{\gamma} - \kappa\,\tilde{\phi}\,\tilde{\boldsymbol{u}}, \tag{5.26}$$

where $\boldsymbol{\alpha} = (\alpha_1, \alpha_2)$ and $\boldsymbol{\gamma} = (\gamma_1, \gamma_2)$ are auxiliary variables. These relations yield the multi-symplectic canonical structure

$$\mathbb{M}\cdot\vec{z}_t + \mathbb{K}_1\cdot\vec{z}_{x_1} + \mathbb{K}_2\cdot\vec{z}_{x_2} = \mathrm{grad}_{\vec{z}}\,\mathcal{S}(\vec{z}), \tag{5.27}$$

where $\vec{z} = (\tilde{\phi}, \eta, \tilde{u}_1, \tilde{u}_2, \gamma_1, \gamma_2, \alpha_1, \alpha_2)^\top \in \mathbb{R}^8$, $\mathcal{S}$ is the generalised Hamiltonian function

$$\mathcal{S}(\vec{z}) = \boldsymbol{\alpha}\cdot\boldsymbol{\gamma} + \kappa\,g\,\eta^2 + \tfrac{1}{2}\left(\kappa\tilde{\phi}\right)^2 - \kappa\,\tilde{\phi}\,\tilde{\boldsymbol{u}}\cdot\boldsymbol{\alpha} - \tfrac{1}{2}\,\tilde{\boldsymbol{u}}\cdot\tilde{\boldsymbol{u}},$$

and where the eight-by-eight skew-symmetric matrices $\mathbb{M}$, $\mathbb{K}_1$ and $\mathbb{K}_2$ are defined as

$$\mathbb{M} = 2\,\kappa\,(\vec{e}_1\otimes\vec{e}_2 - \vec{e}_2\otimes\vec{e}_1),$$
$$\mathbb{K}_1 = \vec{e}_1\otimes\vec{e}_3 - \vec{e}_3\otimes\vec{e}_1 + \vec{e}_5\otimes\vec{e}_2 - \vec{e}_2\otimes\vec{e}_5,$$
$$\mathbb{K}_2 = \vec{e}_1\otimes\vec{e}_4 - \vec{e}_4\otimes\vec{e}_1 + \vec{e}_6\otimes\vec{e}_2 - \vec{e}_2\otimes\vec{e}_6,$$

$\vec{e}_j$ being j-th unitary vector of the Cartesian coordinates for the $\mathbb{R}^8$ space ($\otimes$ the tensor product).

Conservation laws

The local multi-symplectic conservation law for 5.27 is

$$\partial_t \omega + \boldsymbol{\nabla} \cdot \boldsymbol{\tau} = 0,$$

where the pre-symplectic forms are defined, for any solution of the first variation of 5.27, as

$$\omega = \tfrac{1}{2}\, \mathrm{d}\vec{z} \wedge (\mathbb{M} \cdot \mathrm{d}\vec{z}), \qquad \tau_1 = \tfrac{1}{2}\, \mathrm{d}\vec{z} \wedge (\mathbb{K}_1 \cdot \mathrm{d}\vec{z}), \qquad \tau_2 = \tfrac{1}{2}\, \mathrm{d}\vec{z} \wedge (\mathbb{K}_2 \cdot \mathrm{d}\vec{z}),$$

that is to say

$$\omega = 2\,\kappa\, \mathrm{d}\eta \wedge \mathrm{d}\tilde{\phi}, \quad \tau_1 = \mathrm{d}\tilde{u}_1 \wedge \mathrm{d}\tilde{\phi} + \mathrm{d}\gamma_1 \wedge \mathrm{d}\eta, \quad \tau_2 = \mathrm{d}\tilde{u}_2 \wedge \mathrm{d}\tilde{\phi} + \mathrm{d}\eta \wedge \mathrm{d}\gamma_2,$$

where $\wedge$ is the usual exterior or wedge product [37, 186].

Along with the multi-symplectic system solutions, local energy conservation law is verified

$$\partial_t E(\vec{z}) + \boldsymbol{\nabla} \cdot \boldsymbol{F}(\vec{z}) = 0,$$

with

$$E = \mathcal{S} - \tfrac{1}{2}\, \vec{z}^{\,\mathsf{T}} \cdot \mathbb{K}_1 \cdot \vec{z}_{x_1} - \tfrac{1}{2}\, \vec{z}^{\,\mathsf{T}} \cdot \mathbb{K}_2 \cdot \vec{z}_{x_2}, \qquad F_j = \tfrac{1}{2}\, \vec{z}^{\,\mathsf{T}} \cdot \mathbb{K}_j \cdot \vec{z}_t,$$

which can be explicitly expressed in terms of the physical variables as

$$2\,E = 2\,\kappa\, g\, \eta^2 - \tilde{\boldsymbol{u}}^2 + (\kappa\tilde{\phi})^2 - \kappa\, \tilde{\phi}\, \tilde{\boldsymbol{u}} \cdot \boldsymbol{\nabla}\eta + \kappa\, \eta\, \boldsymbol{\nabla} \cdot (\tilde{\phi}\tilde{\boldsymbol{u}}) - \tilde{\phi}\, \boldsymbol{\nabla} \cdot \tilde{\boldsymbol{u}} + \tilde{\boldsymbol{u}} \cdot \boldsymbol{\nabla}\tilde{\phi},$$

$$2\,\boldsymbol{F} = \kappa\, \tilde{\phi}\, \tilde{\boldsymbol{u}}\, \partial_t \eta - \kappa\, \eta\, \partial_t(\tilde{\phi}\tilde{\boldsymbol{u}}) + \tilde{\phi}\, \partial_t \tilde{\boldsymbol{u}} - \tilde{\boldsymbol{u}}\, \partial_t \tilde{\phi}.$$

There exists also two local momentum conservation laws associated with each spatial direction

$$\partial_t I_1(\vec{z}) + \partial_{x_1} G_{11}(\vec{z}) + \partial_{x_2} G_{12}(\vec{z}) = 0,$$

$$\partial_t I_2(\vec{z}) + \partial_{x_1} G_{21}(\vec{z}) + \partial_{x_2} G_{22}(\vec{z}) = 0,$$

the corresponding quantities being

$$2\,I_j = \vec{z}^{\,\mathsf{T}} \cdot \mathbb{M} \cdot \vec{z}_{x_j} = 2\kappa \left(\tilde{\phi}\, \partial_{x_j} \eta - \eta\, \partial_{x_j} \tilde{\phi} \right),$$

$$2\,G_{12} = \vec{z}^{\,\mathsf{T}} \cdot \mathbb{K}_2 \cdot \vec{z}_{x_1} = \kappa\, \tilde{\phi}\, \tilde{u}_2\, \partial_{x_1} \eta - \kappa\, \eta\, \partial_{x_1}(\tilde{\phi}\tilde{u}_2) + \tilde{\phi}\, \partial_{x_1} \tilde{u}_2 - \tilde{u}_2\, \partial_{x_1} \tilde{\phi},$$

$$2\,G_{21} = \vec{z}^{\,\mathsf{T}} \cdot \mathbb{K}_1 \cdot \vec{z}_{x_2} = \kappa\, \tilde{\phi}\, \tilde{u}_1\, \partial_{x_2} \eta - \kappa\, \eta\, \partial_{x_2}(\tilde{\phi}\tilde{u}_1) + \tilde{\phi}\, \partial_{x_2} \tilde{u}_1 - \tilde{u}_1\, \partial_{x_2} \tilde{\phi},$$

$$
\begin{aligned}
2\,G_{11} &= 2\,\mathcal{S} - \vec{z}^{\,\mathsf{T}}\cdot\mathbb{M}\cdot\vec{z}_t - \vec{z}^{\,\mathsf{T}}\cdot\mathbb{K}_2\cdot\vec{z}_{x_2} \\
&= 2\,\kappa\,g\,\eta^2 + (\kappa\tilde{\phi})^2 - \tilde{\boldsymbol{u}}^2 + 2\kappa\left(\eta\,\partial_t\tilde{\phi} - \tilde{\phi}\,\partial_t\eta\right) \\
&\quad - \left(\kappa\,\tilde{\phi}\,\tilde{u}_2\,\partial_{x_2}\eta - \kappa\,\eta\,\partial_{x_2}(\tilde{\phi}\,\tilde{u}_2) + \tilde{\phi}\,\partial_{x_2}\tilde{u}_2 - \tilde{u}_2\,\partial_{x_2}\tilde{\phi}\right), \\
2\,G_{22} &= 2\,\mathcal{S} - \vec{z}^{\,\mathsf{T}}\cdot\mathbb{M}\cdot\vec{z}_t - \vec{z}^{\,\mathsf{T}}\cdot\mathbb{K}_1\cdot\vec{z}_{x_1} \\
&= 2\,\kappa\,g\,\eta^2 + (\kappa\tilde{\phi})^2 - \tilde{\boldsymbol{u}}^2 + 2\kappa\left(\eta\,\partial_t\tilde{\phi} - \tilde{\phi}\,\partial_t\eta\right) \\
&\quad - \left(\kappa\,\tilde{\phi}\,\tilde{u}_1\,\partial_{x_1}\eta - \kappa\,\eta\,\partial_{x_1}(\tilde{\phi}\,\tilde{u}_1) + \tilde{\phi}\,\partial_{x_1}\tilde{u}_1 - \tilde{u}_1\,\partial_{x_1}\tilde{\phi}\right).
\end{aligned}
$$

The multi-symplectic form highlighted above can be used to construct various numerical multi-symplectic schemes, which preserve exactly the multi-symplectic form at the discrete level [37, 38, 173, 199, 247]. These schemes are suitable for long-time integration using rather coarse discretizations [80, 82]. The development and application of these schemes to proposed approximate model equations are left for our future studies.

5.4.3 | Travelling waves

For the sake of simplicity, we will consider hereinafter the special case of two-dimensional wave motions, *i.e.* the dependent variables are independent of, say, the variable x_2; for brevity, we denote $x = x_1$ and $u = u_1$. The equations of motion become

$$
\begin{aligned}
\tilde{u} &= \tilde{\phi}_x - \kappa\,\tilde{\phi}\,\eta_x, \\
\tilde{v} &= \kappa\,\tilde{\phi}, \\
0 &= 2\,\kappa\,\eta_t + \tilde{u}_x - \kappa\,\tilde{v} + \kappa\,\tilde{u}\,\eta_x, \\
0 &= 2\,g\,\kappa\,\eta + 2\,\kappa\,\tilde{\phi}_t + [\,\tilde{u}\,\tilde{v}\,]_x,
\end{aligned}
$$

which can be reduced into a two equations system

$$
\begin{aligned}
\eta_t + \tfrac{1}{2}\,\kappa^{-1}\,\tilde{\phi}_{xx} - \tfrac{1}{2}\,\kappa\,\tilde{\phi} &= \tfrac{1}{2}\,\tilde{\phi}\left[\,\eta_{xx} + \kappa\,\eta_x^2\,\right], \\
\tilde{\phi}_t + g\,\eta &= -\tfrac{1}{2}\left[\,\tilde{\phi}\,\tilde{\phi}_x - \kappa\,\tilde{\phi}^2\,\eta_x\,\right]_x.
\end{aligned}
$$

The equations can be combined to derive useful secondary relations. For instance, we derive the conservative equations

$$
\tilde{u}_t + \left[\,\tfrac{3}{4}\,\tilde{u}^2 + \tfrac{1}{4}\,\tilde{v}^2 + g\,\eta\left(1 - \tfrac{1}{2}\kappa\eta\right)\,\right]_x = 0, \tag{5.28}
$$

$$
\left[\,\tfrac{1}{2}\,g\,\kappa\,\eta^2 + \tfrac{1}{4}\,(\tilde{u}^2 + \tilde{v}^2)\,\right]_t + \left[\,\tfrac{1}{2}\,\tilde{u}\,(\tilde{v}\,\eta_t - \tilde{\phi}_t)\,\right]_x = 0, \tag{5.29}
$$

which physically describe (after division by κ) the conservations of the momentum and energy fluxes, respectively.

For travelling waves of permanent form, the dependent variables are functions of the single independent variable $\xi = x - ct$. The equations 5.28 and 5.29 can then be integrated as

$$\begin{aligned} \tfrac{3}{4}\,\tilde{u}^2 + \tfrac{1}{4}\,\tilde{v}^2 + g\,\eta\,(1 - \tfrac{1}{2}\kappa\eta) - c\,\tilde{u} &= K_p, \\ \tfrac{1}{2}\,g\,\kappa\,\eta^2 - \tfrac{1}{4}\,\tilde{u}^2 + \tfrac{1}{4}\,\tilde{v}^2 &= K_e, \end{aligned}$$

where K_p and K_e are integration constants. Adding these two relations, one obtains

$$\tfrac{1}{2}\,\tilde{u}^2 + \tfrac{1}{2}\,\tilde{v}^2 + g\,\eta - c\,\tilde{u} = K_p + K_e,$$

which is the Bernoulli equation, $K_p + K_e$ being a Bernoulli constant. Subtracting the two relations, one gets at once

$$\tilde{u}^2 + g\,\eta\,(1 - \kappa\eta) - c\,\tilde{u} = K_p - K_e,$$

that can be used to express $\tilde{u}$ in terms of η (or vice-versa), *i.e.*,

$$\tilde{u} = \tfrac{1}{2}\,c \,\pm\, \sqrt{K_p - K_e + \tfrac{1}{4}\,c^2 \,-\, g\,\eta\,(1 - \kappa\eta)}\,, \tag{5.30}$$

$$\tilde{u}_\xi = g\,\eta_\xi\,(1 - 2\kappa\eta)\,/\,(c - 2\tilde{u})\,. \tag{5.31}$$

With these relations, the Lagrangian density 5.16 becomes

$$\begin{aligned} 2\kappa\,\mathscr{L} &= -2\,c\,\tilde{v}\,\eta_\xi - g\,\kappa\,\eta^2 - \tfrac{1}{2}\,\tilde{u}^2 - \tfrac{1}{2}\,\tilde{v}^2 \\ &= 2\,c\,\eta_\xi^2\,[\,2\,c - \tilde{u} - (g/\kappa)\,(1 - 2\kappa\eta)\,/\,(c - 2\tilde{u})\,] \,-\, \tilde{u}^2 - 2\,K_e, \end{aligned}$$

where $\tilde{u}$ should be expressed via 5.30. An equation for η is then obtained from the Beltrami identity

$$\mathscr{L} - \eta_\xi\,\frac{\partial\,\mathscr{L}}{\partial\eta_\xi} = \text{constant} \;\equiv\; (K_b - 2K_e)\,/\,2\kappa,$$

yielding

$$\left(\frac{\mathrm{d}\,\eta}{\mathrm{d}\,\xi}\right)^2 = \frac{\kappa\,(K_b + \tilde{u}^2)\,(c - 2\tilde{u})}{2\,c\,[\,g\,(1 - 2\kappa\eta) + \kappa\,(2c - \tilde{u})\,(c - 2\tilde{u})\,]}, \tag{5.32}$$

where $\tilde{u}$ is given by 5.30. Unfortunately, we were not able to solve the equation 5.32 analytically. However, this solution might be useful for theoretical investigations of travelling waves. In order to

construct these solutions numerically to high accuracy ($\sim 10^{-10}$), we employ a Newton Jacobian-free method combined with the Levenberg–Marquardt algorithm [175]. The computed profiles will be shown below in section 5.4.5.

5.4.4 | Pseudo-spectral method

We briefly describe below a highly accurate Fourier-type pseudo-spectral method [31, 224] that we use to simulate the dynamics of the gKG equations. These methods have been proven to be extremely efficient (practically unbeatable) in the idealized periodic setting [31]. Below, we show that the gKG system can be integrated up to the Riemann wave breaking using the proposed pseudo-spectral scheme. We would like to mention that the pseudo-spectral method presented below does not rely on a variational structure. However, due to the fact that the numerical error committed by this pseudo-spectral method is exponentially small, we may use it confidently to study the dynamics of the gKG equations.

With $V = (\eta, \tilde{\phi})^\top$ denoting the vector of dynamic variables, the gKG system 5.17, 5.18 can be recast in the vector form

$$V_t + \mathcal{L} \cdot V = N(V), \tag{5.33}$$

where the operator N denotes the right-hand side of equations 5.17, 5.18 and the linear operator $\mathcal{L}$ is defined as

$$\mathcal{L} = \begin{bmatrix} 0 & \frac{\boldsymbol{\nabla}^2 - \kappa^2}{2\kappa} \\ g & 0 \end{bmatrix}, \qquad \hat{\mathcal{L}} = \begin{bmatrix} 0 & -\frac{|\boldsymbol{k}|^2 + \kappa^2}{2\kappa} \\ g & 0 \end{bmatrix},$$

where $\hat{\mathcal{L}}$ is the operator $\mathcal{L}$ in the Fourier space. The equation 5.33 is solved by applying the Fourier transform in the spatial variable $\boldsymbol{x}$. The transformed variables is denoted by $\hat{V}(t, \boldsymbol{k}) = \mathcal{F}\{V(t, \boldsymbol{x})\}$, $\boldsymbol{k}$ being the Fourier transform parameter. The nonlinear terms are computed in the physical space, while spatial derivatives are computed spectrally in the Fourier space. For example, the term $\tilde{\phi}\boldsymbol{\nabla}^2\eta$ is discretised as:

$$\mathcal{F}\left\{\tilde{\phi}\,\boldsymbol{\nabla}^2\eta\right\} = \mathcal{F}\left\{\mathcal{F}^{-1}\left(\hat{\phi}\right) \times \mathcal{F}^{-1}\{-|\boldsymbol{k}|^2\hat{\eta}\}\right\}.$$

The other nonlinear terms are treated in a similar way. We note that the usual three-half rule has to be applied for anti-aliasing [58, 102, 224].

In order to improve the stability of the time discretization procedure, we integrate exactly the linear terms. This is achieved by making a change of variables [102, 168]:

$$\hat{W}(t) = \exp\left((t - t_0)\hat{\mathcal{L}}\right) \cdot \hat{V}(t), \qquad \hat{W}(t_0) = \hat{V}(t_0),$$

yielding the equation

$$\hat{W}_t = \exp\left((t-t_0)\hat{\mathcal{L}}\right)\cdot\mathcal{F}\left\{N\left(\exp\left((t_0-t)\hat{\mathcal{L}}\right)\cdot\hat{W}\right)\right\}.$$

The exponential matrix of the operator $\hat{\mathcal{L}}$ can be explicitly computed to give

$$\exp\left((t-t_0)\hat{\mathcal{L}}\right) = \begin{bmatrix} \cos\big(\omega(t-t_0)\big) & -(\omega/g)\sin\big(\omega(t-t_0)\big) \\ (g/\omega)\sin\big(\omega(t-t_0)\big) & \cos\big(\omega(t-t_0)\big) \end{bmatrix},$$

where

$$\omega^2 = \frac{g\,\kappa}{2} + \frac{g\,|\boldsymbol{k}|^2}{2\,\kappa}.$$

Finally, the resulting system of ODEs is discretised in space by the Verner embedded adaptive 9(8) Runge–Kutta scheme [228]. The step size is chosen adaptively using the so-called H211b digital filter [208, 209] to meet the prescribed error tolerance, set as of the order of machine precision.

5.4.5 | Numerical results

Periodic steady solutions

We begin the numerical study of gKG equations by computing numerically steady periodic Stokes-like solutions. We employ the Newton Levenberg–Marquardt method, which tends to the steepest descent far from the solution (to ensure the convergence) and becomes the classical Newton method in the vicinity of the root [175]. Then, we compare the computed profile to the seventh-order Stokes expansion to the full Euler equations A.1–A.3. In order to fix the ideas, we choose the wavelength to be $\lambda \equiv 2\ell = 2\pi$, *i.e.* the computational domain is $[-\ell,\ \ell]$. Consequently, the parameter $\kappa = 2\pi/\lambda = 1$. For simplicity, we take also $g = 1\ \mathrm{m/s^2}$. In steady computations, we use only $N = 128$ Fourier modes. It is sufficient to compute to high accuracy ($\sim\ \mathcal{O}(10^{-9})$) the numerical solution at the collocation points. The results are shown in Figures 5.4, 5.5 and 5.6.

In order to validate further the computed travelling wave profiles, we use the dynamic solver described in section 5.4.4. Consider the computational domain composed of 16 periodic waves with steepness $\varepsilon = 0.095$. The discretization was done with $N = 4096$ Fourier modes. This initial condition was propagated up to $T = 250$, which corresponds to approximately ~ 40 wave periods. As one can see in Figure 5.7, the initial wave system propagates uniformly in space without changing its shape. This simulation shows again that travelling waves were computed correctly. To test the stability of these solutions, we consider the same initial condition with long (~ 4 wavelengths) and short ($\sim 1/4$ wavelength) wave perturbations. Both situations were simulated numerically on the same time scale,

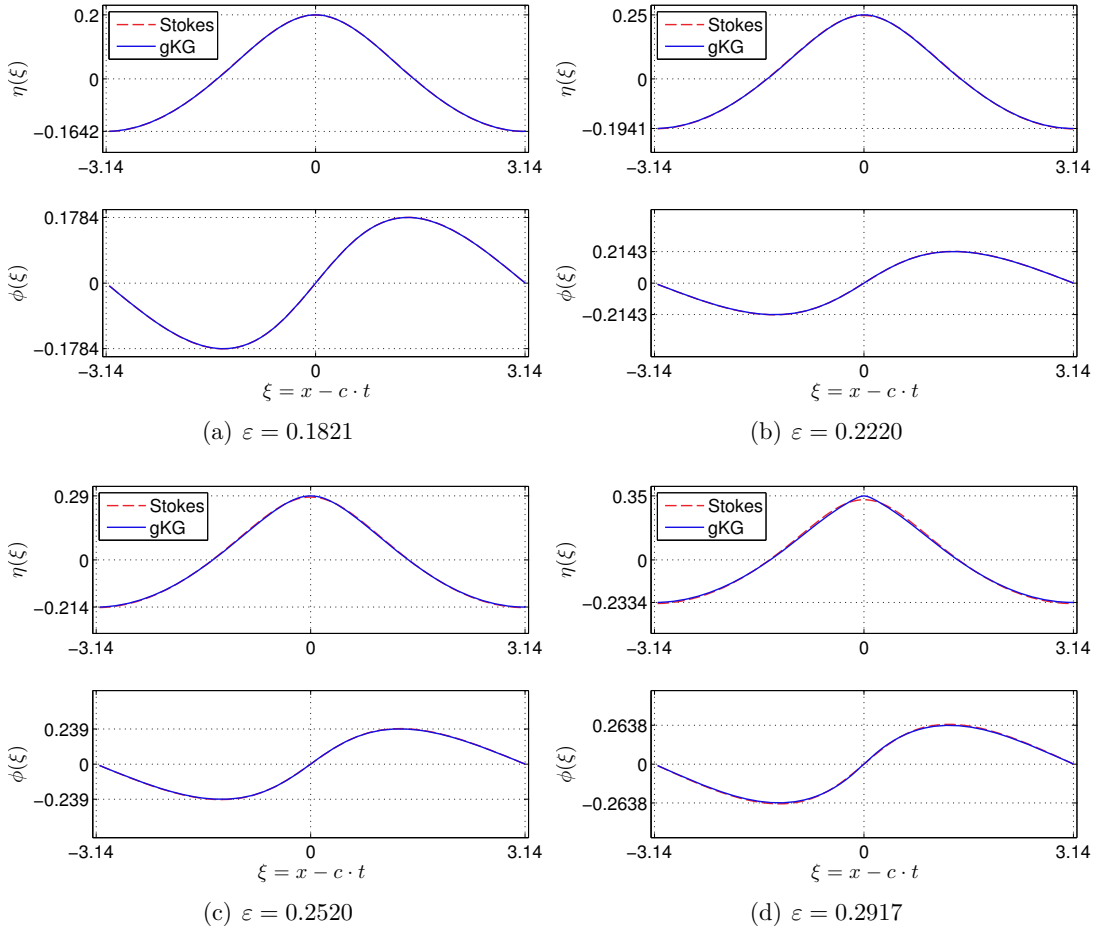

(a) $\varepsilon = 0.1821$ (b) $\varepsilon = 0.2220$

(c) $\varepsilon = 0.2520$ (d) $\varepsilon = 0.2917$

Figure 5.4 | Comparison of the travelling wave solutions to the gKG equations with the seventh-order Stokes solution for various values of the wave steepness parameter. The wavelength is fixed to 2π.

and results are presented in Figures 5.7(*a,b*). We can see that the travelling wave solutions in the gKG equations appear to be stable. However, a more detailed study is needed to answer this question with more certitude.

Envelope soliton

In this Section, we consider an example stemming from the wave packet propagation theory on deep waters. As it was shown for the first time by Zakharov [243], the free surface complex envelope $A(x, t)$ is governed by the classical Nonlinear Schrödinger equation (NSE) [57, 121, 243]:

$$A_t + c_g A_x + \frac{\mathrm{i}\, c_g}{4\, k_0} A_{xx} + \frac{\mathrm{i}\, \omega_0\, k_0^2}{2} A\, |A|^2 = 0, \qquad 5.34$$

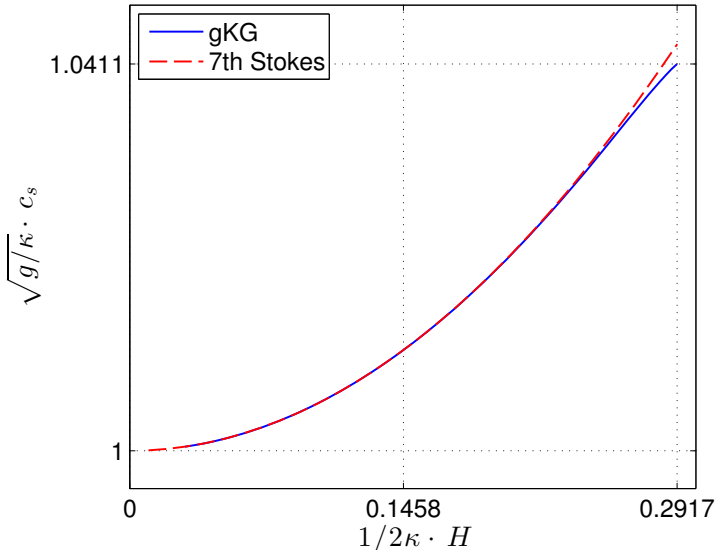

Figure 5.5 | Speed–steepness relation for periodic steady waves: blue solid line — the gKG equations, red dashed line — seventh-order Stokes expansion. The wavelength is fixed to 2π.

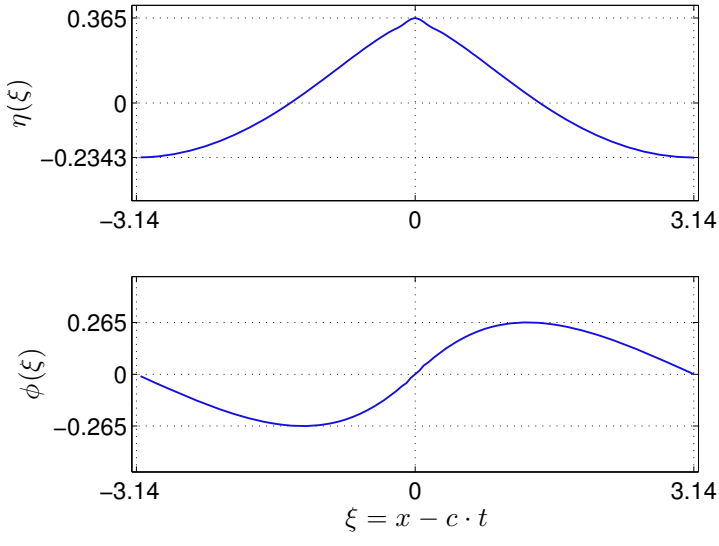

Figure 5.6 | Periodic travelling wave to the gKG equations for the steepness parameter $\varepsilon = 0.29967$.

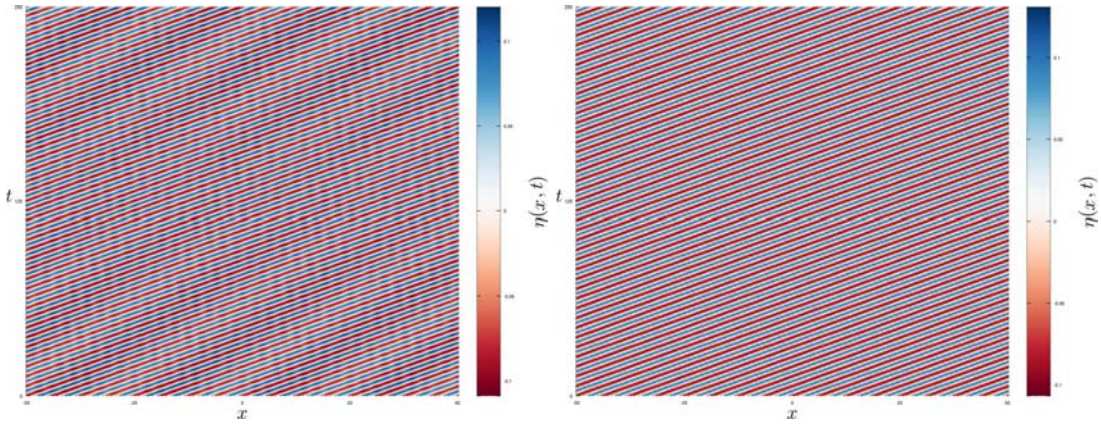

(a) *Long perturbation* (b) *Short perturbation*

Figure 5.7 | Evolution of 16 wavelengths of computed periodic travelling waves for $\varepsilon = 0.0954$ during about 160 periods: (a) long wave perturbation; (b) short wave perturbation.

where $\omega_0 = \sqrt{g k_0}$ and $c_g = \partial\omega_0/\partial k_0 = \omega_0/2k_0$ is the linear group velocity. Equation 5.34 admits the envelope soliton solution:

$$A(x,t) = a\ \mathrm{sech}\left(\sqrt{2}k_0^2(x - c_g t)\right)\exp(-\mathrm{i}a^2 k_0^2\omega_0 t/4). \tag{5.35}$$

The free surface elevation $\eta(x,t)$ and the velocity potential $\phi(x,t)$ can be recovered from the complex envelope $A(x,t)$ in the following way:

$$\eta(x,t) = \mathrm{Re}\left\{A(x,t)\,\mathrm{e}^{\mathrm{i}(k_0 x - \omega_0 t)}\right\}, \qquad \phi(x,t) = \mathrm{Re}\left\{-\frac{\mathrm{i}\omega_0}{k_0}A(x,t)\,\mathrm{e}^{\mathrm{i}(k_0 x - \omega_0 t)}\right\}. \tag{5.36}$$

The evolution of this envelope soliton in higher-order models was studied in [57, 121]. Consequently, we put this localised structure as the initial condition in the gKG equations. Consider the computational domain $[-128, 128]$ with periodic boundary conditions and the envelope soliton 5.35 (transformed to physical variables using formulas 5.36) with $a = 0.1$, $\kappa \equiv k_0 = 1.0$ and $g = 1$. We simulated the evolution of this wave packet until $T = 1000.0$, which was sufficient for the packet to go around the computational domain three times. The space-time evolution is shown in Figure 5.8, and several individual snapshots of the free surface elevation are shown in Figure 5.9. The shape of the envelope soliton is not preserved exactly, of course. However, during short times, the preservation is satisfactory. On snapshots 5.9 (b & c), one can notice a small wavelet travelling in the opposite direction. The general effect is the broadening of the wave packet in agreement with previous investigations [206, 207].

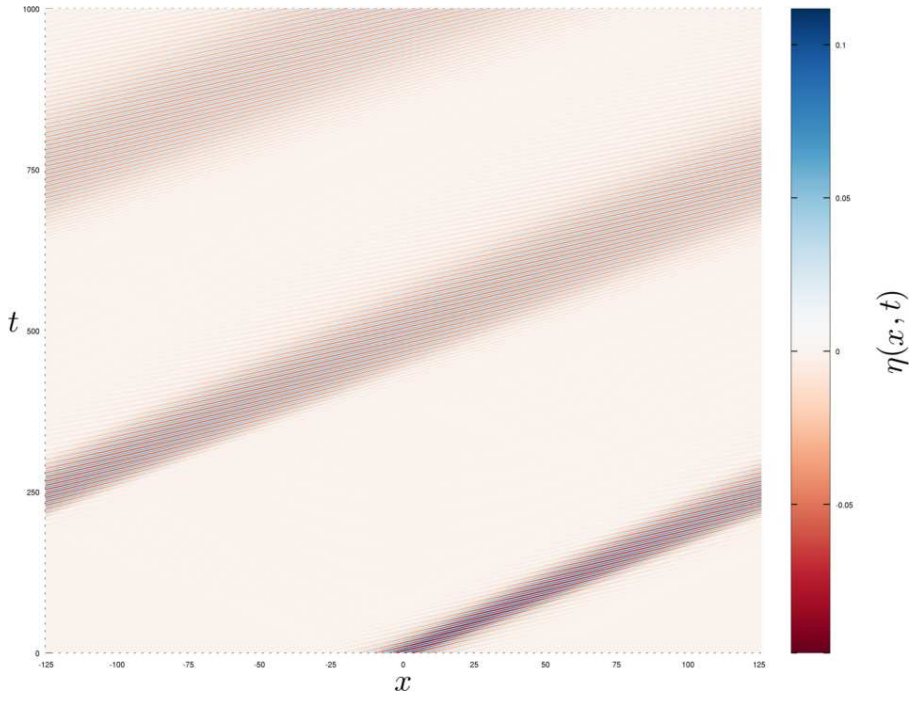

Figure 5.8 | Space–time plot of a localized wave packet under the gKG dynamics.

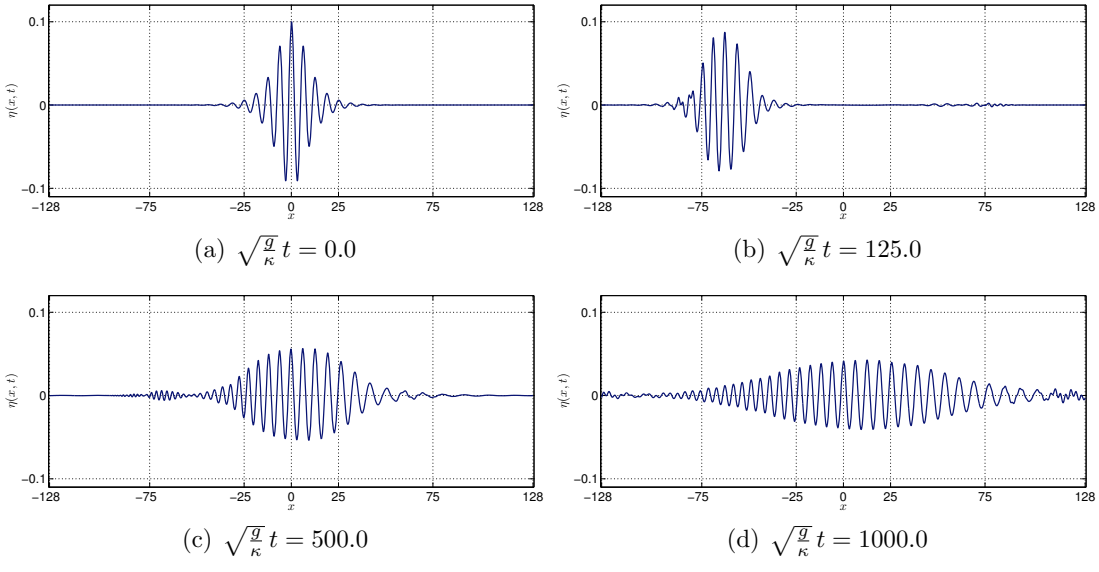

Figure 5.9 | Evolution of initially localized wave packet under the gKG dynamics.

Table 5.1 | Physical and numerical parameters used for the simulation of the shock wave formation in gKG equations.

Gravity acceleration: g [m s^{-2}]	1.0
Characteristic wavenumber: κ [m^{-1}]	0.7
Computational domain half-length: ℓ [m]	π
Final simulation time: T [s]	11.5
Initial condition amplitude: a [m]	0.1
Initial bump width: k [m^{-1}]	π
Number of Fourier modes: N	4096

Shock wave formation

Finally, we present an additional test case where the gKG system shows an interesting behaviour. The initial condition is taken to be a localised bump on the free surface with zero initial velocity:

$$\eta(x,0) = a\ \mathrm{sech}^2(kx), \qquad \tilde{\phi}(x,0) = 0.$$

All the values of physical and numerical parameters are given in Table 5.1. The space-time dynamics of this system are shown in Figure 5.12, and several snapshots of the free surface elevation are depicted in Figure 5.10. The particularity of this simulation consists of two shock waves which develop at the free surface. The snapshot at the final simulation time T is shown on the upper panel of Figure 5.11. One can clearly see the sharp transitions at the free surface. It is even more instructive to look at the energy spectrum, which is depicted on the bottom panel of the same Figure. For the sake of comparison, we also plot the energy spectrum of a breaking Riemann wave, which was recently shown to be exactly of the form $|\hat{\eta}_k|^2 \sim k^{-8/3}$ [178, 188]. This excellent agreement shows that the gKG system may produce wave breaking of a similar type as classical shallow-water type systems. This result was to be expected since the gKG system is a deep water counterpart of the classical Saint-Venant equations [68].

Intermediate conclusions

We discussed the derivation of some gKG equations, which are a new model for water waves propagating in deep water approximation. This model already appeared as an illustration for the relaxed variational formulation [52, 81]. Here, the structure of this model was further investigated, and a multi-symplectic formulation was proposed. Moreover, we computed periodic travelling wave solutions, and we showed that they approximate fairly well the corresponding solutions of the full Euler equations, including the formation of a limiting wave with a singular point at the crest [160, 213]. The dynamics of regular periodic waves were studied, and these solutions appear to be stable under long and short-wave perturbations. Finally, we showed also that solutions of gKG equations may produce the shock wave formation phenomenon of a similar type as the breaking of Riemann waves in

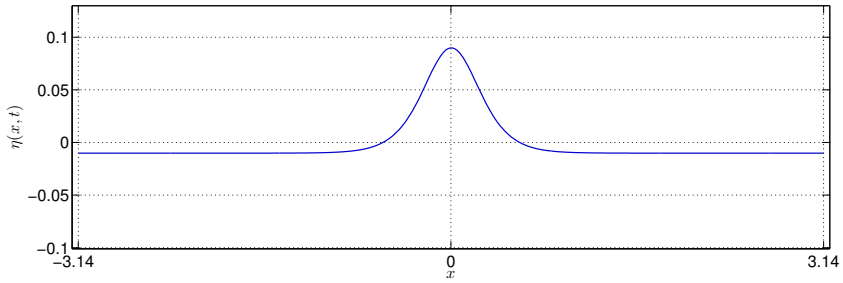

(a) $t = 0$ s

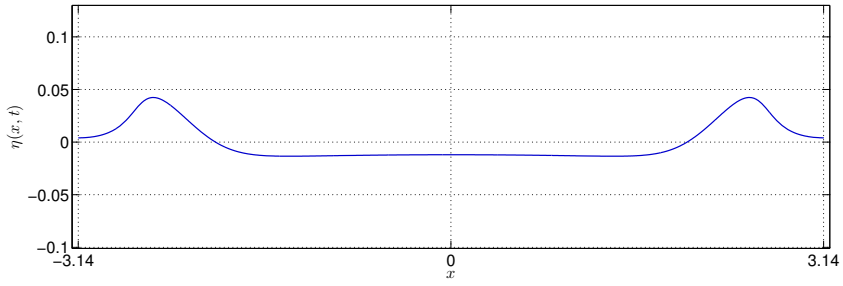

(b) $t = 2.875$ s

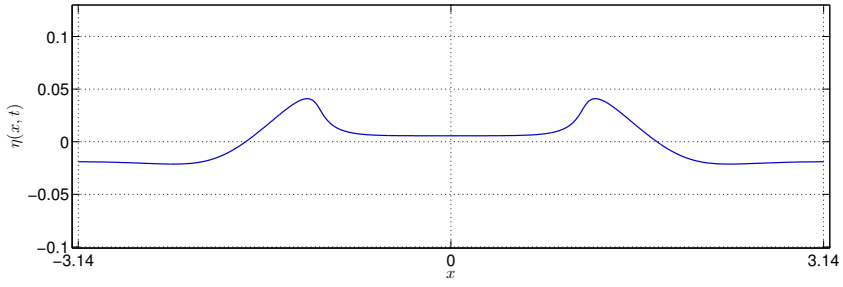

(c) $t = 5.75$ s

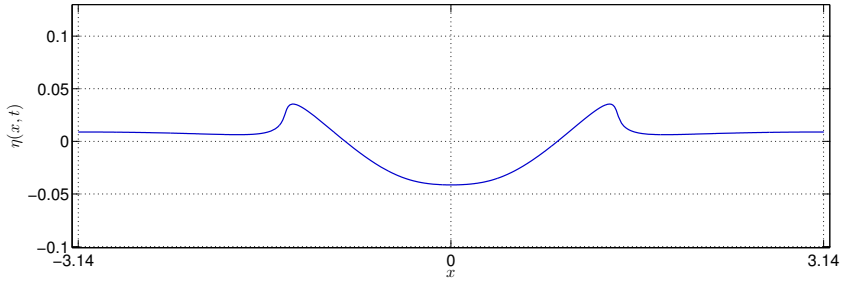

(d) $t = 8.625$ s

Figure 5.10 | Several snapshots of an initial bump evolution. See also Figure 5.12. The free surface at the final simulation time is shown in Figure 5.11.

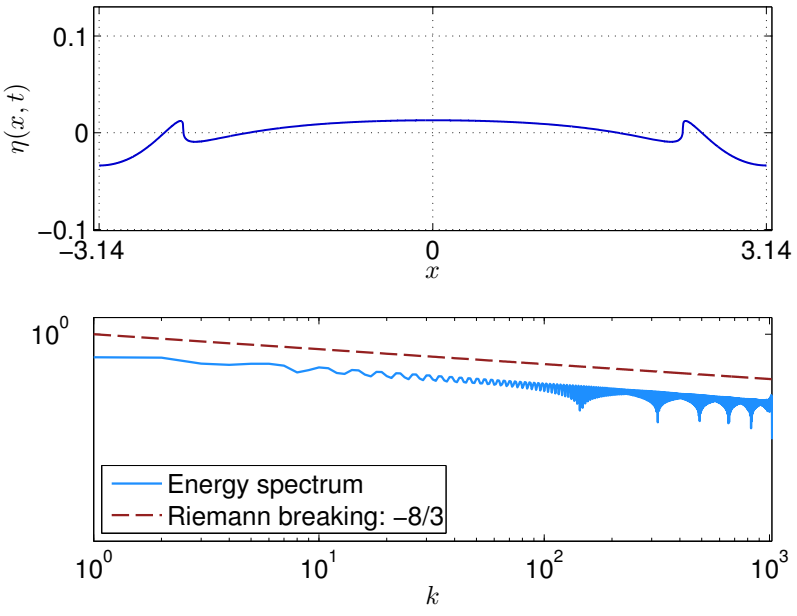

Figure 5.11 | Free surface elevation and the energy spectrum at the final simulation time $T = 11.5$ s. The red dotted line shows the theoretical prediction of a Riemann wave breaking spectrum [178, 188].

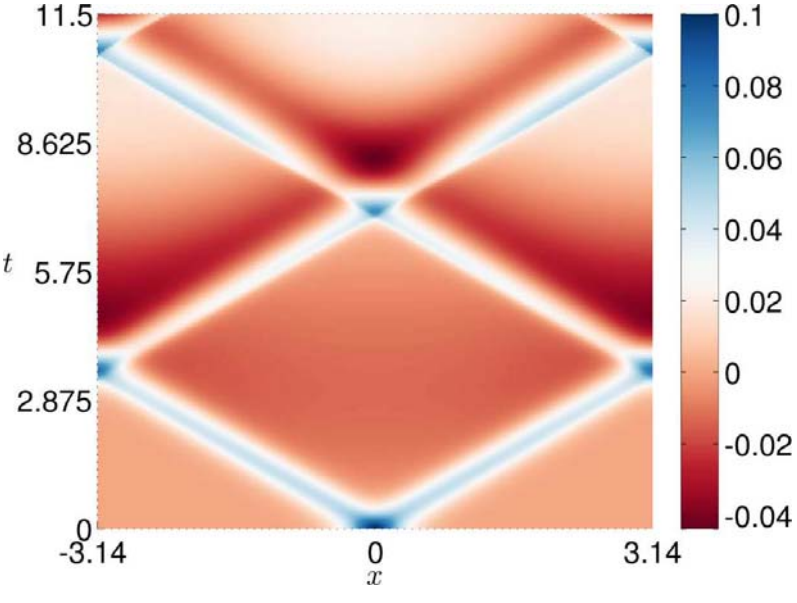

Figure 5.12 | Space-time dynamics of an initial bump posed on the free surface in the gKG equations.

shallow water models [178, 188]. To our knowledge, it is the first approximate model in deep waters which shows this behaviour. Although the results presented here are encouraging, further investigations would be necessary to assess the relevance and limitations of the gKG for modelling water waves in deep water.

5.5 | Constraining with the free surface impermeability

In order to satisfy the free surface impermeability identically, we take

$$\tilde{v} = \eta_t + \tilde{\boldsymbol{u}} \cdot \boldsymbol{\nabla}\eta,$$

and the Lagrangian density 5.16 becomes[24]

$$2\kappa\,\mathscr{L} = \tilde{\phi}\,(\kappa\,\eta_t + \boldsymbol{\nabla}\cdot\tilde{\boldsymbol{u}}) - g\kappa\,\eta^2 + \tfrac{1}{2}\tilde{\boldsymbol{u}}^2 + \tfrac{1}{2}(\eta_t + \tilde{\boldsymbol{u}}\cdot\boldsymbol{\nabla}\eta)^2, \tag{5.37}$$

while the Euler–Lagrange equations yield the relations

$$\delta\,\tilde{\boldsymbol{u}}: \qquad \mathbf{0} = \tilde{\boldsymbol{u}} + (\eta_t + \tilde{\boldsymbol{u}}\cdot\boldsymbol{\nabla}\eta)\boldsymbol{\nabla}\eta - \boldsymbol{\nabla}\tilde{\phi}, \tag{5.38}$$

$$\delta\,\tilde{\phi}: \qquad 0 = \kappa\eta_t + \boldsymbol{\nabla}\cdot\tilde{\boldsymbol{u}}, \tag{5.39}$$

$$\delta\,\eta: \qquad 0 = 2g\kappa\eta + \kappa\tilde{\phi}_t + \eta_{tt} + (\tilde{\boldsymbol{u}}\cdot\boldsymbol{\nabla}\eta)_t + \boldsymbol{\nabla}\cdot(\tilde{\boldsymbol{u}}\eta_t) + \boldsymbol{\nabla}\cdot[(\tilde{\boldsymbol{u}}\cdot\boldsymbol{\nabla}\eta)\tilde{\boldsymbol{u}}]. \tag{5.40}$$

The relation 5.39 implies that $\boldsymbol{\nabla}\cdot\boldsymbol{u} + v_y = 0$, the solution satisfies the incompressibility identically. Notice that we did not require this condition at the level of Ansatz 5.15. On the other hand, the irrotationality being not verified identically, equations 5.38–5.40 cannot be derived from Luke's variational formulation. Note that 5.38 yields $\boldsymbol{\nabla}\tilde{\phi} = \tilde{\boldsymbol{u}} + \tilde{v}\boldsymbol{\nabla}\eta$ that is exact for potential flows [64, 102]. As for the shallow water case, the potential $\tilde{\phi}$ can be eliminated from equations 5.38, thus yielding a deep water analogue of SGN equations. These equations have also been studied in [86].

To the linear approximation, relations 5.38–5.40 can be combined into a single equation for the elevation of the free surface:

$$(\boldsymbol{\nabla}^2 - \kappa^2)\,\eta_{tt} + 2\,g\,\kappa\,\boldsymbol{\nabla}^2\eta = 0,$$

which admits the special $(2\pi/k)$-periodic solution

$$\eta = a\,\cos k(x_1 - ct), \qquad c^2 = 2\,g\,\kappa\,(k^2 + \kappa^2)^{-1}.$$

[24] We refer to section 5.3 for the genesis of this Lagrangian density.

Therefore, if $k = \kappa$, the exact linear approximation is recovered, as it should be. Again, this means that this model is valid for narrow-banded spectra. The question on how narrow was investigated in [52, section §4.3.1].

5.5.1 | Evolution equations

The governing equations 5.38–5.40 may appear complicated to the reader. The main problem with the formulation given above is that equations are not written in an evolutionary form of a system of PDEs with time derivatives separated from other terms. We can recast the model 5.38–5.40 in a more amenable form. In order to obtain a compact form of equations 5.38–5.40, first we are going to *expand* them:

$$\tilde{v} \equiv \eta_t + \tilde{\boldsymbol{u}} \cdot \boldsymbol{\nabla}\eta = \frac{\eta_t + \boldsymbol{\nabla}\tilde{\phi} \cdot \boldsymbol{\nabla}\eta}{1 + |\boldsymbol{\nabla}\eta|^2} \equiv \tilde{\boldsymbol{u}} \cdot \boldsymbol{\nabla}\eta - \kappa^{-1}\, \boldsymbol{\nabla} \cdot \tilde{\boldsymbol{u}},$$

$$\tilde{\boldsymbol{u}} \equiv \boldsymbol{\nabla}\tilde{\phi} - \tilde{v}\, \boldsymbol{\nabla}\eta = \frac{\boldsymbol{\nabla}\tilde{\phi} - \eta_t\, \boldsymbol{\nabla}\eta + |\boldsymbol{\nabla}\eta|^2\, \boldsymbol{\nabla}\tilde{\phi} - \left[\, \boldsymbol{\nabla}\tilde{\phi} \cdot \boldsymbol{\nabla}\eta \,\right] \boldsymbol{\nabla}\eta}{1 + |\boldsymbol{\nabla}\eta|^2},$$

$$0 = \kappa\, \eta_t + \boldsymbol{\nabla} \cdot \tilde{\boldsymbol{u}},$$

$$0 = 2\, \kappa\, g\, \eta + \kappa\, \tilde{\phi}_t + \tilde{v}_t + \boldsymbol{\nabla} \cdot (\tilde{v}\, \tilde{\boldsymbol{u}}).$$

The last equation gives us a hint that the right evolution variable is

$$\tilde{\boldsymbol{q}} \overset{\text{def}}{=} \boldsymbol{\nabla}\left(\tilde{\phi} + \kappa^{-1}\, \tilde{v}\right) = \tilde{\boldsymbol{u}} + \tilde{v}\, \boldsymbol{\nabla}\eta + \kappa^{-1} \boldsymbol{\nabla}(\tilde{\boldsymbol{u}} \cdot \boldsymbol{\nabla}\eta) - \kappa^{-2}\, \boldsymbol{\nabla}(\boldsymbol{\nabla} \cdot \tilde{\boldsymbol{u}}).$$

We can notice that $\boldsymbol{\nabla}(\boldsymbol{\nabla} \cdot \tilde{\boldsymbol{u}})$ can be seen as an application of the operator matrix $\boldsymbol{\nabla} \otimes \boldsymbol{\nabla}$ to the vector $\tilde{\boldsymbol{u}}$, *i.e.*

$$\tilde{\boldsymbol{q}} = \underbrace{\left[\, \mathbb{I} - \kappa^{-2}\, \boldsymbol{\nabla} \otimes \boldsymbol{\nabla} \,\right]}_{\equiv\, \mathbb{D}^{-1}} \cdot \tilde{\boldsymbol{u}} + \tilde{v}\, \boldsymbol{\nabla}\eta + \kappa^{-1} \boldsymbol{\nabla}(\tilde{\boldsymbol{u}} \cdot \boldsymbol{\nabla}\eta),$$

where $\mathbb{I}$ denotes the identity operator. Finally, the system of evolution equations can be written as

$$\kappa\, \eta_t + \boldsymbol{\nabla} \cdot \mathbb{D} \cdot \tilde{\boldsymbol{q}} = \boldsymbol{\nabla} \cdot \mathbb{D} \cdot \left[\, \tilde{v}\, \boldsymbol{\nabla}\eta + \kappa^{-1}\, \boldsymbol{\nabla}(\tilde{\boldsymbol{u}} \cdot \boldsymbol{\nabla}\eta) \,\right], \tag{5.41}$$

$$\tilde{\boldsymbol{q}}_t + 2\, g\, \boldsymbol{\nabla}\eta = -\kappa^{-1}\, (\boldsymbol{\nabla} \otimes \boldsymbol{\nabla}) \cdot (\tilde{v}\, \tilde{\boldsymbol{u}}). \tag{5.42}$$

These equations have to be supplemented by two algebraic-differential relations:

$$\tilde{v} = \tilde{\boldsymbol{u}} \cdot \boldsymbol{\nabla}\eta - \kappa^{-1}\, \boldsymbol{\nabla} \cdot \tilde{\boldsymbol{u}},$$
$$\tilde{\boldsymbol{u}} = \mathbb{D} \cdot \left[\, \tilde{\boldsymbol{q}} - \tilde{v}\, \boldsymbol{\nabla}\eta - \kappa^{-1} \boldsymbol{\nabla}(\tilde{\boldsymbol{u}} \cdot \boldsymbol{\nabla}\eta) \,\right].$$

The pseudo-differential operator $\mathbb{D} = \left[\mathbb{I} - \kappa^{-2}\,\boldsymbol{\nabla}\otimes\boldsymbol{\nabla}\right]^{-1}$ can be easily computed in the Fourier space:

$$\hat{\mathbb{D}} = \left[\mathbb{I} - \kappa^{-2}\,\boldsymbol{k}\otimes\boldsymbol{k}\right]^{-1},$$

where $\boldsymbol{k} = (k_1, k_2)$ is the vector of wavenumbers. Otherwise, one has to invert an elliptic operator numerically as it is custom in the numerical analysis of classical Serre equations [87].

An open problem. By analogy to the classical Serre–Green–Naghdi equations, the canonical Hamiltonian structure for deep water Serre equations 5.41 and 5.42 does not probably exist. The Authors of the present manuscript did not succeed in finding even a non-canonical Hamiltonian formulation which should exist in principle. Consequently, it remains an open problem so far. However, we succeeded in finding the multi-symplectic formulation for deep water Serre-type equations.

5.6 | Multi-symplectic formulation

Here, we give the multi-symplectic structure for deep water Serre equations in the case of one spatial horizontal dimension $x_1 \equiv x$ (and, thus, $\tilde{u} \equiv \tilde{u}_1$) for the sake of notation compactness. The generalization to the case of two horizontal dimensions is straightforward. The general form of multi-symplectic equations (with one spatial variable) is

$$\mathbb{M}\cdot\boldsymbol{z}_t + \mathbb{K}\cdot\boldsymbol{z}_x = \boldsymbol{\nabla}_{\boldsymbol{z}}\,\mathcal{S}(\boldsymbol{z}), \tag{5.43}$$

where $\boldsymbol{z} \in \mathbb{R}^d$ is the vector of state variables and $\mathbb{M},\ \mathbb{K} \in \mathrm{Mat}_{d\times d}(\mathbb{R})$ are some *skew-symmetric* matrices. It is not difficult to check that for deep water Serre equations 5.38–5.40 (in 1D) it is sufficient to take

$$\boldsymbol{z} = \left(\tilde{\phi},\ \eta,\ \tilde{u},\ \gamma,\ \beta,\ \tilde{v}\right)^{\top},$$

$$\mathcal{S}(\boldsymbol{z}) = -g\,\kappa\,\eta^2 + \beta\,(\tilde{u}\,\tilde{v} - \gamma) + \tfrac{1}{2}\left(\tilde{u}^2 - \tilde{v}^2\right),$$

and the skew-symmetric matrices $\mathbb{M}$ and $\mathbb{K}$ are defined as

$$\mathbb{M} \stackrel{\text{def}}{=} \begin{pmatrix} 0 & -\kappa & 0 & 0 & 0 & 0 \\ \kappa & 0 & 0 & 0 & 0 & 1 \\ 0 & 0 & 0 & 0 & 0 & 0 \\ 0 & 0 & 0 & 0 & 0 & 0 \\ 0 & 0 & 0 & 0 & 0 & 0 \\ 0 & -1 & 0 & 0 & 0 & 0 \end{pmatrix}, \qquad \mathbb{K} \stackrel{\text{def}}{=} \begin{pmatrix} 0 & 0 & -1 & 0 & 0 & 0 \\ 0 & 0 & 0 & 1 & 0 & 0 \\ 1 & 0 & 0 & 0 & 0 & 0 \\ 0 & -1 & 0 & 0 & 0 & 0 \\ 0 & 0 & 0 & 0 & 0 & 0 \\ 0 & 0 & 0 & 0 & 0 & 0 \end{pmatrix}.$$

Equation 5.43 can be rewritten in the component-wise form for the sake of clarity:

$$
\begin{aligned}
-\kappa\,\eta_t - \tilde{u}_x &= 0,\\
\kappa\,\tilde{\phi}_t + \tilde{v}_t + \gamma_x &= -2\,g\,\kappa\,\eta,\\
\tilde{\phi}_x &= \tilde{u} + \beta\,\tilde{v},\\
-\eta_x &= -\beta,\\
0 &= \gamma - \tilde{u}\,\tilde{v},\\
-\eta_t &= -\tilde{v} + \beta\,\tilde{u}.
\end{aligned}
$$

Now it is straightforward to check by making substitutions that equation 5.43 is indeed equivalent to the deep Serre equations 5.38–5.40. The generalization to the 2D case is straightforward.

CHAPTER 6

Intermediate depth example

A general Ansatz, for waves in finite constant depth and satisfying identically the bottom impermeability is suggested by the linear theory of water waves:

$$\phi \approx \frac{\cosh \kappa Y}{\cosh \kappa h}\,\tilde{\phi}(x,t), \qquad u \approx \frac{\cosh \kappa Y}{\cosh \kappa h}\,\tilde{u}(x,t), \qquad v \approx \frac{\sinh \kappa Y}{\sinh \kappa h}\,\tilde{v}(x,t), \tag{6.1}$$

where $Y = y+d$. The parameter $\kappa > 0$ is a characteristic wave number to be made precise *a posteriori*. This Ansatz is uniformly valid for all depths because it yields the shallow water one 4.1 as $\kappa \to 0$, and the deep water one 5.15 as $d \to \infty$. Obviously, the Ansatz 6.1 should be valid for wave fields with wavenumber spectra that are narrow-banded around κ.

Substituting the Ansatz 6.1 into 3.7, one obtains

$$\begin{aligned}\mathscr{L} = {} & [\,\eta_t + \tilde{u}\,\eta_x\,]\,\tilde{\phi} - \frac{g\,\eta^2}{2} + \frac{\tilde{v}^2}{2}\,\frac{\sinh(2\kappa h) - 2\kappa h}{2\kappa\cosh(2\kappa h) - 2\kappa} + \frac{\tilde{\phi}\,\tilde{v}}{2}\left[\frac{2\kappa h}{\sinh(2\kappa h)} - 1\right] \\ & + \left[\frac{\tilde{u}^2}{2} + \tilde{\phi}\,\tilde{u}_x - \kappa\tanh(\kappa h)\,\tilde{\phi}\,\tilde{u}\,\eta_x\right]\frac{\sinh(2\kappa h) + 2\kappa h}{2\kappa\cosh(2\kappa h) + 2\kappa}.\end{aligned} \tag{6.2}$$

Applying various constraints, one obtains generalized equations, including the ones derived in the previous sections 4 and 5 as limiting cases. In particular, one can derive arbitrary depth generalizations of the Serre and Klein–Gordon equations. These derivations are left to the reader. The main purpose of this section is to illustrate the easiness of deriving approximations uniformly valid for all depths, contrary to perturbation methods with which the two main theories (*i.e.*, Stokes-like and shallow water expansions) have separated validity domains.

Indeed, the Serre equations of section 4 can also be derived from an asymptotic expansion (with the depth over wavelength ratio as a small parameter). This is not the case for all approximations obtainable from the variational principle (see examples in [52] and [83]). However, this does not mean that approximations obtained this way do not have restricted validity domains, as further discussed below.

CHAPTER 7

Conclusions and perspectives

In the discourse of the current survey, we have elucidated a novel variational principle predicated on a relaxed Lagrangian functional as expounded in [52]. The applicability and versatility of this variational principle have been demonstrated through a plethora of examples emanating from a spectrum of water depths: shallow, deep, and intermediate. It is our aspiration that the wide array of examples furnished herein would serve as a robust guide, aiding our readers in adeptly employing this method to address the challenges inherent in their specific scenarios. However, a word of caution is warranted here: every approximation deployed carries with it a defined domain of validity. Therefore, it is imperative that these approximate models are wielded judiciously, and preferentially in scenarios that align with their foundational design principles. The task of delineating the bounds of a model's validity region is not to be taken lightly and ideally warrants a dedicated study to ensure a nuanced understanding of the model's capabilities and limitations. It is pertinent to note that these observations are not confined to the relaxed variational principle proposed herein but extend to all approximate models harnessed in the realm of applied sciences. The essence of these remarks underscores a broader scientific rigour and discernment requisite in the employment of approximate models, thereby fostering a more informed and judicious application of these tools in unravelling the intricacies of fluid dynamics.

It may be worth reminding the main advantages of using the variational methods in modelling water waves (and not only):

- The approximate model inherits naturally the variational structure of the base model. Thus, it can be studied using similar methods.
- Thanks to the celebrated Noether theorem, we may preserve important symmetries and conservation laws. In particular, in water waves, we believe it is of capital importance to have the momentum and energy conservation (or balance) laws along with the Galilean boost symmetry. This systematic route has not been explored in our study yet.
- The derived model also enjoys the Hamiltonian formulation[25].

[25] Possibly a non-canonical one as it is the case of the classical Serre–Green–Naghdi equations [153].

- This variational structure might be exploited to construct efficient and structure-preserving variational integrators [151]. We started the exploration of this research direction in [82] for the case of the celebrated KdV equation and in [79, 80] for a family of Boussinesq-type equations. However, this methodology should be applied to more complex (in particular, fully nonlinear) water wave models as well.

We have illustrated the advantage of using a variational principle with as many variables as possible. We call it the *relaxed* variational principle, since the Lagrangian density 3.6 involves more degrees of freedom (*i.e.*, the variables η, ϕ, $\boldsymbol{u}$, v, $\boldsymbol{\mu}$ and ν) compared to the two degrees of freedom (η and ϕ) in the classical case. In particular, these extra variables can be used to impose various constraints such as incompressibility, irrotationality, impermeability, *etc.* The practical use of the relaxed formulation was illustrated in numerous examples in shallow, deep and intermediate waters. Thus, we obtained several approximations, some well-known and some new to our knowledge.

In the shallow water regime, we have first obtained the classical nonlinear shallow water (or Saint-Venant) equations 4.19–4.20. Then, with the same Ansatz 4.9 but imposing the constraint of the free surface impermeability, we have derived the irrotational Serre–Green–Naghdi equations 4.27–4.28. Applying the incompressibility constraint and choosing the pseudo-velocity field in a different way, we have obtained two kinds of *generalized Kaup–Boussinesq* equations. Several ways of further generalizations were also outlined. We considered a generalized Ansatz, and we illustrated its consequence in the limiting case of shallow water. In this way, we derived the modified Serre–Green–Naghdi equations (mSGN) and subsequently obtained exact cnoidal and solitary wave solutions. The main purpose of this example was to illustrate the fact that one can introduce an Ansatz which is not inspired by any asymptotic expansion and nevertheless leads to reasonable approximations.

In deep water, two models were considered. Namely, we derived deep water counterparts of the celebrated Saint-Venant and Serre equations. The former has a canonical Hamiltonian formulation and degenerates to the Klein–Gordon equation in the linear approximation; we thus called the new system 5.17, 5.18 *generalized Klein–Gordon* equations. The latter could be solved analytically for a two-dimensional travelling wave. This solution is a striking illustration of the power of the variational formulation compared to asymptotic expansion methods, especially for large amplitudes when the expansion parameter is no longer small. Of course, the validity limits of all these models have to be properly studied and assessed.

The case of arbitrary depth has also been briefly considered. In particular, it has been shown how easily one can introduce an Ansatz valid for all depths. Indeed, the vertical variation of the velocity

field suggested by the linear theory provides at once such a general Ansatz, which degenerates to previous cases when the water is shallow ($\kappa d \to 0$) or deep ($d \to \infty$). This simplicity and flexibility of the variational principle is quite remarkable compared to perturbation methods.

In this survey, some further possibilities for generalizations are also mentioned. However, we have to emphasize that not all Ansätze and constraints will necessarily lead to physically relevant and tractable approximations; the same is true for models derived from asymptotic expansions, however. Nonetheless, the relaxed variational formulation is sufficiently versatile to allow easy derivations of physically sound models. We have illustrated this claim, in particular, by showing how it is simple to obtain approximate equations valid for all depths.

Sometimes, the choice of the constraints may seem to be rather *ad hoc*, but that should not be surprising. Indeed, the water wave theory already knows several *ad hoc* 'tricks' intended to improve the approximation quality. For instance, it was proposed in [157] to replace the polynomial shallow water expansion 4.8 by a (m, n)-Padé approximation, the orders m and n being chosen to improve the linear dispersion relation of progressive waves. Another example is the use of the velocity potential defined at some depth y_0 [183] and, as before, the free parameter y_0 is chosen to improve linear dispersion characteristics. The approach proposed here is not more *ad hoc* than any example mentioned above. Moreover, the variational principle allows for greater flexibility in the choice of the Ansatz. Thus, the approximations derived via the relaxed variational procedure must be studied *a posteriori* in order to verify their mathematical consistency and physical relevance. This is also the case for approximations derived via perturbation techniques, and many such approximations commonly used have not yet been justified on a rigorous mathematical basis. In the several examples presented here, the Ansätze involve free parameters that we have chosen constant for simplicity. One may also consider these parameters as functions and find their values from the stationary point of the Lagrangian. Doing so will lead to more complicated equations, but this is not a major issue if these equations are intended to be treated numerically.

In order to derive approximate models, variational formulations are an attractive alternative to asymptotic expansions. However, both approaches can also be combined. Indeed, once the variational principle has been applied to an Ansatz, asymptotic expansions can be further applied to obtain simpler models. For instance, one could consider 'unidirectionalized' approximations [184, 185] to derive variants of Korteweg and de Vries [140], Dysthe [98], Camassa and Holm [40], Degasperis and Procesi [69], Kraenkel *et al.* [141], and other equations. This possibility will be investigated in future works.

Regarding the perspectives, interested readers could use this method to build new pertinent approximations. The authors of the present survey are already fully engaged in the quest for new models. In particular, a lot of work has still to be done in the three-dimensional setting. Also, new physical effects may be added to the variational principle. The examples presented above stem from the free surface gravity waves [41, 232, 242]. However, the (discretely or continuously) stratified flows can also be considered (such as internal waves [104, 116]). Adding the surface tension [54, 72, 189], flexural-gravity [66] and electro-magneto fluid effects [123, 124] are very promising research directions which have been treated mostly with non-variational approaches so far. It is only for the sake of simplicity that we have considered only gravity waves propagating at the surface of a single layer of a homogeneous fluid. It is trivial to introduce a relaxed variational formulation including, *e.g.*, surface tension, stratifications in several homogeneous layers and obstacles. Such general variational formulations, together with relevant Ansätze and well-chosen constraints, will easily lead to interesting models. For perfect fluids, variational formulations can also be obtained for rotational motions [60, 99, 152, 155, 176, 197]. A relaxed version of such variational principles will facilitate the derivation of approximate models. We invite everybody to join this scientific direction.

Acknowledgments

The Authors would like to acknowledge the very helpful discussions with Prof. Angel Duràn (University of Valladolid, Spain) on the topics of numerical methods and their convergence, especially for the travelling waves computation. Moreover, we would like to thank Prof. Damien Violeau (EDF Chatou, France) for his kind invitation to prepare this IAHR monograph and for organizing a rigorous peer-review process of the present manuscript. We are indebted to three Referees – Onno Bokhove of the University of Leeds and Evgeniy Lokharu of the University of Lund and Boris Kolev (CNRS) of the Laboratory of Mechanics Paris-Saclay – who devoted their time to rereading our work and who provided numerous comments to improve the present text. Without this rigorous peer review process, the quality of this text would be definitely below its current state.

Funding

The work of Denys Dutykh has been supported by the French National Research Agency through the Investments for Future Program (ref. ANR−18−EURE−0016 — Solar Academy). This publication is based upon work supported by the Khalifa University of Science and Technology under Award No. FSU−2023 − 014.

Author contributions

All the Authors contributed equally to this work.

Conflict of interest statement

The Authors certify that they have **no** affiliations with or involvement in any organization or entity with any financial interest (such as honoraria; educational grants; participation in speakers' bureaus; membership, employment, consultancies, stock ownership, or other equity interest; and expert testimony or patent-licensing arrangements), or non-financial interest (such as personal or professional relationships, affiliations, knowledge or beliefs) in the subject matter or materials discussed in this manuscript.

Disclaimer statement

The opinions expressed in this publication/study are those of the authors and do not necessarily reflect the views of their employers or any other affiliated organizations.

APPENDIX A

Exact Stokes wave

In deep water, a seventh-order Stokes expansion (for the exact equations) is

$$\begin{aligned}\kappa\,\eta = {}& \alpha\cos\xi + \tfrac{1}{2}\alpha^2\left(1+\tfrac{17}{12}\alpha^2+\tfrac{233}{64}\alpha^4\right)\cos 2\xi \\ &+ \tfrac{3}{8}\alpha^3\left(1+\tfrac{51}{16}\alpha^2+\tfrac{3463}{320}\alpha^4\right)\cos 3\xi + \tfrac{1}{3}\alpha^4\left(1+\tfrac{307}{60}\alpha^2\right)\cos 4\xi \\ &+ \tfrac{125}{384}\alpha^5\left(1+\tfrac{10697}{1500}\alpha^2\right)\cos 5\xi + \tfrac{27}{80}\alpha^6\cos 6\xi + \tfrac{16807}{46080}\alpha^7\cos 7\xi + \mathcal{O}(\alpha^8),\end{aligned} \tag{A.1}$$

$$\begin{aligned}g^{-\frac{1}{2}}\kappa^{\frac{3}{2}}\,\tilde{\phi} = {}& \alpha\left(1-\tfrac{1}{4}\alpha^2-\tfrac{43}{96}\alpha^4-\tfrac{2261}{1536}\alpha^6\right)\sin\xi + \tfrac{1}{2}\alpha^2\left(1+\tfrac{7}{12}\alpha^2+\tfrac{81}{64}\alpha^4\right)\sin 2\xi \\ &+ \tfrac{3}{8}\alpha^3\left(1+\tfrac{281}{144}\alpha^2+\tfrac{5813}{1080}\alpha^4\right)\sin 3\xi + \tfrac{1}{3}\alpha^4\left(1+\tfrac{431}{120}\alpha^2\right)\sin 4\xi \\ &+ \tfrac{125}{384}\alpha^5\left(1+\tfrac{3369}{625}\alpha^2\right)\sin 5\xi + \tfrac{27}{80}\alpha^6\sin 6\xi + \tfrac{16807}{46080}\alpha^7\sin 7\xi + \mathcal{O}(\alpha^8),\end{aligned} \tag{A.2}$$

$$g^{-\frac{1}{2}}\kappa^{\frac{1}{2}}\,c = 1+\tfrac{1}{2}\alpha^2+\tfrac{1}{2}\alpha^4+\tfrac{707}{384}\alpha^6+\mathcal{O}(\alpha^8), \tag{A.3}$$

where $\theta=\kappa(x-ct)$. Note that, to the leading order, the n^{th} Fourier coefficient is $2^{1-n}n^{n-2}\alpha^n/(n-1)!$ (this is also true for all $n>7$). In the bulk of the fluid, the velocity potential is

$$\begin{aligned}g^{-\frac{1}{2}}\kappa^{\frac{3}{2}}\,\phi = {}& \alpha\left(1-\tfrac{1}{8}\alpha^2-\tfrac{7}{12}\alpha^4-\tfrac{14761}{9216}\alpha^6\right)\mathrm{e}^{\kappa y}\sin\theta + \tfrac{1}{2}\alpha^4\left(1+\tfrac{11}{6}\alpha^2\right)\mathrm{e}^{2\kappa y}\sin 2\theta \\ &+ \tfrac{1}{12}\alpha^5\left(1+\tfrac{191}{24}\alpha^2\right)\mathrm{e}^{3\kappa y}\sin 3\theta + \tfrac{1}{72}\alpha^6\,\mathrm{e}^{4\kappa y}\sin 4\theta \\ &+ \tfrac{1}{480}\alpha^7\,\mathrm{e}^{5\kappa y}\sin 5\theta + \mathcal{O}(\alpha^8),\end{aligned}$$

meaning that harmonics appear in the fourth order only, thus justifying the Ansatz 5.15. Note that, to the leading order, the nth Fourier coefficient is $\alpha^{n+2}/n!(n-1)$ for all $n>1$.

APPENDIX B

Cubic Zakharov's equations

Satisfying exactly the Laplace equation and the bottom impermeability, the gravity waves variational formulation [155] yields the Hamiltonian [243]:

$$\mathcal{H} = \frac{1}{2}\int \left\{ g\,\eta^2 + \tilde{\phi}\,V \right\} \mathrm{d}^2\boldsymbol{x}, \qquad V = \left[\phi_y - \boldsymbol{\nabla}\eta\cdot\boldsymbol{\nabla}\phi\right]_{y=\eta}. \tag{B.1}$$

Introducing a Dirichlet–Neumann operator G, such that $V = G(\eta)\tilde{\phi}$ (Craig and Sulem (1993), [64]), expanding G around $\eta = 0$ and neglecting the terms beyond the quartic nonlinearities, the Hamiltonian B.1 becomes

$$\begin{aligned}\mathcal{H} = \frac{1}{2}\int \Big\{ & g\eta^2 + \tilde{\phi}\Big[\mathfrak{d}\tilde{\phi} - \mathfrak{d}(\eta\mathfrak{d}\tilde{\phi}) - \boldsymbol{\nabla}\cdot(\eta\boldsymbol{\nabla}\tilde{\phi}) \\ & + \tfrac{1}{2}\mathfrak{d}(\eta^2\boldsymbol{\nabla}^2\tilde{\phi}) + \mathfrak{d}(\eta\,\mathfrak{d}(\eta\,\mathfrak{d}\tilde{\phi})) + \tfrac{1}{2}\boldsymbol{\nabla}^2(\eta^2\,\mathfrak{d}\tilde{\phi})\Big]\Big\}\,\mathrm{d}^2\boldsymbol{x},\end{aligned} \tag{B.2}$$

with the pseudo-differential operator[26] $\mathfrak{d} = (-\boldsymbol{\nabla}^2)^{\frac{1}{2}}\tanh[(-\boldsymbol{\nabla}^2)^{\frac{1}{2}}d]$. Thus, the cubic Zakharov equations (CZE) are

$$\eta_t - \mathfrak{d}\tilde{\phi} = -\boldsymbol{\nabla}\cdot(\eta\boldsymbol{\nabla}\tilde{\phi}) - \mathfrak{d}(\eta\mathfrak{d}\tilde{\phi}) + \tfrac{1}{2}\boldsymbol{\nabla}^2(\eta^2\mathfrak{d}\tilde{\phi}) + \mathfrak{d}(\eta\mathfrak{d}(\eta\mathfrak{d}\tilde{\phi})) + \tfrac{1}{2}\mathfrak{d}(\eta^2\boldsymbol{\nabla}^2\tilde{\phi}), \tag{B.3}$$

$$\tilde{\phi}_t + g\eta = \tfrac{1}{2}(\mathfrak{d}\tilde{\phi})^2 - \tfrac{1}{2}(\boldsymbol{\nabla}\tilde{\phi})^2 - (\eta\mathfrak{d}\tilde{\phi})\boldsymbol{\nabla}^2\tilde{\phi} - (\mathfrak{d}\tilde{\phi})\mathfrak{d}(\eta\mathfrak{d}\tilde{\phi}). \tag{B.4}$$

For progressive $(2\pi/\kappa)$-periodic solutions in infinite depth, a seventh-order Stokes expansion is

$$\begin{aligned}\kappa\,\eta = {} & \alpha\cos\theta + \tfrac{1}{2}\alpha^2\left(1 + \tfrac{3}{2}\alpha^2 + \tfrac{445}{96}\alpha^4\right)\cos 2\theta \\ & + \tfrac{3}{8}\alpha^3\left(1 + \tfrac{41}{12}\alpha^2 + \tfrac{5213}{384}\alpha^4\right)\cos 3\theta + \tfrac{7}{24}\alpha^4\left(1 + \tfrac{263}{42}\alpha^2\right)\cos 4\theta \\ & + \tfrac{67}{384}\alpha^5\left(1 + \tfrac{2569}{201}\alpha^2\right)\cos 5\theta - \tfrac{9}{320}\alpha^6\cos 6\theta - \tfrac{16751}{46080}\alpha^7\cos 7\theta + \mathcal{O}(\alpha^8), \\ g^{-\frac{1}{2}}\kappa^{\frac{3}{2}}\,\tilde{\phi} = {} & \alpha\left(1 - \tfrac{1}{4}\alpha^2 - \tfrac{31}{64}\alpha^4 - \tfrac{465}{256}\alpha^6\right)\sin\theta + \tfrac{1}{2}\alpha^2\left(1 + \tfrac{3}{4}\alpha^2 + \tfrac{123}{64}\alpha^4\right)\sin 2\theta \\ & + \tfrac{3}{8}\alpha^3\left(1 + \tfrac{89}{36}\alpha^2 + \tfrac{27271}{3456}\alpha^4\right)\sin 3\theta + \tfrac{7}{24}\alpha^4\left(1 + \tfrac{1795}{336}\alpha^2\right)\sin 4\theta \\ & + \tfrac{67}{384}\alpha^5\left(1 + \tfrac{24769}{2010}\alpha^2\right)\sin 5\theta - \tfrac{9}{320}\alpha^6\sin 6\theta - \tfrac{16751}{46080}\alpha^7\sin 7\theta + \mathcal{O}(\alpha^8), \\ g^{-\frac{1}{2}}\kappa^{\frac{1}{2}}\,c = {} & 1 + \tfrac{1}{2}\alpha^2 + \tfrac{41}{64}\alpha^4 + \tfrac{913}{384}\alpha^6 + \mathcal{O}(\alpha^8),\end{aligned}$$

[26] For one horizontal dimension in infinite depth $\mathfrak{d}f = -\mathscr{H}(f_x)$, $\mathscr{H}$ being the Hilbert transform.

where the incorrect (compared to the exact expansion) coefficients and signs are displayed in boldface. Thus, the CZE matches the exact Stokes wave up to the third-order only. Truncating the Hamiltonian at the order $N + 1$ in nonlinearities, the corresponding Stokes double series is correct up to the order N in the expansion parameter. None of these approximations has the exact asymptotic behaviour 5.21 for their Fourier coefficients.

APPENDIX C

The workflow pattern

The section 4.5.2 would not be complete if we did not explain how we arrived at the multi-symplectic structure 4.48 of the SGN equations. It is not so trivial to see how this structure appears from equations 4.37, 4.38. However, when we derive the SGN system from the relaxed variational principle [52], a more suitable form of the equations appears. Namely, the relaxed Lagrangian [52] under the shallow water Ansatz reads (see also [87])

$$\mathscr{L} = (h_t + \bar{\boldsymbol{\mu}}\, h_x)\,\bar{\phi} - \tfrac{1}{2}\, g\, h^2 + h\left[\,\bar{\boldsymbol{\mu}}\,\bar{\boldsymbol{u}} - \tfrac{1}{2}\,\bar{\boldsymbol{u}}^2 + \tfrac{1}{3}\,\tilde{\nu}\,\tilde{v} - \tfrac{1}{6}\,\tilde{v}^2 \;+\; \bar{\phi}\,\bar{\boldsymbol{\mu}}_x\,\right],$$

where $\bar{\boldsymbol{\mu}}$, $\tilde{\nu}$ are the Lagrange multipliers. An additional constraint of the free surface impermeability is imposed:

$$\tilde{\nu} = h_t + \bar{\boldsymbol{\mu}}\, h_x.$$

The corresponding Euler–Lagrange equations are

$$\delta\,\bar{\boldsymbol{u}}: \qquad 0 = \bar{\boldsymbol{\mu}} \;-\bar{\boldsymbol{u}}, \tag{C.1}$$

$$\delta\,\tilde{v}: \qquad 0 = h_t + \bar{\boldsymbol{\mu}} h_x \;-\; \tilde{v}, \tag{C.2}$$

$$\delta\,\bar{\boldsymbol{\mu}}: \qquad 0 = \bar{\boldsymbol{u}} + \tfrac{1}{3}\,\tilde{v}\, h_x - \bar{\phi}_x, \tag{C.3}$$

$$\delta\,\bar{\phi}: \qquad 0 = h_t + \left[\, h\,\bar{\boldsymbol{\mu}}\,\right]_x, \tag{C.4}$$

$$\delta\, h: \qquad 0 = \bar{\boldsymbol{\mu}}\,\bar{\boldsymbol{u}} - \tfrac{1}{2}\,\bar{\boldsymbol{u}}^2 - \tfrac{1}{6}\,\tilde{v}^2 - \bar{\boldsymbol{\mu}}\bar{\phi}_x - \bar{\phi}_t - g\, h - \tfrac{1}{3}\, h\left[\,\tilde{v}_t + \bar{\boldsymbol{\mu}}\,\tilde{v}_x + \tilde{v}\,\bar{\boldsymbol{\mu}}_x\,\right]. \tag{C.5}$$

After eliminating $\bar{\boldsymbol{\mu}}$ from equations C.2–C.5 thanks to C.1 and introducing the extra variables $p = hv$, $q = hu$, $r = huv$, and $s = h_x$, one almost obtains the required system 4.52–4.59 for the multi-symplectic formulation.

APPENDIX D

Classical variational structures in deep water

In this Appendix, we briefly describe the *main* variational structures of the deep water wave problem in the chronological order of their appearance. Of course, this list is not exhaustive. The water wave problem is known since Petrov [190] and Zakharov [243] to have the Hamiltonian structure. Below, we present the classical Lagrangian and Hamiltonian formulations together since they are naturally related by Legendre transformation.

Let us compute the kinetic $\mathscr{K}$ and potential P energies of a deep fluid moving under the force of gravity g:

$$\mathscr{K} \stackrel{\text{def}}{=} \frac{1}{2} \int_{\mathbb{R}^2} \int_{-\infty}^{\eta} |\boldsymbol{u}|^2 \, \mathrm{d}y \, \mathrm{d}\boldsymbol{x}, \qquad P = \frac{1}{2} g \int_{\mathbb{R}^2} \eta^2 \, \mathrm{d}\boldsymbol{x}.$$

According to Hamilton's principle [15], the fluid motion has to provide a stationary value to the following action functional

$$\mathcal{S} = \int_{t_0}^{t_1} \rho \mathcal{L} \, \mathrm{d}t, \tag{D.1}$$

where $\mathcal{L}$ is the Lagrangian density classically defined as

$$\mathcal{L} \stackrel{\text{def}}{=} \mathscr{K} - P.$$

Below in section D.1, we shall give another Lagrangian density. We have to keep in mind that the flow is incompressible, *i.e.*

$$\boldsymbol{\nabla} \cdot \boldsymbol{u} = 0,$$

and on the free surface, we also have the kinematic boundary condition that we shall write as

$$\eta_t = \sqrt{1 + |\boldsymbol{\nabla}\eta|^2} \cdot u_n,$$

where $u_n \stackrel{\text{def}}{=} \boldsymbol{u} \cdot \boldsymbol{n}$ is the normal velocity at the free surface and $\boldsymbol{n}$ is the the outer unitary normal vector

$$\boldsymbol{n} = \frac{1}{\sqrt{1 + |\boldsymbol{\nabla}\eta|^2}} \begin{pmatrix} -\boldsymbol{\nabla}\eta \\ 1 \end{pmatrix}.$$

We have to incorporate these conditions into Hamilton principle using two Lagrange multipliers $\phi = \phi(\boldsymbol{x}, y, t)$ and $\tilde{\phi} = \tilde{\phi}(\boldsymbol{x}, t)$:

$$\mathcal{L} = \mathscr{K} - P + \int_{\mathbb{R}^2} \int_{-\infty}^{\eta} \phi \, \boldsymbol{\nabla} \cdot \boldsymbol{u} \, \mathrm{d}y \, \mathrm{d}\boldsymbol{x} + \int_{\mathbb{R}^2} \left[\eta_t - \sqrt{1 + |\boldsymbol{\nabla}\eta|^2} \cdot u_n \right] \tilde{\phi} \, \mathrm{d}\boldsymbol{x}.$$

By taking the variation of this functional with respect to $\boldsymbol{u}$ and requiring that it vanishes in the fluid bulk, we obtain

$$\delta \boldsymbol{u} : \ \boldsymbol{u} - \boldsymbol{\nabla}\phi = \boldsymbol{0}. \tag{D.2}$$

Consequently, the flow is necessarily irrotational. It is a direct consequence of assumptions made above, and the Lagrange multiplier ϕ is a velocity potential. From Kelvin's circulation theorem, we know that the flow that is initially irrotational will remain irrotational forever [16]. The variational description of flows with vorticity is out of the scope of the present study.

Taking into account D.2, from now on, we can substitute $\boldsymbol{u} = \boldsymbol{\nabla}\phi$ into the Lagrangian density $\mathcal{L}$. By applying the Gauß–Ostrogradsky theorem to the Lagrangian density we obtain

$$\mathcal{L} = \int_{\mathbb{R}^2} \left[\tilde{\phi} \, \eta_t + u_n \sqrt{1 + |\boldsymbol{\nabla}\eta|^2} \cdot \left(\tilde{\phi} - \phi \big|_{y=\eta} \right) \right] \mathrm{d}\boldsymbol{x} - K - P.$$

By taking the variation with respect to the normal velocity u_n we obtain

$$\delta u_n : \ \tilde{\phi} - \phi \big|_{y=\eta} = 0.$$

Thus, the other Lagrange multiplier $\tilde{\phi}$ is simply the trace of the velocity potential at the free surface, *i.e.*

$$\tilde{\phi}(\boldsymbol{x}, t) \ \equiv \ \phi\big(\boldsymbol{x}, y = \eta(\boldsymbol{x}, t), t\big).$$

Finally, the Lagrangian density $\mathcal{L}$ becomes

$$\mathcal{L} = \int_{\mathbb{R}^2} \tilde{\phi} \, \eta_t \, \mathrm{d}\boldsymbol{x} - \mathcal{H}$$

where $\mathcal{H} \overset{\text{def}}{=} K + P$ is the total fluid energy being also the Hamiltonian of the water wave problem:

$$\mathcal{H} = \frac{1}{2} \int_{\mathbb{R}^2} \int_{-\infty}^{\eta} |\boldsymbol{\nabla}\phi|^2 \, \mathrm{d}\boldsymbol{x} + \frac{1}{2} \, g \int_{\mathbb{R}^2} \eta^2 \, \mathrm{d}\boldsymbol{x}.$$

The last Hamiltonian functional was independently rediscovered by Broer [39], then by Miles [166] and probably several other researchers.

The evolution equations for canonical variables are

$$\eta_t = \frac{\delta \mathcal{H}}{\delta \tilde{\phi}}, \qquad \tilde{\phi}_t = -\frac{\delta \mathcal{H}}{\delta \eta}.$$

By $\delta\mathcal{H}$, we denote the variational (Gâteaux's) derivative. In order to compute the Hamiltonian $\mathcal{H}$ one has to solve the Laplace equation

$$\boldsymbol{\nabla}^2 \phi = 0,$$

with corresponding boundary conditions:

$$\phi\big|_{y=\eta} = \tilde{\phi}, \qquad |\boldsymbol{\nabla}\phi| \to 0, \quad \text{as} \quad y \to -\infty.$$

In general, it is not possible to solve this problem analytically. Consequently, in deep water, one uses in practice asymptotic expansions with respect to the small parameter $\varepsilon \sim \|\boldsymbol{\nabla}\eta\|$.

D.1 | Luke's Lagrangian formulation

In 1967, Luke proposed to use the following functional [155] (in finite depth case):

$$\mathcal{L} = \int_{-d}^{\eta} \left[\phi_t + \tfrac{1}{2} |\boldsymbol{\nabla}\phi|^2 + \tfrac{1}{2} \phi_y^2 + g\, y \right] \mathrm{d}y,$$

where d is the constant water depth. The action integral is defined in D.1 as above. Without free surface effects, this functional was proposed in 1929 by Bateman [17]. One can easily recognize that the expression under the integral sign is the well-known Cauchy–Lagrange integral. In his seminal paper [155], Luke justified the advantages of this functional over the classical Lagrangian $\mathcal{L} = K - P$ described above.

In order to apply the deep water approximation, we have to take the limit $d \to \infty$. The term $g\,y$ is not integrable, so before taking this limit, we integrate it over the depth and remove the constant term $-g\,\dfrac{d^2}{2}$ which disappears under the Gâteaux derivative operation. As a result, we obtain the following Lagrangian density:

$$\mathcal{L} = \int_{-\infty}^{\eta} \left[\phi_t + \tfrac{1}{2} |\boldsymbol{\nabla}\phi|^2 + \tfrac{1}{2} \phi_y^2 \right] \mathrm{d}y\, \mathrm{d}\boldsymbol{x} + \frac{1}{2}\, g\, \eta^2. \qquad \text{D.3}$$

In order to recover the water wave problem equations 2.5–2.8 in deep water, we write down the Euler–Lagrange equations corresponding to the functional D.3:

$$\begin{aligned} \delta\phi: &\quad \boldsymbol{\nabla}^2\phi + \phi_{yy} = 0, \\ \delta\phi\big|_{y=\eta}: &\quad \eta_t + \boldsymbol{\nabla}\phi\cdot\boldsymbol{\nabla}\eta - \phi_y = 0, \\ \delta\eta: &\quad \phi_t + \tfrac{1}{2}\,|\boldsymbol{\nabla}\phi|^2 + \tfrac{1}{2}\,\phi_y^2 + g\,\eta = 0. \end{aligned}$$

Luke's variational principle has at least one important advantage over the Hamiltonian principle: the flow incompressibility 2.5 is incorporated into the variational principle, and it does not have to be additionally assumed as a constraint. It appears as one of Euler–Lagrange equations.

D.2 | Relaxed Lagrangian formulation in deep water

In this Appendix, we shall redevelop the so-called '*relaxed variational principle*' in the deep water approximation. Earlier in the literature, this method was also introduced under the name of a "motivated Legendre transform" (see *e.g.* [122] for more details).

We would like to introduce more variables into the Luke Lagrangian D.3, which has the velocity potential $\phi(\boldsymbol{x}, y, t)$ and free surface elevation $\eta(\boldsymbol{x}, t)$ in its original form. Let us also introduce explicitly the components of the velocity field $\boldsymbol{u} = \boldsymbol{\nabla}\phi$ and $v = \phi_y$ by using two Lagrange multipliers $\boldsymbol{\mu}$ and ν:

$$\mathcal{L} = -\tilde{\phi}\,\eta_t + \frac{1}{2}\,g\,\eta^2 + \int_{-\infty}^{\eta} \left[\tfrac{1}{2}\,(\boldsymbol{u}^2 + v^2) + \boldsymbol{\mu}\cdot(\boldsymbol{\nabla}\phi - \boldsymbol{u}) + \nu\,(\phi_y - v)\right] \mathrm{d}y,$$

where we also took the term ϕ_t out of the integral sign for the sake of convenience. By applying the Gauß–Ostrogradsky theorem we can rewrite the Lagrangian $\mathcal{L}$ in the following *equivalent* form:

$$\begin{aligned} \mathcal{L} = &-\left(\eta_t + \tilde{\boldsymbol{\mu}}\cdot\boldsymbol{\nabla}\eta - \tilde{\nu}\right)\tilde{\phi} + \frac{1}{2}\,g\,\eta^2 \\ &+ \int_{-\infty}^{\eta} \left[\tfrac{1}{2}\,(\boldsymbol{u}^2 + v^2) - \boldsymbol{\mu}\cdot\boldsymbol{u} - \nu\cdot v - (\boldsymbol{\nabla}\cdot\boldsymbol{\mu} + \nu_y)\,\phi\right] \mathrm{d}y. \end{aligned}$$

The tildes denote the quantities evaluated at the free surface, *i.e.* $\tilde{\nu}(\boldsymbol{x}, t) \overset{\text{def}}{=} \nu\big(\boldsymbol{x}, y = \eta(\boldsymbol{x}, t), t\big)$. The last functional $\mathcal{L}$ is the so-called *relaxed variational principle*. Let us count the degrees of freedom:

(1) $\eta(\boldsymbol{x}, t)$ is the free surface elevation
(2) $\phi(\boldsymbol{x}, y, t)$ is the velocity potential
(3) $\boldsymbol{u}(\boldsymbol{x}, y, t)$ is the horizontal velocities vector

(4) $v(\boldsymbol{x}, y, t)$ is the vertical velocity
(5) $\boldsymbol{\mu}(\boldsymbol{x}, y, t)$ is the Lagrange multiplier associated to the horizontal velocities
(6) $\nu(\boldsymbol{x}, y, t)$ is the Lagrange multiplier associated to the vertical velocity

So, instead of having two degrees of freedom in the original Luke Lagrangian, the relaxed Lagrangian has six. This extra freedom can be used to derive various approximations, which was illustrated in [52].

D.2.1 | Lagrange multipliers

For the practical purposes of wave modelling in deep waters, we may content with four degrees of freedom by eliminating the Lagrange multipliers $\boldsymbol{\mu}$ and ν. Indeed, let us compute the variations of the relaxed Lagrangian with respect to $\boldsymbol{u}$ and v:

$$\delta \boldsymbol{u}: \quad \boldsymbol{u} - \boldsymbol{\mu} = \boldsymbol{0},$$

$$\delta v: \quad v - \nu = 0.$$

This computation also gives us the physical sense of Lagrange multipliers — they are pseudo-velocities, which coincide with physical velocities $\boldsymbol{u}$ and v at least in the *unconstrained* case. Thus, we can substitute $\boldsymbol{\mu} = \boldsymbol{u}$ and $\nu = v$ into $\mathcal{L}$ to obtain

$$\mathcal{L} = -\left(\eta_t + \tilde{\boldsymbol{u}} \cdot \boldsymbol{\nabla}\eta - \tilde{v}\right)\tilde{\phi} + \frac{1}{2}\, g\, \eta^2 - \int_{-\infty}^{\eta} \left[\tfrac{1}{2}\left(\boldsymbol{u}^2 + v^2\right) - \left(\boldsymbol{\nabla} \cdot \boldsymbol{u} + v_y\right)\phi\right] \mathrm{d}y. \qquad \text{D.4}$$

The last Lagrangian can also be used for modelling purposes in deep waters; see *e.g.* [86].

The variational structure in general (such as Hamiltonian or Lagrangian functionals) is important in many respects. First of all, since the full water wave equations 2.5–2.8 enjoy this variational structure, we should seek approximate models which enjoy the same structure and, thus, preserve some subset of qualitative properties of the base model. For instance, the Hamiltonian formalism [245] allows to simplify asymptotic developments in powers of the nonlinearity parameter $\varepsilon \overset{\text{def}}{=} a/\lambda$, which is the wave steepness in the deep water regime. Finally, the Hamiltonian formulation also allows us to put the problem of hydrodynamic waves in a unified framework of nonlinear waves in various media [244, 245]. Thus, methods developed in other fields might be directly transposed to water waves.

APPENDIX E

Nomenclature

$\mathbb{R}$ **:** The field of real numbers.
ε **:** A dimensionless nonlinearity parameter.
$\times$ **:** The vector product of two vectors.
$\boldsymbol{\nabla}$ **:** The gradient operator with respect to horizontal independent variables.
∂ **:** A partial derivative operator.
D **:** The total (material) derivative operator.
t **:** Time evolution variable.
$\boldsymbol{x} = (x_1, x_2)$ **:** Vector of horizontal coordinates.
x **:** The short-hand notation for x_1 in 2D.
y **:** Vertical coordinate.
$y = 0$ **:** Still water level.
$\eta(\boldsymbol{x}, t)$ Free-surface elevation above the still water depth.
$d(\boldsymbol{x}, t)$ **:** Bathymetry function.
$h(\boldsymbol{x}, t)$ **:** Total water depth.
h_0 **:** A positive constant having the meaning of the minimal water depth.
h **:** Average water depth.
β **:** A free real parameter.
λ **:** Characteristic wave length.
$\boldsymbol{u} = (u_1, u_2)$ **:** Horizontal velocity of fluid particles.
$\tilde{\boldsymbol{u}}$ **:** Horizontal velocity at the free surface.
$\check{\boldsymbol{u}}$ **:** Horizontal velocity at the bottom.
$\bar{u}$ **:** Depth-averaged horizontal velocity in 2D.
$\bar{\boldsymbol{u}}$ **:** Depth-averaged horizontal velocity in 3D.
v **:** The vertical velocity of fluid particles.
$\tilde{v}$ **:** The vertical velocity of fluid particles at the free surface.
$\check{v}$ **:** The vertical velocity of fluid particles at the solid bottom.
γ **and** $\tilde{\gamma}$ **:** The vertical acceleration of fluid particles at the free surface.
p **:** Fluid pressure divided by the fluid constant density ρ.
B **:** Bernoulli constant.

ϕ : Velocity potential function.
$\tilde{\phi}$: Velocity potential trace at the free surface.
$\check{\phi}$: Velocity potential trace at the bottom.
$\boldsymbol{\mu}$: The Lagrange multiplier corresponding to the horizontal velocity variable $\boldsymbol{u}$.
$\tilde{\boldsymbol{\mu}}$: The Lagrange multiplier $\boldsymbol{\mu}$ evaluated at the free surface.
$\check{\boldsymbol{\mu}}$: The Lagrange multiplier $\boldsymbol{\mu}$ evaluated at the solid bottom.
$\bar{\boldsymbol{\mu}}$ The depth-averaged Lagrange multiplier $\boldsymbol{\mu}$.
ν : The Lagrange multiplier corresponding to the vertical velocity variable v.
$\tilde{\nu}$: The Lagrange multiplier ν evaluated at the free surface.
$\check{\nu}$: The Lagrange multiplier ν evaluated at the solid bottom.
a : (Solitary) Wave amplitude.
c : The travelling wave celerity.
ρ : Constant fluid density.
g : Constant gravity acceleration.
κ : Characteristic wave number.
k : The wave number.
$\bar{q}$: The horizontal momentum.
$\tilde{q}$: The horizontal momentum flux.
σ : The surface tension coefficient.
$\mathscr{K}$: The kinetic energy.
P : The potential energy.
$\mathscr{L}$: The Lagrangian density.
$\mathcal{L}$: The action integral.
$\mathcal{O}$: Landau symbol.
$\mathcal{P}$: The reconstructed pressure distribution.
$\mathcal{F}$: The reconstructed force.
$\mathcal{M}$: The reconstructed tilting moment.
m : A parameter in the cnoidal wave solution.
H : The total cnoidal wave height.
$\varkappa$: The cnoidal wave number.
$\mathbb{J}$: A symplectic operator.
$\mathcal{H}$: A Hamiltonian functional.
$\mathcal{Q}$: A conserved quantity.
E : The total (conserved) energy.
I : The conserved momentum.

F **,** G **:** The conservation laws fluxes.

$\mathbb{M}$ **and** $\mathbb{K}$ **:** Skew-symmetric matrices in the multi-symplectic formulation.

$\boldsymbol{z}$ **:** A vector of state variables in the multi-symplectic formulation.

S **:** The Hamiltonian function in the multi-symplectic formulation.

$c_{1,\,2,\,3,\,4}$ **:** Some real constants.

$\{\,\boldsymbol{e}_i\,\}_{i=1}^{n}$ **:** The standard basis vectors in $\mathbb{R}^n$.

$\boldsymbol{V}$ **:** The vector of conservative variables.

$\boldsymbol{F}$ **:** The flux in the conservation laws.

$\boldsymbol{S}$ **:** The source term in a system of balance laws.

$\mathbb{A}$ **:** The Jacobian matrix of the advective flux $\boldsymbol{F}$ ($\boldsymbol{V}$).

λ **:** Eigenvalue of the Jacobian matrix $\mathbb{A}$.

c_s **:** The speed of infinitely long gravity waves.

$\mathbb{R}$ **:** The matrix of right eigenvectors.

$\mathbb{L}$ **:** The matrix of left eigenvectors.

Δx **:** The length of a discrete cell (control volume) in the finite volume method.

$\bar{\boldsymbol{V}}$ **:** The cell-averaged vector of conservative variables.

$\mathcal{F}$ **:** The numerical flux function.

$\mathbb{U}$ **:** The sign matrix.

$\boldsymbol{Q}$ **:** A quadratic interpolating polynomial.

L **:** A linear interpolant.

$k_{1,\,2,\,3,\,4}$ **:** Intermediate stages in the time-stepper.

Δt **:** The local time step.

N **and** $\mathcal{N}$ **:** A nonlinear operator.

θ **:** A free relaxation paremter in $[\,0,\ 1\,]$.

i **:** The imaginary unit, *i.e.* $\mathrm{i}^2 = -1$.

Bibliography

1 | Abramowitz, M., and Stegun, I. A. *Handbook of Mathematical Functions With Formulas, Graphs, and Mathematical Tables*. Dover Publications, Inc., Washington, DC, 1972.

2 | Airy, G. B. On the laws of the tides on the coasts of Ireland, as inferred from an extensive series of observations made in connexion with the Ordnance Survey of Ireland. *Philos. Trans. R. Soc. London* (1845), 1–124.

3 | Ammon, C. J., Ji, C., Thio, H.-K., Robinson, D. I., Ni, S., Hjorleifsdottir, V., Kanamori, H., Lay, T., Das, S., Helmberger, D., Ichinose, G., Polet, J., and Wald, D. Rupture process of the 2004 Sumatra-Andaman earthquake. *Science 308* (2005), 1133–1139.

4 | Ancey, C., Bain, V., Bardou, E., Borrel, G., Burnet, R., Jarry, F., Kolbl, O., and Meunier, M. *Dynamique des avalanches*. Presses polytechniques et universitaires romandes (Lausanne, Suisse), 2006.

5 | Antonopoulos, D. C., Dougalis, V. A., and Mitsotakis, D. E. Initial-boundary-value problems for the Bona-Smith family of Boussinesq systems. *Advances in Differential Equations 14* (2009), 27–53.

6 | Antonopoulos, D. C., Dougalis, V. A., and Mitsotakis, D. E. Numerical solution of Boussinesq systems of the Bona-Smith family. *Appl. Numer. Math. 30* (2010), 314–336.

7 | Ardakani, H. A., Bridges, T. J., Gay-Balmaz, F., Huang, Y. H., and Tronci, C. A variational principle for fluid sloshing with vorticity, dynamically coupled to vessel motion. *Proceedings of the Royal Society A: Mathematical, Physical and Engineering Sciences 475*, 2224 (apr 2019), 20180642.

8 | Artiles, W., and Nachbin, A. Nonlinear evolution of surface gravity waves over highly variable depth. *Phys. Rev. Lett. 93*, 23 (2004), 234501.

9 | Ascher, U. M., and McLachlan, R. I. On Symplectic and Multisymplectic Schemes for the KdV Equation. *J. Sci. Comput. 25*, 1 (2005), 83–104.

10 | Avilez-Valente, P., and Seabra-Santos, F. J. A high-order Petrov-Galerkin finite element method for the classical Boussinesq wave model. *Int. J. Numer. Meth. Fluids 59* (2009), 969–1010.

11 | Balk, A. M. A Lagragian for water waves. *Phys. Fluids 8* (1996), 416–419.

12 | Barth, T. J. Aspects of unstructured grids and finite-volume solvers for the Euler and Navier-Stokes equations. *Lecture series - van Karman Institute for Fluid Dynamics 5* (1994), 1–140.

13 | Barth, T. J., and Ohlberger, M. Finite Volume Methods: Foundation and Analysis. In *Encyclopedia of Computational Mechanics*, E. Stein, R. de Borst, and T. J. R. Hughes, Eds. John Wiley and Sons, Ltd, Chichester, UK, nov 2004, pp. 439–474.

14 | Barthélémy, E. Nonlinear shallow water theories for coastal waves. *Surveys in Geophysics 25* (2004), 315–337.

15 | Basdevant, J.-L. *Variational Principles in Physics*. Springer-Verlag, New York, 2007.

16 | Batchelor, G. K. *An Introduction to Fluid Dynamics*. Cambridge University Press, Cambridge, 1967.

17 | Bateman, H. Notes on a Differential Equation Which Occurs in the Two-Dimensional Motion of a Compressible Fluid and the Associated Variational Problems. *Proceedings of the Royal Society A: Mathematical, Physical and Engineering Sciences 125* (1929), 598–618.

18 | Beji, S., and Nadaoka, K. A time-dependent nonlinear mild slope equation for water waves. *Proc. R. Soc. Lond. A 453*, 1957 (feb 1997), 319–332.

19 | Benjamin, T. B., Bona, J. L., and Mahony, J. J. Model equations for long waves in nonlinear dispersive systems. *Philos. Trans. Royal Soc. London Ser. A 272* (1972), 47–78.

20 | Benjamin, T. B., and Olver, P. J. Hamiltonian structure, symmetries and conservation laws for water waves. *J. Fluid Mech 125* (1982), 137–185.

21 | Benney, D. J., and Newell, A. C. The propagation of nonlinear wave envelopes. *J. Math. and Physics 46* (1967), 133–139.

22 | Berger, R. C., and Carey, G. F. Free-surface flow over curved surfaces: Part I: Perturbation analysis. *Int. J. Num. Meth. Fluids 28* (1998), 191–200.

23 | Boccotti, P. *Wave Mechanics for Ocean Engineering*. Elsevier Sciences, Oxford, 2000.

24 | Bogacki, P., and Shampine, L. F. A 3(2) pair of Runge-Kutta formulas. *Appl. Math. Lett. 2(4)* (1989), 321–325.

25 | Bona, J. L., and Chen, M. A Boussinesq system for two-way propagation of nonlinear dispersive waves. *Physica D 116* (1998), 191–224.

26 | Bonneton, P., Chazel, F., Lannes, D., Marche, F., and Tissier, M. A splitting approach for the fully nonlinear and weakly dispersive Green-Naghdi model. *J. Comput. Phys. 230* (2011), 1479–1498.

27 | Borisenko, A. I., and Tarapov, I. E. *Vector and Tensor Analysis with Applications*. Dover Publications, New York, 1979.

28 | Bouchut, F., Mangeney-Castelnau, A., Perthame, B., and Vilotte, J.-P. A new model of Saint-Venant and Savage-Hutter type for gravity driven shallow water flows. *C. R. Acad. Sci. Paris I 336* (2003), 531–536.

29 | Boussinesq, J. V. Théorie de l'intumescence liquide appelée onde solitaire ou de translation se propageant dans un canal rectangulaire. *C.R. Acad. Sci. Paris Sér. A-B 72* (1871), 755–759.

30 | Boussinesq, J. V. Théorie des ondes et des remous qui se propagent le long d'un canal rectangulaire horizontal, en communiquant au liquide contenu dans ce canal des vitesses sensiblement pareilles de la surface au fond. *J. Math. Pures Appl. 17* (1872), 55–108.

31 | Boyd, J. P. *Chebyshev and Fourier Spectral Methods*, 2nd ed. Dover Publications, New York, New York, 2000.

32 | Bridges, T. J. Periodic patterns, linear instability, symplectic structure and mean-flow dynamics for three-dimensional surface waves. *Phil. Trans. Royal Soc. London A 354* (1996), 533–574.

33 | Bridges, T. J. Multi-symplectic structures and wave propagation. *Math. Proc. Camb. Phil. Soc. 121*, 1 (jan 1997), 147–190.

34 | Bridges, T. J., and Donaldson, N. M. Variational principles for water waves from the viewpoint of a time dependent moving mesh. *Mathematika 57*, 1 (jan 2011), 147–173.

35 | Bridges, T. J., Hydon, P. E., and Lawson, J. K. Multisymplectic structures and the variational bicomplex. *Mathematical Proceedings of the Cambridge Philosophical Society 148*, 1 (jan 2010), 159–178.

36 | Bridges, T. J., and Needham, D. J. Breakdown of the shallow water equations due to growth of the horizontal vorticity. *J. Fluid Mech 679* (jul 2011), 655–666.

37 | Bridges, T. J., and Reich, S. Multi-symplectic integrators: numerical schemes for Hamiltonian PDEs that conserve symplecticity. *Phys. Lett. A 284*, 4-5 (2001), 184–193.

38 | Bridges, T. J., and Reich, S. Numerical methods for Hamiltonian PDEs. *J. Phys. A: Math. Gen 39* (2006), 5287–5320.

39 | Broer, L. J. F. On the hamiltonian theory of surface waves. *Applied Scientific Research 29*, 1 (1974), 430–446.

40 | Camassa, R., and Holm, D. An integrable shallow water equation with peaked solitons. *Phys. Rev. Lett. 71(11)* (1993), 1661–1664.

41 | Carrier, G. F. Gravity waves on water of variable depth. *J. Fluid Mech 24*, 04 (1966), 641–659.

42 | Chambarel, J., Kharif, C., and Touboul, J. Head-on collision of two solitary waves and residual falling jet formation. *Nonlin. Processes Geophys. 16* (2009), 111–122.

43 | Chan, R. K.-C., and Street, R. L. A computer study of finite-amplitude water waves. *J. Comp. Phys. 6*, 1 (aug 1970), 68–94.

44 | Chazel, F. Influence of bottom topography on long water waves. *M2AN 41* (2007), 771–799.

45 | Chazel, F., Lannes, D., and Marche, F. Numerical simulation of strongly nonlinear and dispersive waves using a Green-Naghdi model. *J. Sci. Comput. 48* (2011), 105–116.

46 | Chehab, J.-P., and Dutykh, D. On time relaxed schemes and formulations for dispersive wave equations. *AIMS Mathematics 4*, 2 (2019), 254–278.

47 | Chen, Y., Song, S., and Zhu, H. The multi-symplectic Fourier pseudospectral method for solving two-dimensional Hamiltonian PDEs. *J. Comp. Appl. Math. 236*, 6 (oct 2011), 1354–1369.

48 | Chhay, M., Dutykh, D., and Clamond, D. On the multi-symplectic structure of the Serre-Green-Naghdi equations. *J. Phys. A: Math. Gen 49*, 3 (jan 2016), 03LT01.

49 | Cienfuegos, R., Barthélémy, E., and Bonneton, P. A fourth-order compact finite volume scheme for fully nonlinear and weakly dispersive Boussinesq-type equations. Part I: Model development and analysis. *Int. J. Numer. Meth. Fluids 51* (2006), 1217–1253.

50 | Cienfuegos, R., Barthélemy, E., and Bonneton, P. A fourth-order compact finite volume scheme for fully nonlinear and weakly dispersive Boussinesq-type equations. Part II: boundary conditions and validation. *Int. J. Num. Meth. Fluids 53*, 9 (mar 2007), 1423–1455.

51 | Clamond, D., and Dutykh, D. http://www.mathworks.com/matlabcentral/fileexchange/39189-solitary-water-wave, 2012.

52 | Clamond, D., and Dutykh, D. Practical use of variational principles for modeling water waves. *Phys. D 241*, 1 (2012), 25–36.

53 | Clamond, D., and Dutykh, D. Fast accurate computation of the fully nonlinear solitary surface gravity waves. *Computers and Fluids 84* (jun 2013), 35–38.

54 | Clamond, D., Dutykh, D., and Durán, A. A plethora of generalised solitary gravity-capillary water waves. *J. Fluid Mech. 784* (2015), 664–680.

55 | Clamond, D., Dutykh, D., and Galligo, A. Computer Algebra Applied to a Solitary Waves Study. In *Proceedings of the 2015 ACM on International Symposium on Symbolic and Algebraic Computation - ISSAC '15* (New York, USA, 2015), ACM Press, pp. 125–132.

56 | Clamond, D., Dutykh, D., and Galligo, A. Algebraic method for constructing singular steady solitary waves: a case study. *Proc. R. Soc. Lond. A 472*, 2191 (2016).

57 | Clamond, D., Francius, M., Grue, J., and Kharif, C. Long time interaction of envelope solitons and freak wave formations. *Eur. J. Mech. B/Fluids 25*, 5 (2006), 536–553.

58 | Clamond, D., and Grue, J. A fast method for fully nonlinear water-wave computations. *J. Fluid. Mech. 447* (2001), 337–355.

59 | Clauss, G. F., and Klein, M. F. The New Year Wave in a sea keeping basin: Generation, propagation, kinematics and dynamics. *Ocean Engineering 38* (2011), 1624–1639.

60 | Constantin, A., Sattinger, D. H., and Strauss, W. Variational formulations for steady water waves with vorticity. *J. Fluid Mech. 548* (2006), 151–163.

61 | Cotter, C., and Bokhove, O. Variational water-wave model with accurate dispersion and vertical vorticity. *J. Eng. Math. 67*, 1-2 (oct 2010), 33–54.

62 | Craig, W., and Groves, M. D. Hamiltonian long-wave approximations to the water-wave problem. *Wave Motion 19* (1994), 367–389.

63 | Craig, W., Guyenne, P., Hammack, J., Henderson, D., and Sulem, C. Solitary water wave interactions. *Phys. Fluids 18(5)* (2006), 57106.

64 | Craig, W., and Sulem, C. Numerical simulation of gravity waves. *J. Comput. Phys. 108* (1993), 73–83.

65 | Craik, A. D. D. The origins of water wave theory. *Ann. Rev. Fluid Mech. 36* (2004), 1–28.

66 | Das, S., Sahoo, T., and Meylan, M. H. Dynamics of flexural gravity waves: from sea ice to Hawking radiation and analogue gravity. *Proceedings of the Royal Society A: Mathematical, Physical and Engineering Sciences 474*, 2209 (jan 2018), 20170223.

67 | de Donder, T. *Théorie invariantive du calcul des variations*. Gauthier-Villars, Paris, 1930.

68 | de Saint-Venant, A. J. C. Théorie du mouvement non-permanent des eaux, avec application aux crues des rivières et à l'introduction des marées dans leur lit. *C. R. Acad. Sc. Paris 73* (1871), 147–154.

69 | Degasperis, A., and Procesi, M. Asymptotic integrability. In *Symmetry and Perturbation Theory*, A. Degasperis and G. Gaeta, Eds. World Scientific, 1999, ch. Asymptotic, pp. 23–37.

70 | Dewals, B. J., Erpicum, S., Archambeau, P., Detrembleur, S., and Pirotton, M. Depth-integrated flow modelling taking into account bottom curvature. *Journal of Hydraulic Research 44*, 6 (nov 2006), 785–795.

71 | Dias, F., and Dutykh, D. Dynamics of tsunami waves. In *Extreme Man-Made and Natural Hazards in Dynamics of Structures*, A. Ibrahimbegovic and I. Kozar, Eds. Springer Netherlands, 2007, pp. 35–60.

72 | Dias, F., and Kharif, C. Nonlinear gravity and capillary-gravity waves. *Ann. Rev. Fluid Mech. 31* (1999), 301–346.

73 | Dias, F., and Milewski, P. On the fully-nonlinear shallow-water generalized Serre equations. *Phys. Lett. A 374(8)* (2010), 1049–1053.

74 | Dougalis, V. A., and Mitsotakis, D. E. Solitary waves of the Bona-Smith system. In *Advances in scattering theory and biomedical engineering*, D. Fotiadis and C. Massalas, Eds. World Scientific, New Jersey, 2004, pp. 286–294.

75 | Dougalis, V. A., and Mitsotakis, D. E. Theory and numerical analysis of Boussinesq systems: A review. In *Effective Computational Methods in Wave Propagation* (2008), N. A. Kampanis, V. A. Dougalis, and J. A. Ekaterinaris, Eds., CRC Press, pp. 63–110.

76 | Dougalis, V. A., Mitsotakis, D. E., and Saut, J.-C. On some Boussinesq systems in two space dimensions: Theory and numerical analysis. *Math. Model. Num. Anal. 41*, 5 (2007), 254–825.

77 | Drazin, P. G., and Johnson, R. S. *Solitons: An introduction*. Cambridge University Press, Cambridge, 1989.

78 | Dressler, R. F. New nonlinear shallow-flow equations with curvature. *Journal of Hydraulic Research 16(3)* (1978), 205–222.

79 | Durán, A., Dutykh, D., and Mitsotakis, D. On the multi-symplectic structure of Boussinesq-type systems. I: Derivation and mathematical properties. *Physica D: Nonlinear Phenomena 388* (jan 2019), 10–21.

80 | Durán, A., Dutykh, D., and Mitsotakis, D. On the multi-symplectic structure of Boussinesq-type systems. II: Geometric discretization. *Physica D: Nonlinear Phenomena 397* (oct 2019), 1–16.

81 | Dutykh, D., Chhay, M., and Clamond, D. Numerical study of the generalised Klein-Gordon equations. *Phys. D 304-305* (jun 2015), 23–33.

82 | Dutykh, D., Chhay, M., and Fedele, F. Geometric numerical schemes for the KdV equation. *Comp. Math. Math. Phys. 53*, 2 (2013), 221–236.

83 | Dutykh, D., and Clamond, D. Shallow water equations for large bathymetry variations. *J. Phys. A: Math. Theor. 44*, 33 (2011), 332001.

84 | Dutykh, D., and Clamond, D. Efficient computation of steady solitary gravity waves. *Wave Motion 51*, 1 (jan 2014), 86–99.

85 | Dutykh, D., and Clamond, D. Modified shallow water equations for significantly varying seabeds. *Appl. Math. Model. 40*, 23-24 (dec 2016), 9767–9787.

86 | Dutykh, D., Clamond, D., and Chhay, M. Serre-type equations in deep water. *Mathematical Modelling of Natural Phenomena 12*, 1 (2017).

87 | Dutykh, D., Clamond, D., Milewski, P., and Mitsotakis, D. Finite volume and pseudo-spectral schemes for the fully nonlinear 1D Serre equations. *Eur. J. Appl. Math. 24*, 05 (2013), 761–787.

88 | Dutykh, D., and Dias, F. Water waves generated by a moving bottom. In *Tsunami and Nonlinear Waves*, A. Kundu, Ed. Springer Berlin Heidelberg, Berlin, Heidelberg, 2007, pp. 65–95.

89 | Dutykh, D., and Dias, F. Energy of tsunami waves generated by bottom motion. *Proc. R. Soc. Lond. A 465*, 2103 (mar 2009), 725–744.

90 | Dutykh, D., Dias, F., and Kervella, Y. Linear theory of wave generation by a moving bottom. *Comptes Rendus Mathématique 343*, 7 (oct 2006), 499–504.

91 | Dutykh, D., Hoefer, M., and Mitsotakis, D. Solitary wave solutions and their interactions for fully nonlinear water waves with surface tension in the generalized Serre equations. *Theoretical and Computational Fluid Dynamics 32*, 3 (jun 2018), 371–397.

92 | Dutykh, D., Katsaounis, T., and Mitsotakis, D. Finite volume schemes for dispersive wave propagation and runup. *J. Comput. Phys. 230*, 8 (apr 2011), 3035–3061.

93 | Dutykh, D., Katsaounis, T., and Mitsotakis, D. Finite volume methods for unidirectional dispersive wave models. *Int. J. Num. Meth. Fluids 71* (2013), 717–736.

94 | Dutykh, D., Labart, C., and Mitsotakis, D. Long wave run-up on random beaches. *Phys. Rev. Lett 107* (2011), 184504.

95 | Dutykh, D., and Mitsotakis, D. On the relevance of the dam break problem in the context of nonlinear shallow water equations. *Discrete and Continuous Dynamical Systems - Series B 13(4)* (2010), 799–818.

96 | Dutykh, D., Poncet, R., and Dias, F. The VOLNA code for the numerical modeling of tsunami waves: Generation, propagation and inundation. *Eur. J. Mech. B/Fluids 30*, 6 (2011), 598–615.

97 | Dyachenko, A. I., Korotkevich, A. O., and Zakharov, V. E. Weak turbulence of gravity waves. *JETP Lett. 77* (2003), 546–550.

98 | Dysthe, K. B. Note on a modification to the nonlinear Schrödinger equation for application to deep water. *Proc. R. Soc. Lond. A 369* (1979), 105–114.

99 | Eckart, C. Variation principles of hydrodynamics. *Phys. Fluids 3* (1960), 421–427.

100 | Feynman, R., Leighton, R. B., and Sands, M. *The Feynman Lectures on Physics, Vol. 1: Mainly Mechanics, Radiation, and Heat*, 2 ed. Addison Wesley, 2005.

101 | Frank, J., Moore, B. E., and Reich, S. Linear PDEs and Numerical Methods That Preserve a Multisymplectic Conservation Law. *SIAM J. Sci. Comput. 28*, 1 (jan 2006), 260–277.

102 | Fructus, D., Clamond, D., Kristiansen, O., and Grue, J. An efficient model for threedimensional surface wave simulations. Part I: Free space problems. *J. Comput. Phys. 205* (2005), 665–685.

103 | Galligo, A., Dutykh, D., and Clamond, D. On detection of solitary waves, using phase diagrams and real discriminant. In *Encuentros de Algebra Computacional y aplicaciones*. Barcelona, Spain, 2014, pp. 119–122.

104 | Garrett, C., and Munk, W. Internal Waves in the Ocean. *Ann. Rev. Fluid Mech. 11*, 1 (jan 1979), 339–369.

105 | Ghidaglia, J.-M., Kumbaro, A., and Le Coq, G. Une méthode volumes-finis à flux caractéristiques pour la résolution numérique des systèmes hyperboliques de lois de conservation. *C. R. Acad. Sci. I 322* (1996), 981–988.

106 | Ghidaglia, J.-M., Kumbaro, A., and Le Coq, G. On the numerical solution to two fluid models via cell centered finite volume method. *Eur. J. Mech. B/Fluids 20* (2001), 841–867.

107 | Gobbi, M. F., and Kirby, J. T. Wave evolution over submerged sills: Tests of a high-order Boussinesq model. *Coastal Engineering 37*, 1 (1999), 57–96.

108 | Godunov, S. K., Zabrodine, A., Ivanov, M., Kraiko, A., and Prokopov, G. *Résolution numérique des problèmes multidimensionnels de la dynamique des gaz*. Editions Mir, Moscow, 1979.

109 | Goldschmidt, H., and Sternberg, S. The Hamilton-Cartan formalism in the calculus of variations. *Ann. Inst. Fourier 23*, 1 (1973), 203–267.

110 | Goldstein, H., Poole, C., and Safko, J. *Classical Mechanics*, 3 ed. Addison-Wesley Pub. Co., San Francisco, CA, 2001.

111 | Gong, Y., Cai, J., and Wang, Y. Multi-Symplectic Fourier Pseudospectral Method for the Kawahara Equation. *Commun. Comput. Phys. 16*, 1 (2014), 35–55.

112 | Gramstad, O., and Trulsen, K. Hamiltonian form of the modified nonlinear Schrödinger equation for gravity waves on arbitrary depth. *J. Fluid Mech 670* (2011), 404–426.

113 | Gray, J., Wieland, M., and Hutter, K. Gravity-driven free surface flow of granular avalanches over complex basal topography. *Proc. R. Soc. Lond. A 455* (1998), 1841–1874.

114 | Green, A. E., Laws, N., and Naghdi, P. M. On the theory of water waves. *Proc. R. Soc. Lond. A 338* (1974), 43–55.

115 | Green, A. E., and Naghdi, P. M. A derivation of equations for wave propagation in water of variable depth. *J. Fluid Mech. 78* (1976), 237–246.

116 | Grimshaw, R. Internal Solitary Waves. In *Environmental Stratified Flows*, R. Grimshaw, Ed. Springer US, 2002, pp. 1–27.

117 | Grue, J., Clamond, D., Huseby, M., and Jensen, A. Kinematics of extreme waves in deep water. *Applied Ocean Research 25* (2003), 355–366.

118 | Hammack, J. A note on tsunamis: their generation and propagation in an ocean of uniform depth. *J. Fluid Mech. 60* (1973), 769–799.

119 | Harten, A. ENO schemes with subcell resolution. *J. Comput. Phys 83* (1989), 148–184.

120 | Harten, A., and Osher, S. Uniformly high-order accurate nonscillatory schemes. I. *SIAM J. Numer. Anal. 24* (1987), 279–309.

121 | Henderson, K. L., Peregrine, D. H., and Dold, J. W. Unsteady water wave modulation: fully nonlinear solutions and comparison with the nonlinear Schrödinger equation. *Wave Motion 29* (1999), 341–361.

122 | Henyey, F. S. Hamiltonian description of stratified fluid dynamics. *Phys. Fluids 26* (1983), 40.

123 | Hunt, M., and Dutykh, D. Visco-potential flows in electrohydrodynamics. *Physics Letters, Section A: General, Atomic and Solid State Physics 378*, 24-25 (2014), 1721–1726.

124 | Hunt, M. J., and Dutykh, D. Free Surface Flows in Electrohydrodynamics with a Constant Vorticity Distribution. *Water Waves 3*, 2 (jul 2021), 297–317.

125 | Iguchi, T. Isobe-kakinuma model for water waves as a higher order shallow water approximation. *J. Diff. Eqs. 265* (8 2018), 935–962.

126 | Isaacson, E., and Keller, H. B. *Analysis of Numerical Methods*. Dover Publications, 1966.

127 | Jensen, A., Clamond, D., Huseby, M., and Grue, J. On local and convective accelerations in steep wave events. *Ocean Engineering 34* (2007), 426–435.

128 | Johnson, R. S. Camassa-Holm, Korteweg-de Vries and related models for water waves. *J. Fluid Mech. 455* (2002), 63–82.

129 | Johnson, R. S. *A Modern Introduction to the Mathematical Theory of Water Waves*, 2 ed. Cambridge University Press, Cambridge, 2004.

130 | Kameyama, M., Kageyama, A., and Sato, T. Multigrid iterative algorithm using pseudo-compressibility for three-dimensional mantle convection with strongly variable viscosity. *J. Comput. Phys 206* (2005), 162–181.

131 | Kaup, D. J. A higher-order water-wave equation and method for solving it. *Prog. Theor. Phys. 54* (1975), 396–408.

132 | Keller, J. B. Shallow-water theory for arbitrary slopes of the bottom. *J. Fluid Mech. 489* (2003), 345–348.

133 | Kervella, Y., Dutykh, D., and Dias, F. Comparison between three-dimensional linear and nonlinear tsunami generation models. *Theor. Comput. Fluid Dyn. 21*, 4 (jun 2007), 245–269.

134 | Khakimzyanov, G., Dutykh, D., Fedotova, Z., and Gusev, O. *Dispersive Shallow Water Waves*. Lecture Notes in Geosystems Mathematics and Computing. Springer International Publishing, Cham, 2020.

135 | Kijowki, J. Multiphase spaces and gauge in calculus of variations. *Bull. Acad. Polon. des Sci., Série Sci. Math., Astr. et Phys. XXII* (1974), 1219–1225.

136 | Kim, J. W., Bai, K. J., Ertekin, R. C., and Webster, W. C. A derivation of the Green-Naghdi equations for irrotational flows. *J. Eng. Math. 40*, 1 (2001), 17–42.

137 | Kolgan, N. E. Finite-difference schemes for computation of three dimensional solutions of gas dynamics and calculation of a flow over a body under an angle of attack. *Uchenye Zapiski TsaGI [Sci. Notes Central Inst. Aerodyn] 6(2)* (1975), 1–6.

138 | Komen, G. J., Cavalieri, L., Donelan, M., Hasselmann, K., Hasselmann, S., and Janssen, P. A. E. M. *Dynamics and Modelling of Ocean Waves*. Cambridge University Press, Cambridge, 1996.

139 | Korotkevich, A. O., Pushkarev, A. N., Resio, D., and Zakharov, V. E. Numerical verification of the weak turbulent model for swell evolution. *Eur. J. Mech. B/Fluids 27(4)* (2008), 361–387.

140 | Korteweg, D. J., and de Vries, G. On the change of form of long waves advancing in a rectangular canal, and on a new type of long stationary waves. *Phil. Mag. 39*, 5 (1895), 422–443.

141 | Kraenkel, R. A., Leon, J., and Manna, M. A. Theory of small aspect ratio waves in deep water. *Physica D 211* (2005), 377–390.

142 | Krupka, D. A geometric theory of ordinary first order variational problems in fibered manifolds. I. Critical sections. *Journal of Mathematical Analysis and Applications 49*, 1 (jan 1975), 180–206.

143 | Krupka, D. A geometric theory of ordinary first order variational problems in fibered manifolds. II. Invariance. *Journal of Mathematical Analysis and Applications 49*, 2 (feb 1975), 469–476.

144 | Kupershmidt, B. A. Mathematics of dispersive water waves. *Commun. Math. Phys. 99* (1985), 51–73.

145 | Lagrange, J.-L. Mémoire sur la théorie du mouvement des fluides. *Nouv. Mém. Acad. Berlin 196* (1781).

146 | Lagrange, J.-L. *Mécanique analytique*, 3 ed. Hallet-Bachelier, Paris, 1853.

147 | Lanczos, C. *The Variational Principles of Mechanics*. New York: Dover Publications, 1970.

148 | Laughlin, R. B. Anomalous Quantum Hall Effect: An Incompressible Quantum Fluid with Fractionally Charged Excitations. *Phys. Rev. Lett. 50*, 18 (may 1983), 1395–1398.

149 | Leimkuhler, B., and Reich, S. *Simulating Hamiltonian Dynamics*, vol. 14 of *Cambridge Monographs on Applied and Computational Mathematics*. Cambridge University Press, Cambridge, 2005.

150 | Lepage, T. Sur les champs géodésiques du calcul des variations. *Bull. Acad. Roy. Belg., Cl. Sci 27* (1936), 716–729, 1036–1046.

151 | Lew, A., Marsden, J., Ortiz, M., and West, M. An overview of variational integrators. In *Finite Element Methods: 1970s and beyond (CIMNE, 2003)* (Barcelona, Spain, 2004), p. 18.

152 | Lewis, D., Marsden, J., Montgomery, R., and Ratiu, T. The Hamiltonian structure for dynamic free boundary problems. *Physica D 18* (1986), 391–404.

153 | Li, Y. A. Hamiltonian structure and linear stability of solitary waves of the Green-Naghdi equations. *J. Nonlin. Math. Phys. 9*, 1 (2002), 99–105.

154 | Li, Y. A., Hyman, J. M., and Choi, W. A Numerical Study of the Exact Evolution Equations for Surface Waves in Water of Finite Depth. *Stud. Appl. Maths. 113* (2004), 303–324.

155 | Luke, J. C. A variational principle for a fluid with a free surface. *J. Fluid Mech. 27* (1967), 375–397.

156 | Ma, Q. Advances in numerical simulation of nonlinear water waves. In *Adv. Coastal Ocean Engng*. World Scientific, 2010.

157 | Madsen, P. A., Bingham, H. B., and Schäffer, H. A. Boussinesq-type formulations for fully nonlinear and extremely dispersive water waves: derivation and analysis. *Proc. R. Soc. Lond. A 459* (2003), 1075–1104.

158 | Madsen, P. A., and Schäffer, H. A. A review of Boussinesq-type equations for surface gravity waves. *Adv. Coastal Ocean Engng 5* (1999), 1–94.

159 | Majda, A. J., and Bertozzi, A. L. *Vorticity and Incompressible Flow*. Cambridge University Press, Cambridge, 2001.

160 | Maklakov, D. Almost-highest gravity waves on water of finite depth. *European Journal of Applied Mathematics 13* (2002), 67–93.

161 | Marsden, J. E., Patrick, G. W., and Shkoller, S. Multisymplectic geometry, variational integrators, and nonlinear PDEs. *Comm. Math. Phys. 199*, 2 (1998), 351–395.

162 | Marsden, J. E., and Shkoller, S. Multisymplectic geometry, covariant Hamiltonians, and water waves. *Mathematical Proceedings of the Cambridge Philosophical Society 125*, 3 (jan 1999), 553–575.

163 | Maxworthy, T. Experiments on collisions between solitary waves. *J. Fluid Mech 76* (1976), 177–185.

164 | Medeiros, S. C., and Hagen, S. C. Review of wetting and drying algorithms for numerical tidal flow models. *Int. J. Num. Meth. Fluids 71*, 4 (feb 2013), 473–487.

165 | Mei, C. C. *The applied dynamics of water waves*. World Scientific, 1989.

166 | Miles, J. W. On Hamilton's principle for surface waves. *J. Fluid Mech 83*, 1 (nov 1977), 153–158.

167 | Miles, J. W., and Salmon, R. Weakly dispersive nonlinear gravity waves. *J. Fluid Mech. 157* (1985), 519–531.

168 | Milewski, P., and Tabak, E. A pseudospectral procedure for the solution of nonlinear wave equations with examples from free-surface flows. *SIAM J. Sci. Comput. 21(3)* (1999), 1102–1114.

169 | Mirie, S. M., and Su, C. H. Collision between two solitary waves. Part 2. A numerical study. *J. Fluid Mech. 115* (1982), 475–492.

170 | Mitsotakis, D., Dutykh, D., and Carter, J. On the nonlinear dynamics of the traveling-wave solutions of the Serre system. *Wave Motion 70* (apr 2017), 166–182.

171 | Mitsotakis, D., Ilan, B., and Dutykh, D. On the Galerkin/Finite-Element Method for the Serre Equations. *J. Sci. Comput. 61*, 1 (feb 2014), 166–195.

172 | Mitsotakis, D. E. Boussinesq systems in two space dimensions over a variable bottom for the generation and propagation of tsunami waves. *Math. Comp. Simul. 80* (2009), 860–873.

173 | Moore, B., and Reich, S. Backward error analysis for multi-symplectic integration methods. *Numerische Mathematik 95*, 4 (2003), 625–652.

174 | Moore, B., and Reich, S. Multi-symplectic integration methods for Hamiltonian PDEs. *Future Generation Computer Systems 19*, 3 (2003), 395–402.

175 | Moré, J. J. The Levenberg-Marquardt algorithm: Implementation and theory. In *Proceedings of the Biennial Conference Held at Dundee, June 28-July 1, 1977* (1978), G. A. Watson, Ed., Springer Berlin Heidelberg, pp. 105–116.

176 | Morrison, P. J. Hamiltonian description of the ideal fluid. *Rev. Mod. Phys. 70(2)* (1998), 467–521.

177 | Mura, T., and Koya, T. *Variational Methods in Mechanics*. Oxford University Press, Oxford, 1992.

178 | Muraki, D. J. A Simple Illustration of a Weak Spectral Cascade. *SIAM J. Appl. Math 67*, 5 (2007), 1504–1521.

179 | Murayama, H. Berkley's Quantum Mechanics I Lecture Notes: Variational Method. Tech. rep., University of California, Berkeley, CA, 2006.

180 | Nachbin, A. A terrain-following Boussinesq system. *SIAM Appl. Math. 63(3)* (2003), 905–922.

181 | Nadaoka, K., Beji, S., and Nakagawa, Y. A fully dispersive weakly nonlinear model for water waves. *Proc. R. Soc. Lond. A 453*, 1957 (feb 1997), 303–318.

182 | Neetu, S., Suresh, I., Shankar, R., Shankar, D., Shenoi, S. S. C., Shetye, S. R., Sundar, D., and Nagarajan, B. Comment on "The Great Sumatra-Andaman Earthquake of 26 December 2004". *Science 310* (2005), 1431a———1431b.

183 | Nwogu, O. Alternative form of Boussinesq equations for nearshore wave propagation. *J. Waterway, Port, Coastal and Ocean Engineering 119* (1993), 618–638.

184 | Olver, P. J. Hamiltonian perturbation theory and water waves. *Contemp. Math. 28* (1984), 231–249.

185 | Olver, P. J. Unidirectionalization of hamiltonian waves. *Phys. Lett. A 126* (1988), 501–506.

186 | Olver, P. J. *Applications of Lie groups to differential equations*, 2 ed., vol. 107 of *Graduate Texts in Mathematics*. Springer-Verlag, New York, 1993.

187 | Osborne, A. *Nonlinear ocean waves and the inverse scattering transform*, vol. 97. Elsevier, 2010.

188 | Pelinovsky, D. E., Pelinovsky, E. N., Kartashova, E., Talipova, T., and Giniyatullin, A. Universal power law for the energy spectrum of breaking Riemann waves. *JETP Lett. 98*, 4 (2013), 237–241.

189 | Perlin, M., and Schultz, W. W. Capillary Effects on Surface Waves. *Ann. Rev. Fluid Mech. 32*, 1 (jan 2000), 241–274.

190 | Petrov, A. A. Variational statement of the problem of liquid motion in a container of finite dimensions. *Prikl. Math. Mekh. 28*, 4 (1964), 917–922.

191 | Purser, W. F. C., and Synge, J. L. Water Waves and Hamilton's Method. *Nature 194*, 4825 (apr 1962), 268–268.

192 | Radder, A. C. Hamiltonian dynamics of water waves. *Adv. Coastal Ocean Engng 4* (1999), 21–59.

193 | Rajchenbach, J., Clamond, D., and Leroux, A. Observation of Star-Shaped Surface Gravity Waves. *Phys. Rev. Lett. 110*, 9 (feb 2013), 094502.

194 | Rajchenbach, J., Leroux, A., and Clamond, D. New Standing Solitary Waves in Water. *Phys. Rev. Lett. 107*, 2 (jul 2011), 024502.

195 | Renouard, D. P., Seabra-Santos, F. J., and Temperville, A. M. Experimental study of the generation, damping, and reflexion of a solitary wave. *Dynamics of Atmospheres and Oceans 9(4)* (1985), 341–358.

196 | Roeber, V., Cheung, K. F., and Kobayashi, M. H. Shock-capturing Boussinesq-type model for nearshore wave processes. *Coastal Engineering 57*, 4 (apr 2010), 407–423.

197 | Salmon, R. Hamiltonian fluid mechanics. *Ann. Rev. Fluid Mech. 20* (1988), 225–256.

198 | Savage, S. B., and Hutter, K. The motion of a finite mass of granular material down a rough incline. *J. Fluid Mech. 199* (1989), 177–215.

199 | Schober, C. M., and Wlodarczyk, T. H. Dispersive properties of multisymplectic integrators. *J. Comput. Phys 227*, 10 (may 2008), 5090–5104.

200 | Seabra-Santos, F. J. *Contribution à l'étude des ondes de gravité bidimensionnelles en eau peu profonde*. PhD thesis, Institut National Polytechnique de Grenoble, 1985.

201 | Seabra-Santos, F. J., Renouard, D. P., and Temperville, A. M. Numerical and Experimental study of the transformation of a Solitary Wave over a Shelf or Isolated Obstacle. *J. Fluid Mech 176* (1987), 117–134.

202 | Seliger, R. L., and Whitham, G. B. Variational principle in continuous mechanics. *Proc. R. Soc. Lond. A 305* (1968), 1–25.

203 | Serre, F. Contribution à l'étude des écoulements permanents et variables dans les canaux. *La Houille blanche*, 3 (1953), 374–388.

204 | Serre, F. Contribution à l'étude des écoulements permanents et variables dans les canaux. *La Houille blanche*, 8 (1953), 830–872.

205 | Shampine, L. F., and Reichelt, M. W. The MATLAB ODE Suite. *SIAM J. Sci. Comput. 18* (1997), 1–22.

206 | Shemer, L., and Sergeeva, A. An experimental study of spatial evolution of statistical parameters in a unidirectional narrow-banded random wavefield. *J. Geophys. Res. 114*, C1 (jan 2009), C01015.

207 | Shemer, L., Sergeeva, A., and Liberzon, D. Effect of the initial spectrum on the spatial evolution of statistics of unidirectional nonlinear random waves. *J. Geophys. Res. 115*, C12 (dec 2010), C12039.

208 | Söderlind, G. Digital filters in adaptive time-stepping. *ACM Trans. Math. Software 29* (2003), 1–26.

209 | Söderlind, G., and Wang, L. Adaptive time-stepping and computational stability. *J. Comp. Appl. Math. 185(2)* (2006), 225–243.

210 | Sørensen, R. M. *Basic coastal engineering*. Springer, 1997.

211 | Souriau, J.-M. *Structure of Dynamical Systems: a Symplectic View of Physics*. Birkhäuser, Boston, MA, 1997.

212 | Stoker, J. J. *Water Waves: The Mathematical Theory with Applications*. John Wiley and Sons, Inc., Hoboken, NJ, USA, jan 1992.

213 | Stokes, G. G. On the theory of oscillatory waves. *Trans. Camb. Phil. Soc. 8* (1847), 441–455.

214 | Stokes, G. G. Considerations relative to the greatest height of oscillatory irrotational waves which can be propagated without change of form. *Collected Papers 1* (1880), 225–228.

215 | Su, C. H., and Gardner, C. S. KdV equation and generalizations. Part III. Derivation of the Korteweg-de Vries equation and Burgers equation. *J. Math. Phys. 10* (1969), 536–539.

216 | Su, C. H., and Mirie, R. M. On head-on collisions between two solitary waves. *J. Fluid Mech. 98* (1980), 509–525.

217 | Synge, J. L. The Hamiltonian Method and Its Application to Water Waves. *Proceedings of the Royal Irish Academy. Section A: Mathematical and Physical Sciences 63* (1963), 1–34.

218 | Synolakis, C. E. *The runup of long waves*. PhD thesis, California Institute of Technology, 1986.

219 | Synolakis, C. E., and Bernard, E. N. Tsunami science before and beyond Boxing Day 2004. *Phil. Trans. R. Soc. A 364* (2006), 2231–2265.

220 | Thomas, M. D., and Craik, A. D. D. Three-wave resonance for free-surface flows over flexible boundaries. *J. Fluids Structures 2* (1988), 323–338.

221 | Thorpe, S. A. *The Turbulent Ocean*. Cambridge University Press, Cambridge, 2005.

222 | Titov, V. V., Rabinovich, A. B., Mofjeld, H. O., Thomson, R. E., and González, F. I. The global reach of the 26 December 2004 Sumatra tsunami. *Science 309* (2005), 2045–2048.

223 | Todorovska, M. I., and Trifunac, M. D. Generation of tsunamis by a slowly spreading uplift of the seafloor. *Soil Dynamics and Earthquake Engineering 21* (2001), 151–167.

224 | Trefethen, L. N. *Spectral methods in MatLab*. Society for Industrial and Applied Mathematics, Philadelphia, PA, USA, 2000.

225 | Trulsen, K., Kliakhandler, I., Dysthe, K. B., and Velarde, M. G. On weakly nonlinear modulation of waves on deep water. *Phys. Fluids 12* (2000), 2432–2437.

226 | van Leer, B. Towards the ultimate conservative difference scheme V: a second order sequel to Godunov' method. *J. Comput. Phys. 32* (1979), 101–136.

227 | van Leer, B. Upwind and High-Resolution Methods for Compressible Flow: From Donor Cell to Residual-Distribution Schemes. *Commun. Comput. Phys. 1* (2006), 192–206.

228 | Verner, J. H. Explicit Runge-Kutta methods with estimates of the local truncation error. *SIAM J. Num. Anal. 15(4)* (1978), 772–790.

229 | Volterra, V. Sopra una estensione della teoria Jacobi-Hamilton del calcolo delle variazioni. *Rend. Cont. Acad. Lincei, ser. IV VI* (1890), 127–138.

230 | Volterra, V. Sulle equazioni differenziali che provengono da questiono di calcolo delle variazioni. *Rend. Cont. Acad. Lincei, ser. IV VI* (1890), 42–54.

231 | Wang, Y., Wang, B., and Qin, M. Z. Numerical Implementation of the Multisymplectic Preissman Scheme and Its Equivalent Schemes. *Appl. Math. Comput. 149*, 2 (2003), 299–326.

232 | Wehausen, J. V., and Laitone, E. V. Surface waves. *Handbuch der Physik 9* (1960), 446–778.

233 | Wei, G., Kirby, J. T., Grilli, S. T., and Subramanya, R. A fully nonlinear Boussinesq model for surface waves. Part 1. Highly nonlinear unsteady waves. *J. Fluid Mech. 294* (1995), 71–92.

234 | Wessel, P. Analysis of Observed and Predicted Tsunami Travel Times for the Pacific and Indian Oceans. *Pure Appl. Geophys. 166*, 1-2 (feb 2009), 301–324.

235 | Weyl, H. Geodesic Fields in the Calculus of Variation for Multiple Integrals. *Annals of Mathematics 36*, 3 (jul 1935), 607–629.

236 | Whitham, G. B. A general approach to linear and non-linear dispersive waves using a Lagrangian. *J. Fluid Mech. 22* (1965), 273–283.

237 | Whitham, G. B. *Linear and Nonlinear Waves*. John Wiley & Sons, Inc., Hoboken, NJ, USA, jun 1999.

238 | Wu, T. Y. Long Waves in Ocean and Coastal Waters. *Journal of Engineering Mechanics 107* (1981), 501–522.

239 | Wu, T. Y. A unified theory for modeling water waves. *Adv. App. Mech. 37* (2001), 1–88.

240 | Xing, Y., and Shu, C.-W. High order finite difference WENO schemes with the exact conservation property for the shallow water equations. *J. Comput. Phys. 208* (2005), 206–227.

241 | Yahalom, A., and Lynden-Bell, D. Simplified variational principles for barotropic magnetohydrodynamics. *J. Fluid Mech 607* (2008), 235–265.

242 | Yuen, H. C., and Lake, B. M. Nonlinear dynamics of deep-water gravity waves. *Adv. App. Mech. 22* (1982), 67–229.

243 | Zakharov, V. E. Stability of periodic waves of finite amplitude on the surface of a deep fluid. *J. Appl. Mech. Tech. Phys. 9* (1968), 190–194.

244 | Zakharov, V. E. Turbulence in Integrable Systems. *Studies in Applied Mathematics 122*, 3 (apr 2009), 219–234.

245 | Zakharov, V. E., and Kuznetsov, E. A. Hamiltonian formalism for nonlinear waves. *Usp. Fiz. Nauk 167* (1997), 1137–1168.

246 | Zakharov, V. E., Lvov, V. S., and Falkovich, G. *Kolmogorov Spectra of Turbulence I. Wave Turbulence.* Series in Nonlinear Dynamics, Springer-Verlag, Berlin, 1992.

247 | Zhao, P. F., and Qin, M. Z. Multisymplectic geometry and multisymplectic Preissmann scheme for the KdV equation. *J. Phys. A: Math. Gen. 33*, 18 (may 2000), 3613–3626.

248 | Zheleznyak, M. I. Influence of long waves on vertical obstacles. In *Tsunami Climbing a Beach*, E. N. Pelinovsky, Ed. Applied Physics Institute Press, Gorky, 1985, pp. 122–139.

249 | Zheleznyak, M. I., and Pelinovsky, E. N. Physical and mathematical models of the tsunami climbing a beach. In *Tsunami Climbing a Beach*, E. N. Pelinovsky, Ed. Applied Physics Institute Press, Gorky, 1985, pp. 8–34.

This IAHR Water Monograph takes the subject of variational principles for water waves to a new level. Lagrangians such as Luke's are improved via relaxation where a sequence of constraints are added, enforced by Lagrange multipliers, that may be exact or approximate and, in the latter case, a range of new and surprising model equations for water waves emerge, without the need to introduce a small parameter. It is a highly effective strategy and produces Lagrangian, Hamiltonian and multisymplectic structures with equal ease.

Tom Bridges

ABOUT THE AUTHORS

Didier Clamond was educated in Theoretical Mechanics at the University of Grenoble, France. He is now a full Professor at the Mathematics Department of the Université Côte d'Azur in Nice, France. His main field of research is mathematical and numerical modelling, particularly for nonlinear water waves.

Denys Dutykh was born in the quaint Ukrainian town of Polohy, located in the Zaporizhzhia region. His academic journey began at Oles Honchar Dnipro National University, where he earned a Bachelor of Science in Applied Mathematics in 2003, followed by a Master of Science in 2004. After earning a prestigious international scholarship, Dr. Dutykh relocated to France to continue his studies at the École Normale Supérieure de Cachan. There, he pursued a second Master's degree in numerical methods for continuum mechanics. Dr. Dutykh then embarked on his doctoral studies at the Centre de Mathématiques et de Leurs Applications (CMLA). He successfully defended his PhD thesis, which focused on the mathematical modelling of tsunami waves, in a two-year span, completing it in 2007. In 2008, Dr. Dutykh joined the highly selective Centre National de la Recherche Scientifique (CNRS) as a permanent researcher. He further enhanced his academic credentials by defending a habilitation thesis on mathematical modelling in environmental sciences at the same University of Savoie in 2010. In 2012–2013, Dr. Dutykh expanded his international experience by joining the University College Dublin's School of Mathematics and Statistics in Ireland, contributing to the ERC Advanced Grant project MULTIWAVE. In 2022, Dr. Dutykh embarked on a new chapter, joining the Mathematics Department of Khalifa University of Science and Technology (Abu Dhabi, United Arab Emirates) as an Associate Professor.

Dimitrios Mitsotakis received his bachelor's degree from the University of Crete with the highest honours (first in class) in 2000. He received a master's degree in Applied and Numerical Analysis in 2003 and a PhD in Mathematics in 2007 from the University of Athens. His experience with high performance computing started while a visiting student at the Edinburgh Parallel Computing Center at The University of Edinburgh in 2000. Dimitrios worked at the Université Paris-Sud (2008–2010) as a Marie Curie fellow, at the University of Minnesota (2010–2012) as an associate postdoc and at the University of California, Merced (2012–2014) as a visiting Assistant Professor. Dimitrios is currently a reader/associate professor at the School of Mathematics and Statistics of Victoria University of Wellington.

ISBN 978-90-833476-6-0
9 789083 347660

IAHR Global Secretariat
iahr@iahr.org

Madrid Office
Paseo Bajo Virgen del Puerto, 3
28005 Madrid, SPAIN
T +34 91 335 7908
F +34 91 335 7935

Beijing Office
A-1 Fuxing Road, Haidian District
100038 Beijing, CHINA
T +86 10 6878 1128
F +86 10 6878 1890

IAHR.org